

**EXTRACELLULAR REDOX BIOCHEMISTRY:
QUIESCIN SULFHYDRYL OXIDASE IN MAMMALIAN SERUM
AND
PROBING THE THIOL-DISULFIDE STATUS OF THE CELL SURFACE**

by

Lingxi Jiang

A dissertation submitted to the Faculty of the University of Delaware in partial fulfillment of the requirements for the degree of Doctor of Philosophy in Chemistry and Biochemistry

Summer 2018

© 2018 Lingxi Jiang
All Rights Reserved

**EXTRACELLULAR REDOX BIOCHEMISTRY:
QUIESCIN SULFHYDRYL OXIDASE IN MAMMALIAN SERUM
AND
PROBING THE THIOL-DISULFIDE STATUS OF THE CELL SURFACE**

by

Lingxi Jiang

Approved: _____
Brian J. Bahnson, Ph.D.
Chair of the Department of Chemistry and Biochemistry

Approved: _____
George H. Watson, Ph.D.
Dean of the College of Arts and Sciences

Approved: _____
Douglas J. Doren, Ph.D.
Interim Vice Provost for Graduate and Professional Education

I certify that I have read this dissertation and that in my opinion it meets the academic and professional standard required by the University as a dissertation for the degree of Doctor of Philosophy.

Signed:

Colin Thorpe, Ph.D.
Professor in charge of dissertation

I certify that I have read this dissertation and that in my opinion it meets the academic and professional standard required by the University as a dissertation for the degree of Doctor of Philosophy.

Signed:

Brian J. Bahnson, Ph.D.
Member of dissertation committee

I certify that I have read this dissertation and that in my opinion it meets the academic and professional standard required by the University as a dissertation for the degree of Doctor of Philosophy.

Signed:

Catherine L. Grimes, Ph.D.
Member of dissertation committee

I certify that I have read this dissertation and that in my opinion it meets the academic and professional standard required by the University as a dissertation for the degree of Doctor of Philosophy.

Signed:

Tanya F. Gressley, Ph.D.
Member of dissertation committee

ACKNOWLEDGMENTS

My PhD life at University of Delaware has developed with supports and help from many people, and I would like to extend my appreciation and gratitude to all of them. First and foremost, I would like to thank my advisor, Dr. Colin Thorpe. His continuous guidance and support to my research have immensely helped me to grow as a scientist. I always admire his brilliant ideas and patience in experiments, his excellent skills of presentation and communication, and his passion and dedication towards scientific research. I have greatly benefited from hundreds of discussions with him about my research and my life, and I feel fortunate that I have worked under his mentorship.

I would like to thank my committee members Dr. Bahnson, Dr. Grimes and Dr. Gressley for their time and advice, which have enriched my PhD research work. I would like to acknowledge the Department of Chemistry and Biochemistry for providing such a good collaborative environment that enabled me to develop as a researcher. I would like to thank Dr. John Koh for providing the tissue culture facility and Dr. Haoyu Wang for the mammalian cell culture training. I would also like to thank Dr. Jeffrey Caplan and Dr. Michael Moore at Delaware Biotechnical Institute for the help with confocal microscopy, and Dr. Jessica Tanis and Michael Clupper at Department of Biological Science for collaboration of the *C. elegans* project.

I am grateful to the current and past members of the Thorpe Laboratory for their help and encouragement throughout the PhD journey. Especially I would like to thank Dr. Benjamin Israel for not only being my mentor of biochemistry techniques

and collaborating with me to publish a paper, but also encouraging me when I struggled in first years and offering so many helps towards my daily life. I would also like to thank Dr. Stephanie Ramadan for the FPLC training, Dr. Shawn Gannon for collaborating in the publication, Dr. Jennifer Coddling-Bui, Dr. Vidyadhar Daithankar, Dr. Aparna Sapra, Dr. Devin Hudson, Celia Foster, Tiantian Yu, and Reetika Dutt for scientific and non-scientific discussions. I am thankful for the invaluable friends that I have made during the whole period at University of Delaware, and the experience here would not have been the same without them.

Finally, I would like to thank my family. I feel very lucky that I have my husband Hai with me during these years, we went through both good and bad times together and were constantly supportive to each other. I am grateful for the love of my parents, my parents-in-law, uncle, auntie and sisters; their constant support has been an invaluable source of strength. I am also thankful to my little baby Mofei (Bubu); having him with me is the luckiest thing in my life and he makes me a better person.

TABLE OF CONTENTS

LIST OF TABLES	xi
LIST OF FIGURES	xii
ABSTRACT	xxiv

Chapter

1	OXIDATIVE PROTEIN FOLDING AND REDOX REGULATION	1
1.1	Introduction to Oxidative Protein Folding	1
1.2	Oxidative Protein Folding in Prokaryotes	4
1.3	Oxidative Protein Folding Systems in Eukaryotes	7
1.3.1	Mitochondrial IMS	7
1.3.2	Endoplasmic Reticulum (ER).....	10
1.3.2.1	Protein Disulfide Isomerase (PDI)	10
1.3.2.2	Endoplasmic Reticulum Oxidoreductin 1 (ERO1).....	14
1.3.2.3	Erv2p	14
1.3.2.4	Peroxiredoxin IV	15
1.3.2.5	Vitamin K Epoxide Reductase (VKOR)	15
1.3.2.6	L-Ascorbate	16
1.3.3	Disulfide Bond Formation Post ER.....	16
1.4	Quiescin Sulfhydryl Oxidase (QSOX)	17
1.4.1	History of QSOX.....	17
1.4.2	Structure and Catalytic Mechanism of QSOX	19
1.4.3	Substrates of QSOX	23
1.4.4	Intracellular and Extracellular Distribution of QSOX.....	23
1.4.5	QSOX and Diseases	27
1.5	Extracellular Redox Regulation	28
1.5.1	Glutathione/glutathione Disulfide Couple.....	28
1.5.2	Cysteine/cystine Couple	30
1.5.3	Thioredoxin	31

1.5.4	PDI.....	32
1.5.5	Extracellular Redox State and Cancer.....	33
	REFERENCES	36
2	QSOX ASSAY DEVELOPMENT AND PURIFICATION OF THE OXIDASE FROM SERUM	51
2.1	Introduction	51
2.2	Experimental Procedures.....	53
2.2.1	Materials and Reagents.....	53
2.2.2	General Methods	55
2.2.3	Sulfhydryl Oxidase Fluorescence Assays	55
2.2.3.1	Homovanillic Acid (HVA) Assay	55
2.2.3.2	Amplex UltraRed (AUR) Assay.....	56
2.2.4	Purification of QSOX1 from Bovine Serum	57
2.2.4.1	Cation Exchange Column (Salt Gradient).....	57
2.2.4.2	Hydrophobic Interaction Column.....	57
2.2.4.3	Cation Exchange Column (Eluting with a pH Gradient).....	58
2.2.4.4	Protein Digestion and Analysis	58
2.3	Results and Discussion	59
2.3.1	AUR Assay Development with Recombinant Human QSOX1 ..	59
2.3.2	Optimization of AUR Assay for Serum	61
2.3.3	Bovine Serum from Animals of Different Ages Show Comparable Sulfhydryl Oxidase Activities.....	67
2.3.4	A Survey of Mammalian Sera	67
2.3.5	Modest QSOX Activity at Low Levels of Monothiol Substrates.....	67
2.3.6	The Activity in Serum is due to Bovine QSOX1	71
2.4	Conclusions	79
	REFERENCES	80

3	VISUALIZATION OF THE THIOL/DISULFIDE REDOX STATE OF THE MAMMALIAN CELL SURFACE USING CONFOCAL MICROSCOPY: METHODS AND APPLICATIONS.....	84
3.1	Introduction	84
3.2	Experimental Procedures.....	87
3.2.1	Materials and Reagents.....	87
3.2.2	Mammalian Cell Culture	88
3.2.3	Chemical Staining	88
3.2.4	Fluorescent Beads Construction	89
3.2.5	Treatment with Macromolecular Crowding Agents.....	89
3.2.6	Surface Dye Internalization.....	90
3.2.7	DTNB Assay	90
3.2.8	Membrane Fraction Collection, Sodium Dodecyl Sulfate Polyacrylamide Gel Electrophoresis (SDS-PAGE).....	91
3.2.9	Microscope Imaging and Image Analysis	91
3.2.10	Platereader Experiments Proving the Effects of PSS or β -ME on Cy3B Dye	92
3.3	Results and Discussion	93
3.3.1	Cell Surface SH/SS and SH/NH ₂ Labeling	93
3.3.2	The Maleimide Dye Staining is Thiol Specific	96
3.3.3	Quantitation Calibration Using Fluorescent Beads	103
3.3.4	Quantitation of SH/SS Ratio for Mammalian Cell Surfaces	103
3.3.5	SH/SS Ratio Depends on the Reductants	108
3.3.6	Quantitation of SH/NH ₂ Ratio for Mammalian Cell Surfaces ..	108
3.3.7	QSOX Activates on Cell Surface SH Oxidation	111
3.3.8	Footprints of Cells on Cover Slides.....	111
3.3.9	Macromolecular Crowding Agents Increase Cell Surface SH Levels	114
3.3.10	PSS Effect is SH Specific.....	120
3.3.11	Further Experiments to Investigate the PSS Effect	126
3.3.12	Surface Thiols Exposed with PSS Can be Internalized by Live Cells.....	131
3.3.13	Investigation of Protein Targets of PSS Effect.....	134
3.4	Conclusion and Discussion.....	136
	REFERENCES	139

4	THE APPLICATION OF THIOL/DISULFIDE AND THIOL/NH ₂ IMAGING TO A MULTICELLULAR ORGANISM AND A DISULFIDE-RICH BIOMATERIAL	143
4.1	General Introduction.....	143
4.2	<i>C. elegans</i> – an Introduction to Relevant Aspects.....	143
4.2.1	General	143
4.2.2	Cuticle Structure.....	146
4.2.3	Moulting	146
4.2.4	Experimental Procedures.....	148
4.2.4.1	Worm Preparation	148
4.2.4.2	Redox Staining of Worms	148
4.2.4.3	Microscope Imaging and Image Analysis	149
4.2.5	Results and Discussion	149
4.2.5.1	Redox Staining in Esophagus and Grinder.....	149
4.2.5.2	Level 1 Worms Show Strong Surface Staining.....	152
4.2.5.3	Redox Staining on Molting Worms.....	153
4.2.5.4	Conclusion.....	153
4.3	Egg Shell Membrane	157
4.3.1	General Introduction.....	157
4.3.2	Experimental Procedures.....	160
4.3.2.1	Preparation of ESM	160
4.3.2.2	Redox Labeling of ESM.....	161
4.3.2.3	Microscope Imaging and Image Analysis	161
4.3.3	Results and Discussion	161
4.3.3.1	Disulfide Staining on Both Sides of Membrane.....	161
4.3.3.2	GnCl and Reductants Disrupt the Thiol Distribution on the Membrane.....	165
4.3.3.3	The Limiting Membrane is Disulfide Rich and Proteinaceous.....	168
4.3.4	Conclusion.....	171
	REFERENCES	172

Appendix

A COPYRIGHTS 174

LIST OF TABLES

Table 1.1 Catalytic activity of QSOXs towards different substrates (Data taken from references in the table).....	25
Table 2.1 Sulphydryl oxidase activity levels toward DTT in bovine, human, and mouse commercial sera.	70
Table 2.2 Purification of sulphydryl oxidase from adult bovine serum.....	74

LIST OF FIGURES

Figure 1.1	The oxidative reaction of oxidative protein folding. Removal of a pair of electrons generates a disulfide linkage.....	2
Figure 1.2	Structure of some disulfide bond-containing proteins. Disulfide bonds are shown as yellow sticks. Codes from the Protein Data Base (PDB) are listed.	3
Figure 1.3	The Dsb system in prokaryotes. Figure modified from Cho and Collet ²⁰	6
Figure 1.4	Oxidative protein folding within the mammalian mitochondrial inter membrane space. The arrows depict the flow of reducing equivalents.....	9
Figure 1.5	Scheme of a PDI-first model of oxidative protein folding.....	12
Figure 1.6	Yeast Protein Disulfide Isomerase (PDI). PDB code: 2B5E. The CxxC motifs in the α and α' domains are depicted in yellow spheres.	13
Figure 1.7	A scheme for QSOX mediated oxidative protein folding. The role of PDI is restricted to that of an isomerase.....	18
Figure 1.8	Domain structure of QSOX proteins. Panel A shows metazoan QSOXs which have two thioredoxin domains (Trx1 and Trx2) followed by a helix-rich region (HRR) and an ERV domain. Panel B shows QSOXs of plants and protists, which lack the Trx2 domain. The redox-active CxxC motifs are shown as single solid yellow lines. The flavin cofactor is shown as hexagons in yellow. The approximate position of signal sequence is shown as the solid red line at left.	20
Figure 1.9	A simplified depiction of the flow of reducing equivalents accompanying disulfide bond formation by a metazoan QSOX.	21
Figure 1.10	Crystal structure of <i>Trypanosoma brucei</i> QSOX. Open (panel A, PDB file:3QCP) and closed (panel B, PDB file:3QD9) conformations are shown. The closed conformation was captured by trapping a mixed-disulfide between CI of the Trx domain and CIII of the ERV domain. The Trx domain is shown in blue, the HRR in grey and the ERV domain in green. CI and CIII are shown as yellow spheres.	22

Figure 1.11	High expression of QSOX1 in epithelial tissues with heavy secretory loads (reprinted from Thorpe & Coppock ⁹¹). Brown staining represents QSOX1 in (A) epidermis; (B) sebaceous gland; (C) hair follicle; (D) seminal vesicle; (E) placenta; (F) eccrine gland.	26
Figure 2.1	Horseradish peroxidase-catalyzed oxidation of homovanillic acid by hydrogen peroxide.	54
Figure 2.2	Amplex Red based assays for QSOX. Panel A shows Amplex Red being converted to the strongly fluorescent resorufin in the presence of horseradish peroxidase and hydrogen peroxide. A proprietary variant of Amplex Red, Amplex Ultra Red (AUR), of undisclosed structure is more stable and was used throughout this work. Panel B shows the scheme of the AUR assay.	54
Figure 2.3	AUR assay with increasing concentrations of recombinant human QSOX1. The inset shows the linearity of initial rates, corrected for the nonenzymatic background oxidation of thiols, as a function of enzyme concentration.	60
Figure 2.4	Thiol-dependent attenuation of the development of fluorescence using AUR, horseradish peroxidase and hydrogen peroxide. The plate-reader was implemented as described in Methods using 10 μ M AUR, 50 nM HRP and the indicated thiol concentrations contributed from DTT, reduced RNase, GSH or cysteine (panels A-D, respectively). A single aliquot of 0.8 μ M H ₂ O ₂ was then added to generate the fluorescent product and the fluorescence was recorded at 1.5 and 2 min and averaged. The observed intensities were subtracted from the signal in the absence of hydrogen peroxide and the data were normalized to 100% for the zero thiol control. The data are the average of 2 independent determinations.	62
Figure 2.5	AUR assay in phosphate buffers with various pH values. At pH 7.5 the assay provides sufficient enzyme activity while maintaining a workably low nonenzymatic rate of metal catalyzed thiol oxidation (indicated by intercepts in the vertical axis).	63
Figure 2.6	EDTA decreases the nonenzymatic background at pH 7.5. The plate-reader method was implemented using 10 μ M AUR, 50 nM HRP and 100 μ M thiols from DTT in phosphate buffers with or without 1 mM EDTA (5 mM EDTA shows a comparable minimizing effect (data not shown).	64

Figure 2.7	Bovine serum albumin-mediated inhibition of the AUR assay using recombinant human QSOX1. The AUR assay was conducted using 1 nM human QSOX1 with the inclusion of 1 or 2 mg/mL of bovine serum albumin and 0.5% Tween 80 as indicated. Detergent largely reversed the apparent inhibition of the AUR assay by serum albumin. ...	65
Figure 2.8	Effect of Tween 80 on AUR assays of adult bovine serum. Panel A shows representative traces from the plate reader. Panel B depicts the initial rates with increasing volumes of added serum.	66
Figure 2.9	Amplex UltraRed assay of bovine serum. Amplex UltraRed assay using 5 μ L of fetal (FBS), newborn (NBS), or adult bovine serum (DBS) in a total assay volume of 150 μ L in phosphate buffer, pH 7.5, containing 1 mM EDTA in the presence of 0.5% Tween 80 (see Experimental Procedures). Control assays without added serum are represented by CON. Two additional controls, lacking either DTT or both DTT and serum, showed no detectable increase in fluorescence over the measurement period (data not shown). The inset presents initial rates normalized to the protein concentration of the serum samples.	68
Figure 2.10	Homovanillic acid assay of bovine serum. Homovanillic acid assay in phosphate buffer, pH 7.5, containing 1 mM EDTA using 5 μ L of fetal (FBS), newborn (NBS), or adult bovine serum (DBS) in a total assay volume of 150 μ L (see Experimental Procedures). The inset provides rates corrected for the protein content of the samples.	69
Figure 2.11	Comparison of the rates of hydrogen peroxide generation by recombinant human QSOX1 in the presence of submillimolar concentrations of glutathione and cysteine. The data were corrected for background nonenzymatic peroxide generation and for the attenuation of fluorescence signal that is observed in the presence of increasing thiol concentration (Figure 2.4). Panel A and B show data for GSH and cysteine, respectively. Panel C shows that reduction of QSOX by monothiols involves capture of the mixed disulfide intermediate formed in Equilibrium (1), with a second molecule of monothiol depicted in Reaction (2).	73

Figure 2.12	Elution of sulfhydryl oxidase activity on the first cation-exchange column and the HIC column. The cation-exchange column (Panel A) was developed with an increasing gradient of NaCl and 5 μ L from each 5 mL fraction were assayed as described in Experimental Procedures. Panel B shows the HIC column. The offset is due to a lag between the flow cell record and the collection of material in the fraction collector.....	75
Figure 2.13	SDS-PAGE of fractions. Panel A shows an SDS-PAGE analysis of fractions from the first cation-exchange (CE) column and HIC. There are two main bands in HIC. The Western blot analysis of pooled HIC fractions with activity using chicken QSOX1 antibody in panel B suggests the band at 63kD is QSOX1. Panel C shows the SDS-PAGE analysis of the purified protein after the second cation-exchange column.	76
Figure 2.14	UV-Vis spectrum of the sulfhydryl oxidase purified from adult bovine serum. The spectrum of the oxidase recorded in 50 mM phosphate buffer, pH 7.5, containing 1 mM EDTA is shown. The dashed line highlights the flavin region of the spectrum.....	77
Figure 2.15	Bovine QSOX1 sequence. The amino acid sequence of the quiescin sulfhydryl oxidase 1 precursor is shown. Peptides identified by MS/MS are underlined, yielding a total coverage of 59% over the 537 residues remaining after cleavage of the signal sequence (shown boxed). The cysteine residues from the two redox-active CxxC motifs are indicated in inverse font.	78
Figure 3.1	Scheme of the reaction between DTNB (5,5'-Dithiobis[2-nitrobenzoic acid]) and a thiolate. P represents a protein. TNB (2-nitro-5-mercaptobenzoic acid) is a yellow compound, $\lambda_{\text{max}}=412$ nm at neutral pH values.	86
Figure 3.2	Structures of the fluorescent reagents used in this work. These sulfonated reagents are membrane impermeant and therefore exclusively label the cell surface and extracellular matrix components.	94
Figure 3.3	Schemes of cell surface labeling. Panel A shows the SH/SS labeling. Single yellow spheres represent free thiols while double yellow spheres represent disulfide bonds. Panel B shows the SH/NH ₂ staining (see Experimental procedures).	95

Figure 3.4	SH/SS redox state of the cell surface of 3 cell lines. The green channel indicates surface thiol staining and the red channel shows the surface disulfide staining. The nuclei are visualized with DAPI (blue). The differential interference contrast (DIC) channel shows the cell outlines at the left of the Figure. The intensities of green and red signals are adjusted here for ease of visualization.	98
Figure 3.5	Cells lacking a functional plasma membrane stain uniformly with sulfo-Cy3B-maleimide. The white arrows show compromised cells that are permeant to fluorescent dyes. The nuclei are visualized with DAPI (blue).	99
Figure 3.6	Inactivated maleimide dyes cannot label cell surface thiols. Panel A shows a schematic depiction of β -mercaptoethanol treated maleimide-dye conjugate. The maleimide dyes were pre-incubated with β -mercaptoethanol in a 1:1 molar ratio. Panel B shows the unmodified maleimide dye leads to clear cell surface staining while the β -mercaptoethanol-treated dyes cannot label the cells. Each laser intensity was maintained constant for comparison between non-treated and β -mercaptoethanol images. Signal intensities are increased uniformly for ease of visualization.....	100
Figure 3.7	Pretreatment with N-ethylmaleimide (NEM) prevents subsequent SH labeling on cell surfaces using either Cy3B or Cy5 maleimides. NEM (1 mM) in DPBS was applied to the fixed cells for 10 min before the maleimide dyes were added. The NEM pretreatment significantly decrease the thiol labeling of the cell surface. Each laser intensity was maintained constant for comparison.....	101
Figure 3.8	DTNB pretreatment ablates cell surface thiol labeling. HeLa cells were treated with DPBS only (control) or DPBS containing 1 mM DTNB for 10 min. Then the Cy3B-maleimide dye was applied to label the cell surface. The green channel shows the Cy3B fluorescence and the DIC channel shows the cell outlines. The laser intensity was maintained constant for comparison.....	102
Figure 3.9	Scheme for double labeling of thiopropyl bead with green and red fluorescent maleimides. Activated thiol Sepharose 4B beads were treated with 10 mM DTT in PBS to expose free thiols (Panel A). The beads were incubated with limiting concentrations of mixture of Cy3B- and Cy5-maleimides (see Experimental procedures). Upon completion, the large excess of unreacted bead -SH groups were alkylated with 10 mM NEM (Panel B). Panel C shows two channels of one bead stained with two maleimides.	105

- Figure 3.10 Fluorescent beads can be used for ratiometric calculations. Panel A, B show proportional fluorescence signals against increasing concentration of Cy3B and Cy5 loaded on the beads, respectively. The x-axis represents the dye concentration of the solution incubating the beads, the y-axis represents the integrated fluorescent signals of 1-3 beads at each concentration. Panel C shows the data of one bead loaded with equal amount of two fluorophores. The integrated fluorescent intensity of each channel is proportional with increasing laser power. Panel D shows the data of another batch of beads. Here beads were loaded with green and red maleimides at the three ratios shown. The fluorescence intensity is proportional to the ratio of dye (n=4 at each concentration ratio)..... 106
- Figure 3.11 Quantitation of SH/SS ratio for mammalian cell surfaces. Panel A shows some representative cells under confocal microscopy. The green channel (with 10-fold higher laser power compared to the red channel) shows the free thiol staining while red channel shows the disulfide staining. Panel B shows the bar graph of SH/SS ratio of each cell lines calculated as before. Images were analyzed using ImageJ. Four representative images of each cell line were selected and 4-6 cell membrane areas of interest were picked in each image using ImageJ selection tools and calculated for fluorescence intensity (see Experimental procedures. U-118, n=20; HeLa, n=20; HEK293T, n=23; J774A.1, n=23)..... 107
- Figure 3.12 SH/SS ratio depends on the reductants. Panel A shows the HeLa cell surface SS/SH ratio with TCEP as the reductant. After labeling the free thiols with Cy3B-maleimide, a variety of concentrations of TCEP were applied to reduce the disulfide on the cell surface (at room temperature for 15 min) and then Cy5-maleimide was used for liberated SH labeling. Two representative images of each cell line were selected and 6 cell membrane areas of interest were picked in each image using ImageJ selection tools and calculated for fluorescence intensity (see Experimental procedures). For each concentration n=12. Panel B shows a comparable experiment using GSH as the reductant (here n=10). 109

- Figure 3.13 Quantitation of SH/NH₂ ratio for mammalian cell surfaces. Panel A shows some representative cells under confocal microscopy. The green channel shows the free thiol staining while the red channel shows the amino group staining. Panel B shows a bar graph of SH/NH₂ ratio for each cell line. Images were analyzed using ImageJ. Three representative images of each cell line were selected and 5 cell membrane areas of interest were picked using ImageJ selection tools and calculated for fluorescence intensity (see Experimental procedures). The errors reflect the following measurements: U-118, n=15; HeLa, n=15; HEK293T, n=15; and J774A.1, n=15..... 110
- Figure 3.14 QSOX catalyzes cell surface SH oxidation. Panel A shows the staining of J774A.1 cells. Cells were incubated in media with or without 20 mM GSH at 37 °C for 20 min. Then 30 nM recombinant human QSOX1, or a DPBS control, was added and the cells were incubated for 40 min. Finally the cells were fixed using 2% PFA and stained with the regular SH/NH₂ procedure. Panel B shows the data, n=4. T-test ** P<0.01. The laser intensity was maintained constant within each cell type for comparison. Signal intensity was increased with the same level to show better view..... 112
- Figure 3.15 Cells leave footprints on coverslips. In these images green represents Cy3B-maleimide staining for thiols while red represents Cy5-NHS ester staining for protein as before. Nuclei are shown by DAPI (blue). Panel A shows the J774A.1 cells. The image focuses on the coverslip surface (coincident with the base of the macrophage cells). J774A.1 macrophage cells remain very tightly bound to the glass coverslip and it is clear that while the base of the cells and the substrate they occlude contain protein NH₂ group (staining red), thiol staining is notably absent within the margins of the cell. Thiol green staining covers the coverslip and is concentrated in the surrounding of certain cells. Panel B shows the stained coverslips that previously supported HeLa cells. Cells were dislodged by chelators before the regular SH/NH₂ staining procedure. 113

- Figure 3.16 Crowding agent utilization. Under traditional 2-D cell culture conditions, the concentrations of extracellular matrix precursors and enzymes are low. The addition of polydispersed macromolecules (presented as spheres with different sizes) leads to a higher effective concentration of ECM precursors and enzymes that are involved in ECM generation, leading to increases in ECM deposition. Panel B shows several standard macromolecular crowding agents. Among these Ficoll is a neutral polysaccharide while CR, DxS and PSS are negatively charged sulfonated polymers. 116
- Figure 3.17 PSS exerts a particular dramatic effect on HeLa cell surface SH staining. The green channel shows the Cy3B-MAL labeled cell surface. The DIC channel shows the cell outlines. The laser intensity was maintained constant for comparison of SH staining. 117
- Figure 3.18 PSS effect on cell surface thiol labeling is found in a range of cell lines. Cells were washed and treated with DPBS (control) or DPBS containing 25 $\mu\text{g}/\text{mL}$ PSS (PSS) for 5 min at room temperature, in the control and PSS column, respectively. For the third column, cells were fixed with 2% PFA first and then treated with 25 $\mu\text{g}/\text{mL}$ of PSS. All the cells were labeled with 1 μM Cy3B-MAL for 10 min at room temperature. Laser power was maintained constant for each cell type. The 12 panels were then uniformly brightened for better visualization of the PSS effects. 118
- Figure 3.19 Low concentration of PSS increases cell surface thiol labeling. J774A.1 cells were fixed first for 15 min with 2% PFA, and then incubated with DPBS containing different concentrations of PSS. After washing the standard SH/ NH_2 staining procedure was applied. Panel A shows the images of cells. The green channel shows the thiol labeling by Cy3B-MAL while the red channel shows the NH_2 labeling by Cy5-NHS ester. The laser intensity was maintained constant for comparison. All images were brightened by the same factor for presentation purposes. Panel B shows the calculation of SH labeling normalized with NH_2 levels. 119
- Figure 3.20 PSS effect involves labeling of cell surface thiols by Cy3B-MAL. J774A.1 cells were treated with or without 20 $\mu\text{g}/\text{mL}$ PSS for 10 min. The PSS treated cells were then incubated with or without 100 μM methyl-PEG₂₄-maleimide. The cells were labeled with the original maleimide dye or with β -mercaptoethanol inactivated dye (Cy3B-MAL-2-ME; see Experimental procedures). The green channel shows the SH labeling and the blue channel shows nuclei (DAPI). 121

- Figure 3.21 PSS effect on cell surface thiol labeling is not a dye-specific effect. J774A.1 cells were stained with 1 μ M Alexa 568-maleimide or 1 μ M Cy5-maleimide after treatment for 10 min with or without 25 μ g/mL PSS in DPBS at room temperature. The green channel shows the Alexa 568 fluorescence. The red channel shows the Cy5 fluorescence. In both cases nuclei are shown by DAPI. The laser intensity of each channel was maintained constant for comparison of the thiol levels for each dye set. 122
- Figure 3.22 PSS effect on cell surface thiol labeling is abolished by pretreatment with DTNB. HEK293T cells were treated with DPBS (control) or DPBS containing 20 μ g/mL PSS for 10 min. The PSS treated cells were then incubated with or without 1 mM DTNB for 10 min. The green channel shows the SH labeling using Cy3B-MAL and the blue channel shows nuclei (Hoechst 33342). 123
- Figure 3.23 PSS effect on cell surface thiol labeling can be reversed by recombinant human QSOX1. J774A.1 cells were fixed with 2% PFA first and incubated with or without 20 μ g/mL PSS for 5 min. After washing with DPBS, the cells were treated for 15 min at 37 $^{\circ}$ C and then 10 min at room temperature with or without 50 nM recombinant human QSOX1. The green channel shows the SH staining with Cy3B-MAL. Nuclei are shown as blue (DAPI). The red channel (Cy5-NHS ester labeling NH_2) is not shown. 124
- Figure 3.24 PSS does not increase the fluorescence signal of Cy3B. A variety of concentrations of Cy3B-MAL were added into a 96-well plate containing DPBS with (close squares) or without (open diamonds) 23 μ g/mL PSS. 125
- Figure 3.25 PSS does not bind Cy5-maleimide dyes. Panel A shows the two PD-10 columns with Cy5-MAL only (left column) and Cy5-MAL with PSS (right column). The numbers on the left hand presents the elution volume. Panel B shows the elution of Cy5-MAL (absorbance at 645 nm in UV-vis). Panel C shows the elution of PSS (absorbance at 255 nm in UV-vis)..... 128

Figure 3.26	The PSS monomeric unit, 4-vinylbenzenesulfonate, does not induce surface labeling. Panel A illustrates the structure of the monomer of PSS. Panel B shows the effect of both compounds on surface thiols of J774A.1 cells. Cells were treated with DPBS containing 25 $\mu\text{g}/\text{mL}$ PSS or 25 $\mu\text{g}/\text{mL}$ monomer for 5 min, followed with the typical thiol staining procedure. The green channel shows the thiols labeled with Cy3B-MAL.	129
Figure 3.27	Polyacrylic acid is unable to mimic the effects of polystyrene sulfonate. Panel A shows the structure of PAA. Panel B shows the effect of PSS and PAA on HeLa surface thiols levels. The green channel shows the thiols labeled with Cy3B-MAL.....	130
Figure 3.28	PSS increased thiol labeling are internalized into cells. J774A.1 cells were treated with DPBS or DPBS containing 20 $\mu\text{g}/\text{mL}$ PSS. Then cells were incubated with 1 μM Cy3B-MAL and 1 μM Cy5-NHS ester for 30 min at 37 $^{\circ}\text{C}$. The blue channel shows the nuclei, the green channel shows the Cy3B-MAL labeled thiols, the red channel shows the Cy5-NHS ester labeled proteins.	132
Figure 3.29	Thiols internalized into cells do not co-localized with lysosomes. J774A.1 cells were first incubated in complete DMEM media with 75 nM of LysoTracker Deep Red for 1 h at 37 $^{\circ}\text{C}$. Then cells were washed and treated with or without 20 $\mu\text{g}/\text{mL}$ PSS for 5 min, and then followed with 1 μM Cy3B-MAL and 1 μM Cy5-NHS ester incubation for 30 min at 37 $^{\circ}\text{C}$. The green channel shows the thiols labeled with Cy3B-MAL, the red channel shows the lysosomes labeled by LysoTracker Deep Red.	133
Figure 3.30	SDS-PAGE shows higher thiol labeling on cell surface but same total protein levels after PSS treatment. Panel A shows the flow of the experiment (see Experimental procedure). Panel B shows the SDS-PAGE results of three cell lines. The left 3 (HEK293T and J774A.1) or 2 (U-118) lanes show the Cy5 fluorescent channel, while the right lanes show the Coomassie channel. M, marker; C, control; P, PSS.	135
Figure 4.1	Schematic Depiction of a male <i>C. elegans</i> nematode. Figure is from Wikipedia.	144
Figure 4.2	Life cycle of <i>C. elegans</i> . Figure is adapted from Clark and Hodgkin ³	145

Figure 4.3	The organization and structure of the <i>C. elegans</i> cuticle. This figure is reprinted from Page ⁶ . Panel A is depicting a cross-section of the adult cuticle with distinct structural layers. Panel B depicts the synthesis of a new cuticle and the associated detachment of the old cuticle.	147
Figure 4.4	Redox staining in esophagus and grinder of adult worms. Panel A and B shows the two representative adult worms, the green channel shows SH staining and the red channel shows SS staining. Panel C shows a 3D reconstruction of a stained esophagus. The white arrows show the cross-like grinder structure at the end of the esophagus.	151
Figure 4.5	Redox staining of two of the level 1 worms. The green channel indicates the SH staining and the red channel shows the SS staining. Nuclei are shown in blue (DAPI). Panel A shows one section of a z-stack imaging of a level 1 worm. Panel B is the 3D reconstruction of the same worm. Panel C shows another worm with the esophagus and grinder (white arrow) stained as green.	152
Figure 4.6	Redox staining on a molting worm. The green channel indicates the SH and the red channel shows the SS. Panel A shows the head part of the worm. Panel B shows the tail of the same worm.	155
Figure 4.7	Redox staining on a molting worm. The red channel shows the SS, nuclei are stained with DAPI (blue). The green channel was not shown here because there is not signals.	156
Figure 4.8	Key components of a bird's egg. The detail is not drawn to scale. The external cuticle layer is largely formed from protein, and may serve as a barrier to microbial attack and water loss. The calcified cell is a composite material consisting of calcium carbonate and small amounts of proteins that form a fibrous network. Outer and inner eggshell membranes are formed largely from protein fibers (see the Text). Not shown in this illustration is the limiting membrane. It lies between the egg white and the inner membrane. Illustration taken from: https://commons.wikimedia.org/wiki/File:Anatomy_of_an_egg_labeled.jpg	158
Figure 4.9	Disulfide staining on both sides of egg shell membrane. The red channel shows the Cy5-maleimide labeling disulfides, the grey channel is the DIC channel. Panel A shows the side facing the egg white. Panel B shows the side facing the egg shell. These two images are with the same magnification.....	163

Figure 4.10	The labeling of ESM by Cy5-maleimide is dependent on pre-reduction of protein disulfides. The ESM was treated with or without 5 mM TCEP and stained with 1 μ M Cy5-maleimide diluted with 10 μ M PEG ₂₄ -maleimide.....	164
Figure 4.11	GnCl and reductant disrupts the structure on ESM. ESM pieces were treated with DPBS, 4 M GnCl, and 4 M GnCl with 10 mM DTT for 14 h with rocking. The treated membranes were reduced by TCEP and stained with Cy5-maleimide.....	166
Figure 4.12	GnCl and reductant disrupts the morphology of the inner layer of the ESM. The green channel shows the SS labeling, the red channel shows the NH ₂ labeling.	167
Figure 4.13	The limiting membrane is a thiol rich structure. The red channel shows the SS labeling of the cross sections of ESM. Panel A shows a typical cross section of ESM, the white arrow shows the limiting membrane. Panel B shows the limiting membrane that is broken (white arrows). Panel C shows a double layer of limiting membrane (white arrow). Panel D shows a magnification of the double layer area. Panel E shows three of the 3D reconstruction of z-stack ESM images.....	170

ABSTRACT

The extracellular SH/SS redox status has been shown to play critical roles in a range of mammalian cell behaviors, including migration, proliferation, cancer invasion, and virus fusion. Quiescin-sulfhydryl oxidase (QSOX), a facile disulfide-generating enzyme discovered in our laboratory, is believed to contribute to extracellular SH/SS status. Although the enzymological properties of QSOX have been studied extensively in our laboratory, its contribution to disulfide bond formation in biological contexts is still cryptic. This dissertation includes two projects that impact extracellular redox state regulation.

In the first part of this work, a simple and sensitive fluorescence-based microplate assay for QSOX activity is described. This assay couples hydrogen peroxide formation generated by sulfhydryl oxidases to the generation of the strong red fluorescence formed during HRP-catalyzed oxidation of Amplex UltraRed and is suitable for testing QSOX activity in small samples of serum, plasma, or other biological fluids. This work shows that murine, bovine, and human sera contain significant levels of sulfhydryl oxidase activity. We also found similar levels of enzymatic activity between fetal and adult bovine sera in contrast to a prior report. A three-step purification protocol using adult bovine serum showed that this activity reflects circulating, soluble QSOX1. Peptide digests and mass spectrometric analysis confirmed that this disulfide-generating activity was indeed due to QSOX1. The presence of a facile oxidase for a wide range of thiol-containing peptides and proteins

in mammalian plasma suggests a new dimension to the study of thiol/disulfide redox biochemistry in blood.

In the second project, novel ratiometric fluorescence imaging methods for surface thiols and disulfides and their applications to studying a range of cellular phenomena were described. Membrane-impermeant fluorescent maleimide reagents were used throughout, and these new methods can visualize and quantitatively assess the status of surface proteins on normal and cancer cells. In addition, a dramatic effect of very low concentrations of polystyrene sulfonate (PSS) on cell surface SH/SS redox status was investigated. This effect is thiol specific, general to different cell types, and reversed, in part, by exogenous QSOX. PSS is also found to increase the endocytosis of exofacial thiols and proteins. Finally, we showed that the new ratiometric methods can be extended to multicellular organisms and biomaterials. These procedures are amenable for future super-resolution studies.

Chapter 1

OXIDATIVE PROTEIN FOLDING AND REDOX REGULATION

1.1 Introduction to Oxidative Protein Folding

Oxidative protein folding, the process that involves generation of disulfide bonds during the attainment of the native fold, is one of the most widely recognized post-translational modifications. After translation from messenger ribonucleic acids (mRNA) by ribosomes, the nascent chains undergo folding with the assistance of molecular chaperones¹. Chemically disulfide bond formation involves a 2-electron oxidation reaction between cysteinyl sulfhydryl groups, see Figure 1.1. In the absence of catalysts the reaction is slow when molecular oxygen is the oxidant². After, or during, this oxidative phase mispaired disulfide bonds are rearranged by disulfide exchange isomerization reactions.

About 25% of eukaryotic proteins are secreted and most of these contain one or more disulfide bonds³. In contrast, most intracellular proteins lack these linkages. A common argument for the selective presence of disulfide bond in extracellular proteins is that these crosslinks reinforce tertiary or quaternary structures⁴. Examples of small proteins that are stabilized by structural disulfide bonds are shown in Figure 1.2. Additionally, some disulfides serve regulatory roles. These “allosteric” disulfide bonds engage in redox reactions acting as switches to control protein functions⁵.

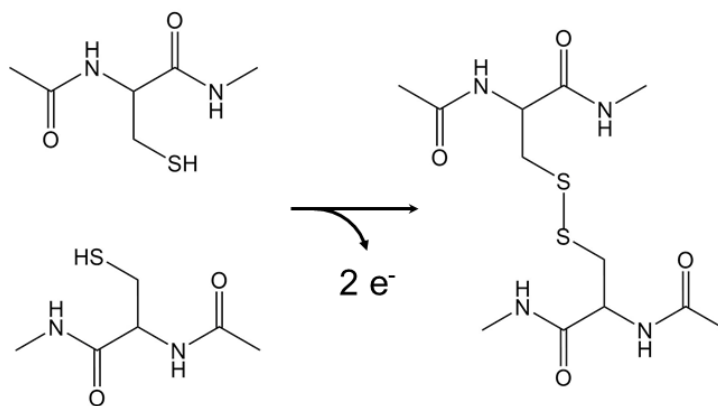


Figure 1.1 **The oxidative reaction of oxidative protein folding.** Removal of a pair of electrons generates a disulfide linkage.

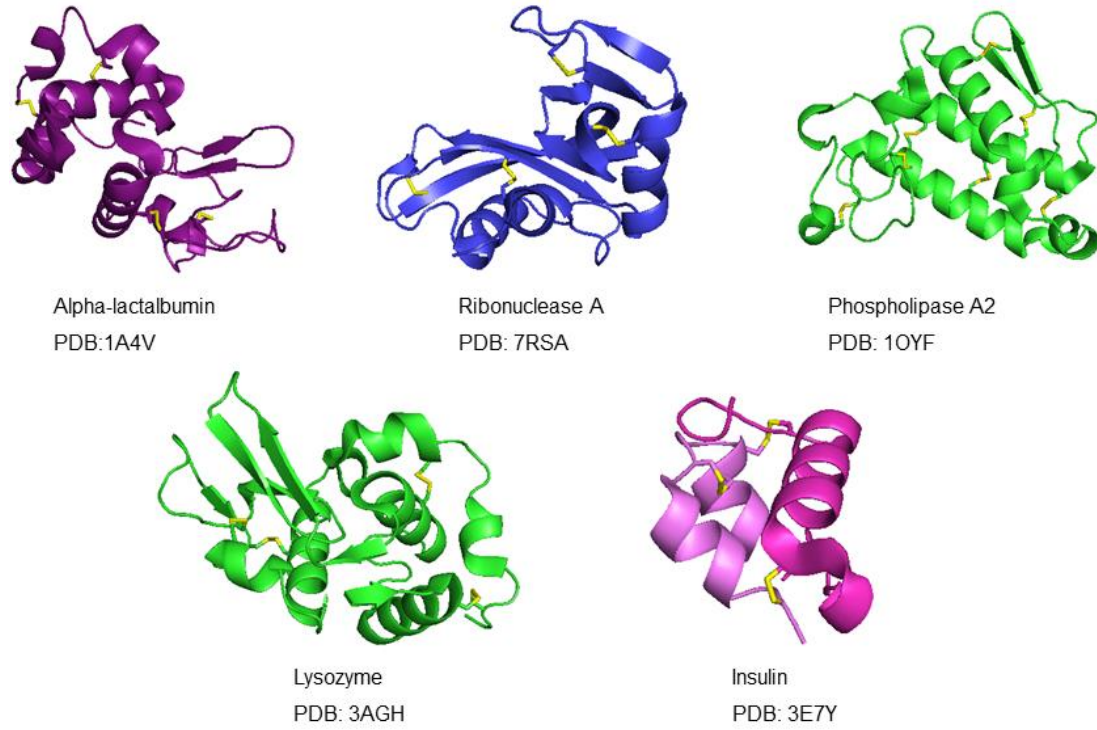


Figure 1.2 **Structure of some disulfide bond-containing proteins.** Disulfide bonds are shown as yellow sticks. Codes from the Protein Data Base (PDB) are listed.

1.2 Oxidative Protein Folding in Prokaryotes

The current understanding of disulfide bond generation in prokaryotes was strongly influenced by research in the Gram-negative bacterium *Escherichia coli*. Here, oxidative protein folding occurs in the periplasmic space, driven by a family of thiol oxidoreductase known as disulfide bond forming (Dsb) proteins⁶. Figure 1.3 shows a simplified scheme of this pathway. The first step involves the generation of disulfide bonds in reduced client proteins by DsbA. This monomeric 21 kDa oxidoreductase has a highly oxidizing redox-active CxxC motif⁷. The reacting reduced DsbA then transfers reducing equivalents through disulfide exchange with the membrane-bound protein DsbB⁸. Under aerobic conditions, DsbB then passes the electrons to ubiquinone. Reducing equivalents are then passed to cytochrome oxidases and finally to molecular oxygen⁹. Under anaerobic conditions, DsbB transfers reducing equivalents to menaquinone and further to anaerobic electron acceptors such as fumarate¹⁰. Both aerobic and anaerobic processes link oxidative folding to the respiratory chain^{6,11}. In those bacteria that lack DsbB, DsbA transfers electrons to bacterial homologs of vitamin K epoxide reductase (VKOR) and further to vitamin K epoxide, the final electron acceptor^{12,13}. Mismatched disulfide bonds introduced by the DsbA/DsbB system are corrected by another periplasmic component, the isomerase DsbC¹⁴. DsbC is a homodimer of ~25 kDa subunits with two redox-active CxxC motifs in two thioredoxin domains and a V shaped peptide binding site¹⁵. This isomerase is maintained in its active, reduced, state by disulfide exchange with DsbD (Figure 1.3)¹⁶. DsbD is a membrane protein (~60 kDa) that spans cytosolic and periplasmic spaces. Thus it receives electron equivalents from reduced cytosolic thioredoxin, which is generated by NADPH in the presence of thioredoxin reductase^{11,14}. The

reducing equivalents now on DsbD are then delivered at the outer plasma membrane surface to DsbC (Figure 1.3).

The oxidative protein folding pathways in Gram-positive bacteria are still cryptic. Ishihara et al.¹⁷ discovered a DsbA homolog, BdbD (Bacillus disulfide bond formation), in *Bacillus brevis*. Currently, ComGC is the only identified substrate of BdbD in *Bacillus brevis*¹⁸. BdbD is re-oxidized by BdbC, a protein that is 40% identical to DsbB sequence¹⁹. Thus, the BdbC/ BdbD system appears to be a clear counterpart of the DsbA/DsbB system in *E. coli*.

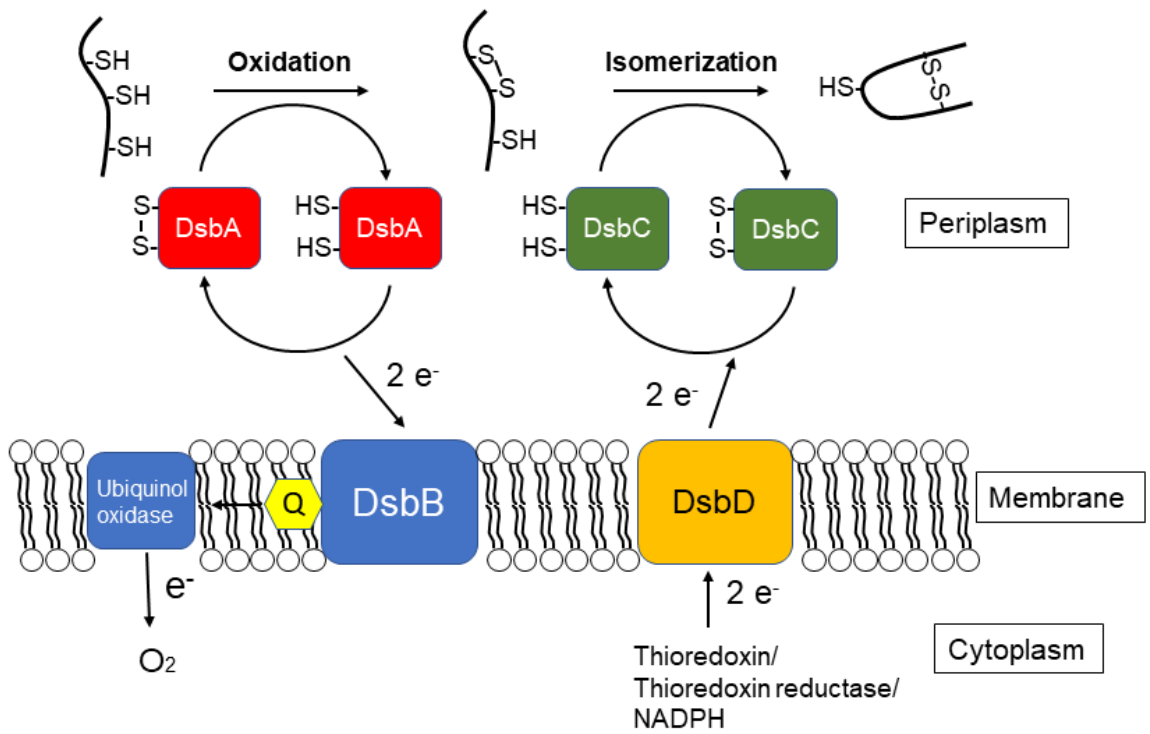


Figure 1.3 **The Dsb system in prokaryotes.** Figure modified from Cho and Collet²⁰.

1.3 Oxidative Protein Folding Systems in Eukaryotes

In Eukaryotes, the redox potential is tightly controlled in a location-specific manner inside cells, and most oxidative protein folding occurs in specialized membrane bounded organelles, such as the mitochondrial inner membrane space (IMS), the endoplasmic reticulum (ER) and the Golgi apparatus. In contrast to the highly reducing environment in the cytoplasm (with a GSH/GSSG ratio $\sim 3300/1$, corresponding to a redox potential of -290 mV)²¹, the ER is comparatively oxidizing (with a GSH/GSSG ratio reported in the $1.5/1$ to $5/1$ range, equivalent to a redox potential of -180 mV)^{22,23}. The mitochondrial IMS is another relatively oxidizing location (with a GSH/GSSG ratio $250/1$ and a redox potential of -256 mV). In addition to these intracellular locations, disulfide bond generation also takes place in the extracellular environment. In the next section, we will discuss the oxidative folding system of the mitochondrial IMS, followed by the disulfide bond generation pathways in the ER and Golgi apparatus. Disulfide bond generation within the extracellular space will be described later.

1.3.1 Mitochondrial IMS

As a eukaryotic organelle, the mitochondrion is believed to be a consequence of the endosymbiosis of an ancient oxygen-metabolizing prokaryote with a primitive eukaryotic cell. While the structure of the mitochondrial IMS seems a functional equivalent of the prokaryotic periplasmic space, the oxidative protein folding machinery in these two compartments are completely different. Figure 1.4 shows a scheme of the human mitochondrial oxidative folding machinery. In the first step,

reduced and unfolded polypeptides in the cytosol pass through the mitochondrial outer membrane via a membrane-bound protein translocase pore. Those peptides are then oxidized by Mia40 in the IMS using a small helix-coil-helix oxidoreductase with a redox active CxC disulfide motif and a binding site for unfolded substrate proteins^{24,25}. Reduced Mia40 transfers reducing equivalents to augment liver regeneration (ALR) via thiol-disulfide exchange reactions^{26,27}.

ALR is a homodimeric flavoenzyme with FAD as the cofactor as well as two disulfides for oxidation reactions²⁶⁻²⁸. While ALR can use molecular oxygen as an electron acceptor, our laboratory found that cytochrome C was a better kinetic substrate *in vitro*^{26,28}. *In vivo*, reduced cytochrome C could deliver electrons to the respiratory chain. In yeast, there is a close homolog of ALR named essential for respiration and viability 1 (ERV1)²⁹, with 29% identity to ALR³⁰. Reduced ERV1 can pass electrons to the fumarate reductase protein (Osm1) so as to regenerate the catalyst.

Research on oxidative protein folding in the mitochondrial IMS has not yet identified a dedicated disulfide isomerase. Several proteomic studies identify protein substrates of the IMS oxidative folding pathway with complicated patterns of disulfide connectivity^{31,32}. Our laboratory has clearly shown that Mia40 is a poor isomerase towards both native and non-cognate substrates²⁷. Hence mispaired IMS disulfide bonds may undergo correction by cycles of reduction using resident reductases followed by reoxidation using Mia40³³⁻³⁵.

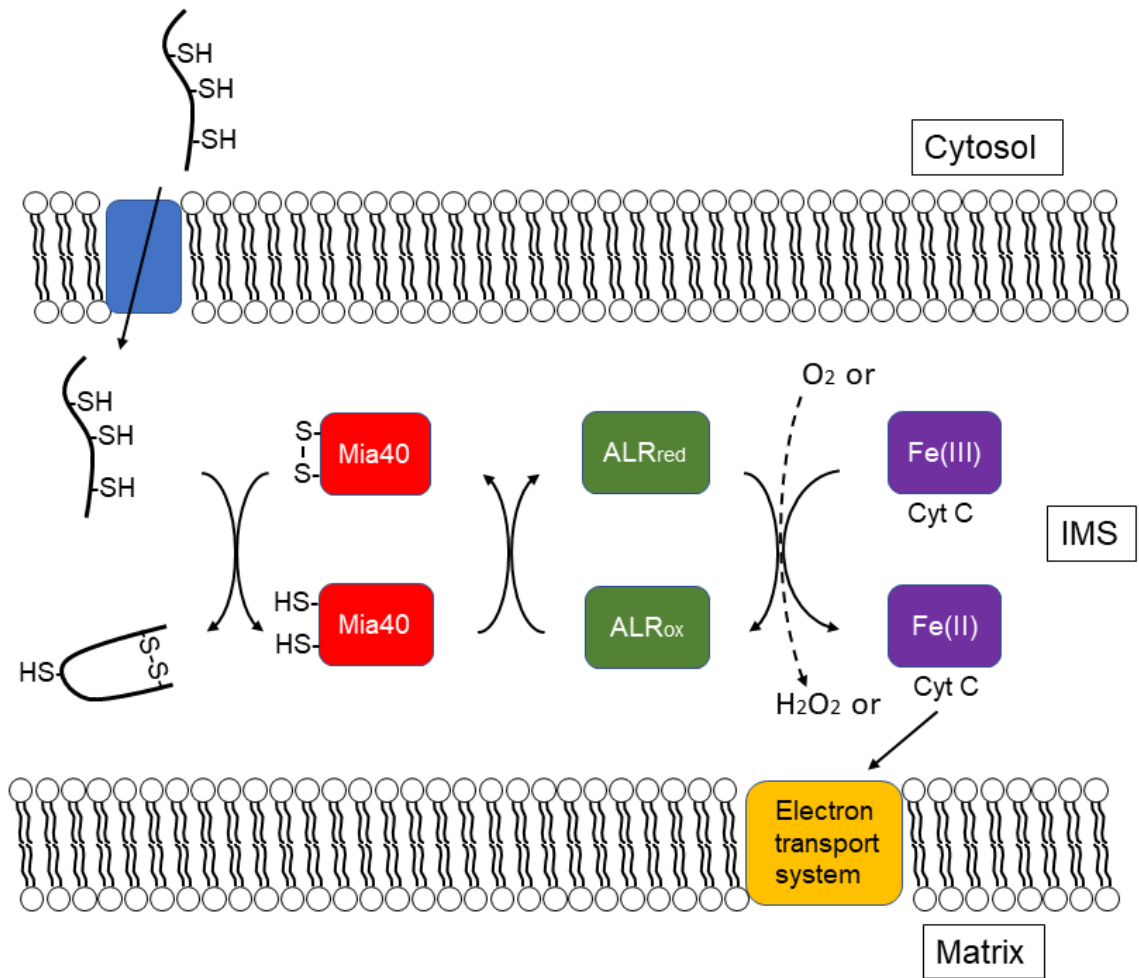


Figure 1.4 **Oxidative protein folding within the mammalian mitochondrial intermembrane space.** The arrows depict the flow of reducing equivalents.

1.3.2 Endoplasmic Reticulum (ER)

Approximately 25% human proteins transit the endoplasmic reticulum (ER) before being secreted, and the ER has been long recognized as the main compartment for oxidative protein folding. Protein disulfide isomerase (PDI) often acts as the immediate oxidant for proteins undergoing oxidative folding in the ER (Figure 1.5). To sustain catalysis reduced PDI must then be reoxidized by secondary oxidants depicted in the Figure. This scheme has been termed the PDI-first model of oxidative folding because PDI intervenes at the initial oxidation step. Figure 1.5 also shows that PDI operates in a second capacity to isomerize any mispaired disulfides introduced in the first step. Here, PDI associates with mispaired proteins and performs multiple rounds of thiol disulfide exchange reaction ultimately leading to the appearance of the native fold. The next section will expand in the PDI-first route to oxidative folding. An alternate pathway involving QSOX will be described later.

1.3.2.1 Protein Disulfide Isomerase (PDI)

Protein disulfide isomerase (PDI) is a 57 kDa multidomain enzyme which belong to the thioredoxin superfamily. Figure 1.6 shows a structure of a yeast PDI; it is a U-shaped protein that contains four consecutive thioredoxin domains: a, b, b', and a' ³⁶. There are catalytically active Cys-Gly-His-Cys motifs on each of a and a' domains. The N-terminal cysteine of the motif is comparatively solvent accessible. In contrast the C-terminal cysteine is buried from solvent towards the core of the protein. There is a putative hydrophobic protein binding site in the b' domain that has affinity for reduced, unfolded protein substrates³⁷. In the PDI-first model of oxidative folding,

PDI oxidizes reduced client peptides and transfers the pair of electrons to other proteins, such as Ero1, peroxiredoxin 4, glutathione peroxidase 7/8, VKOR, dehydroascorbate, H_2O_2 and GSSG^{38,39}.

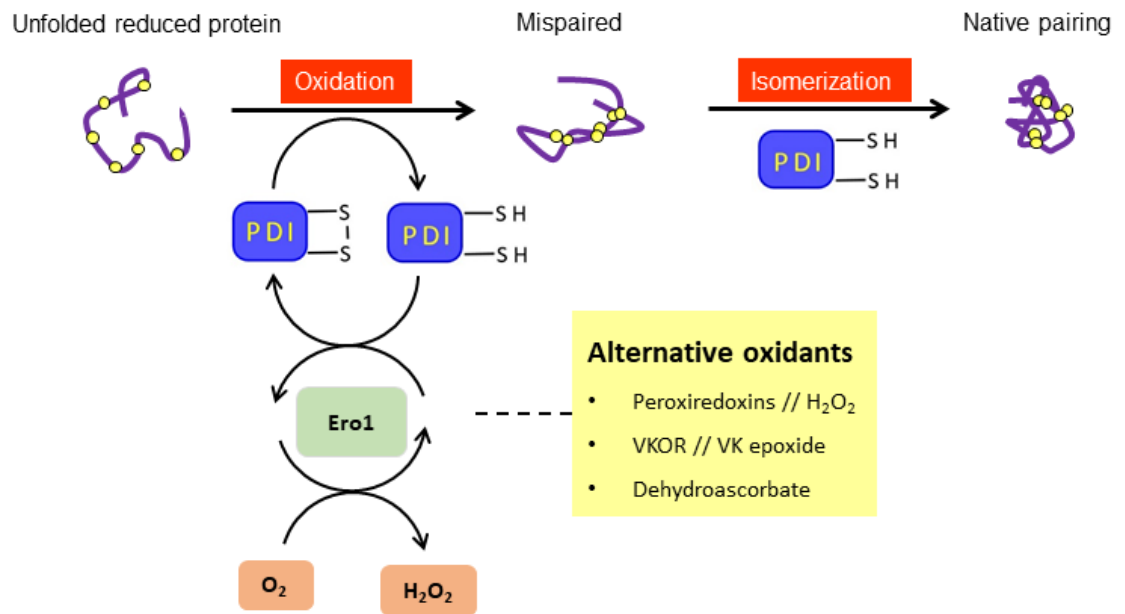


Figure 1.5 Scheme of a PDI-first model of oxidative protein folding.

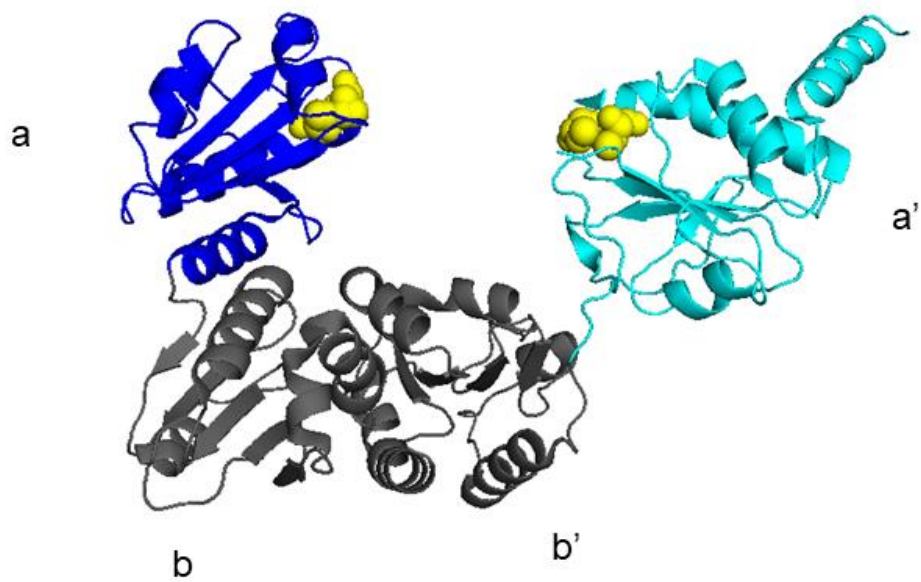


Figure 1.6 **Yeast Protein Disulfide Isomerase (PDI)**. PDB code: 2B5E. The CxxC motifs in the a and a' domains are depicted in yellow spheres.

1.3.2.2 Endoplasmic Reticulum Oxidoreductin 1 (ERO1)

The yeast ERO1p was uncovered independently by two groups in 1998^{40,41}. Two orthologs in mammals, Ero1 α and Ero1 β , were discovered later^{42,43}. ERO1p is a 65 kDa flavin adenine dinucleotide (FAD) bound thiol oxidoreductase that oxidizes PDI with an N-terminal shuttle CxxC disulfide and a C-terminal CxxCxxC motif. Following a series of disulfide exchange reactions the reducing equivalents are passed to the flavin cofactor for the subsequent reduction of molecular oxygen to hydrogen peroxide^{44,45}. ERO1p localizes to the ER, but does not have an ER retention sequence⁴¹; it is tightly associated with ER membrane via interaction with its C-terminal tail⁴⁶.

The PDI-Ero1 oxidative folding pathway was considered as the major pathway for disulfide generation in mammals. However simultaneous knockout of both isoforms of Ero1 (α and β) in mouse only caused a very mild diabetic phenotype⁴⁷. This surprising result stimulated the search for other pathway for the oxidative of PDI within the ER (see later).

1.3.2.3 Erv2p

Erv2p (Essential for respiration and viability in yeast²⁹) is a membrane-bound ER-resident fungal FAD-dependent sulfhydryl oxidase that catalyzes disulfide bond generation in the ER lumen in parallel with ERO1^{48,49}. Overexpression of Erv2p in yeast suppresses the lethality of a complete deletion of Ero1 strain under aerobic conditions⁴⁹. As a dimeric protein, Erv2p has a CxxC motif on each subunit near the flavin ring, and a shuttle disulfide located on the C-terminal flexible loop^{48,49}. Erv2p

receives electrons from reduced PDI using the shuttle disulfide with the ultimate reduction of the flavin and the final reoxidation of the enzyme using molecular oxygen^{48,49}.

1.3.2.4 Peroxiredoxin IV

The ER-resident protein Peroxiredoxin IV (PRDX4) reduces H₂O₂ produced, for example, by the PDI-Ero1 oxidative folding pathway^{50,51}. In this way peroxiredoxin can use the potentially dangerous hydrogen peroxide generated by ER-oxidases to generate a second disulfide bond.

Peroxiredoxin reacts efficiently with hydrogen peroxide because of reaction with cysteine 124 that forms a sulfenate (-S-OH). Subsequent nucleophilic cleavage of the sulfenate by a second cysteine generates an intersubunit disulfide. This new disulfide then can drive further oxidative folding⁵²⁻⁵⁴. Iuchi et al⁵⁵ reported that a PRDX4 knockout mouse was viable and fertile, indicating PRDX4 is not an essential ER enzyme. However, Zito and colleagues⁵² performed RNA interference (RNAi) of PRDX4 in mice embryo fibroblasts cells that also lack Ero1. They found this treatment is lethal, indicating that the two enzymes are partially redundant for oxidative folding.

1.3.2.5 Vitamin K Epoxide Reductase (VKOR)

VKOR is a transmembrane ER resident protein that links dithiol-dependent oxidative protein folding to protein γ -carboxylation^{56,57}. In the VKOR pathway, PDI donates two pairs of electrons to VKOR through disulfide exchange, and electrons are

finally transferred to vitamin K epoxide to form the hydroquinone^{57,58}. This reduced form of vitamin K is an essential cofactor for the γ -glutamyl carboxylase that catalyzes the glutamate carboxylation reactions. Several Vitamin K-dependent proteins, such as blood clotting factors VII, IX and X, are post-translationally modified by γ -glutamyl carboxylase in the ER⁵⁹.

1.3.2.6 L-Ascorbate

L-Ascorbate (or vitamin C) can serve as an antioxidant in the ER. This molecule is oxidized by an unidentified ascorbate oxidase enzyme to generate dehydroascorbate (DHA). DHA may contribute to disulfide bond generation⁶⁰. However, although a variety of thiol compounds, including reduced PDI, can be oxidized by DHA, Saaranen et al⁶¹ reported that the PDI-DHA reaction is kinetically too slow to contribute to oxidative folding in the ER. As an alternative they proposed that DHA is sufficiently rapidly reduced non-enzymatically by GSH.

1.3.3 Disulfide Bond Formation Post ER

After the oxidative protein folding process in the ER, folded proteins are transported to the Golgi apparatus and undergo additional posttranslational modifications and sorting. Mispaired proteins are screened out and returned to the ER via retrograde transport. Correctly folded secreted proteins are transferred through the Golgi apparatus and packaged into vesicles targeted for fusion with the plasma membrane^{62,63}. Some of these proteins become incorporated at the cell surface, others

are secreted into the bulk extracellular matrix space. An important potential catalyst of disulfide bond generation outside the cell is a main focus of our laboratory. In the next sections we will introduce the Quiescin Sulfhydryl Oxidase (QSOX).

1.4 Quiescin Sulfhydryl Oxidase (QSOX)

As previously mentioned, there is another potential oxidative protein folding pathway in the ER. Here, QSOX acts as an immediate oxidant and PDI acts only as an isomerase (Figure 1.7). Notice that these two enzymes work independently because PDI is not a substrate of QSOX²².

1.4.1 History of QSOX

QSOX is a FAD-bound protein that was first purified in our laboratory from chicken egg white by following the yellow color of FAD⁶⁴. The chicken QSOX was later found to be homologous to the human Quiescin Q6 protein which was upregulated when human fibroblasts enter quiescence⁶⁵⁻⁶⁷. Quiescin Q6 was then shown to have sulfhydryl oxidase activity⁶⁷. Two earlier studies about sulfhydryl oxidases from rabbit skin⁶⁸ and bovine milk⁶⁹ were revisited based on the discovery of chicken QSOX. Both enzymes were found to be QSOX family members^{70,71}. Another flavoprotein sulfhydryl oxidase, discovered in seminal vesicles⁷², was also found to be a QSOX family member⁷³. The kinetic mechanism of avian egg white⁷⁴ as well as recombinant human⁷⁵ and *Trypanosoma brucei*⁷⁶ were also investigated. Crystal structures of *Trypanosoma brucei* QSOX1 and mouse QSOX1 were obtained by Alon et al.⁷⁷.

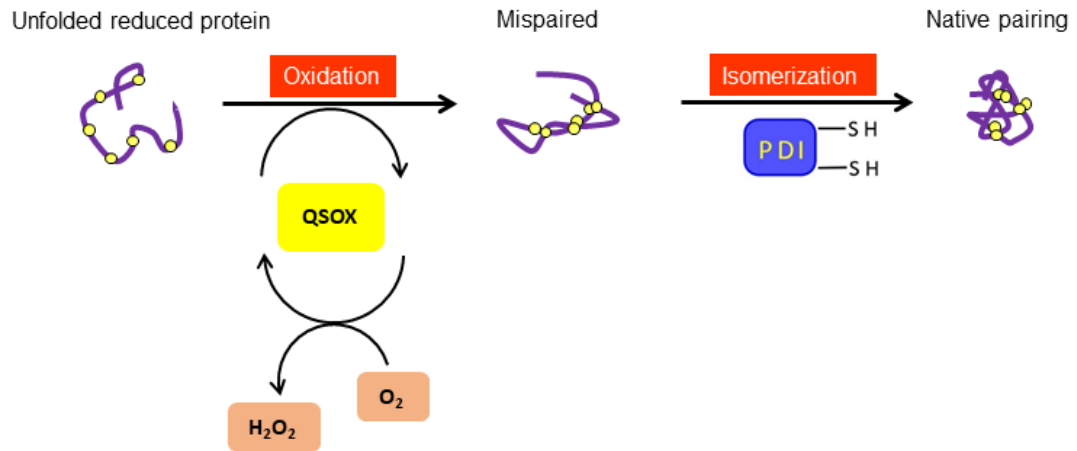


Figure 1.7 **A scheme for QSOX mediated oxidative protein folding.** The role of PDI is restricted to that of an isomerase.

1.4.2 Structure and Catalytic Mechanism of QSOX

QSOX enzymes are multi-domain proteins that represent an ancient fusion of two proteins: thioredoxin and Erv1^{65,78} (Figure 1.8). All QSOXs contain an N-terminal signal sequence that leads the protein through the secretory pathway. In metazoan QSOXs there are four recognizable domains. From the N-terminal the first two domains are PDI-like thioredoxin domains and the first one contains a redox-active CxxC motif (labeled as C_IxxC_{II} in Figure 1.8)⁷⁹. The second thioredoxin domain does not have a redox-active disulfide and its function is still unknown. Plant and protist QSOXs lack the second thioredoxin domain⁷⁸ (Figure 1.8). The third domain is a helix rich region (HRR), which appears to be an Erv/ALR like domain without redox centers⁸⁰. The fourth domain is also an Erv/ALR domain but contains FAD as a non-covalently bound cofactor and a second CxxC motif (labeled as C_{III}xxC_{IV} in Figure 1.8). A third CxxC motif which is catalytically non-essential is in the Erv/ALR domain; its function is still unclear⁷⁵.

QSOXs are present in metazoans and plants, but not in fungi⁸¹. Multicellular organisms contain various QSOX paralogs, e.g. *Drosophila* have four, *Caenorhabditis elegans* have three⁷⁸, and higher metazoans have two QSOX paralogs. *Human* QSOX1 and QSOX2 retain the same domain organization and share 37% overall amino acid sequence identity and 68% identity in their functional structures (that is the thioredoxin and Erv domains)⁸¹. There are two mRNAs encoding human QSOX1. Caused by an alternative splice site on exon 12, the long form, QSOX1a, has 747 amino acids and retains a long C-terminal region with a transmembrane region close to the C-terminus⁸². In contrast, the short form, QSOX1b, contains 604 amino acids and

lacks the transmembrane domain. The QSOX2 gene encodes a 698 amino acid protein⁸³, but this the enzyme remains to be characterized.

The catalytic mechanism of QSOX is schematically shown in Figure 1.9. A thiolate of a protein substrate attacks the first cysteine residue C_I of the first CxxC motif, generating a mixed disulfide^{84,85}. Another thiolate of the substrate resolves the mixed disulfide, leading to a disulfide bond formation in the substrate and releasing the Trx1 in its reduced form^{74,75}. The two electrons are then transferred to the second CxxC motif in the ERV/ALR domain via a mixed disulfide between C_I and C_{III}. This process involves an extensive rotation of the thioredoxin domain and docking with the ERV domain surface^{76,77} (Figure 1.10). This mixed disulfide is resolved, in a rate-limiting step, by C_{II}⁷⁵. The reducing equivalents are then transferred to the flavin ring and finally to molecular oxygen^{75,76}. QSOX lacks a significant binding site for protein substrates and seems to perform a hit-and-run mode of catalysis⁸⁶.

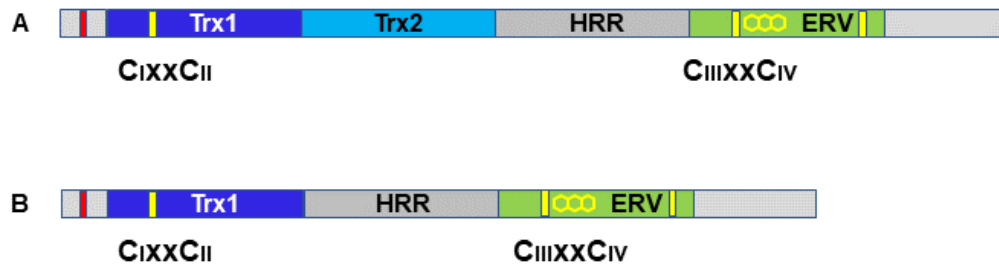


Figure 1.8 **Domain structure of QSOX proteins.** Panel A shows metazoan QSOXs which have two thioredoxin domains (Trx1 and Trx2) followed by a helix-rich region (HRR) and an ERV domain. Panel B shows QSOXs of plants and protists, which lack the Trx2 domain. The redox-active CxxC motifs are shown as single solid yellow lines. The flavin cofactor is shown as hexagons in yellow. The approximate position of signal sequence is shown as the solid red line at left.

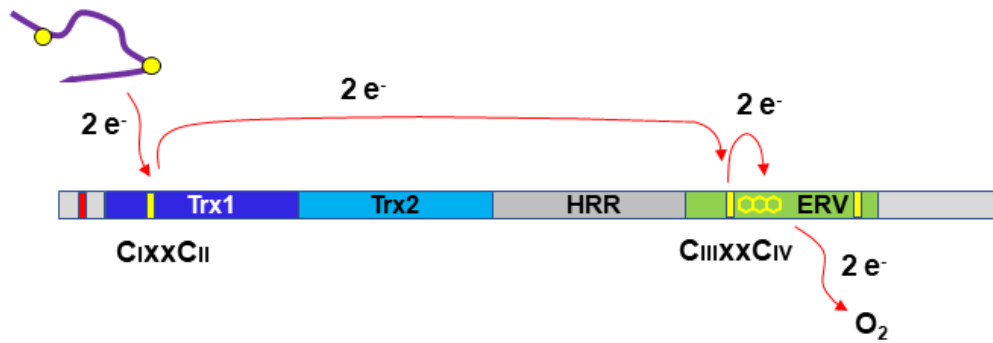


Figure 1.9 A simplified depiction of the flow of reducing equivalents accompanying disulfide bond formation by a metazoan QSOX.

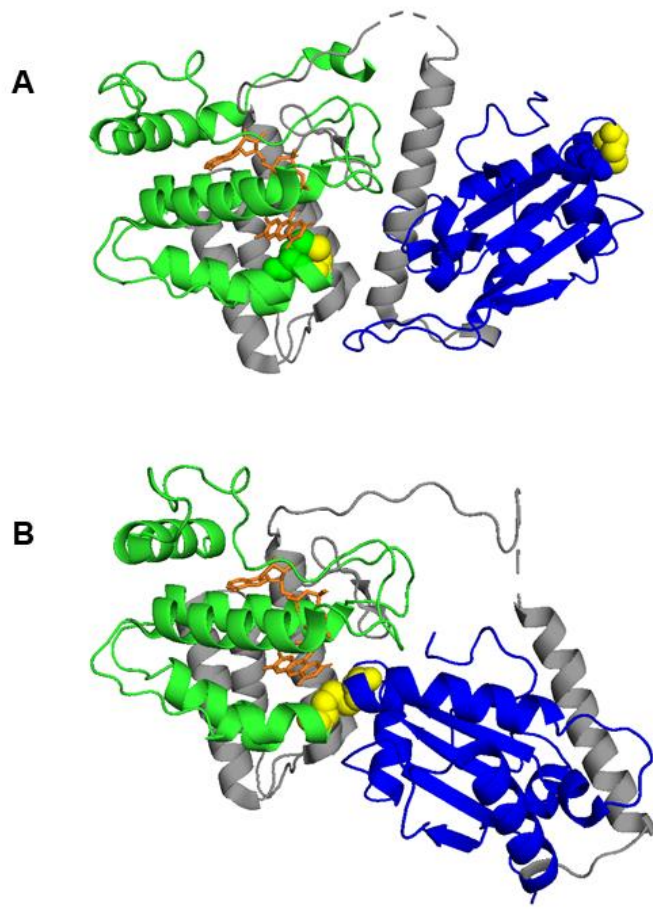


Figure 1.10 **Crystal structure of *Trypanosoma brucei* QSOX.** Open (panel A, PDB file:3QCP) and closed (panel B, PDB file:3QD9) conformations are shown. The closed conformation was captured by trapping a mixed-disulfide between CI of the Trx domain and CIII of the ERV domain. The Trx domain is shown in blue, the HRR in grey and the ERV domain in green. CI and CIII are shown as yellow spheres.

1.4.3 Substrates of QSOX

The in vitro enzymological properties of QSOX have been studied extensively in our laboratory. The kinetic parameters of QSOX with different substrates are shown in Table 1.1. QSOX is the most proficient catalyst for disulfide bond generation known to date⁸⁴. The k_{cat} entries are largely dependent on the rate of inter-domain electron transfer, the rate-limiting step, thus these values are comparable between various substrates⁷⁹. K_m values, however, show a dominant role in catalytic efficiency and substrate discrimination. Monothiols (e.g. β -mercaptoethanol, cysteine, and GSH) are relatively poor substrates of QSOX, while dithiols such as DTT shows catalytic efficiencies similar to that of reduced, unfolded, proteins like RNase⁷⁵. QSOX strongly favors unfolded protein substrates and cannot generate disulfide from cysteine residues in folded proteins⁸⁶.

1.4.4 Intracellular and Extracellular Distribution of QSOX

As mentioned in the previous section, an N-terminal signal sequence of QSOX leads this enzyme through the secretory pathway. Intracellularly, QSOX1 has been found in the ER^{87,88} and Golgi^{87,89,90}. Cytochemical studies have shown that QSOX expression is particularly high in epithelial tissues with heavy secretory loads, see Figure 1.11⁹¹. For this reason we proposed that QSOX serves as an oxidant in oxidative protein folding pathways as shown in Figure 1.7.

QSOX has also been identified at the cell surface⁹² and in the extracellular environment, e.g. including seminal vesicle fluids^{72,73}, chicken egg white⁶⁴, mammalian cell secretions⁷⁹, bovine serum^{93,94} and milk⁷¹. It has been suggested that

QSOX1 plays important roles in modulating the extracellular matrix⁷⁸. Katchman et al.⁹⁵ proposed that extracellular QSOX1 can activate matrix metalloproteinases (MMP-2 and MMP-9) during pancreatic and breast cancer invasion. Ilani et al.⁸⁸ found that QSOX1 plays efficient roles in extracellular matrix formation and modulation, including the incorporation of laminin into the matrix.

Table 1.1 Catalytic activity of QSOXs towards different substrates (Data taken from references in the table).

	Substrate	kcat (min⁻¹)	Km (mM)	kcat/Km (M⁻¹s⁻¹)	Reference
Avian QSOX	Cysteine	1275	10.9	1.95 x 10 ³	64
	β-Mercaptoethanol	1215	54	3.75 x 10 ²	
	Glutathione	1385	20	1.15 x 10 ³	
	Dithiothreitol	1033	0.15	1.15 x 10 ⁵	
	N-acetyl-EAQCGTS	1420	1.72	1.4 x 10 ⁴	96
	Aldolase	200	0.16	2.1 x 10 ⁴	
	Insulin chain A	1000	0.215	7.8 x 10 ⁴	
	Insulin Chain B	700	0.3	3.9 x 10 ⁴	
	Lysozyme	860	0.11	1.3 x 10 ⁵	
	RfBP	1100	0.23	8.0 x 10 ⁴	
	RNase	610	0.115	8.8 x 10 ⁴	
	Pyruvate kinase	475	1.25	6.3 x 10 ³	
	Ovalbumin	565	0.33	2.9 x 10 ⁴	
	PDI	-	-	<10 ²	
<i>Trypanosoma brucei</i> QSOX	Glutathione	-	>50	1.35 x 10 ²	76
	Dithiothreitol	1350	0.086	2.6 x 10 ⁵	
	Trypanothione	480	3.23	2.5 x 10 ³	
	RNase	660	0.36	3.0 x 10 ⁴	
	RfBP	420	0.3	2.25 x 10 ⁴	
Bovine QSOX	Glutathione	880	4.9	3.0 x 10 ³	71
	Dithiothreitol	940	0.086	1.83 x 10 ⁵	
	RNase	670	0.060	1.87 x 10 ⁵	
Human QSOX	Glutathione	740	0.10	1.0 x 10 ³	75
	Dithiothreitol	620	12.4	1.0 x 10 ⁵	
	RNase	2160	0.32	1.1 x 10 ⁵	

Turnover numbers are expressed in terms of disulfides generated per minute. Proteins with disulfide were first reduced before the kinetic measurements. Dashes represent undetectable rates.

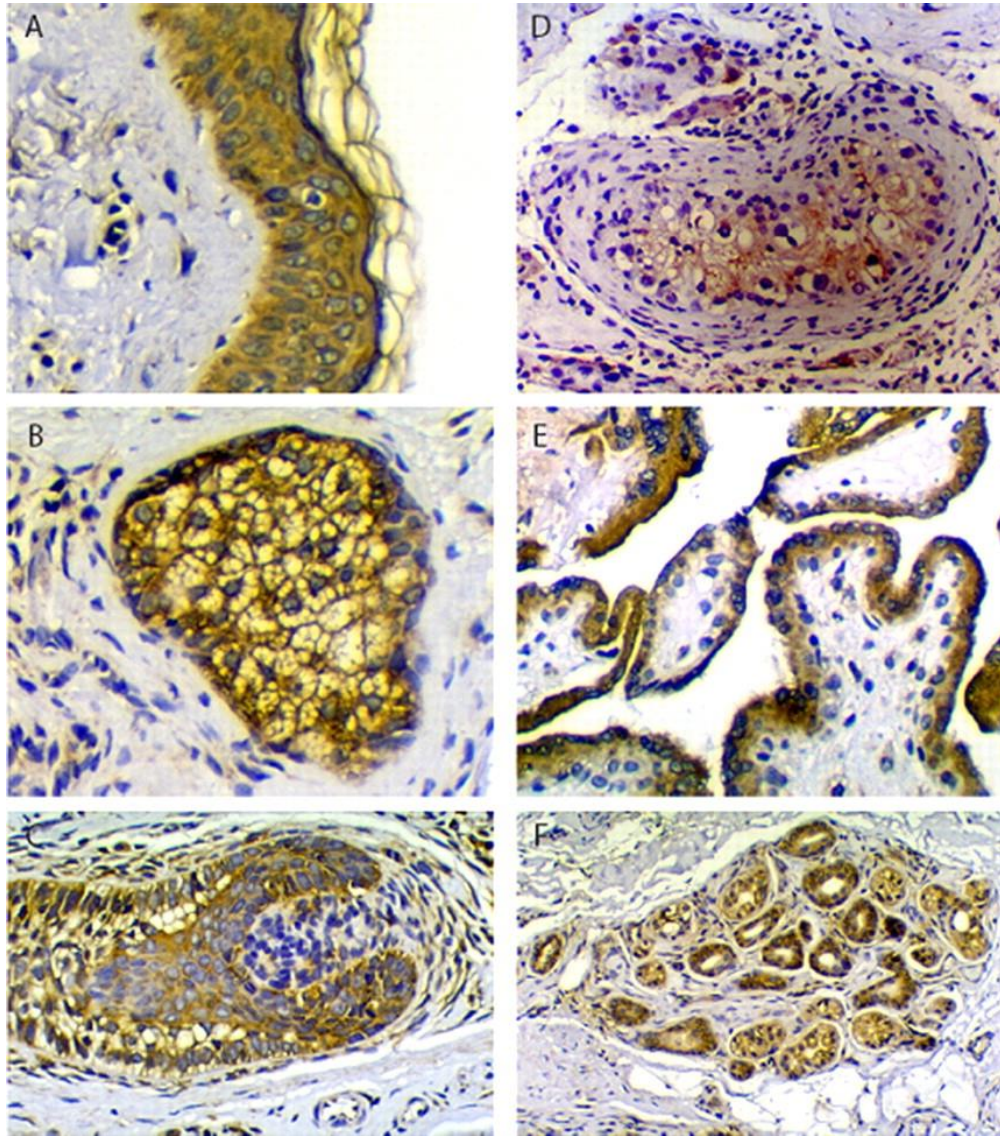


Figure 1.11 **High expression of QSOX1 in epithelial tissues with heavy secretory loads** (reprinted from Thorpe & Coppock⁹¹). Brown staining represents QSOX1 in (A) epidermis; (B) sebaceous gland; (C) hair follicle; (D) seminal vesicle; (E) placenta; (F) eccrine gland.

1.4.5 QSOX and Diseases

In humans, QSOX1 expression has been found to be significantly upregulated in prostate^{97,98}, pancreas^{95,99} and breast^{100,101} cancers. For instance, Song *et al.* reported that mRNA level of QSOX1 are significantly upregulated at early stages of prostate tumorigenesis⁹⁷. Lake et al. identified a C-terminal QSOX1 peptide in plasma that he could use as a biomarker for pancreatic ductal carcinoma⁹⁹. The same group also showed that QSOX1 is involved in post-translational modifications in metalloproteinases that facilitate pancreatic tumor cell invasion⁹⁵. Katchman et al. found that QSOX1 expression is associated with a highly invasive phenotype and correlates with a poor prognosis in Luminal B breast cancer¹⁰⁰. Depressing QSOX1 levels with RNAi or inhibiting its activity using an inhibitory antibody leads to a significant decline of invasiveness in cell migration assays^{88,95,100,102}. It should be noted that the findings of this study have been challenged by several groups¹⁰³⁻¹⁰⁵; they have indicated that QSOX1 expression may be negatively correlated with cell growth. For other diseases, Mebazaa and colleagues identified QSOX1 peptide in plasma as a biomarker for acute decompensated heart failure that significantly increases the diagnostic accuracy for this condition¹⁰⁶. Julian et al. found a 3-fold increase of QSOX1 expression in patients with acute mountain sickness¹⁰⁷.

The mechanisms for QSOX expression regulation in diseases have been studied. Several studies suggested that QSOX1 in human MCF-7 breast cancer cells¹⁰⁸, MDA-MB-231 breast cancer cells¹⁰⁹, and rat pituitary glands⁸⁷ is regulated by estrogen. Also, autophagy, a pro-oncogenic process during the late stages of tumor growth, has been suggested to be linked with QSOX1 expression in MCF-7 breast cancer cells¹¹⁰. Another regulatory mechanism for QSOX1 expression was demonstrated by Shi et al. They showed that QSOX1 was significantly upregulated

during hypoxia in pancreatic tumor cells¹¹¹. In this study, hypoxia-inducible factor 1 alpha (HIF-1 α) overexpression correlates with a 7-fold QSOX1 upregulation, and the QSOX1 gene sequence contains two hypoxia response elements (HREs). It has been well established that during carcinogenesis, hypoxia is one limitation slowing metastasis of cancer cells¹¹². Hypoxia also correlates with acute heart failure due to shortness of breath¹⁰⁶ and acute mountain sickness due to the low oxygen concentrations at high altitudes¹⁰⁷. Since oxygen is a co-substrate for thiol oxidation by QSOX1, a response to hypoxia might include elevated levels of the oxidase.

1.5 Extracellular Redox Regulation

The secretion of a potent thiol-oxidizing catalyst would be expected to modulate the thiol/disulfide poise of the extracellular matrix. While the extracellular environment is widely regarded as oxidizing, cells also can secrete significant levels of small molecular weight thiols and reduced proteins. In the next sections we discuss some of these additional components that may impact the extracellular redox status.

1.5.1 Glutathione/glutathione Disulfide Couple

As mentioned before, the extracellular glutathione/glutathione disulfide (GSH/GSSG) couple reflects very small concentrations in the plasma (e.g. $\sim 3 \mu\text{M}$ of GSH and $\sim 0.1 \mu\text{M}$ of GSSG). There are minimal compared to aggregate intracellular levels of glutathione (10 mM)¹¹³. In healthy adult individual plasma the redox potential of the GSH/GSSG is about -137 mV. Oxidizing GSH/GSSG ratios are correlated with disease states, smoking and aging¹¹⁴. One function of GSH involves

protecting cells from oxidative damage via reducing peroxides. Brown et al.¹¹⁵ showed that decreased glutathione availability results in rat alveolar macrophage dysfunction and decreased viability via oxidative stress. Glutathione precursors reversed this effect¹¹⁵. GSH/GSSG ratios can also indicate unusual cell conditions such as oxidative stress or cell death¹¹⁶. Adams and colleagues¹¹⁷ reported that rats with oxidative stress show a 17-fold increase in plasma GSSG concentration but almost unchanged GSH level. GSH/GSSG levels function as regulators of the cell signaling pathways via the reversible glutathionylation of proteins¹¹⁸. For example, extracellular GSH binds specific receptors in brain and stimulates signal cascades in astrocytes¹¹⁹.

Intracellularly synthesized GSH is exported to the extracellular environment by multidrug-resistance-associated protein (MRP) and organic anion-transporting polypeptide (OATP) families of membrane proteins¹²⁰. Substantial decrease of plasma GSH levels by inhibition of intracellular GSH synthesis suggests the intimate relationship between intracellular and extracellular GSH regulation and the importance of GSH transport¹¹⁸. Extracellular GSH can undergo several fates¹¹⁸. One is to be cleaved by γ -glutamyltransferase and subsequently dipeptidase to glutamate, cysteine and glycine, thus providing a systemic source of Cys and keeping a low level of plasma GSH. γ -glutamyltransferase deficiency has been shown to lead to high circulating levels of GSH and to severe behavioral problems¹²¹. A second fate of GSH is as a reducing agent to reduce H_2O_2 and lipid hydroperoxides in a reaction catalyzed by glutathione peroxidase (GPx-3) found in extracellular body fluids¹²². A third way is for GSH to be oxidized to GSSG nonenzymatically in a reaction mediated by metal ions. S-glutathionylation of proteins represents another mode by which GSH can be

consumed. Finally, GSH can also be oxidized by disulfide exchange with cystine (CySS) to yield CySSG¹¹⁸.

1.5.2 Cysteine/cystine Couple

The cysteine/cystine (Cys/CySS) couple is the most abundant small-molecule redox-active species in plasma¹²³, where CySS is about 50 μM while Cys is between 8 to 10 μM . The extracellular Cys/CySS pair plays significant roles in cell behaviors, such as adhesion¹²⁴ and proliferation¹²⁵⁻¹²⁷ through cell signaling. For instance, Go and Jones¹²⁴ have reported that a more oxidizing Cys/CySS redox state causes an increase of cell-cell adhesion molecule expression in endothelial cells by stimulating the production of H_2O_2 , which activates the NF- κB signaling pathway. Ramirez et al.¹²⁵ demonstrated that a more oxidizing Cys/CySS redox state triggers the intracellular protein kinase C signaling pathway that stimulate extracellular fibronectin production in fibroblasts and facilitates cell proliferation. However, Nkabyo and colleagues¹²⁶ showed that in the case of Caco-2 intestinal cell line, a more reducing Cys/CySS redox state favors cell proliferation via activation of the p44/p42 MAPK pathway, suggesting that the effect of redox state is cell line specific.

The physiological Cys/CySS redox potential in healthy human plasma is approximately -80 mV ¹¹³, and a higher potential (more oxidizing) is usually correlated with various malignancies, such as aging^{114,128}, cardiovascular disease¹²⁹, and cirrhosis¹³⁰. Studies of animal models also showed that the plasma Cys/CySS potential was significantly oxidized in overweight animals while GSH/GSSG potential did not change¹³¹. Interestingly, a more oxidizing Cys/CySS potential can also occur

with diets without any sulfur-containing amino acids, with decreased Cys level but constant CySS levels¹³².

There is no known dedicated CySS reductase, and the reduction of extracellular CySS is assumed to be achieved by GSH or via reduced thioredoxin^{118,133,134}. Some cells express an x_c^- antiporter system that imports CySS into cells with concomitant export of glutamate. Internalized CySS is then converted to Cys in the reducing environment of cytosol^{133,135,136}. Cys can undergo oxidation to CySS or be transported between the intracellular and extracellular environment via transporters like alanine-serine-cysteine (ASC) transporter¹³⁷ and system L (LAT2)¹¹⁸. Those cells that lack x_c^- antiporter system, such as T cells, are dependent on Cys supply from antigen-presenting cells, such as dendritic cells¹³⁸. With these transport systems, the extracellular Cys/CySS potential can be regulated. Yan et al.¹³⁹ demonstrated that elevated cystine consumption and cysteine release by dendritic cells lead to a significant drop in the extracellular Cys/CySS potential, and this reductive remodeling is conducive for T cell proliferation as well as a shift of membrane thiols to a more reducing status. In spite of the close interrelation between Cys and glutathione biosynthesis, the Cys/CySS and GSH/GSSG redox couple appear to function independently^{123,127,140}.

1.5.3 Thioredoxin

Although intracellular thioredoxin (Trx) is considered a critical protein disulfide reductant and a key regulator in cell proliferation and survival¹⁴¹, extracellular Trx has been found to be secreted by a variety of normal and transformed cells such as fibroblasts, airway epithelial cells, and activated B and T

lymphocytes even though it lacks a canonical secretion-signal sequence and does not follow the classical ER-Golgi route¹⁴². Although in healthy individuals the extracellular Trx is in the low nanomolar range, it is released from cells in response to oxidative stress-related signals and considered as a biomarker for diseases^{143,144}. For example, Nakamura et al.¹⁴⁵ reported that thioredoxin protects endothelial F-2 cell injury caused by activated neutrophils or hydrogen peroxide. Schwertassek and colleagues¹⁴⁶ showed that Trx1 catalytically interacts with CD30, a cytokine receptor of activated lymphocytes involved in the regulation of inflammation. Trx was also found to be involved in HIV infection. Studies have shown that Trx-mediated disulfide cleavage of domain 2 of CD4 is essential for HIV entry into T cells^{147,148}. Moreover, extracellular Trx has been found to be involved in proliferation¹⁴⁹⁻¹⁵¹, migration¹⁴⁴ and cell membrane channel function¹⁵² of different cell types. Although intracellular Trx regeneration involving thioredoxin reductase (TR) and NADPH has been well studied^{153,154}, it is still unknown how Trx is regenerated in the extracellular environment. TR is generally located in the cytoplasm, but an extracellular TR1 form was found to be secreted from multiple blood cell lines and fresh human blood plasma¹⁵⁵. The exact function of TR1 and how it might reduce Trx in the absence of NADPH is still unclear.

1.5.4 PDI

PDI was long considered an intracellular protein localized exclusively in the endoplasmic reticulum until it was found to be expressed on the cell surfaces of platelets by Essex et al.^{156,157}. Later it was also found on the surface of lymphocytes¹⁵⁸ together with cancer cells such as fibrosarcoma cells¹⁵⁹ and glioblastoma¹⁶⁰. The role

of extracellular PDI on platelet thrombus formation and fibrin generation has been extensively studied. A significant decrease of thrombus formation was observed after inhibition¹⁶¹⁻¹⁶³ or knockout¹⁶⁴ of platelet surface PDI, and an exogenous addition of PDI to blood can recover this formation¹⁶⁴. The mechanism of PDI effect on thrombus formation was demonstrated to be reduction of disulfide bonds in β -integrins^{164,165}. Other PDI family members such as ERp57¹⁶⁶⁻¹⁶⁸ and ERp5¹⁶⁹ are also involved in the process of thrombus formation. Moreover, PDI has been also found to be involved in virus fusion. Barbouche et al.¹⁵⁸ reported that extracellular PDI is responsible for cell recognition and fusion of the HIV virus by mediating the reduction of two disulfide bonds of the glycoprotein gp120 on the virus. Wan et al.¹⁷⁰ found that endothelial cell surface PDI activates β 1 and β 3 integrins and facilitates dengue virus infection. The retention of PDI on the cell surface has been shown to be regulated by binding of galectin-9 that subsequently alters the redox status of T cell membranes¹⁷¹.

1.5.5 Extracellular Redox State and Cancer

Alterations of small-molecule thiols or redox-modulated proteins in the extracellular environment may lead to disturbances of the extracellular redox state and to impacts on cancer progression¹⁷².

Chaiswing et al.¹⁷³ demonstrated that GSH/GSSG ratios in the culture media of highly aggressive prostate cancer cells were higher than those in immortalized prostate epithelial cells. The same group also found that highly aggressive PC3 prostate cancer cells show higher extracellular GSH/GSSG ratios compared with those in less aggressive LNCaP prostate cancer cells¹⁷⁴. These results suggest that in prostate cancer cells, a more-reducing state is correlated with more-aggressive phenotypes. The

enhanced extracellular GSH level might be in response of hypoxia and to the high glycolysis level in tumor growth¹⁷⁵.

As a resource for GSH synthesis, extracellular CySS is often required for cancer growth, and starvation of extracellular CySS uptake has been demonstrated as potential therapeutic strategies for breast carcinoma¹⁷⁶, leukemia¹⁷⁷, prostate cancer cells¹⁷⁸, pancreatic cancer cells¹⁷⁹, and triple-negative breast cancer cells¹⁸⁰. The decrease of CySS uptake results in depletion of intracellular GSH, leading to cancer growth arrest. Interestingly, the Chaiswing group¹⁷² reported that oxidized CyS/CySS enhanced prostate cancer cell growth, whereas reduced CyS/CySS increased prostate cancer cell invasion. However, the CyS/CySS ratio didn't affect normal prostate epithelial cell growth or altered invasion behavior. Thus the CyS/CySS modulation of cell growth might be cell type or cancer specific.

The downregulation of GPx-3 in cancer cells might be another mechanism to allow extracellular GSH to increase. Downregulation of GPx-3 expression has been reported in renal cell carcinoma¹⁸¹, thyroid cancer¹⁸², colorectal cancer¹⁸³, and prostate cancer¹⁸⁴. Moreover, the activity of this enzyme was also found to be reduced in blood of individuals with different cancers¹⁸⁵. Since GPx-3 can scavenge H₂O₂ with GSH as the reducing agent, it has been considered as a tumor-suppressor protein. Yu et al.¹⁸⁴ demonstrated that overexpression of GPx-3 in prostate cancer cell lines can suppress tumor growth and metastasis both *in vitro* and *in vivo*. Thus restoration of Gpx3 protein level in tumor cells might be a treatment of cancers.

Thioredoxin has been detected in serum of patients with hepatocellular carcinoma, and these levels decreased significantly after surgical removal of the tumor¹⁸⁶. This study suggests that thioredoxin is released directly from cancer tissues.

In leukemia cells thioredoxin was found to perform significant mitogenic activity but only in a reduced extracellular environment¹⁴⁹. Elevated secretion of thioredoxin in cancer cells might be due to its function in maintaining an appropriate extracellular redox state. Reduced extracellular thioredoxin could stimulate the activity of growth factors for cancer and protect cancer cells from oxidative stress accompanying chemotherapy. Trx1 has been considered to be a biomarker for cancers, and inhibitors against Trx1 have been used in clinic¹⁸⁷. However, administration of recombinant Trx1 did not promote tumor growth nor affect chemosensitivity in a xenotransplantation model, suggesting the safety of thioredoxin as an anti-inflammatory therapy for cancer patients¹⁸⁸.

Highly reducing extracellular tumor microenvironments favors electron flux from reductants to oxygen leading to superoxide generation¹⁸⁹. Reduced metal ions such as Fe^{2+} or Cu^+ are well-known reducing agents for oxygen. Cysteinyl-glycine is a potent reductant for Fe^{3+} and Cu^{2+} , and is synthesized from extracellular GSH via γ -glutamyltransferase^{190,191}. Thus, the elevated activity of γ -glutamyltransferase and the expression of GSH export transporters in cancer cells contributes to a more reducing environment for tumors with the extracellular consumption of oxygen.

In summary much needs to be learnt concerning the interplay between the many redox-active species in the extracellular environment. It appears that different cell types and stages of cancer progression may show different redox profiles and may show differing sensitivities to pharmaceutical intervention with redox-based strategies.

REFERENCES

- 1 Mamathambika, B. S. & Bardwell, J. C. Disulfide-Linked Protein Folding Pathways. *Annual Review of Cell and Developmental Biology* **24**, 211-235, doi:10.1146/annurev.cellbio.24.110707.175333 (2008).
- 2 Munday, R., Munday, C. M. & Winterbourn, C. C. Inhibition of copper-catalyzed cysteine oxidation by nanomolar concentrations of iron salts. *Free Radical Biology and Medicine* **36**, 757-764, doi:10.1016/j.freeradbiomed.2003.12.015 (2004).
- 3 Voet, D. & Voet, J. G. *Biochemistry*. (J. Wiley & Sons, 2004).
- 4 Thornton, J. M. Disulfide bridges in globular proteins. *Journal of Molecular Biology* **151**, 261-287 (1981).
- 5 Schmidt, B., Ho, L. & Hogg, P. J. Allosteric Disulfide Bonds [†]. *Biochemistry* **45**, 7429-7433, doi:10.1021/bi0603064 (2006).
- 6 Inaba, K. & Ito, K. Structure and mechanisms of the DsbB-DsbA disulfide bond generation machine. *Biochimica et Biophysica Acta - Molecular Cell Research* **1783**, 520-529, doi:10.1016/j.bbamcr.2007.11.006 (2008).
- 7 Bardwell, J. C., McGovern, K. & Beckwith, J. Identification of a protein required for disulfide bond formation in vivo. *Cell* **67**, 581-589, doi:0092-8674(91)90532-4 [pii] (1991).
- 8 Regeimbal, J. & Bardwell, J. C. A. DsbB catalyzes disulfide bond formation de novo. *Journal of Biological Chemistry* **277**, 32706-32713, doi:10.1074/jbc.M205433200 (2002).
- 9 Bader, M., Muse, W., Ballou, D. P., Gassner, C. & Bardwell, J. C. A. Oxidative protein folding is driven by the electron transport system. *Cell* **98**, 217-227, doi:10.1016/S0092-8674(00)81016-8 (1999).
- 10 Takahashi, Y. H., Inaba, K. & Ito, K. Characterization of the menaquinone-dependent disulfide bond formation pathway of Escherichia coli. *Journal of Biological Chemistry* **279**, 47057-47065, doi:10.1074/jbc.M407153200 (2004).
- 11 Tan, J. T. & Bardwell, J. C. A. Key players involved in bacterial disulfide-bond formation. *ChemBioChem* **5**, 1479-1487, doi:10.1002/cbic.200400036 (2004).
- 12 Dutton, R. J., Boyd, D., Berkmen, M. & Beckwith, J. Bacterial species exhibit diversity in their mechanisms and capacity for protein disulfide bond formation. *Proceedings of the National Academy of Sciences of the United States of America* **105**, 11933-11938, doi:10.1073/pnas.0804621105 (2008).
- 13 Li, W. *et al.* Structure of a bacterial homologue of vitamin K epoxide reductase. *Nature* **463**, 507-512, doi:10.1038/nature08720 (2010).
- 14 Rietsch, A., Bessette, P., Georgiou, G. & Beckwith, J. Reduction of the periplasmic disulfide bond isomerase, DsbC, occurs by passage of electrons

- from cytoplasmic thioredoxin. *Journal of Bacteriology* **179**, 6602-6608, doi:10.1128/jb.179.21.6602-6608.1997 (1997).
- 15 McCarthy, A. A. *et al.* Crystal structure of the protein disulfide bond isomerase, DsbC, from *Escherichia coli*. *Nature structural biology* **7**, 196-199, doi:10.1038/73295 (2000).
- 16 Katzen, F. & Beckwith, J. Transmembrane electron transfer by the membrane protein DsbD occurs via a disulfide bond cascade. *Cell* **103**, 769-779, doi:10.1016/S0092-8674(00)00180-X (2000).
- 17 Ishihara, T. *et al.* Cloning and characterization of the gene for a protein thiol-disulfide oxidoreductase in *Bacillus brevis*. *J Bacteriol* **177**, 745-749 (1995).
- 18 Meima, R. *et al.* The bdbDC operon of *Bacillus subtilis* encodes thiol-disulfide oxidoreductases required for competence development. *Journal of Biological Chemistry* **277**, 6994-7001, doi:10.1074/jbc.M111380200 (2002).
- 19 Depuydt, M., Messens, J. & Collet, J.-F. How Proteins Form Disulfide Bonds. *Antioxidants & Redox Signaling* **15**, 49-66, doi:10.1089/ars.2010.3575 (2011).
- 20 Cho, S.-H. & Collet, J.-F. Many roles of the bacterial envelope reducing pathways. *Antioxidants & redox signaling* **18**, 1690-1698, doi:10.1089/ars.2012.4962 (2013).
- 21 Hu, J., Dong, L. & Outten, C. E. The redox environment in the mitochondrial intermembrane space is maintained separately from the cytosol and matrix. *Journal of Biological Chemistry* **283**, 29126-29134, doi:10.1074/jbc.M803028200 (2008).
- 22 Rancy, P. C. & Thorpe, C. Oxidative protein folding in vitro: A study of the cooperation between quiescin-sulfhydryl oxidase and protein disulfide isomerase. *Biochemistry* **47**, 12047-12056, doi:10.1021/bi801604x (2008).
- 23 Dixon, B. M., Heath, S.-H. D., Kim, R., Suh, J. H. & Hagen, T. M. Assessment of Endoplasmic Reticulum Glutathione Redox Status Is Confounded by Extensive *Ex Vivo* Oxidation. *Antioxidants & Redox Signaling* **10**, 963-972, doi:10.1089/ars.2007.1869 (2008).
- 24 Banci, L. *et al.* MIA40 is an oxidoreductase that catalyzes oxidative protein folding in mitochondria. *Nature Structural and Molecular Biology* **16**, 198-206, doi:10.1038/nsmb.1553 (2009).
- 25 Sideris, D. P. *et al.* A novel intermembrane space-targeting signal docks cysteines onto Mia40 during mitochondrial oxidative folding. *Journal of Cell Biology* **187**, 1007-1022, doi:10.1083/jcb.200905134 (2009).
- 26 Daithankar, V. N., Wang, W., Trujillo, J. R. & Thorpe, C. Flavin-linked Erv-family sulfhydryl oxidases release superoxide anion during catalytic turnover. *Biochemistry* **51**, 265-272, doi:10.1021/bi201672h (2012).
- 27 Hudson, D. A. & Thorpe, C. Mia40 is a facile oxidant of unfolded reduced proteins but shows minimal isomerase activity. *Archives of Biochemistry and Biophysics* **579**, 1-7, doi:10.1016/j.abb.2015.05.005 (2015).

- 28 Farrell, S. R. & Thorpe, C. Augmenter of Liver Regeneration : A Flavin-
Dependent Sulphydryl Oxidase with Cytochrome c Reductase Activity †. 1532-
1541 (2005).
- 29 Lisowsky, T. Dual function of a new nuclear gene for oxidative
phosphorylation and vegetative growth in yeast. *Molecular & general genetics*
: *MGG* **232**, 58-64, doi:10.1007/BF00299137 (1992).
- 30 Stein, G. & Lisowsky, T. Functional comparison of the yeast scERV1 and
scERV2 genes. *Yeast* **14**, 171-180, doi:10.1002/(SICI)1097-
0061(19980130)14:2<171::AID-YEA209>3.0.CO;2-U (1998).
- 31 Nuebel, E., Manganas, P. & Tokatlidis, K. Orphan proteins of unknown
function in the mitochondrial intermembrane space proteome: New pathways
and metabolic cross-talk. *Biochimica et Biophysica Acta - Molecular Cell*
Research **1863**, 2613-2623, doi:10.1016/j.bbamcr.2016.07.004 (2016).
- 32 Hung, V. *et al.* Proteomic Mapping of the Human Mitochondrial
Intermembrane Space in Live Cells via Ratiometric APEX Tagging. *Molecular*
Cell **55**, 332-341, doi:10.1016/j.molcel.2014.06.003 (2014).
- 33 Vögtle, F.-N. *et al.* Intermembrane Space Proteome of Yeast Mitochondria.
Molecular & Cellular Proteomics **11**, 1840-1852,
doi:10.1074/mcp.M112.021105 (2012).
- 34 Kojer, K. & Riemer, J. Balancing oxidative protein folding: The influences of
reducing pathways on disulfide bond formation. *Biochimica et biophysica acta*
1844, 1383-1390, doi:10.1016/j.bbapap.2014.02.004 (2014).
- 35 Cardenas-Rodriguez, M. & Tokatlidis, K. Cytosolic redox components
regulate protein homeostasis via additional localisation in the mitochondrial
intermembrane space. *FEBS Letters* **591**, 2661-2670, doi:10.1002/1873-
3468.12766 (2017).
- 36 Tian, G., Xiang, S., Noiva, R., Lennarz, W. J. & Schindelin, H. The crystal
structure of yeast protein disulfide isomerase suggests cooperativity between
its active sites. *Cell* **124**, 61-73, doi:10.1016/j.cell.2005.10.044 (2006).
- 37 Klappa, P., Ruddock, L. W., Darby, N. J. & Freedman, R. B. The b' domain
provides the principal peptide-binding site of protein disulfide isomerase but
all domains contribute to binding of misfolded proteins. *EMBO Journal* **17**,
927-935, doi:10.1093/emboj/17.4.927 (1998).
- 38 Hudson, D. A., Gannon, S. A. & Thorpe, C. Oxidative protein folding: From
thiol-disulfide exchange reactions to the redox poise of the endoplasmic
reticulum. *Free Radical Biology and Medicine* **80**, 171-182,
doi:10.1016/j.freeradbiomed.2014.07.037 (2015).
- 39 Hatahet, F. & Ruddock, L. W. Protein disulfide isomerase: a critical evaluation
of its function in disulfide bond formation. *Antioxid Redox Signal* **11**, 2807-
2850, doi:10.1089/ars.2009.2466 (2009).
- 40 Pollard, M. G. *et al.* Ero1p: a novel and ubiquitous protein with an essential
role in oxidative protein folding in the endoplasmic reticulum. *Molecular cell*
1, 171-182, doi:10.1016/S1097-2765(00)80018-0 (1998).

- 41 Frand, A. R. & Kaiser, C. A. The ERO1 gene of yeast is required for oxidation of protein dithiols in the endoplasmic reticulum. *Molecular Cell* **1**, 161-170, doi:10.1016/S1097-2765(00)80017-9 (1998).
- 42 Pagani, M. *et al.* Endoplasmic reticulum oxidoreductin 1-L β (ERO1-L β), a human gene induced in the course of the unfolded protein response. *Journal of Biological Chemistry* **275**, 23685-23692, doi:10.1074/jbc.M003061200 (2000).
- 43 Mezghrani, A. *et al.* Manipulation of oxidative protein folding and PDI redox state in mammalian cells. *The EMBO journal* **20**, 6288-6296, doi:10.1093/emboj/20.22.6288 (2001).
- 44 Frand, A. R. & Kaiser, C. A. Ero1p oxidizes protein disulfide isomerase in a pathway for disulfide bond formation in the endoplasmic reticulum. *Molecular Cell* **4**, 469-477, doi:10.1016/S1097-2765(00)80198-7 (1999).
- 45 Sevier, C. S. & Kaiser, C. a. Ero1 and redox homeostasis in the endoplasmic reticulum. *Biochimica et biophysica acta* **1783**, 549-556, doi:10.1016/j.bbamcr.2007.12.011 (2008).
- 46 Pagani, M., Pilati, S., Bertoli, G., Valsasina, B. & Sitia, R. The C-terminal domain of yeast Ero1p mediates membrane localization and is essential for function. *FEBS Letters* **508**, 117-120, doi:10.1016/S0014-5793(01)03034-4 (2001).
- 47 Zito, E., Chin, K. T., Blais, J., Harding, H. P. & Ron, D. ERO1- β , a pancreas-specific disulfide oxidase, promotes insulin biogenesis and glucose homeostasis. *Journal of Cell Biology* **188**, 821-832, doi:10.1083/jcb.200911086 (2010).
- 48 Gerber, J., Mühlenhoff, U., Hofhaus, G., Lill, R. & Lisowsky, T. Yeast Erv2p Is the First Microsomal FAD-linked Sulfhydryl Oxidase of the Erv1p/Alrp Protein Family. *Journal of Biological Chemistry* **276**, 23486-23491, doi:10.1074/jbc.M100134200 (2001).
- 49 Sevier, C. S., Cuozzo, J. W., Vala, A., Åslund, F. & Kaiser, C. A. A flavoprotein oxidase defines a new endoplasmic reticulum pathway for biosynthetic disulphide bond formation. *Nature Cell Biology* **3**, 874-882, doi:10.1038/ncb1001-874 (2001).
- 50 Tavender, T. J. & Bulleid, N. J. Peroxiredoxin IV protects cells from oxidative stress by removing H₂O₂ produced during disulphide formation. *Journal of Cell Science* **123**, 2672-2679, doi:10.1242/jcs.067843 (2010).
- 51 Ramming, T. & Appenzeller-Herzog, C. Destroy and exploit: Catalyzed removal of hydroperoxides from the endoplasmic reticulum. *International Journal of Cell Biology* **2013**, doi:10.1155/2013/180906 (2013).
- 52 Zito, E. *et al.* Oxidative Protein Folding by an Endoplasmic Reticulum-Localized Peroxiredoxin. *Molecular Cell* **40**, 787-797, doi:10.1016/j.molcel.2010.11.010 (2010).
- 53 Zito, E. PRDX4, an Endoplasmic Reticulum-Localized Peroxiredoxin at the Crossroads Between Enzymatic Oxidative Protein Folding and Nonenzymatic

- Protein Oxidation. *Antioxidants & Redox Signaling* **18**, 1666-1674, doi:10.1089/ars.2012.4966 (2013).
- 54 Hall, A., Karplus, P. A. & Poole, L. B. Typical 2-Cys peroxiredoxins - Structures, mechanisms and functions. *FEBS Journal* **276**, 2469-2477, doi:10.1111/j.1742-4658.2009.06985.x (2009).
- 55 Iuchi, Y. *et al.* Peroxiredoxin 4 knockout results in elevated spermatogenic cell death via oxidative stress. *Biochemical Journal* **419**, 149-158, doi:10.1042/BJ20081526 (2009).
- 56 Wang, Y. *et al.* Vitamin K Epoxide Reductase : A Protein Involved in Angiogenesis Vitamin K Epoxide Reductase : A Protein Involved in Angiogenesis. **3**, 317-323 (2005).
- 57 Wajih, N., Hutson, S. M. & Wallin, R. Disulfide-dependent protein folding is linked to operation of the vitamin K cycle in the endoplasmic reticulum: A protein disulfide isomerase-VKORC1 redox enzyme complex appears to be responsible for vitamin K1 2,3-epoxide reduction. *Journal of Biological Chemistry* **282**, 2626-2635, doi:10.1074/jbc.M608954200 (2007).
- 58 Berkner, K. L. Vitamin K-Dependent Carboxylation. *Vitamins and Hormones* **78**, 131-156, doi:10.1016/S0083-6729(07)00007-6 (2008).
- 59 Furie, B., Bouchard, B. A. & Furie, B. C. Vitamin K-Dependent Biosynthesis of γ -Carboxyglutamic Acid. *Blood* **93**, 1798 LP - 1808 (1999).
- 60 Szarka, A. & Lőrincz, T. The role of ascorbate in protein folding. *Protoplasma* **251**, 489-497, doi:10.1007/s00709-013-0560-5 (2013).
- 61 Saaranen, M. J., Karala, A.-R., Lappi, A.-K. & Ruddock, L. W. The role of dehydroascorbate in disulfide bond formation. *Antioxidants & redox signaling* **12**, 15-25, doi:10.1089/ars.2009.2674 (2010).
- 62 Glick, B. S. & Nakano, A. Membrane Traffic Within the Golgi Apparatus. *Annual Review of Cell and Developmental Biology* **25**, 113-132, doi:10.1146/annurev.cellbio.24.110707.175421 (2009).
- 63 Teasdale, R. D. & Jackson, M. R. Signal-mediated sorting of membrane proteins between the endoplasmic reticulum and the golgi apparatus. *Annu. Rev. Cell Dev. Biol.* **12**, 27-54, doi:10.1146/annurev.cellbio.12.1.27 (1996).
- 64 Hooper, K. L., Joneja, B., White, H. B. & Thorpe, C. A sulfhydryl oxidase from chicken egg white. *Journal of Biological Chemistry* **271**, 30510-30516, doi:10.1074/jbc.271.48.30510 (1996).
- 65 Coppock, D. L., Cina-Poppe, D. & Gilleran, S. The quiescin Q6 gene (QSCN6) is a fusion of two ancient gene families: thioredoxin and ERV1. *Genomics* **54**, 460-468, doi:10.1006/geno.1998.5605 (1998).
- 66 Coppock, D. L., Kopman, C., Scandalis, S. & Gilleran, S. Preferential gene expression in quiescent human lung fibroblasts. *Cell growth & differentiation : the molecular biology journal of the American Association for Cancer Research* **4**, 483-493 (1993).
- 67 Hooper, K. L., Glynn, N. M., Burnside, J., Coppock, D. L. & Thorpe, C. Homology between egg white sulfhydryl oxidase and quiescin Q6 defines a

- new class of flavin-linked sulfhydryl oxidases. *J Biol Chem* **274**, 31759-31762 (1999).
- 68 Rony, H. R., Schieff, G. J., Cohen, D. M. & Rennagel, W. R. Sulfhydryl oxidase activity in skin homogenates. *The Journal of investigative dermatology* **30**, 43-50 (1958).
- 69 Janolino, V. G. & Swaisgood, H. E. Isolation and characterization of sulfhydryl oxidase from bovine milk. *J Biol Chem* **250**, 2532-2538 (1975).
- 70 Brohawn, S. G. *et al.* Avian Sulfhydryl Oxidase Is Not a Metalloenzyme : Adventitious Binding of Divalent Metal Ions to the Enzyme †. 11074-11082 (2003).
- 71 Jaje, J. *et al.* A flavin-dependent sulfhydryl oxidase in bovine milk. *Biochemistry* **46**, 13031-13040, doi:10.1021/bi7016975 (2007).
- 72 Ostrowski, M. C. & Kistler, W. S. Properties of a flavoprotein sulfhydryl oxidase from rat seminal vesicle secretion. *Biochemistry* **19**, 2639-2645 (1980).
- 73 Benayoun, B., Esnard-Feve, A., Castella, S., Courty, Y. & Esnard, F. Rat seminal vesicle FAD-dependent sulfhydryl oxidase. Biochemical characterization and molecular cloning of a member of the new sulfhydryl oxidase/quiescin Q6 gene family. *J Biol Chem* **276**, 13830-13837, doi:10.1074/jbc.M010933200 (2001).
- 74 Hooper, K. L. & Thorpe, C. Egg white sulfhydryl oxidase: kinetic mechanism of the catalysis of disulfide bond formation. *Biochemistry* **38**, 3211-3217, doi:10.1021/bi9820816 (1999).
- 75 Heckler, E. J., Alon, A., Fass, D. & Thorpe, C. Human quiescin-sulfhydryl oxidase, QSOX1: Probing internal redox steps by mutagenesis. *Biochemistry* **47**, 4955-4963, doi:10.1021/bi702522q (2008).
- 76 Kodali, V. K. & Thorpe, C. Quiescin sulfhydryl oxidase from trypanosoma brucei: Catalytic activity and mechanism of a QSOX family member with a single thioredoxin domain. *Biochemistry* **49**, 2075-2085, doi:10.1021/bi902222s (2010).
- 77 Alon, A. *et al.* The dynamic disulphide relay of quiescin sulphhydryl oxidase. *Nature* **488**, 414-418, doi:10.1038/nature11267 (2012).
- 78 Coppock, D. L. & Thorpe, C. Multidomain flavin-dependent sulfhydryl oxidases. *Antioxidants & redox signaling* **8**, 300-311, doi:10.1089/ars.2006.8.300 (2006).
- 79 Kodali, V. K. & Thorpe, C. Oxidative protein folding and the Quiescin-sulfhydryl oxidase family of flavoproteins. *Antioxidants & redox signaling* **13**, 1217-1230, doi:10.1089/ars.2010.3098 (2010).
- 80 Alon, A., Heckler, E. J., Thorpe, C. & Fass, D. QSOX contains a pseudo-dimer of functional and degenerate sulfhydryl oxidase domains. *FEBS letters* **584**, 1521-1525, doi:10.1016/j.febslet.2010.03.001 (2010).
- 81 Thorpe, C. *et al.* Sulfhydryl oxidases: emerging catalysts of protein disulfide bond formation in eukaryotes. **405**, 1-12 (2002).

- 82 Radom, J. *et al.* Identification and expression of a new splicing variant of FAD-sulfhydryl oxidase in adult rat brain. *Biochimica et biophysica acta* **1759**, 225-233, doi:10.1016/j.bbaexp.2006.04.008 (2006).
- 83 Wittke, I. *et al.* Neuroblastoma-Derived Sulfhydryl Oxidase , a New Member of the Sulfhydryl Oxidase / Quiescin6 Family , Regulates Sensitization to Interferon γ -Induced Cell Death in Human Neuroblastoma Cells Neuroblastoma-Derived Sulfhydryl Oxidase , a New Member of the (2003).
- 84 Heckler, E. J., Rancy, P. C., Kodali, V. K. & Thorpe, C. Generating disulfides with the Quiescin-sulfhydryl oxidases. *Biochimica et biophysica acta* **1783**, 567-577, doi:10.1016/j.bbamcr.2007.10.002 (2008).
- 85 Raje, S. & Thorpe, C. Inter-domain redox communication in flavoenzymes of the quiescin/sulfhydryl oxidase family: role of a thioredoxin domain in disulfide bond formation. *Biochemistry* **42**, 4560-4568, doi:10.1021/bi030003z (2003).
- 86 Coddling, J. a., Israel, B. a. & Thorpe, C. Protein substrate discrimination in the quiescin sulfhydryl oxidase (QSOX) family. *Biochemistry* **51**, 4226-4235, doi:10.1021/bi300394w (2012).
- 87 Tury, A. *et al.* QSOX sulfhydryl oxidase in rat adenohypophysis: localization and regulation by estrogens. *The Journal of endocrinology* **183**, 353-363, doi:10.1677/joe.1.05842 (2004).
- 88 Ilani, T. *et al.* A secreted disulfide catalyst controls extracellular matrix composition and function. *Science (New York, N.Y.)* **341**, 74-76, doi:10.1126/science.1238279 (2013).
- 89 Mairet-Coello, G. *et al.* FAD-linked sulfhydryl oxidase QSOX: topographic, cellular, and subcellular immunolocalization in adult rat central nervous system. *The Journal of comparative neurology* **473**, 334-363, doi:10.1002/cne.20126 (2004).
- 90 Chakravarthi, S., Jessop, C. E., Willer, M., Stirling, C. J. & Bulleid, N. J. Intracellular catalysis of disulfide bond formation by the human sulfhydryl oxidase, QSOX1. *The Biochemical journal* **404**, 403-411, doi:10.1042/BJ20061510 (2007).
- 91 Thorpe, C. & Coppock, D. L. Generating disulfides in multicellular organisms: Emerging roles for a new flavoprotein family. *Journal of Biological Chemistry* **282**, 13929-13933, doi:10.1074/jbc.R600037200 (2007).
- 92 Portes, K. F. *et al.* Tissue distribution of quiescin Q6/sulfhydryl oxidase (QSOX) in developing mouse. *Journal of molecular histology* **39**, 217-225, doi:10.1007/s10735-007-9156-8 (2008).
- 93 Zanata, S. M. *et al.* High levels of active quiescin Q6 sulfhydryl oxidase (QSOX) are selectively present in fetal serum. *Redox report : communications in free radical research* **10**, 319-323, doi:10.1179/135100005X83699 (2005).
- 94 Israel, B. A., Jiang, L., Gannon, S. A. & Thorpe, C. Disulfide bond generation in mammalian blood serum: Detection and purification of quiescin-sulfhydryl

- oxidase. *Free Radical Biology and Medicine* **69**, 129-135, doi:10.1016/j.freeradbiomed.2014.01.020 (2014).
- 95 Katchman, B. a. *et al.* Quiescin sulfhydryl oxidase 1 promotes invasion of pancreatic tumor cells mediated by matrix metalloproteinases. *Molecular cancer research : MCR* **9**, 1621-1631, doi:10.1158/1541-7786.MCR-11-0018 (2011).
- 96 Hooper, K. L., Sheasley, S. L., Gilbert, H. F. & Thorpe, C. Sulfhydryl oxidase from egg white. A facile catalyst for disulfide bond formation in proteins and peptides. *J Biol Chem* **274**, 22147-22150 (1999).
- 97 Song, H. *et al.* Loss of Nkx3.1 leads to the activation of discrete downstream target genes during prostate tumorigenesis. *Oncogene* **28**, 3307-3319, doi:10.1038/onc.2009.181 (2009).
- 98 Ouyang, X., Dewese, T. L., Nelson, W. G. & Abate-shen, C. Loss-of-Function of Nkx3 . 1 Promotes Increased Oxidative Damage in Prostate Carcinogenesis Damage in Prostate Carcinogenesis. 6773-6779 (2005).
- 99 Antwi, K. *et al.* Analysis of the Plasma Peptidome from Pancreas Cancer Patients Connects a Peptide in Plasma to Overexpression of the Parent Protein in Tumors research articles. 4722-4731 (2009).
- 100 Katchman, B. a. *et al.* Expression of quiescin sulfhydryl oxidase 1 is associated with a highly invasive phenotype and correlates with a poor prognosis in Luminal B breast cancer. *Breast cancer research : BCR* **15**, R28, doi:10.1186/bcr3407 (2013).
- 101 Lake, D. F. & Faigel, D. O. The Emerging Role of QSOX1 in Cancer. *Antioxidants & Redox Signaling* **21**, 485-496, doi:10.1089/ars.2013.5572 (2014).
- 102 Grossman, I., Alon, A., Ilani, T. & Fass, D. An inhibitory antibody blocks the first step in the dithiol/disulfide relay mechanism of the enzyme QSOX1. *Journal of molecular biology* **425**, 4366-4378, doi:10.1016/j.jmb.2013.07.011 (2013).
- 103 Pernodet, N. *et al.* High expression of QSOX1 reduces tumorigenesis, and is associated with a better outcome for breast cancer patients. *Breast cancer research : BCR* **14**, R136, doi:10.1186/bcr3341 (2012).
- 104 Hellebrekers, D. M. *et al.* Identification of epigenetically silenced genes in tumor endothelial cells. *Cancer research* **67**, 4138-4148, doi:10.1158/0008-5472.Can-06-3032 (2007).
- 105 Morel, C. *et al.* Involvement of sulfhydryl oxidase QSOX1 in the protection of cells against oxidative stress-induced apoptosis. *Experimental cell research* **313**, 3971-3982, doi:10.1016/j.yexcr.2007.09.003 (2007).
- 106 Mebazaa, A. *et al.* Unbiased plasma proteomics for novel diagnostic biomarkers in cardiovascular disease: identification of quiescin Q6 as a candidate biomarker of acutely decompensated heart failure. *European heart journal* **33**, 2317-2324, doi:10.1093/eurheartj/ehs162 (2012).

- 107 Julian, C. G. *et al.* Exploratory proteomic analysis of hypobaric hypoxia and acute mountain sickness in humans. *Journal of applied physiology (Bethesda, Md. : 1985)* **116**, 937-944, doi:10.1152/jappphysiol.00362.2013 (2014).
- 108 Inoue, A. *et al.* Development of cDNA microarray for expression profiling of estrogen-responsive genes. *Journal of molecular endocrinology* **29**, 175-192 (2002).
- 109 Moggs, J. G. *et al.* Anti-proliferative effect of estrogen in breast cancer cells that re-express ERalpha is mediated by aberrant regulation of cell cycle genes. *Journal of molecular endocrinology* **34**, 535-551, doi:10.1677/jme.1.01677 (2005).
- 110 Poillet, L. *et al.* QSOX1 Inhibits Autophagic Flux in Breast Cancer Cells. *PLoS one* **9**, e86641, doi:10.1371/journal.pone.0086641 (2014).
- 111 Shi, C.-Y., Fan, Y., Liu, B. & Lou, W.-H. HIF1 contributes to hypoxia-induced pancreatic cancer cells invasion via promoting QSOX1 expression. *Cellular physiology and biochemistry : international journal of experimental cellular physiology, biochemistry, and pharmacology* **32**, 561-568, doi:10.1159/000354460 (2013).
- 112 Gatenby, R. A. & Gillies, R. J. A microenvironmental model of carcinogenesis. *Nature reviews. Cancer* **8**, 56-61, doi:10.1038/nrc2255 (2008).
- 113 Jones, D. P. *et al.* Redox state of glutathione in human plasma. *Free Radic Biol Med* **28**, 625-635 (2000).
- 114 Jones, D. P. Extracellular Redox State: Refining the Definition of Oxidative Stress in Aging. *Rejuvenation research* **9**, 169-181, doi:10.1089/rej.2006.9.169 (2006).
- 115 Brown, L. A., Ping, X. D., Harris, F. L. & Gauthier, T. W. Glutathione availability modulates alveolar macrophage function in the chronic ethanol-fed rat. *American journal of physiology. Lung cellular and molecular physiology* **292**, L824-832, doi:10.1152/ajplung.00346.2006 (2007).
- 116 Franco, R. & Cidlowski, J. A. Glutathione efflux and cell death. *Antioxid Redox Signal* **17**, 1694-1713, doi:10.1089/ars.2012.4553 (2012).
- 117 Adams, J. D., Jr., Lauterburg, B. H. & Mitchell, J. R. Plasma glutathione and glutathione disulfide in the rat: regulation and response to oxidative stress. *The Journal of pharmacology and experimental therapeutics* **227**, 749-754 (1983).
- 118 Yi, M. C. & Khosla, C. Thiol–Disulfide Exchange Reactions in the Mammalian Extracellular Environment. *Annual Review of Chemical and Biomolecular Engineering* **7**, 197-222, doi:10.1146/annurev-chembioeng-080615-033553 (2016).
- 119 Dringen, R. Metabolism and functions of glutathione in brain. *Progress in neurobiology* **62**, 649-671 (2000).
- 120 Ballatori, N., Hammond, C. L., Cunningham, J. B., Krance, S. M. & Marchan, R. Molecular mechanisms of reduced glutathione transport: role of the MRP/CFTR/ABCC and OATP/SLC21A families of membrane proteins.

- Toxicology and applied pharmacology* **204**, 238-255, doi:10.1016/j.taap.2004.09.008 (2005).
- 121 Wright, E. C., Stern, J., Ersser, R. & Patrick, A. D. Glutathionuria: gamma-glutamyl transpeptidase deficiency. *Journal of inherited metabolic disease* **2**, 3-7 (1980).
- 122 Lurie, S. *et al.* Different degrees of fetal oxidative stress in elective and emergent cesarean section. *Neonatology* **92**, 111-115, doi:10.1159/000100965 (2007).
- 123 Jones, D. P. *et al.* Cysteine/cystine couple is a newly recognized node in the circuitry for biologic redox signaling and control. *FASEB journal : official publication of the Federation of American Societies for Experimental Biology* **18**, 1246-1248, doi:10.1096/fj.03-0971fje (2004).
- 124 Go, Y. M. & Jones, D. P. Intracellular proatherogenic events and cell adhesion modulated by extracellular thiol/disulfide redox state. *Circulation* **111**, 2973-2980, doi:10.1161/circulationaha.104.515155 (2005).
- 125 Ramirez, A. *et al.* Extracellular cysteine/cystine redox potential controls lung fibroblast proliferation and matrix expression through upregulation of transforming growth factor-beta. *American journal of physiology. Lung cellular and molecular physiology* **293**, L972-L981, doi:10.1152/ajplung.00010.2007 (2007).
- 126 Nkabyo, Y. S., Go, Y.-M., Ziegler, T. R. & Jones, D. P. Extracellular cysteine/cystine redox regulates the p44/p42 MAPK pathway by metalloproteinase-dependent epidermal growth factor receptor signaling. *American journal of physiology. Gastrointestinal and liver physiology* **289**, G70-G78, doi:10.1152/ajpgi.00280.2004 (2005).
- 127 Jonas, C. R., Ziegler, T. R., Gu, L. H. & Jones, D. P. Extracellular thiol/disulfide redox state affects proliferation rate in a human colon carcinoma (Caco2) cell line. *Free Radical Biology and Medicine* **33**, 1499-1506, doi:10.1016/S0891-5849(02)01081-X (2002).
- 128 Hildebrandt, W., Kinscherf, R., Hauer, K., Holm, E. & Droge, W. Plasma cystine concentration and redox state in aging and physical exercise. *Mechanisms of ageing and development* **123**, 1269-1281 (2002).
- 129 Go, Y. M. & Jones, D. P. Cysteine/cystine redox signaling in cardiovascular disease. *Free Radic Biol Med* **50**, 495-509, doi:10.1016/j.freeradbiomed.2010.11.029 (2011).
- 130 Chawla, R. K. *et al.* Plasma cysteine, cystine, and glutathione in cirrhosis. *Gastroenterology* **87**, 770-776 (1984).
- 131 Imhoff, B. R. & Hansen, J. M. Extracellular redox environments regulate adipocyte differentiation. *Differentiation; research in biological diversity* **80**, 31-39, doi:10.1016/j.diff.2010.04.005 (2010).
- 132 Jones, D. P. *et al.* Dietary sulfur amino acid effects on fasting plasma cysteine/cystine redox potential in humans. *Nutrition (Burbank, Los Angeles County, Calif.)* **27**, 199-205, doi:10.1016/j.nut.2010.01.014 (2011).

- 133 Mandal, P. K. *et al.* System x(c)- and thioredoxin reductase 1 cooperatively rescue glutathione deficiency. *J Biol Chem* **285**, 22244-22253, doi:10.1074/jbc.M110.121327 (2010).
- 134 Iwata, S. *et al.* Adult T cell leukemia (ATL)-derived factor/human thioredoxin prevents apoptosis of lymphoid cells induced by L-cystine and glutathione depletion: possible involvement of thiol-mediated redox regulation in apoptosis caused by pro-oxidant state. *Journal of immunology (Baltimore, Md. : 1950)* **158**, 3108-3117 (1997).
- 135 Bannai, S. Transport of cystine and cysteine in mammalian cells. *Biochimica et biophysica acta* **779**, 289-306 (1984).
- 136 Lewerenz, J. *et al.* The Cystine/Glutamate Antiporter System x_c in Health and Disease: From Molecular Mechanisms to Novel Therapeutic Opportunities. *Antioxidants & Redox Signaling* **18**, 522-555, doi:10.1089/ars.2011.4391 (2013).
- 137 Christensen, H. N. Role of amino acid transport and countertransport in nutrition and metabolism. *Physiological reviews* **70**, 43-77, doi:10.1152/physrev.1990.70.1.43 (1990).
- 138 Droge, W., Eck, H. P., Gmunder, H. & Mihm, S. Modulation of lymphocyte functions and immune responses by cysteine and cysteine derivatives. *The American journal of medicine* **91**, 140s-144s (1991).
- 139 Yan, Z., Garg, S. K., Kipnis, J. & Banerjee, R. Extracellular redox modulation by regulatory T cells. **5**, 721-723, doi:10.1038/nchembio.212 (2009).
- 140 Blanco, R. A. *et al.* Diurnal variation in glutathione and cysteine redox states in human plasma. *The American journal of clinical nutrition* **86**, 1016-1023, doi:10.1093/ajcn/86.4.1016 (2007).
- 141 Powis, G. & Montfort, W. R. Properties and biological activities of thioredoxins. *Annual review of pharmacology and toxicology* **41**, 261-295, doi:10.1146/annurev.pharmtox.41.1.261 (2001).
- 142 Rubartelli, A., Bajetto, A., Allavena, G., Wollman, E. & Sitia, R. Secretion of thioredoxin by normal and neoplastic cells through a leaderless secretory pathway. *J Biol Chem* **267**, 24161-24164 (1992).
- 143 Kondo, N. *et al.* Redox-sensing release of human thioredoxin from T lymphocytes with negative feedback loops. *Journal of immunology (Baltimore, Md. : 1950)* **172**, 442-448 (2004).
- 144 Bertini, R. *et al.* Thioredoxin, a redox enzyme released in infection and inflammation, is a unique chemoattractant for neutrophils, monocytes, and T cells. *The Journal of experimental medicine* **189**, 1783-1789 (1999).
- 145 Nakamura, H. *et al.* Adult T cell leukemia-derived factor/human thioredoxin protects endothelial F-2 cell injury caused by activated neutrophils or hydrogen peroxide. *Immunology letters* **42**, 75-80 (1994).
- 146 Schwertassek, U. *et al.* Selective redox regulation of cytokine receptor signaling by extracellular thioredoxin-1. *The EMBO journal* **26**, 3086-3097, doi:10.1038/sj.emboj.7601746 (2007).

- 147 Matthias, L. J. & Hogg, P. J. Redox Control on the Cell Surface: Implications for HIV-1 Entry. *Antioxidants & Redox Signaling* **5**, 133-138, doi:10.1089/152308603321223621 (2003).
- 148 Cerutti, N., Killick, M., Jugnarain, V., Papathanasopoulos, M. & Capovilla, A. Disulfide reduction in CD4 domain 1 or 2 Is essential for interaction with HIV glycoprotein 120 (gp120), which impairs thioredoxin-driven CD4 dimerization. *Journal of Biological Chemistry* **289**, 10455-10465, doi:10.1074/jbc.M113.539353 (2014).
- 149 Wakasugi, N. *et al.* Adult T-cell leukemia-derived factor/thioredoxin, produced by both human T-lymphotropic virus type I- and Epstein-Barr virus-transformed lymphocytes, acts as an autocrine growth factor and synergizes with interleukin 1 and interleukin 2. *Proceedings of the National Academy of Sciences of the United States of America* **87**, 8282-8286 (1990).
- 150 Oblong, J. E., Berggren, M., Gasdaska, P. Y. & Powis, G. Site-directed mutagenesis of active site cysteines in human thioredoxin produces competitive inhibitors of human thioredoxin reductase and elimination of mitogenic properties of thioredoxin. *J Biol Chem* **269**, 11714-11720 (1994).
- 151 Gasdaska, J. R., Berggren, M. & Powis, G. Cell growth stimulation by the redox protein thioredoxin occurs by a novel helper mechanism. *Cell growth & differentiation : the molecular biology journal of the American Association for Cancer Research* **6**, 1643-1650 (1995).
- 152 Xu, S. Z. *et al.* TRPC channel activation by extracellular thioredoxin. *Nature* **451**, 69-72, doi:10.1038/nature06414 (2008).
- 153 Arner, E. S. & Holmgren, A. The thioredoxin system in cancer. *Seminars in cancer biology* **16**, 420-426, doi:10.1016/j.semcancer.2006.10.009 (2006).
- 154 Carvalho, A. P., Fernandes, P. A. & Ramos, M. J. Similarities and differences in the thioredoxin superfamily. *Progress in biophysics and molecular biology* **91**, 229-248, doi:10.1016/j.pbiomolbio.2005.06.012 (2006).
- 155 Soderberg, A., Sahaf, B. & Rosen, A. Thioredoxin reductase, a redox-active selenoprotein, is secreted by normal and neoplastic cells: presence in human plasma. *Cancer research* **60**, 2281-2289 (2000).
- 156 Chen, K., Detwiler, T. C. & Essex, D. W. Characterization of protein disulphide isomerase released from activated platelets. *British journal of haematology* **90**, 425-431 (1995).
- 157 Essex, D. W., Chen, K. & Swiatkowska, M. Localization of protein disulfide isomerase to the external surface of the platelet plasma membrane. *Blood* **86**, 2168-2173 (1995).
- 158 Barbouche, R., Miquelis, R., Jones, I. M. & Fenouillet, E. Protein-disulfide isomerase-mediated reduction of two disulfide bonds of HIV envelope glycoprotein 120 occurs post-CXCR4 binding and is required for fusion. *Journal of Biological Chemistry* **278**, 3131-3136, doi:10.1074/jbc.M205467200 (2003).

- 159 Jiang, X. M., Fitzgerald, M., Grant, C. M. & Hogg, P. J. Redox control of exofacial protein thiols/disulfides by protein disulfide isomerase. *J Biol Chem* **274**, 2416-2423 (1999).
- 160 Goplen, D. *et al.* Protein disulfide isomerase expression is related to the invasive properties of malignant glioma. *Cancer research* **66**, 9895-9902, doi:10.1158/0008-5472.CAN-05-4589 (2006).
- 161 Cho, J., Furie, B. C., Coughlin, S. R. & Furie, B. A critical role for extracellular protein disulfide isomerase during thrombus formation in mice. *The Journal of clinical investigation* **118**, 1123-1131, doi:10.1172/jci34134 (2008).
- 162 Flaumenhaft, R. Protein disulfide isomerase as an antithrombotic target. *Trends in cardiovascular medicine* **23**, 264-268, doi:10.1016/j.tcm.2013.03.001 (2013).
- 163 Jasuja, R. *et al.* Protein disulfide isomerase inhibitors constitute a new class of antithrombotic agents. *Journal of Clinical Investigation* **122**, 2104-2113, doi:10.1172/JCI61228 (2012).
- 164 Kim, K. *et al.* Platelet protein disulfide isomerase is required for thrombus formation but not for hemostasis in mice. *Blood* **122**, 1052-1061, doi:10.1182/blood-2013-03-492504 (2013).
- 165 Lahav, J. *et al.* Sustained integrin ligation involves extracellular free sulfhydryls and enzymatically catalyzed disulfide exchange. *Blood* **100**, 2472-2478, doi:10.1182/blood-2001-12-0339 (2002).
- 166 Holbrook, L. M. *et al.* The platelet-surface thiol isomerase enzyme ERp57 modulates platelet function. *Journal of thrombosis and haemostasis : JTH* **10**, 278-288, doi:10.1111/j.1538-7836.2011.04593.x (2012).
- 167 Wang, L. *et al.* Platelet-derived ERp57 mediates platelet incorporation into a growing thrombus by regulation of the α IIb β 3 integrin. *Blood* **122**, 3642-3650, doi:10.1182/blood-2013-06-506691 (2013).
- 168 Wu, Y. *et al.* The disulfide isomerase ERp57 mediates platelet aggregation, hemostasis, and thrombosis. *Blood* **119**, 1737-1746, doi:10.1182/blood-2011-06-360685 (2012).
- 169 Passam, F. H. *et al.* Both platelet- and endothelial cell-derived ERp5 support thrombus formation in a laser-induced mouse model of thrombosis. *Blood* **125**, 2276-2285, doi:10.1182/blood-2013-12-547208 (2015).
- 170 Wan, S.-W. *et al.* Endothelial cell surface expression of protein disulfide isomerase activates β 1 and β 3 integrins and facilitates dengue virus infection. *Journal of cellular biochemistry* **113**, 1681-1691, doi:10.1002/jcb.24037 (2012).
- 171 Bi, S., Hong, P. W., Lee, B. & Baum, L. G. Galectin-9 binding to cell surface protein disulfide isomerase regulates the redox environment to enhance T-cell migration and HIV entry. *Proceedings of the National Academy of Sciences* **108**, 10650-10655, doi:10.1073/pnas.1017954108 (2011).

- 172 Chaiswing, L. & Oberley, T. D. Extracellular/microenvironmental redox state. *Antioxid Redox Signal* **13**, 449-465, doi:10.1089/ars.2009.3020 (2010).
- 173 Chaiswing, L., Zhong, W., Cullen, J. J., Oberley, L. W. & Oberley, T. D. Extracellular redox state regulates features associated with prostate cancer cell invasion. *Cancer research* **68**, 5820-5826, doi:10.1158/0008-5472.CAN-08-0162 (2008).
- 174 Chaiswing, L., Bourdeau-Heller, J. M., Zhong, W. & Oberley, T. D. Characterization of redox state of two human prostate carcinoma cell lines with different degrees of aggressiveness. *Free Radical Biology and Medicine* **43**, 202-215, doi:10.1016/j.freeradbiomed.2007.03.031 (2007).
- 175 Ogunrinu, T. A. & Sontheimer, H. Hypoxia increases the dependence of glioma cells on glutathione. *J Biol Chem* **285**, 37716-37724, doi:10.1074/jbc.M110.161190 (2010).
- 176 Narang, V. S., Pauletti, G. M., Gout, P. W., Buckley, D. J. & Buckley, A. R. Suppression of cystine uptake by sulfasalazine inhibits proliferation of human mammary carcinoma cells. *Anticancer research* **23**, 4571-4579 (2003).
- 177 Iglehart, J. K., York, R. M., Modest, A. P., Lazarus, H. & Livingston, D. M. Cystine requirement of continuous human lymphoid cell lines of normal and leukemic origin. *J Biol Chem* **252**, 7184-7191 (1977).
- 178 Doxsee, D. W. *et al.* Sulfasalazine-induced cystine starvation: potential use for prostate cancer therapy. *The Prostate* **67**, 162-171, doi:10.1002/pros.20508 (2007).
- 179 Lo, M., Ling, V., Wang, Y. Z. & Gout, P. W. The xc- cystine/glutamate antiporter: a mediator of pancreatic cancer growth with a role in drug resistance. *British journal of cancer* **99**, 464-472, doi:10.1038/sj.bjc.6604485 (2008).
- 180 Tang, X. *et al.* Cystine addiction of triple-negative breast cancer associated with EMT augmented death signaling. *Oncogene* **36**, 4379, doi:10.1038/onc.2017.192 (2017).
- 181 Sarto, C. *et al.* Modified expression of plasma glutathione peroxidase and manganese superoxide dismutase in human renal cell carcinoma. *Electrophoresis* **20**, 3458-3466, doi:10.1002/(sici)1522-2683(19991101)20:17<3458::Aid-elps3458>3.0.Co;2-5 (1999).
- 182 Schmutzler, C. *et al.* Selenoproteins of the thyroid gland: expression, localization and possible function of glutathione peroxidase 3. *Biological chemistry* **388**, 1053-1059, doi:10.1515/bc.2007.122 (2007).
- 183 Murawaki, Y. *et al.* Aberrant expression of selenoproteins in the progression of colorectal cancer. *Cancer letters* **259**, 218-230, doi:10.1016/j.canlet.2007.10.019 (2008).
- 184 Yu, Y. P. *et al.* Glutathione peroxidase 3, deleted or methylated in prostate cancer, suppresses prostate cancer growth and metastasis. *Cancer research* **67**, 8043-8050, doi:10.1158/0008-5472.Can-07-0648 (2007).

- 185 Pawlowicz, Z. *et al.* Blood selenium concentrations and glutathione peroxidase activities in patients with breast cancer and with advanced gastrointestinal cancer. *Journal of trace elements and electrolytes in health and disease* **5**, 275-277 (1991).
- 186 Miyazaki, K. *et al.* Elevated serum level of thioredoxin in patients with hepatocellular carcinoma. *Biotherapy (Dordrecht, Netherlands)* **11**, 277-288 (1998).
- 187 Becker, K., Gromer, S., Schirmer, R. H. & Muller, S. Thioredoxin reductase as a pathophysiological factor and drug target. *European journal of biochemistry* **267**, 6118-6125 (2000).
- 188 Ueda, S. *et al.* Recombinant human thioredoxin suppresses lipopolysaccharide-induced bronchoalveolar neutrophil infiltration in rat. *Life sciences* **79**, 1170-1177, doi:10.1016/j.lfs.2006.03.026 (2006).
- 189 Khramtsov, V. V. & Gillies, R. J. Janus-Faced Tumor Microenvironment and Redox. *Antioxidants & Redox Signaling* **21**, 723-729, doi:10.1089/ars.2014.5864 (2014).
- 190 Dominici, S., Paolicchi, A., Corti, A., Maellaro, E. & Pompella, A. Prooxidant reactions promoted by soluble and cell-bound gamma-glutamyltransferase activity. *Methods in enzymology* **401**, 484-501, doi:10.1016/s0076-6879(05)01029-3 (2005).
- 191 Corti, A., Franzini, M., Paolicchi, A. & Pompella, A. Gamma-glutamyltransferase of cancer cells at the crossroads of tumor progression, drug resistance and drug targeting. *Anticancer research* **30**, 1169-1181 (2010).

Chapter 2

QSOX ASSAY DEVELOPMENT AND PURIFICATION OF THE OXIDASE FROM SERUM

2.1 Introduction

The enzymological properties of QSOX have been studied extensively in our laboratory¹⁻⁴. As we discussed in Chapter 1, QSOX catalyzes the rapid generation of disulfides from a wide range of substrates—from small monothiols to large reduced proteins⁵⁻⁷. The *in vitro* substrate specificity of this oxidase has been extensively studied, but its contribution to disulfide bond formation in biological contexts is still cryptic.

In humans, QSOX1 expression has been found to be significantly elevated in prostate^{8,9}, pancreas¹⁰ and breast^{11,12} cancers, and studies have suggested that higher QSOX1 levels are correlated with a poorer prognosis. Depressing QSOX1 levels with RNAi or inhibiting its activity using an inhibitory antibody leads to a significant decline of invasiveness in cell migration assays^{11,13-15}. In 2009 Lake et al.^{10,14} identified a QSOX1 peptide circulating in plasma that was strongly correlated with pancreatic cancer patients. In 2012 Mebazaa and colleagues¹⁶ demonstrated that mass spectroscopic analysis of QSOX1 peptide levels in plasma significantly increased the diagnostic accuracy for acute decompensated heart failure. These studies suggest plasma QSOX protein and/or peptides may represent potential diagnostic markers. However, it was uncertain whether QSOX in plasma is catalytically active and what role(s) it might play in these diseases.

Although oxygen electrode assays are reliable for QSOX activity determination¹⁷, they exhibit low sensitivity, require relatively large sample volume, and are unsuited for high throughput screening. For this reason, Raje et al., in this laboratory, developed an assay in which the hydrogen peroxide generated by QSOX catalysis reacts with homovanillic acid (HVA) to yield a fluorescent product in a reaction catalyzed by horseradish peroxidase¹⁸ (Figure 2.1). This HVA assay has two apparent limitations. One is that the HVA dimer fluoresces in the blue region of the spectrum (excitation at 320 nm, emission at 420 nm). For this reason the assay is particularly prone to interference in media with high absorbance or scattering in the near UV. The other problem is that this assay may not be suitable for high-throughput screening application because a significant fraction of compounds in many small-molecule libraries fluoresce in the blue region and would therefore interfere¹⁹.

Here, we describe a simple and sensitive fluorescence-based microplate assay for QSOX activity. This method couples hydrogen peroxide formation generated by sulfhydryl oxidases to the generation of the strong red fluorescence formed during HRP-catalyzed oxidation of Amplex UltraRed²⁰ (AUR; Figure 2.2). This assay was first developed by Dr. Benjamin Israel for screening small molecule libraries for QSOX inhibitors. After optimization, this assay is suitable for testing small samples of serum, plasma, or other biological fluids. While evaluating the performance of this assay, we discovered that adult bovine serum contained relatively high levels of sulfhydryl oxidase activity. This finding was in apparent conflict with that of Zanata et al.²¹. While reported active QSOX1 in fetal bovine serum, they found the oxidase activity and protein levels of QSOX1 in serum declined rapidly after birth and became undetectable in 60-day-old animals²¹. Using the assay we developed, we performed a

3-step chromatographic purification of QSOX from adult bovine serum. Peptide digests and mass spectrometric analysis confirmed that this disulfide-generating activity was indeed due to QSOX1. The presence of a facile oxidase for a wide range of thiol-containing peptides and proteins in mammalian plasma suggests a new dimension to the study of thiol/disulfide redox biochemistry in blood.

2.2 Experimental Procedures

2.2.1 Materials and Reagents

Bovine serum albumin, cysteine, dithiothreitol, glutathione, homovanillic acid, horseradish peroxidase type II, hydrogen peroxide, and ribonuclease A were from Sigma-Aldrich. Amplex UltraRed (AUR) was from Life Technologies. Tween 80 (Surfact-Amps, low peroxide) was from Thermo Fisher Scientific. ProBond nickel chelating resin was from Invitrogen. Commercial sera were as follows: defined fetal bovine serum, newborn bovine serum (less than 10 days of age), and donor adult bovine serum were from Hyclone; normal human serum and normal adult mouse serum were from Atlanta Biologicals; Balb C, C57BL6, CD-1, and non-Swiss albino mouse sera were from Innovative Research. Adult non-heat-treated bovine donor serum for chromatographic purification was from Atlanta Biologicals. HiTrap SP HP cation-exchange column, HiTrap Butyl HP hydrophobic interaction column and HiTrap SP XL cation-exchange column were from GE Healthcare Life Sciences. Microcon YM-30 Ultrafiltration device was from Millipore. Sequencing Grade modified trypsin was from Promega.

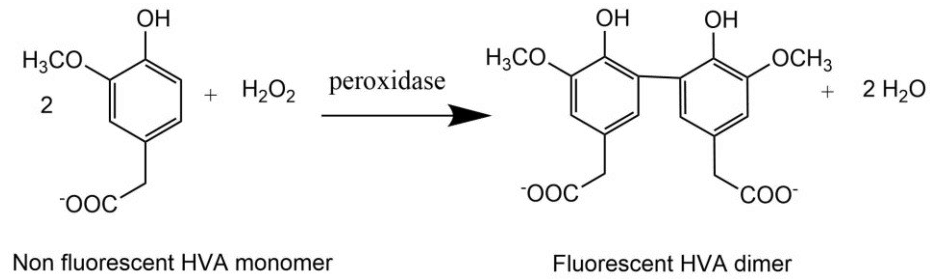


Figure 2.1 **Horseradish peroxidase-catalyzed oxidation of homovanillic acid by hydrogen peroxide.**

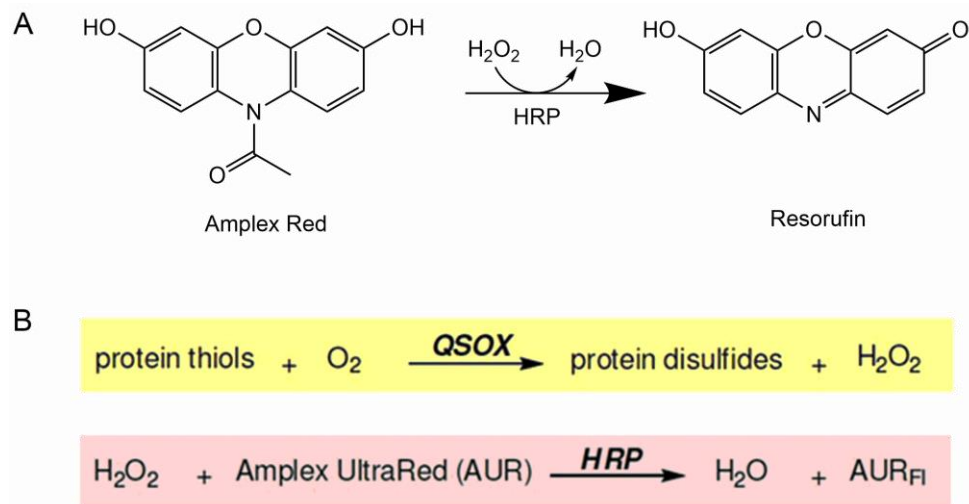


Figure 2.2 **Amplex Red based assays for QSOX.** Panel A shows Amplex Red being converted to the strongly fluorescent resorufin in the presence of horseradish peroxidase and hydrogen peroxide. A proprietary variant of Amplex Red, Amplex Ultra Red (AUR), of undisclosed structure is more stable and was used throughout this work. Panel B shows the scheme of the AUR assay.

2.2.2 General Methods

The buffer used in this work was 50 mM potassium phosphate containing 1 mM ethylenediaminetetraacetic acid (EDTA), adjusted to pH 7.5, unless otherwise stated. Visible and ultraviolet spectra were recorded in self-masking microcells using Hewlett-Packard 8452A or Agilent 8453 instruments. Reduced RNase was prepared and stored as a lyophilized powder⁶. Thiols and hydrogen peroxide were standardized as described previously⁶. Recombinant human QSOX1 (hQSOX1) was expressed and purified as described previously⁶ and activity was evaluated with the oxygen electrode¹⁷. Protein concentrations were determined using the Bradford assay. Western blots used rabbit anti chicken QSOX1 primary antibody and anti-rabbit IgG secondary antibody. Chromatographic purifications utilized an ÄKTA FPLC operated at room temperature. Data were plotted and fit using Microsoft Office Excel and GraphPad Prism software.

2.2.3 Sulphydryl Oxidase Fluorescence Assays

2.2.3.1 Homovanillic Acid (HVA) Assay

Homovanillic acid (HVA) fluorescence assays were conducted in an SLM Aminco Bowman Series 2 luminescence spectrometer as described previously¹⁸. The final assay mixture contained 1 mM HVA, 1.4 μ M horseradish peroxidase (HRP), and 50 μ M dithiothreitol (DTT). A 100 μ L premixed cocktail of buffer, HVA, and HRP was added to the cuvette, DTT and water were added to make a total 150 μ L and the baseline was recorded for 1 min. A 5 μ L serum sample was added to start the reaction. The increase in fluorescence emission was followed at 420 nm with excitation at 320 nm at a sensitivity set to correspond to 3% of the full scale.

2.2.3.2 Amplex UltraRed (AUR) Assay

The Amplex UltraRed (AUR) fluorescence assay was conducted in a BMG POLARstar OMEGA plate reader with 96-well black flat-bottomed polystyrene plates (Corning). The following reagents were used in a total volume of 150 μL in phosphate buffer: 10 μM AUR, 50 nM HRP and 0.5% v/v low-peroxide Tween 80 (included for serum samples; see Results). Typically for biological samples, 125 μL of a cocktail formed by mixing AUR, HRP, and Tween 80 in buffer was delivered to each well, followed by 5 μL of the sample. Care was taken throughout this procedure to minimize exposure of the AUR reagent to light²² by wrapping AUR solutions with aluminum foil, as well as shading the 96-well plate where practical. EDTA (1 mM) was included to suppress a background signal generated by nonenzymatic oxidation of thiols by traces of copper and iron²³. The reaction was started by the addition of 20 μL of 0.75 mM thiols (e.g., 0.375 mM DTT or 94 μM reduced RNase) in each well to give a final concentration of 100 μM thiols. Thiol solutions were prepared daily either from concentrated stocks stored at $-20\text{ }^{\circ}\text{C}$ or freshly from solid reagents to minimize background signals. Recombinant human QSOX1 (hQSOX1) was used for some optimization trials. The measurement started immediately after the addition of thiols. Assays were conducted in fluorescence intensity mode (excitation filter 544 nm and emission filter 590-10 nm) with measurement every 0.5 min for 10 min. Initial rates were typically determined over the first 3 min of data acquisition. Gain adjustment was obtained by the addition of excess H_2O_2 to 10 μM AUR in 150 μL of assay solution. The assay was calibrated by adding increasing concentrations of H_2O_2 (0-1.6 μM) in the presence of the assay cocktail and thiol substrate. The linear fluorescence increase with peroxide enabled conversion of relative fluorescence to micromolar hydrogen peroxide.

2.2.4 Purification of QSOX1 from Bovine Serum

2.2.4.1 Cation Exchange Column (Salt Gradient)

Adult non-heat-treated bovine donor serum (500 mL) was diluted with 2 L of distilled water at 4 °C and centrifuged at 13,700 RCF (Sorvall RC-5B) for 8 min to remove a small amount of precipitate. Two 5-mL HiTrap SP HP cation-exchange columns were connected in series and equilibrated at 1.5 mL/min at 4 °C with a 5-fold-diluted solution of phosphate-buffered saline (0.2× PBS) containing 1.62 mM Na₂HPO₄, 0.38 mM K₂HPO₄, and 29.8 mM NaCl. The 2.5 L diluted serum was then applied to the connected columns at 2 mL/min using a peristaltic pump at 4 °C. The combined columns were then connected to an ÄKTA FPLC operated at room temperature and developed at 1 mL/min using a 200-min linear gradient from 100% buffer A (0.2× PBS) to 100% buffer B (50 mM potassium phosphate, pH 7.5, containing 500 mM NaCl and 1 mM EDTA) followed by a further 20 min of buffer B. 5 mL fractions were automatically collected. AUR assays, using 5 µL of each fraction, were performed. The fractions with peak sulfhydryl oxidase activity were analyzed by UV-Vis spectroscopy and by SDS-PAGE.

2.2.4.2 Hydrophobic Interaction Column

Three fractions from the first cation exchange chromatography, containing 77% of sulfhydryl oxidase activity, were pooled and brought to 40% saturation with ammonium sulfate at room temperature. The solution was centrifuged at 2700 RCF for 2 min to remove precipitate. The supernatant was applied at 0.3 mL/min to a 1-mL HiTrap Butyl HP hydrophobic interaction column (HIC) equilibrated with 40% saturated ammonium sulfate in 50 mM phosphate buffer, pH 7.5, containing 1 mM

EDTA. The column was developed with a decreasing linear gradient to 50 mM phosphate buffer alone at 1 mL/min over a total volume of 20 mL. Fractions (0.5 mL) were collected and analyzed for sulfhydryl oxidase activity as before. The peak fractions were analyzed by UV-Vis spectroscopy, SDS-PAGE and Western blots.

2.2.4.3 Cation Exchange Column (Eluting with a pH Gradient)

Three fractions with peak sulfhydryl oxidase activity recovered from the HIC chromatography were pooled and dialyzed at 4 °C against 50 mM phosphate buffer, pH 7.5, containing 1 mM EDTA. The dialyzed pool was diluted with an equal volume of water and then applied at 0.5 mL/min to a 1-mL HiTrap SP XL cation-exchange column equilibrated with 25 mM phosphate buffer, pH 7.5, containing 1 mM EDTA. The column was then developed at 0.5 mL/min with a 40-min linear gradient starting with 100% 25 mM Tris buffer, pH 7.4, containing 1 mM EDTA, and ending with the same buffer adjusted to pH 9.4. Sulfhydryl oxidase activity was then eluted with a 4-mL wash using the pH 9.4 buffer supplemented with 200 mM NaCl and active fractions were adjusted to pH 7.5 by the addition of 50 µl of 1 M Tris buffer, pH 7.2. Pooled fractions were concentrated and washed into 50 mM phosphate buffer, pH 8.0, containing 1 mM EDTA using a Microcon YM-30 Ultrafiltration device. The purified material was characterized by UV-Vis spectroscopy and SDS-PAGE.

2.2.4.4 Protein Digestion and Analysis

Approximately 15 µg of pure sulfhydryl oxidase in 0.1 mL of 50 mM phosphate buffer, pH 8.0, in a polypropylene centrifuge tube was incubated in a

boiling water bath for 10 min, then cooled on ice and then incubated with 0.75 μ g of Sequencing Grade modified trypsin for 2 h at 37 °C. The peptide digest was stored frozen. Separation and sequencing of peptides was performed by Dr. Shawn Gannon. In brief, chromatography used a Waters Acquity UPLC system equipped with a BEH C18 100 \times 1-mm, 1.7- μ m particle size column utilizing a linear gradient composed of 0.1% formic acid in water (solvent A) and 0.1% formic acid in methanol (solvent B). After a 3-min isocratic hold at 5% solvent B, the column was developed with an increasing gradient to 65% solvent B over an additional 67 min. Peptides were detected using a Thermo Scientific Orbitrap Velos mass spectrometer. The data were acquired using the data-dependent analysis mode, which allowed for the collection of both full-scan and MS/MS data of the peptides. The MS/MS data were further analyzed using the Sequest peptide search algorithm of Thermo Scientific Proteome Discoverer (version 1.3.0.339).

2.3 Results and Discussion

2.3.1 AUR Assay Development with Recombinant Human QSOX1

In the new plate reader assay presented here hydrogen peroxide generated by QSOX is coupled to the horseradish peroxidase-mediated oxidation of Amplex UltraRed (AUR) to yield a product fluorescing in the red region of the spectrum. Figure 2.3 shows a demonstration of the readout from this assay with recombinant human QSOX1 (hQSOX1), together with an indication of the linearity of the assay up to 2 nM hQSOX1. This assay is sensitive to 0.1 nM of hQSOX1.

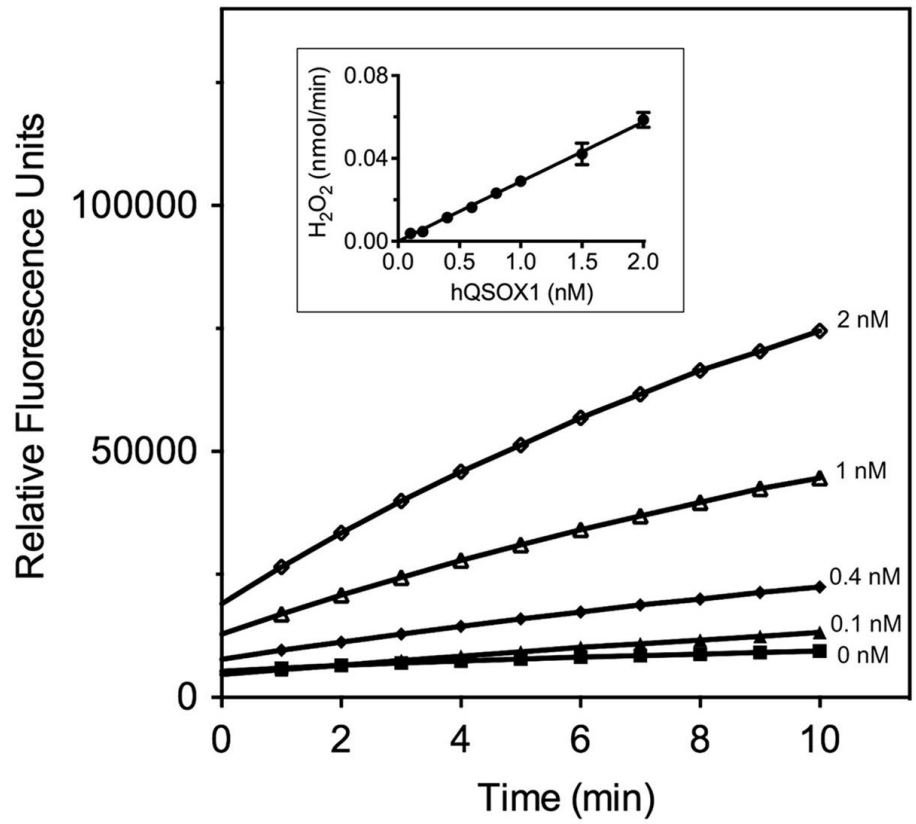


Figure 2.3 **AUR assay with increasing concentrations of recombinant human QSOX1.** The inset shows the linearity of initial rates, corrected for the nonenzymatic background oxidation of thiols, as a function of enzyme concentration.

It is important to note that although this microplate assay is a sensitive and convenient way to measure sulfhydryl oxidase activity levels, it cannot be used to determine K_m values for thiol substrates. This reason is that thiols depress fluorophore generation (Figure 2.4), probably by intercepting the radical intermediates in the generation of the resorufin-like fluorophore¹⁸. The concentration of substrate thiols (100 μ M) used in these assays represents a suitable compromise between sufficient linearity of hydrogen peroxide production and avoiding excessive nonenzymatic metal-catalyzed thiol oxidation.

During the development of the AUR assay, a variety of pH values were tested. Figure 2.5 shows AUR assays in phosphate buffers with various pH, and at pH 7.5 the assay provides sufficient enzyme activity while maintaining a workable nonenzymatic trace metal-catalyzed thiol oxidation of the reagents. Figure 2.6 shows the presence of the metal chelating agent EDTA proved critical in minimizing nonenzymatic background at pH 7.5.

2.3.2 Optimization of AUR Assay for Serum

Initial experiments using serum suggested that the activity of QSOX was being suppressed. Serum contains high concentration of serum albumin and we found that 1 or 2 mg of bovine serum albumin strongly interfered with the AUR assay using recombinant hQSOX1 (Figure 2.7). Presumably this attenuation reflects the well-known ability of albumin to bind a range of aromatic ligands²⁴ including, perhaps, the AUR substrate or its fluorescent product. Inclusion of Tween 80 (at 0.5% v/v) significantly reversed this apparent inhibition (Figure 2.7). Tween 80 at 0.5% v/v also proved suitable for analyzing QSOX in serum, as shown in Figure 2.8.

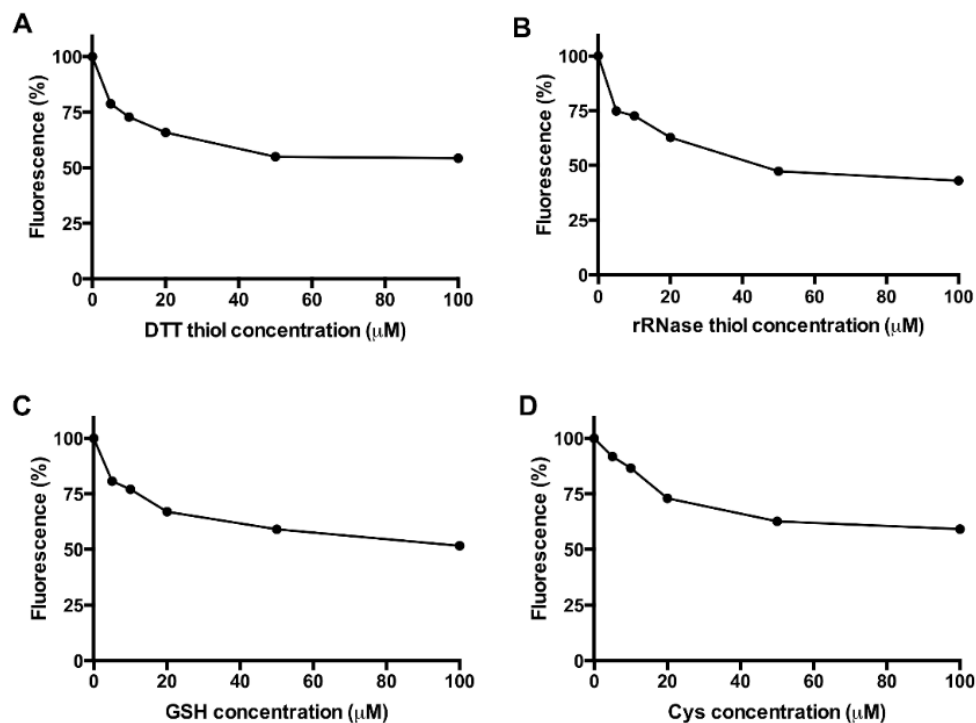


Figure 2.4 **Thiol-dependent attenuation of the development of fluorescence using AUR, horseradish peroxidase and hydrogen peroxide.** The plate-reader was implemented as described in Methods using 10 μM AUR, 50 nM HRP and the indicated thiol concentrations contributed from DTT, reduced RNase, GSH or cysteine (panels A-D, respectively). A single aliquot of 0.8 μM H_2O_2 was then added to generate the fluorescent product and the fluorescence was recorded at 1.5 and 2 min and averaged. The observed intensities were subtracted from the signal in the absence of hydrogen peroxide and the data were normalized to 100% for the zero thiol control. The data are the average of 2 independent determinations.

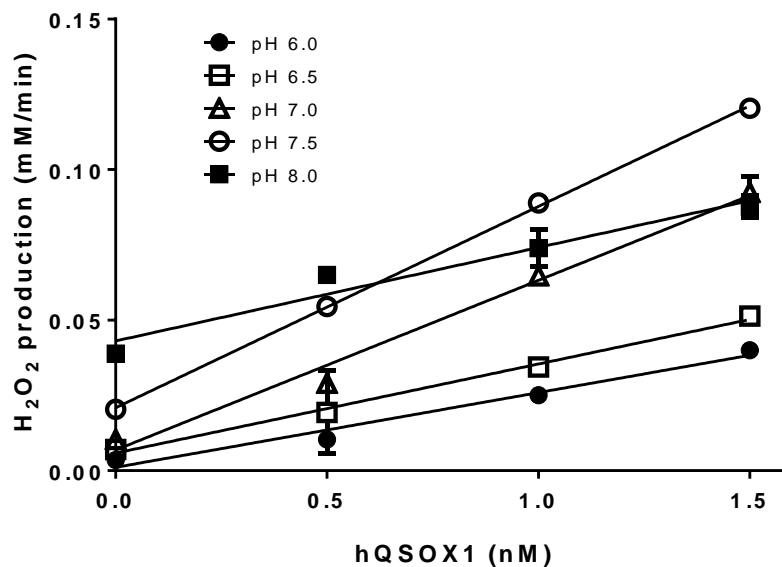


Figure 2.5 **AUR assay in phosphate buffers with various pH values.** At pH 7.5 the assay provides sufficient enzyme activity while maintaining a workably low nonenzymatic rate of metal catalyzed thiol oxidation (indicated by intercepts in the vertical axis).

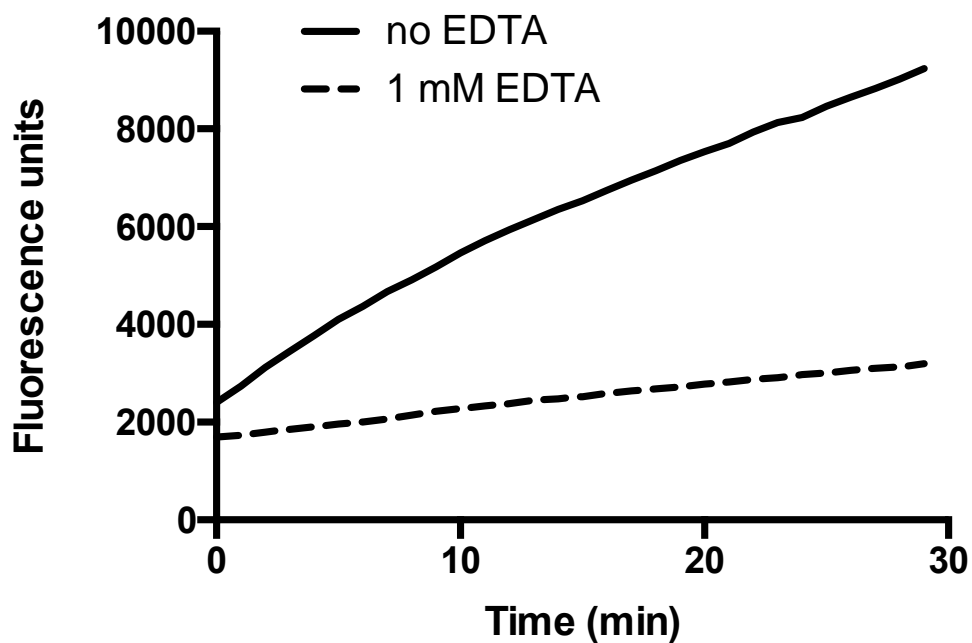


Figure 2.6 **EDTA decreases the nonenzymatic background at pH 7.5.** The plate-reader method was implemented using 10 μM AUR, 50 nM HRP and 100 μM thiols from DTT in phosphate buffers with or without 1 mM EDTA (5 mM EDTA shows a comparable minimizing effect (data not shown)).

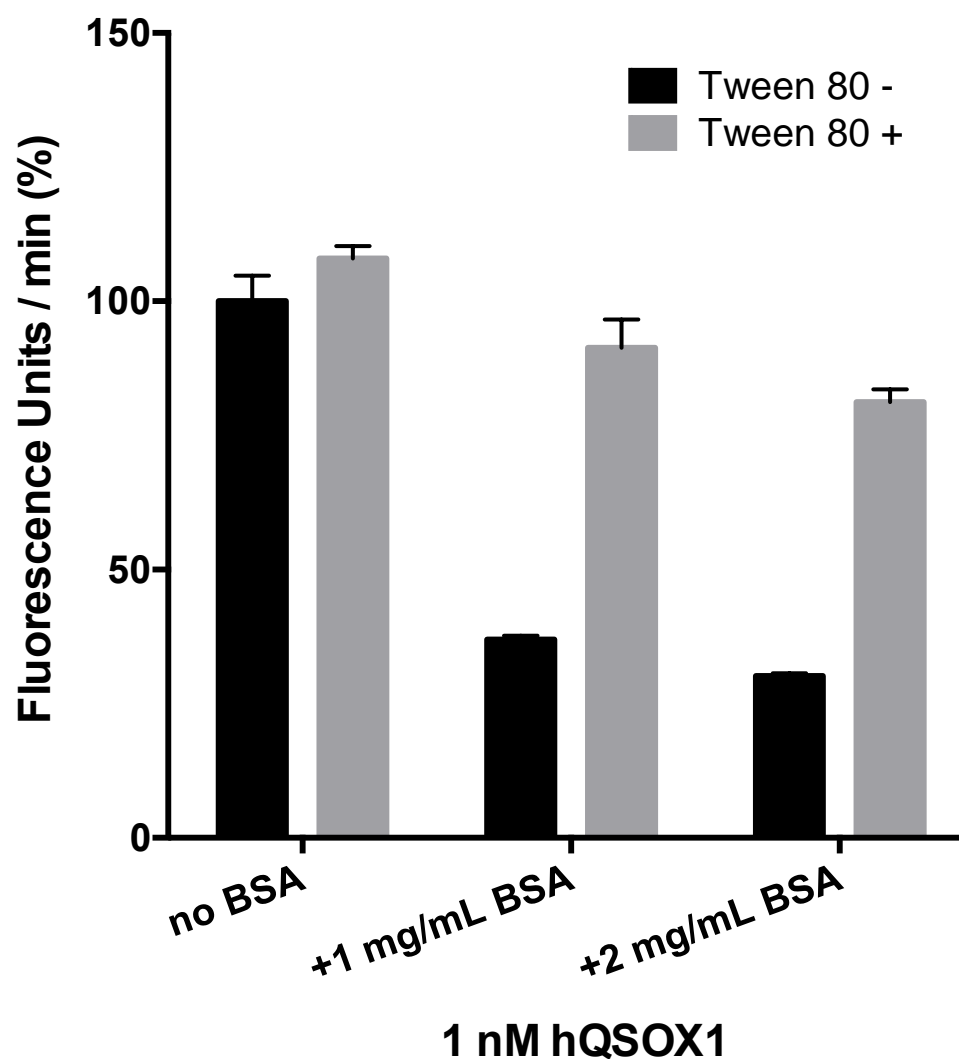


Figure 2.7 **Bovine serum albumin-mediated inhibition of the AUR assay using recombinant human QSOX1.** The AUR assay was conducted using 1 nM human QSOX1 with the inclusion of 1 or 2 mg/mL of bovine serum albumin and 0.5% Tween 80 as indicated. Detergent largely reversed the apparent inhibition of the AUR assay by serum albumin.

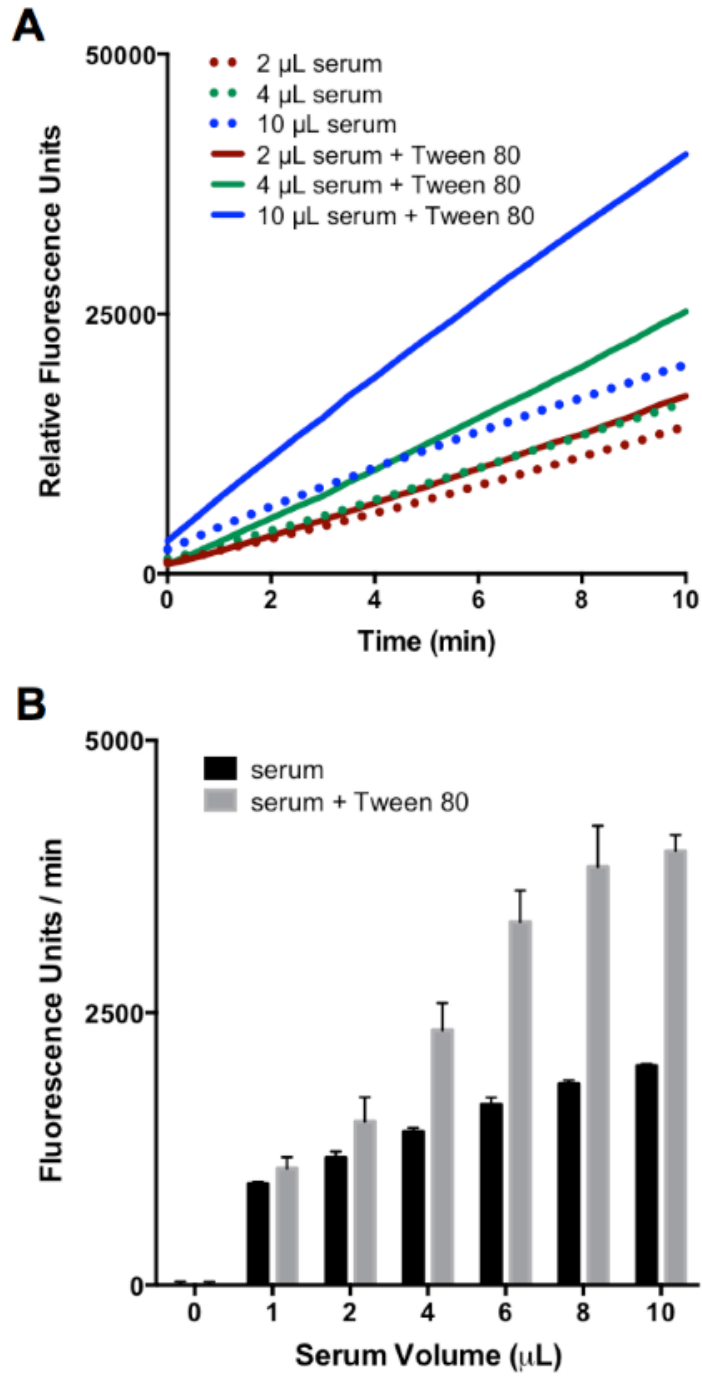


Figure 2.8 **Effect of Tween 80 on AUR assays of adult bovine serum.** Panel A shows representative traces from the plate reader. Panel B depicts the initial rates with increasing volumes of added serum.

2.3.3 Bovine Serum from Animals of Different Ages Show Comparable Sulphydryl Oxidase Activities

With optimization described above, Figure 2.9 shows AUR assays of bovine sera. We found that bovine fetal, newborn, and adult commercial sera revealed approximately the same levels of sulphydryl oxidase activities irrespective of age when the samples are normalized for protein content. Since this result differed from that of Zanata²¹ we also employed the assay technique used in that work. Figure 2.10 shows that when the older HVA assay is employed we again found that the sulphydryl oxidase activity does not decline significantly in adult bovine serum.

2.3.4 A Survey of Mammalian Sera

A survey of sera from different mammals (Table 2.1) show that sulphydryl oxidase activities are generally rather comparable between bovine and human samples. A concentration of ~25 nM QSOX in human serum is deduced by comparing the activity of human blood serum with that of the recombinant human enzyme under standard assay conditions using DTT. Mouse sera reproducibly show an almost 10-fold higher level of activity.

2.3.5 Modest QSOX Activity at Low Levels of Monothiol Substrates

The confirmation of QSOX1 activity in mammalian sera raises questions about the potential of QSOX to oxidize the low concentrations of the monothiols cysteine and glutathione that are normally present in blood plasma^{25,26}. With K_m and k_{cat} values for vertebrate QSOX1 enzymes toward these thiols of about 10 mM and about 2000 thiols/min, respectively^{27,28}, a concentration of ~25 nM QSOX1 in human serum

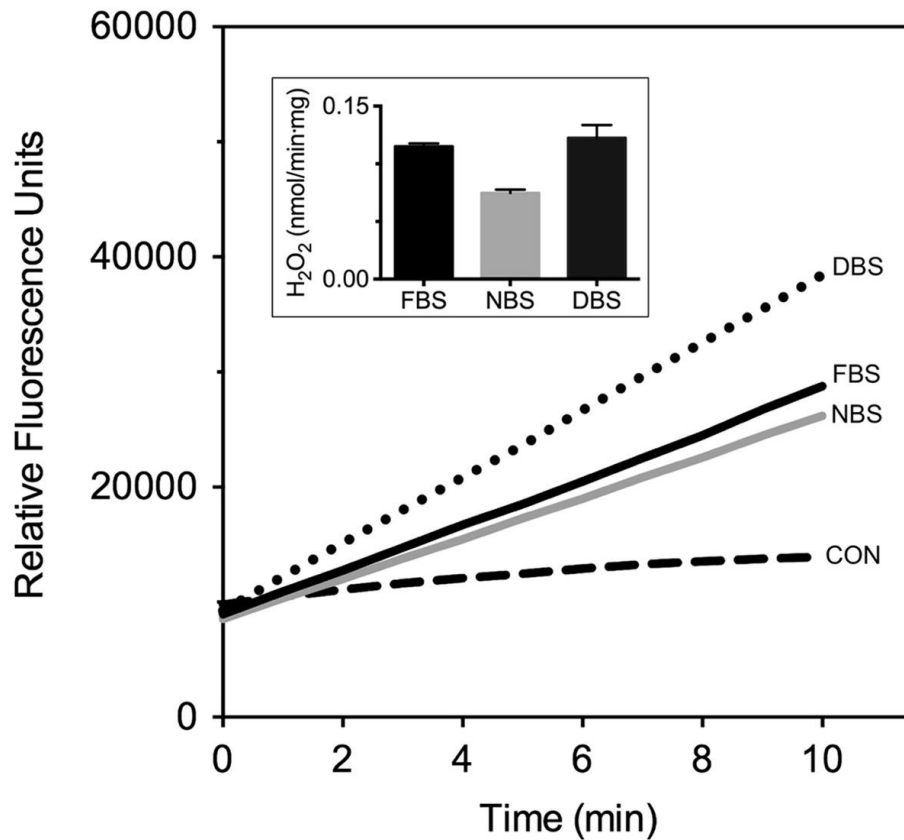


Figure 2.9 **Amplex UltraRed assay of bovine serum.** Amplex UltraRed assay using 5 μL of fetal (FBS), newborn (NBS), or adult bovine serum (DBS) in a total assay volume of 150 μL in phosphate buffer, pH 7.5, containing 1 mM EDTA in the presence of 0.5% Tween 80 (see Experimental procedures). Control assays without added serum are represented by CON. Two additional controls, lacking either DTT or both DTT and serum, showed no detectable increase in fluorescence over the measurement period (data not shown). The inset presents initial rates normalized to the protein concentration of the serum samples.

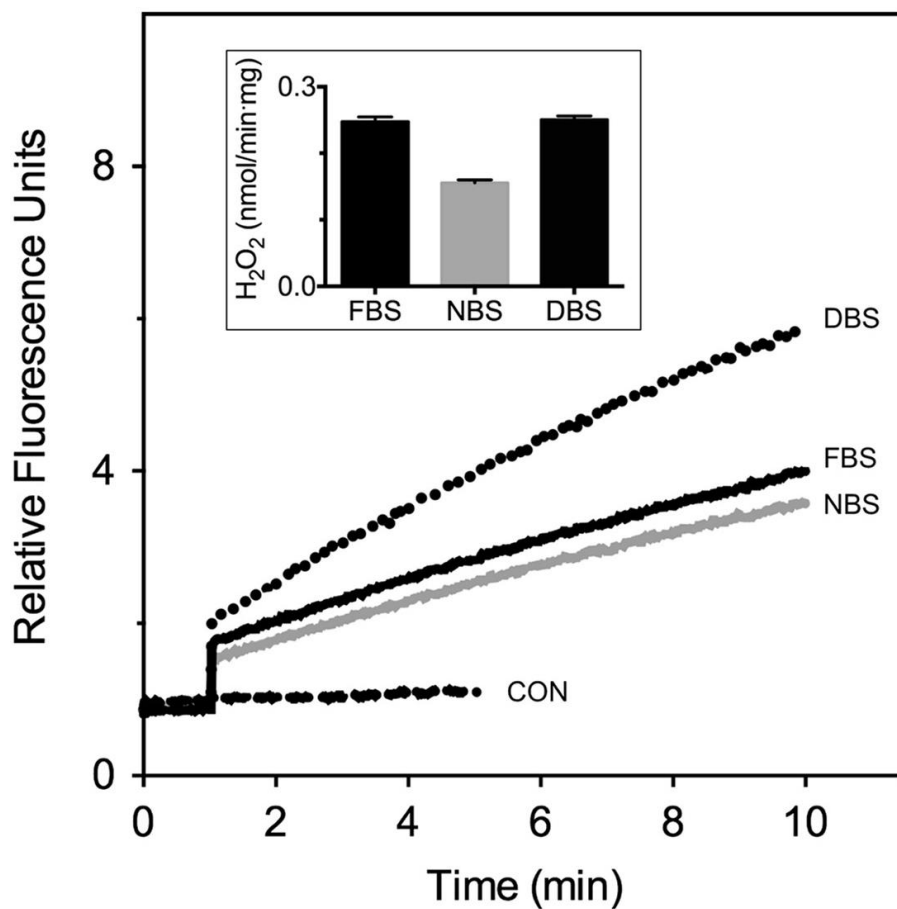


Figure 2.10 **Homovanillic acid assay of bovine serum.** Homovanillic acid assay in phosphate buffer, pH 7.5, containing 1 mM EDTA using 5 μ L of fetal (FBS), newborn (NBS), or adult bovine serum (DBS) in a total assay volume of 150 μ L (see Experimental procedures). The inset provides rates corrected for the protein content of the samples.

Table 2.1 Sulphydryl oxidase activity levels toward DTT in bovine, human, and mouse commercial sera.

Serum type	H ₂ O ₂ production (nmol/min.mg)
Human normal	0.082±0.011
Mouse ^a	0.687±0.056
Fetal bovine	0.099±0.002
Newborn bovine	0.070±0.003
Adult donor bovine	0.119±0.011

Assays were conducted as described under Experimental procedures. Errors represent standard deviations of three determinations.

^aNormal mouse serum; sera from four additional mouse strains (see Experimental procedures) yielded an average of 0.893±0.197 nmol/min/mg.

would seem to imply a significant generation of low-molecular-weight disulfides and H₂O₂ by this circulating oxidase. This is not the case; Figure 2.11 reveals the behavior of recombinant human QSOX1 at low thiol concentrations with the new assay. Here, the activity of QSOX with GSH and cysteine is barely detectable but becomes significant as the thiol concentration is raised into the millimolar range. This type of upward curvature of enzyme activity has also been observed during the oxidation of β-mercaptoethanol by another flavin-linked sulfhydryl oxidase, augmentin of liver regeneration²⁹, and in the oxidation of glutathione by protein disulfide isomerase³⁰. Panel C of Figure 2.11 presents a probable explanation. The hit-and-run mode of QSOX catalysis⁶ requires that a monothiol substrate first reversibly generate a mixed-disulfide intermediate followed by capture of this species with a second monothiol. This sequential intervention of two thiols leads to the observed upward curvature and to the unexpectedly low reactivity of QSOX at low micromolar levels of monothiol substrates. Hence circulating soluble QSOX1 is unlikely to significantly influence the cysteine or glutathione redox pools in blood directly, although it could contribute to the accumulation of hydrogen peroxide in stored plasma³¹.

2.3.6 The Activity in Serum is due to Bovine QSOX1

In order to ascertain whether the sulfhydryl oxidase activity detected in the AUR assay reflected the presence of QSOX or other unrecognized hydrogen peroxide-generating catalyst, we then tried to purify the activity from bovine serum. The initial step is to separate the oxidase activity from the albumin and globulins that are present at an aggregate concentration of about 70 mg/mL in mammalian sera. At pH 7.5 QSOX1 is positively charged, while albumin and globulins are negatively charged, so

cation-exchange column was applied. Table 2.2 shows that the initial cation-exchange chromatography resulted in a dramatic (~1200-fold) purification of activity. Figure 2.12 A shows a single peak of enzyme activity as judged by the plate-reader assay emerging during a salt gradient. At this stage several bands on SDS-PAGE were evident (Figure 2.13 A). The pooled pale-yellow fractions were then applied to a hydrophobic-interaction column with recovery of a single peak of enzyme activity (Figure 2.12 B), SDS-PAGE have shown only two main bands and Western blot using chicken QSOX1 antibody suggested the band at 63kD is QSOX1 (Figure 2.13 A, B). A second cation-exchange step, in which the protein was eluted from the column using Tris buffer/NaCl at pH 9.4, led to an overall three-step purification of ~5300-fold (Table 2.2). The progress of the purification is shown in the Figure 2.13 C. The resulting preparation was ~90% pure protein and showed a visible spectrum with absorbance peaks at 365 and 456 nm consistent with that of mammalian flavin-linked QSOX enzymes^{28,32} (Figure 2.14).

Trypsin digest of the purified activity (Figure 2.15) followed by MS/MS (see Experimental procedures) led to the identification of bovine QSOX1. The sequence coverage was 59% and the peptides were confined to the short form of the enzyme lacking the ~150-residue C-terminal extension that terminates in a transmembrane helix^{1,3}. This conclusion is also supported by the apparent molecular weight deduced from SDS-PAGE analysis (~63 kDa estimated from Figure 2.15 compared to >82 kDa expected for the full-length form of the oxidase³²). Since only one peak of sulfhydryl oxidase was evident in the chromatographic profiles shown in Figure 2.12, our data show that the sulfhydryl oxidase activity observed in serum is substantially to almost completely due to QSOX1.

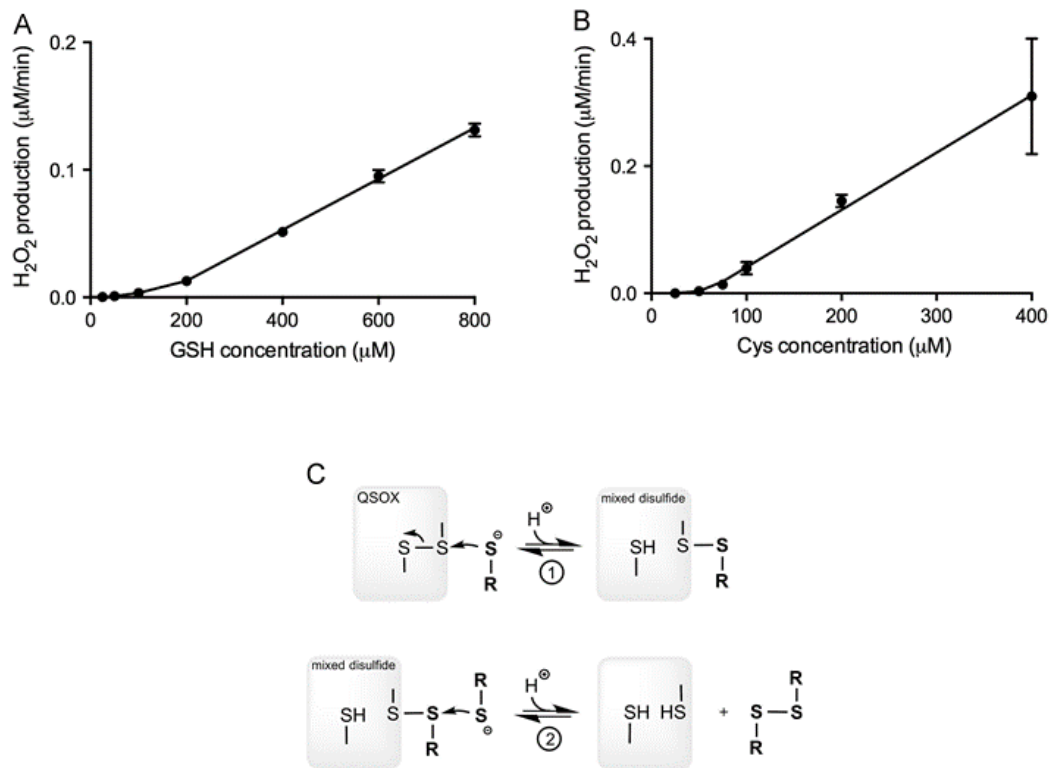


Figure 2.11 **Comparison of the rates of hydrogen peroxide generation by recombinant human QSOX1 in the presence of submillimolar concentrations of glutathione and cysteine.** The data were corrected for background nonenzymatic peroxide generation and for the attenuation of fluorescence signal that is observed in the presence of increasing thiol concentration (Figure 2.4). Panel A and B show data for GSH and cysteine, respectively. Panel C shows that reduction of QSOX by monothiols involves capture of the mixed disulfide intermediate formed in Equilibrium (1), with a second molecule of monothiol depicted in Reaction (2).

Table 2.2 Purification of sulfhydryl oxidase from adult bovine serum.

Step	Total protein (mg)	A ₂₈₀ /A ₄₅₆	Total activity (nmol H ₂ O ₂ /min)	Yield (%)	Specific activity (nmol/min.mg)	Fold purification
Serum (500 ml diluted 5-fold)	31,350	140	4148	100	0.132	1
Cation exchange (salt gradient)	10.3	31	1686	41 ^a	164	1240
Hydrophobic interaction	1.52	22	560	13.5	369	2793
Cation exchange (pH gradient)	0.57	12	402	10	706	5345

^a During loading of the 2.5 L of diluted serum, the cation-exchange column was intentionally overloaded as described under Experimental Procedures. Without such overloading 82% of the sulfhydryl oxidase applied to the column could be recovered from the salt gradient in a single peak of enzyme activity.

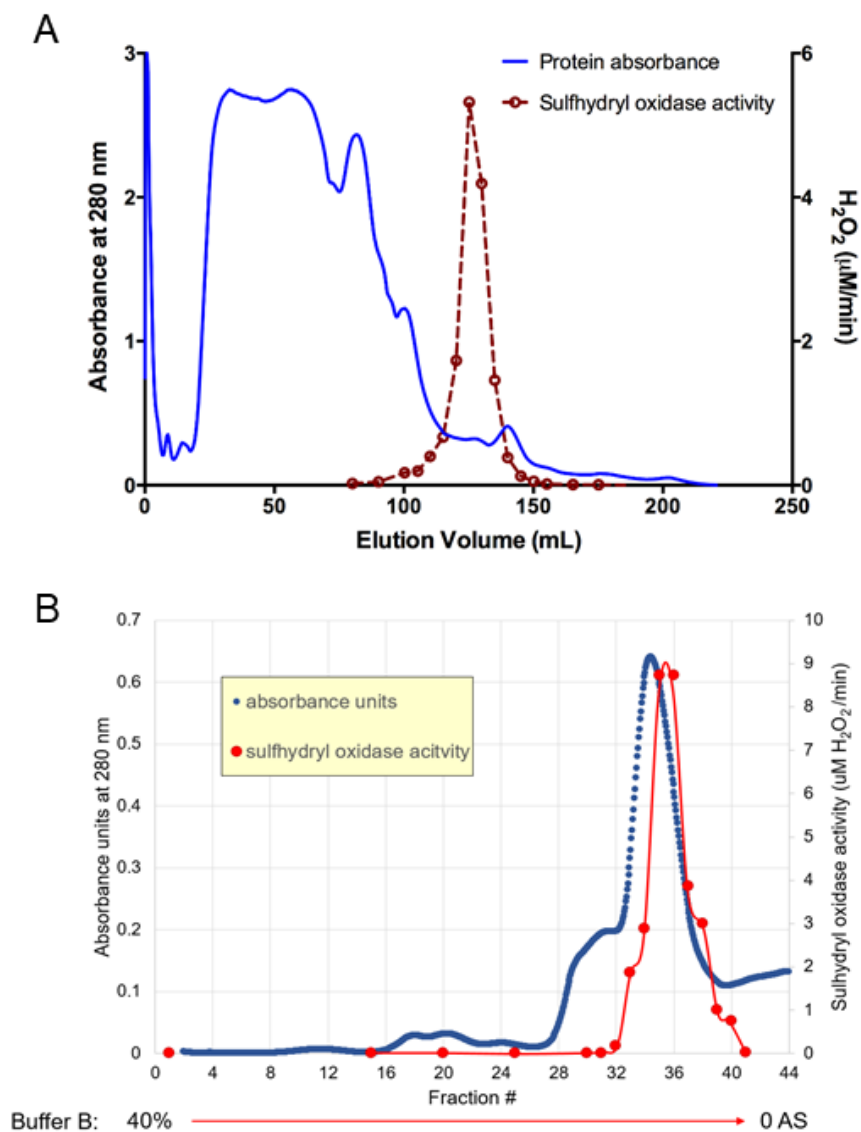


Figure 2.12 **Elution of sulfhydryl oxidase activity on the first cation-exchange column and the HIC column.** The cation-exchange column (Panel A) was developed with an increasing gradient of NaCl and 5 μL from each 5 mL fraction were assayed as described in Experimental procedures. Panel B shows the HIC column. The offset is due to a lag between the flow cell record and the collection of material in the fraction collector.

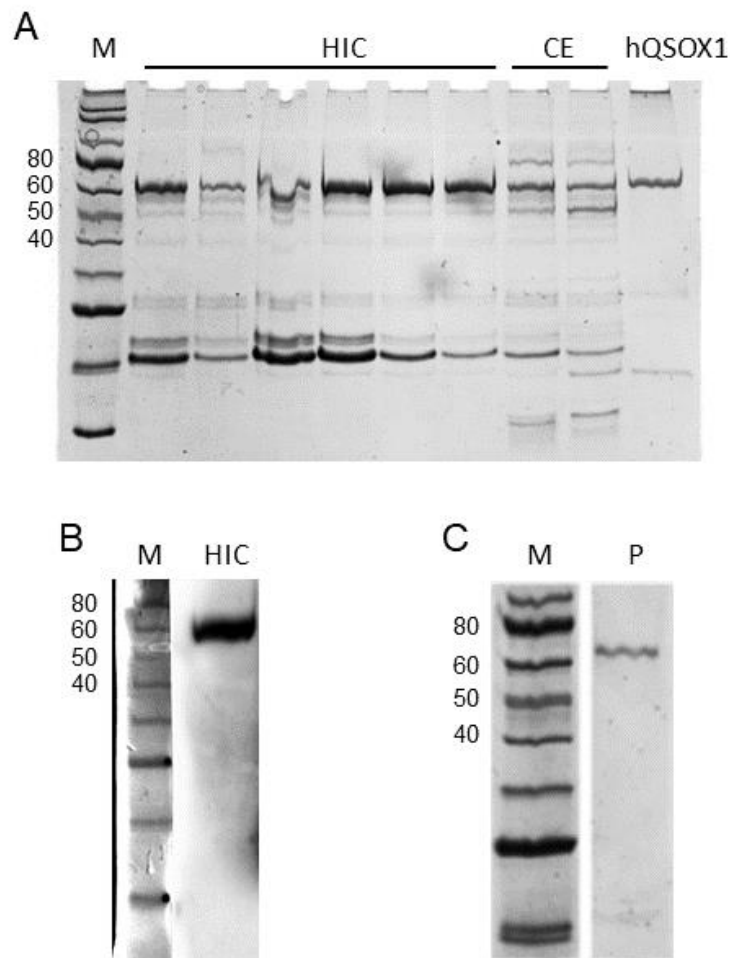


Figure 2.13 **SDS-PAGE of fractions.** Panel A shows an SDS-PAGE analysis of fractions from the first cation-exchange (CE) column and HIC. There are two main bands in HIC. The Western blot analysis of pooled HIC fractions with activity using chicken QSOX1 antibody in panel B suggests the band at 63kD is QSOX1. Panel C shows the SDS-PAGE analysis of the purified protein after the second cation-exchange column.

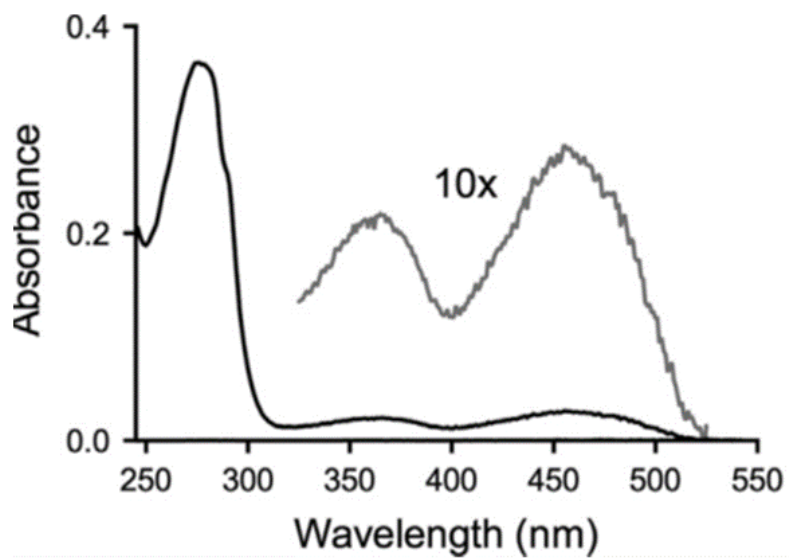


Figure 2.14 **UV-Vis spectrum of the sulfhydryl oxidase purified from adult bovine serum.** The spectrum of the oxidase recorded in 50 mM phosphate buffer, pH 7.5, containing 1 mM EDTA is shown. The dashed line highlights the flavin region of the spectrum.

```

001 MGWCGRGSGP PPSRLLMLLS LLLAVRGAGA APRSALYSSS DPLTLLRADT VRSTVLGSSS
061 AWAVEFFASW CGHCIAFAPT WKALANDVKD WRPALNLAAL DCAEETNSAV CRDFNIPGFP
121 TVRFFKAFSK TGSGTTLVA GADVQTLRER LIDALESHSD TWPPACPPLE PARLEEITGF
181 FARNNEEYLA LIFEKEGSYL GREVTLDLISQ HQGIARRVL NTERDVVNRV GVTNFPSCYL
241 LSRNGSFSRV PALTESRSFY TTYLRKFSGS TSGAVQTAA PATTSAVAPT VWKVADRSKI
301 YMADLESALH YILRIEVGKF SVLEGQRLVA LKKFMAVLAK YFRGRPLVQN FLHSMNDWLK
361 KQQRKKIPYG FFKNALDSRK EGTVIAEKVN WVGCOGSEPH FRGFPCSLWI LFHFLTVQAA
421 QEGVDHPQER AKAQEVLOAI RGYVRRFFC REAGHFEQM ASGSMHRVGS LNSAVLWFWS
481 SHNKVNARLA GAPSEDPQFP KVQWPPREL C SACHNELRGT PVWDLNLIK FLKTHFSPSN
541 IVLDFPSAGP GPWRGAERMA VIPQLI

```

Figure 2.15 **Bovine QSOX1 sequence.** The amino acid sequence of the quiescin sulphydryl oxidase 1 precursor is shown. Peptides identified by MS/MS are underlined, yielding a total coverage of 59% over the 537 residues remaining after cleavage of the signal sequence (shown boxed). The cysteine residues from the two redox-active CxxC motifs are indicated in inverse font.

2.4 Conclusions

This work shows that murine, bovine, and human sera contain significant levels of sulfhydryl oxidase activity. We found similar levels of enzymatic activity between fetal and adult bovine sera. A three-step purification protocol using adult bovine serum showed that this activity reflects circulating, soluble QSOX1. Although the levels of QSOX1 in blood are unlikely to significantly contribute to the oxidation of circulating cysteine and glutathione, there is a wealth of data showing that the redox poise of thiols and disulfides located in exofacial protein domains on a range of blood cells, including platelets and lymphocytes, is a key modulator of biological function³³⁻⁴². For example, protein secretion, adhesion, and integrin-mediated association in platelets are regulated by the thiol/disulfide exchange and redox transformations that are modulated by membrane-bound thiol/disulfide oxidoreductases/isomerases^{33-35,42}. Because QSOX is a direct and facile oxidant of conformationally mobile protein thiols, some of these proteins may be effective substrates of QSOX1 and the activities of this oxidase may oppose those of circulating or membrane-bound reductants.

The finding from mass spectroscopic analyses that the levels of QSOX1 peptides and/or protein in serum have diagnostic applications in pancreatic cancer¹⁰ and in acute decompensated heart failure¹⁶ suggests that these approaches may be complemented by the simple and cost-effective QSOX assay described here. More generally, the observation that QSOX1 enzyme activity is found in blood plasma of all developmental stages suggests that renewed consideration should be directed toward the origins, substrate specificity, and physiological roles of this catalytically most proficient stand-alone oxidant of protein and peptide thiols.

REFERENCES

- 1 Kodali, V. K. & Thorpe, C. Oxidative protein folding and the Quiescin-sulfhydryl oxidase family of flavoproteins. *Antioxid Redox Signal* **13**, 1217-1230, doi:10.1089/ars.2010.3098 (2010).
- 2 Liebert, M. A., Coppock, D. L. & Thorpe, C. Multidomain Flavin-Dependent Sulfhydryl Oxidases. **8** (2006).
- 3 Thorpe, C. & Coppock, D. L. Generating disulfides in multicellular organisms: emerging roles for a new flavoprotein family. *J Biol Chem* **282**, 13929-13933, doi:10.1074/jbc.R600037200 (2007).
- 4 Thorpe, C. *et al.* Sulfhydryl oxidases: emerging catalysts of protein disulfide bond formation in eukaryotes. *Arch Biochem Biophys* **405**, 1-12 (2002).
- 5 Hooper, K. L., Sheasley, S. L., Gilbert, H. F. & Thorpe, C. Sulfhydryl oxidase from egg white. A facile catalyst for disulfide bond formation in proteins and peptides. *J Biol Chem* **274**, 22147-22150 (1999).
- 6 Coddling, J. a., Israel, B. a. & Thorpe, C. Protein substrate discrimination in the quiescin sulfhydryl oxidase (QSOX) family. *Biochemistry* **51**, 4226-4235, doi:10.1021/bi300394w (2012).
- 7 Cline, D. J., Thorpe, C. & Schneider, J. P. Structure-based design of a fluorimetric redox active peptide probe. *Analytical Biochemistry* **325**, 144-150, doi:10.1016/j.ab.2003.10.014 (2004).
- 8 Song, H. *et al.* Loss of Nkx3.1 leads to the activation of discrete downstream target genes during prostate tumorigenesis. *Oncogene* **28**, 3307-3319, doi:10.1038/onc.2009.181 (2009).
- 9 Ouyang, X., Dewese, T. L., Nelson, W. G. & Abate-shen, C. Loss-of-Function of Nkx3 . 1 Promotes Increased Oxidative Damage in Prostate Carcinogenesis Damage in Prostate Carcinogenesis. 6773-6779 (2005).
- 10 Antwi, K. *et al.* Analysis of the Plasma Peptidome from Pancreas Cancer Patients Connects a Peptide in Plasma to Overexpression of the Parent Protein in Tumors research articles. 4722-4731 (2009).
- 11 Katchman, B. a. *et al.* Expression of quiescin sulfhydryl oxidase 1 is associated with a highly invasive phenotype and correlates with a poor prognosis in Luminal B breast cancer. *Breast cancer research : BCR* **15**, R28, doi:10.1186/bcr3407 (2013).
- 12 Lake, D. F. & Faigel, D. O. The Emerging Role of QSOX1 in Cancer. *Antioxidants & Redox Signaling* **21**, 485-496, doi:10.1089/ars.2013.5572 (2014).
- 13 Grossman, I., Alon, A., Ilani, T. & Fass, D. An inhibitory antibody blocks the first step in the dithiol/disulfide relay mechanism of the enzyme QSOX1. *Journal of molecular biology* **425**, 4366-4378, doi:10.1016/j.jmb.2013.07.011 (2013).

- 14 Katchman, B. a. *et al.* Quiescin sulfhydryl oxidase 1 promotes invasion of pancreatic tumor cells mediated by matrix metalloproteinases. *Molecular cancer research : MCR* **9**, 1621-1631, doi:10.1158/1541-7786.MCR-11-0018 (2011).
- 15 Ilani, T. *et al.* A secreted disulfide catalyst controls extracellular matrix composition and function. *Science (New York, N.Y.)* **341**, 74-76, doi:10.1126/science.1238279 (2013).
- 16 Mebazaa, A. *et al.* Unbiased plasma proteomics for novel diagnostic biomarkers in cardiovascular disease: identification of quiescin Q6 as a candidate biomarker of acutely decompensated heart failure. *European heart journal* **33**, 2317-2324, doi:10.1093/eurheartj/ehs162 (2012).
- 17 Hooper, K. L., Joneja, B., White, H. B. & Thorpe, C. A sulfhydryl oxidase from chicken egg white. *Journal of Biological Chemistry* **271**, 30510-30516, doi:10.1074/jbc.271.48.30510 (1996).
- 18 Raje, S., Glynn, N. M. & Thorpe, C. A continuous fluorescence assay for sulfhydryl oxidase. *Analytical Biochemistry* **307**, 266-272, doi:10.1016/S0003-2697(02)00050-7 (2002).
- 19 Simeonov, A. *et al.* Fluorescence spectroscopic profiling of compound libraries. *Journal of Medicinal Chemistry* **51**, 2363-2371, doi:10.1021/jm701301m (2008).
- 20 Zhou, M., Diwu, Z., Panchuk-Voloshina, N. & Haugland, R. P. A stable nonfluorescent derivative of resorufin for the fluorometric determination of trace hydrogen peroxide: Applications in detecting the activity of phagocyte NADPH oxidase and other oxidases. *Analytical Biochemistry* **253**, 162-168, doi:10.1006/abio.1997.2391 (1997).
- 21 Zanata, S. M. *et al.* High levels of active quiescin Q6 sulfhydryl oxidase (QSOX) are selectively present in fetal serum. *Redox report : communications in free radical research* **10**, 319-323, doi:10.1179/135100005X83699 (2005).
- 22 Summers, F. A., Zhao, B., Ganini, D. & Mason, R. P. Photooxidation of amplex red to resorufin: Implications of exposing the amplex red assay to light. *Methods in enzymology* **526**, 1-17, doi:10.1016/B978-0-12-405883-5.00001-6 (2013).
- 23 Munday, R., Munday, C. M. & Winterbourn, C. C. Inhibition of copper-catalyzed cysteine oxidation by nanomolar concentrations of iron salts. *Free Radical Biology and Medicine* **36**, 757-764, doi:10.1016/j.freeradbiomed.2003.12.015 (2004).
- 24 Fasano, M. *et al.* The extraordinary ligand binding properties of human serum albumin. *IUBMB life* **57**, 787-796, doi:10.1080/15216540500404093 (2005).
- 25 Turell, L., Radi, R. & Alvarez, B. The thiol pool in human plasma: The central contribution of albumin to redox processes. *Free Radical Biology and Medicine* **65**, 244-253, doi:10.1016/j.freeradbiomed.2013.05.050 (2013).

- 26 Jones, D. P. & Liang, Y. Measuring the poise of thiol/disulfide couples in vivo. *Free Radical Biology and Medicine* **47**, 1329-1338, doi:10.1016/j.freeradbiomed.2009.08.021 (2009).
- 27 Joneja, B. A Sulfhydryl Oxidase from Chicken Egg White. *Journal of Biological Chemistry* **271**, 30510-30516, doi:10.1074/jbc.271.48.30510 (1996).
- 28 Heckler, E. J., Alon, A., Fass, D. & Thorpe, C. Human quiescin-sulfhydryl oxidase, QSOX1: Probing internal redox steps by mutagenesis. *Biochemistry* **47**, 4955-4963, doi:10.1021/bi702522q (2008).
- 29 Schaefer-Ramadan, S., Gannon, S. A. & Thorpe, C. Human augments liver regeneration: Probing the catalytic mechanism of a flavin-dependent sulfhydryl oxidase. *Biochemistry* **52**, 8323-8332, doi:10.1021/bi401305w (2013).
- 30 Lappi, A. K. & Ruddock, L. W. Reexamination of the role of interplay between glutathione and protein disulfide isomerase. *Journal of Molecular Biology* **409**, 238-249, doi:10.1016/j.jmb.2011.03.024 (2011).
- 31 Halliwell, B., Clement, M. V., Ramalingam, J. & Long, L. H. Hydrogen peroxide. Ubiquitous in cell culture and in vivo? *IUBMB Life* **50**, 251-257, doi:10.1080/15216540051080930 (2000).
- 32 Jaje, J. *et al.* A flavin-dependent sulfhydryl oxidase in bovine milk. *Biochemistry* **46**, 13031-13040, doi:10.1021/bi7016975 (2007).
- 33 Essex, D. W. Redox control of platelet function. *Antioxidants & redox signaling* **11**, 1191-1225, doi:10.1089/ARS.2008.2322 (2009).
- 34 Jordan, P. A. & Gibbins, J. M. Extracellular Disulfide Exchange and the Regulation of Cellular Function. *Antioxidants & Redox Signaling* **8**, 312-324, doi:10.1089/ars.2006.8.312 (2006).
- 35 Matthias, L. J. & Hogg, P. J. Redox Control on the Cell Surface: Implications for HIV-1 Entry. *Antioxidants & Redox Signaling* **5**, 133-138, doi:10.1089/152308603321223621 (2003).
- 36 Sahaf, B., Heydari, K., Herzenberg, L. A. & Herzenberg, L. A. Lymphocyte surface thiol levels. (2002).
- 37 Yan, Z., Garg, S. K., Kipnis, J. & Banerjee, R. Extracellular redox modulation by regulatory T cells. **5**, 721-723, doi:10.1038/nchembio.212 (2009).
- 38 Go, Y. M. & Jones, D. P. Cysteine/cystine redox signaling in cardiovascular disease. *Free Radical Biology and Medicine* **50**, 495-509, doi:10.1016/j.freeradbiomed.2010.11.029 (2011).
- 39 Acosta-Serrano, A. *et al.* The surface coat of procyclic Trypanosoma brucei: Programmed expression and proteolytic cleavage of procyclin in the tsetse fly. *Proceedings of the National Academy of Sciences* **98**, 1513-1518, doi:10.1073/pnas.98.4.1513 (2001).
- 40 Metcalfe, C., Cresswell, P., Ciaccia, L., Thomas, B. & Barclay, A. N. Labile disulfide bonds are common at the leucocyte cell surface. *Open Biology* **1**, 110010-110010, doi:10.1098/rsob.110010 (2011).

- 41 Stegmann, M., Metcalfe, C. & Barclay, A. N. Immunoregulation through membrane proteins modified by reducing conditions induced by immune reactions. *European Journal of Immunology* **43**, 15-21, doi:10.1002/eji.201242849 (2013).
- 42 Swiatkowska, M. *et al.* Ero1 α is expressed on blood platelets in association with protein-disulfide isomerase and contributes to redox-controlled remodeling of α IIb β 3. *Journal of Biological Chemistry* **285**, 29874-29883, doi:10.1074/jbc.M109.092486 (2010).

Chapter 3

VISUALIZATION OF THE THIOL/DISULFIDE REDOX STATE OF THE MAMMALIAN CELL SURFACE USING CONFOCAL MICROSCOPY: METHODS AND APPLICATIONS

3.1 Introduction

As we discussed in previous chapters, the thiol/disulfide (SH/SS) redox state of the mammalian cell surface plays critical roles in modulation of different cell behaviors including cell adhesion¹, migration², proliferation³, metastasis^{4,5}, and viral fusion⁶⁻⁸. Extending from the cell surface, the extracellular matrix (ECM) is an additional locus for potentially interacting SH/SS redox couples that impact cellular behavior. To better understand the extracellular SH/SS redox states, we hope to develop a global method to independently visualize protein thiols and disulfides.

Several earlier methods have been used for the detection of free SH groups on the cell surface. The most widely used is the DTNB assay⁹⁻¹². Figure 3.1 shows the scheme. Briefly, washed cells are incubated in solution containing DTNB for a time interval and the yellow color is recorded. However, this method is not exclusive to the cell surface; it reflects both exofacial thiol and thiol containing molecules secreted from cells¹³ (also data from our lab, not shown). A variety of alternate methods involve covalently labeling of free thiols with maleimides or other alkylating agents. Commercially available impermeable fluorescent thiol-reactive probes, such as Alexa Fluor dyes, followed by fluorescence-activated cell sorting (FACS) were used in several investigations¹⁴⁻¹⁶. While this approach is sensitive and rapid, it is important to

note that this assay does not give spatial information about the labeling. In particular, FACS analysis could not distinguish surface labeling from dye internalization. In an interesting study Laragione et al.⁹ examined redox-sensitive thiols at the surface of Chinese Hamster Ovary (CHO) cells. They used Oregon green as an impermeant maleimide visualizing the cells with confocal microscopy. However under the conditions of their experiment (40 μ M maleimide incubated for 20 min at 37 °C) significant internalization of the label will likely occur by endocytic trafficking (see later). The study was further unable to quantitate SH labeling at the cell surface. Another strategy to examine thiols on the cell surface is to use a non-fluorescent SH alkylating agent, e.g. biotinylated iodoacetamide (BIAM), and then isolate the plasma membrane fraction of cells. Laragione et al.⁹ used the BIAM-labeling method followed by ELISA and proteomics to examine the effects of oxidants and antioxidants on the SH groups at the surface of CHO cells. Skalska et al.¹⁶ also utilized this approach in their investigations of the anticancer effects of parthenolide during the targeting of exofacial SH groups in Granta mantle lymphoma cells. Again, cellular location and ratiometric data are not accessible in this study.

In this chapter we describe ratiometric fluorescence imaging methods for surface thiols and disulfides and their applications to studying a range of cellular phenomena. In the last chapter we briefly show that these ratiometric confocal microscopy methods can be extended to multicellular organisms and biomaterials. All these procedures are amenable for future super-resolution studies.

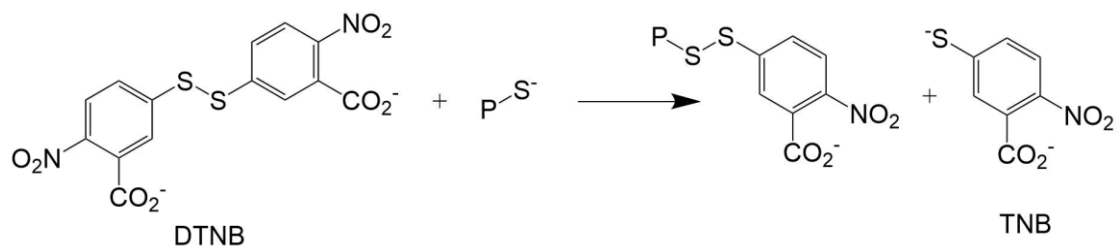


Figure 3.1 **Scheme of the reaction between DTNB (5,5'-Dithiobis[2-nitrobenzoic acid]) and a thiolate.** P represents a protein. TNB (2-nitro-5-mercaptobenzoic acid) is a yellow compound, $\lambda_{\max}=412$ nm at neutral pH values.

3.2 Experimental Procedures

3.2.1 Materials and Reagents

Sulfo-Cy3B-maleimide was obtained from GE Healthcare and sulfo-Cy5-maleimide and sulfo-Cy5-NHS ester was from Lumiprobe. Stock solutions of maleimide were prepared in water and stored at -80 °C. Concentration of dyes were measured spectrophotometrically using the following extinction coefficient: sulfo-Cy3B-maleimide $\epsilon_{558}=130,000 \text{ M}^{-1}\text{cm}^{-1}$, sulfo-Cy5-maleimide $\epsilon_{646}=271,000 \text{ M}^{-1}\text{cm}^{-1}$. Methyl-PEG₂₄-maleimide was from Thermo Scientific; Hoechst 33342 was from Molecular Probes; Fluoromount-G mounting media was purchased from SouthernBiotech. Poly-D-lysine (molecular weight 70,000-150,000) was obtained from Sigma, and methanol-free paraformaldehyde (PFA) was from Pierce. The following cell lines were generous gifts from colleagues at the University of Delaware: human embryonic kidney cell line (HEK293T) and human prostate adenocarcinoma cells (LNCaP) from Dr. John Koh; human cervix epithelial cell line (HeLa) from Dr. Jeff Caplan from Delaware Biotech Institute; human glioblastoma cell line (U-118) from Dr. Deni Galileo; mouse macrophage (J774A.1) from Dr. Catherine Grimes. The mycoplasma Detection Kit was from Lonza. Activated thiol Sepharose 4B was obtained from GE Healthcare. High performance glass coverslips (22 mm x 22 mm, D=0.17 mm) were from Zeiss. Cell culture consumables were obtained from Stellar Scientific.

3.2.2 Mammalian Cell Culture

HEK293T, HeLa cells were cultured in Eagle's Minimum Essential Medium from Corning containing 1.5 g/L sodium bicarbonate, 2 mM L-glutamine, and sodium pyruvate. The media was further supplemented with 10% fetal bovine serum (FBS, from Atlanta Biologicals) and 100 U penicillin-streptomycin (Sigma). Cells were grown at 37 °C in a 5% CO₂ humidified incubator. U-118 and J774A cells were maintained in high-glucose Dulbecco's modified Eagle medium (DMEM, from Sigma). LNCaP cells were cultured in RPMI media (Corning).

3.2.3 Chemical Staining

Cells were seeded on Poly-D-lysine coated sterile high-performance glass coverslips in 6-well plates at 2×10^5 cells per chamber. After 24 or 48 hours (approaching ~70% confluency) cells were washed 3 times with Dulbecco's Phosphate-Buffered Salt Solution (DPBS, from Corning) and fixed with 2% methanol-free PFA at 4 °C for 20 min. For SH/SS staining, after 3 washes in DPBS, cells were incubated in the dark with 1 μM sulfo-Cy3B-maleimide and 10 μM methyl-PEG₂₄-maleimide in DPBS at room temperature for 10 min. After 3 washes in DPBS, 5 mM tris (2-carboxyethyl) phosphine (TCEP) in DPBS (adjusted to pH 7.4) was applied on cells at room temperature for 10 min. After 3 washes the released SH groups were stained with 1 μM sulfo-Cy5-maleimide and 10 μM methyl-PEG₂₄-maleimide treatment again for 10 min at room temperature in the dark. Following 3 washes, cell nuclei were stained with DAPI or Hoechst 33342 and the slides were mounted with Fluoromount-G sealing the edges of the slide with nail polish. For SH/NH₂ staining, after 3 washes in DPBS, cells were incubated in the dark at room temperature with 1

μM sulfo-Cy3B-maleimide mixed with 10 μM methyl-PEG₂₄-maleimide and 1 μM sulfo-Cy5-NHS ester. Procedures for cell nuclei staining and mounting were as above.

3.2.4 Fluorescent Beads Construction

Activated thiol sepharose 4B beads (0.2 g freeze dried powder) were suspended in distilled water to give a 0.8 mL slurry. Following swelling the slurry was loaded into a small empty column and washed with 5 times of 2 mL aliquots of PBS. The solution phase was then replaced with 10 mM DTT in PBS and incubated for 1 h at room temperature. The treated beads were then washed by applying PBS to the column until the eluates were thiol free (as judged by DTNB). The beads were resuspended in PBS and evenly aliquoted into 5 tubes, so that each contains 0.16 mL beads (equivalent to ~ 0.16 μmole thiols). Then, 16, 32, 64, 128, 256 pmoles of a 1:1 ratio Cy3B-maleimide and Cy5-maleimide in PBS was quickly added into each tube, amounting to 16, 32, 64, 128, 256 pmoles of the maleimides. After 30 min of incubation with occasional vortex, all the dye-maleimides were captured on the beads. The large excess of unreacted bead -SH groups were then alkylated with 10 mM NEM, followed by washing in Eppendorf tubes with PBS. Beads with ratios of 4:0, 3:1, 2:2, 1:3, 0:4 of Cy3B to Cy5 were also prepared using a total of 1.6 nmoles of maleimides.

3.2.5 Treatment with Macromolecular Crowding Agents

Cells were seeded on sterile high-performance glass coverslips in 6-well plates at 2×10^5 cells per chamber. After 24 h incubation at 37 °C and 5% CO₂, growth media

were replaced with media supplemented, where indicated, with the following individual reagents serving as macromolecular crowding agents (100 $\mu\text{g}/\text{mL}$ D \times S 500 kD, 25 mg/mL Ficoll 400 kD, 80 mg/mL BSA, 0-50 $\mu\text{g}/\text{mL}$ polystyrene sulfonate (PSS) 200 kD, or 75 $\mu\text{g}/\text{mL}$ carrageenan). Cells were then cultured for another 24 h. In some trials, cells were seeded on glass coverslips for 48 h, fixed with 2% paraformaldehyde, and then treated with PBS with or without macromolecular crowders.

3.2.6 Surface Dye Internalization

Cells were seeded on glass coverslips for 48 hours (to 70-80% confluence) then washed 3 times with DPBS. Cells were then exposed to treatments described later and incubated with 1 μM impermeant fluorescent probes conjugated with maleimide or NHS ester probes at 37 °C in a 5% CO₂ humidified incubator. Some cells were washed to remove unbound maleimide and then returned to the incubator. At the indicated time intervals cells were fixed with 2% paraformaldehyde.

3.2.7 DTNB Assay

Cells were seeded on sterile dishes, after incubated in growth media for 48 h (achieving 80% confluence). After 3 rinses with phenol red free DMEM, cells were incubated with 2 mL DMEM at room temperature for 5, 15, and 60 min. At these times 100 μL media were taken and mixed with DTNB to give a final concentration of 200 μM . The released 2-nitro-5-thiobenzoic acid was measured at 412 nm using an extinction coefficient of 14,150 $\text{M}^{-1}\text{cm}^{-1}$.

3.2.8 Membrane Fraction Collection, Sodium Dodecyl Sulfate Polyacrylamide Gel Electrophoresis (SDS-PAGE)

Cells were seeded in 10 mm dishes for 48 h (achieving 80% confluence) and treated with or without 2 mL of 25 μ g/mL PSS in PBS at room temperature for 10 min. After washing with 12 mL of ice cold PBS, a 2 mL volume of 1 μ M sulfo-Cy5-maleimide in cold PBS was applied for 10 min incubation. Washed cells were then scraped from the dishes and the suspension (2 mL) was centrifuged at 200 g. The cells were resuspended in 1 mL of cold homogenization buffer (10 mM HEPES, 250 mM sucrose, pH 7.4) with protease inhibitor and homogenized using 30 strokes of a Dounce homogenizer. The extracts were centrifuged at 1000 g for 10 min to sediment nuclei and the supernatants were recentrifuged at 16,000 g for 10 min to remove mitochondria, lysosome and peroxisomes. Supernatants were finally in a Beckman centrifuge subject to ultracentrifugation for 3 h at 100,000 g at 4 °C. Sedimented plasma membrane pellets were collected and washed with PBS, and then solubilized in PBS containing 30 mM CHAPS or 6 mM SDS. After 1 h dissolved membrane solutions were boiled for 10 min in Laemmli buffer containing 5% β -mercaptoethanol and analysed by 10% acrylamide SDS-PAGE at 120 V using a Bio-Rad mini gel system. The gel was fixed with 7% acetic acid in 40% methanol for 1 h and the labelled band was visualized using a FluorChem Q Imaging System (Excitation 632/22 nm, Emission filter 699/62 nm). Subsequently, the gel was stained with Coomassie blue for 30 min and destained overnight.

3.2.9 Microscope Imaging and Image Analysis

Fluorescence images were acquired using a Zeiss LSM 780 upright confocal microscope in the Biological Department at the University of Delaware. The laser and

filter sets are as follows: for Cy3B fluorophore, excitation at 561 nm, emission at 560-630 nm. For Cy5 fluorophore, excitation at 633 nm, emission at 637-758 nm. A 40x oil objective was used. Zeiss Zen software was used for image acquisition.

To estimate the level of labeled thiols and proteins on cell surface, images were analyzed using ImageJ (National Institutes of Health, USA), the green channel of a 16-bit RGB image was used. For each scanned section, three representative images were selected. Obvious artifacts in each image were discarded. In each image, 4-5 cell membrane areas of interest were picked using selection tools, and the area-integrated intensity was calculated for both channels. Then a background region was selected to yield a mean grey value. The following formula was used to calculate the corrected cell membrane area fluorescence (CTCF). Notice that each CTCF is area dependent, but the ratio of the two channels normalizes for this.

CTCF = Integrated Density of selection – (Area of selection x Mean fluorescence of background readings)

3.2.10 Platerreader Experiments Proving the Effects of PSS or β -ME on Cy3B Dye

Different combination of PBS, Cy3B-maleimide and β -ME were added in each well in a black 96-well plate and mixed well. The plate was then read by the plate reader (BMG POLARstar OMEGA) at excitation 544 nm and emission 590-10 nm for 30 min, and the first 2 min data were calculated.

3.3 Results and Discussion

3.3.1 Cell Surface SH/SS and SH/NH₂ Labeling

Figure 3.2 shows the structure of four membrane impermeable protein-labeling reagents used in this work. The three maleimides target thiol groups. When normalization to total protein at the surface is needed, the NHS ester was used. All fluorophores are sulfonated and they are found to label the cell surface and the extracellular matrix (see below).

Two-color strategies for evaluating surface SH/SS or SH/NH₂ ratios are shown in Figure 3.3. In panel A is the SH/SS labeling scheme. Two cell membrane impermeant fluorescent maleimides (e.g. sulfo-cyanine3B (Cy3B) and sulfo-cyanine5 (Cy5), or their equivalents) were used. Figure 3.3 B shows the SH/NH₂ labeling scheme; in this case the sulfo-Cy3B-maleimide and sulfo-Cy5-NHS ester were routinely used. It should be noted that in most cases the cells were fixed with 2% paraformaldehyde (PFA) before staining. These lightly-fixed cells are still able to exclude the sulfonated fluorescent dyes as shown later.

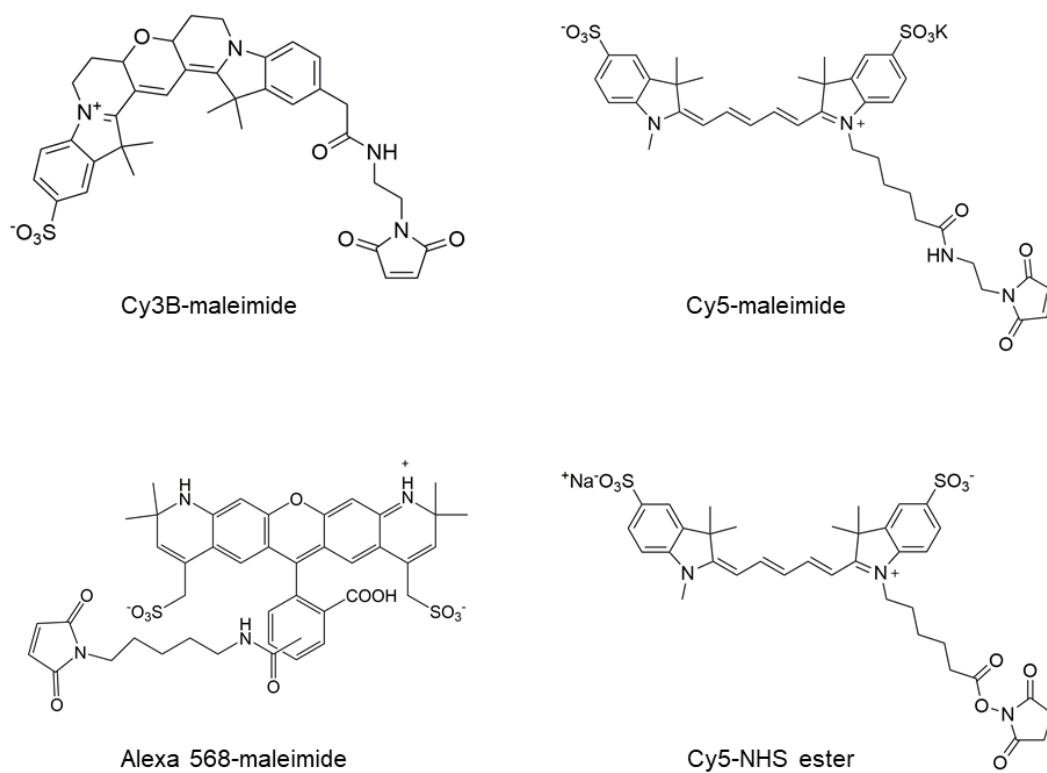


Figure 3.2 **Structures of the fluorescent reagents used in this work.** These sulfonated reagents are membrane impermeant and therefore exclusively label the cell surface and extracellular matrix components.

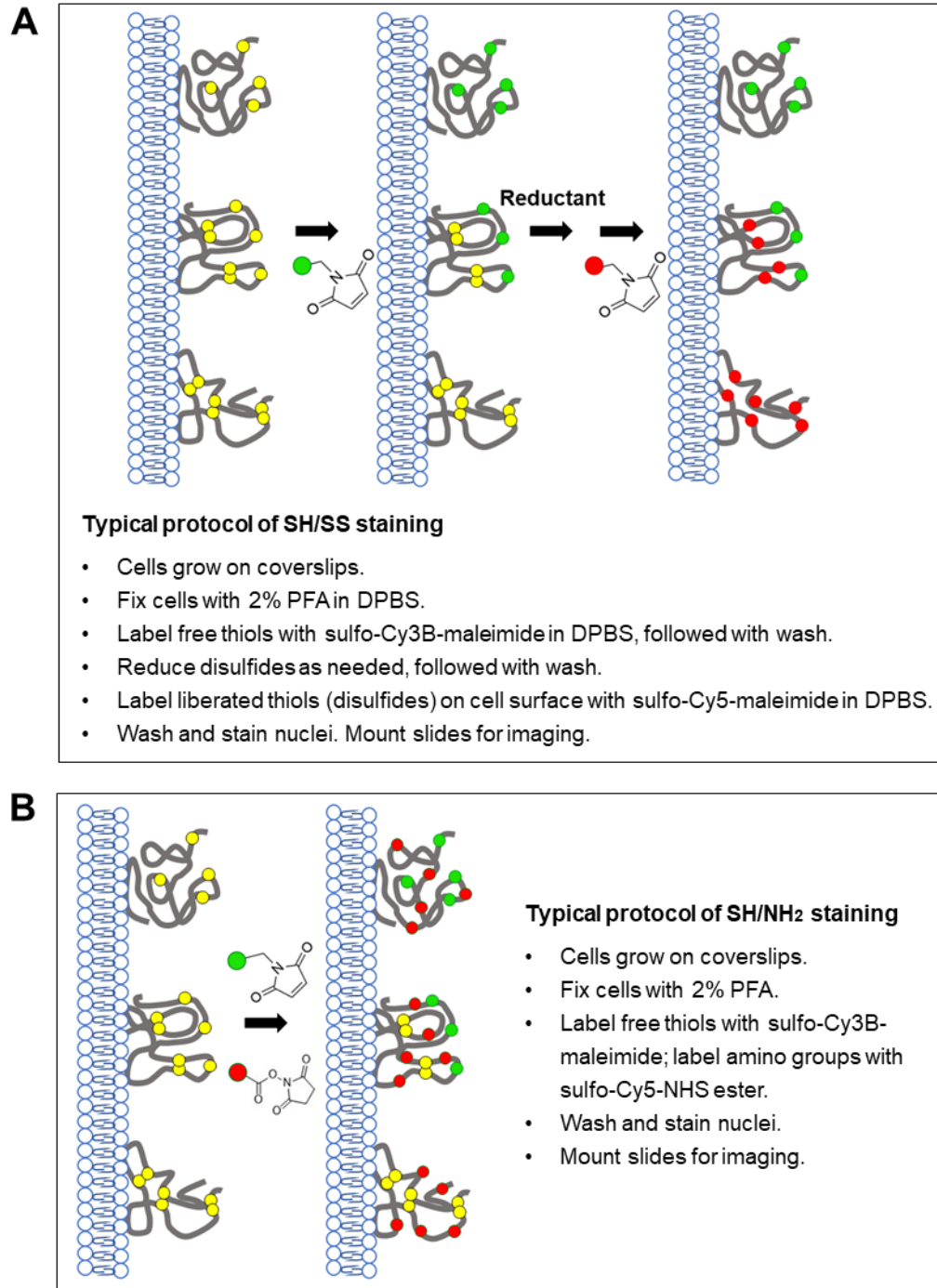


Figure 3.3 **Schemes of cell surface labeling.** Panel A shows the SH/SS labeling. Single yellow spheres represent free thiols while double yellow spheres represent disulfide bonds. Panel B shows the SH/NH₂ staining (see Experimental procedures).

These methods are applicable to all cell types investigated. Figure 3.4 demonstrates SH/SS labeling on three cell lines (HeLa, LNCaP and J774A.1). Here, the green channel shows Cy3B-maleimide labeling of free SH, and the red channel shows Cy5-maleimide labeling of liberated thiols after reduction of surface disulfides with 5 mM of the membrane-impermeant tris(carboxyethyl)phosphine (TCEP). Note that the cell surface is cleanly delineated in these images. In contrast compromised cells, that have lost plasma membrane integrity, allow the maleimide access to the enormous intracellular content of -SH residues. This is shown in Figure 3.5. To avoid proximity-based self-quenching of fluorescence, a non-permeant methyl-PEG₂₄-maleimide conjugate was applied to “dilute” each fluorescent maleimide with a 10-fold molar ratio. However, we found that the effect of this “dilution” is not significant at low ratio (data not shown). Images of SH/NH₂ labeled (scheme in Figure 3.3 B) cells will be shown in later sections.

3.3.2 The Maleimide Dye Staining is Thiol Specific

Several approaches were taken to show the SH specificity of the labeling. Figure 3.6 shows one experiment. The maleimide function of Cy3B was first reacted with a stoichiometric amount of β -mercaptoethanol (see Experimental procedures and the schematic structure in Fig 3.6 A). This pre-deactivated dye failed to stain the cells significantly (Figure 3.6 B). We have also used plate reader assay to show that β -mercaptoethanol treatment does not inhibit the Cy3B fluorescence (data not shown). We also used N-ethylmaleimide (NEM) pretreatment to first label cell surface SH groups (see Experimental procedures). No subsequent staining of the surface with the fluorescent maleimide was evident (Figure 3.7). A third strategy to verify that the

method is responsive to surface SH status is to use DTNB pretreatment. DTNB oxidizes free thiols, making them unavailable for subsequent staining. Figure 3.8 shows that after the DTNB treatment the cell surface labeling is prevented. Thus, staining is not due to a non-specific binding of the dye to the cell surface.

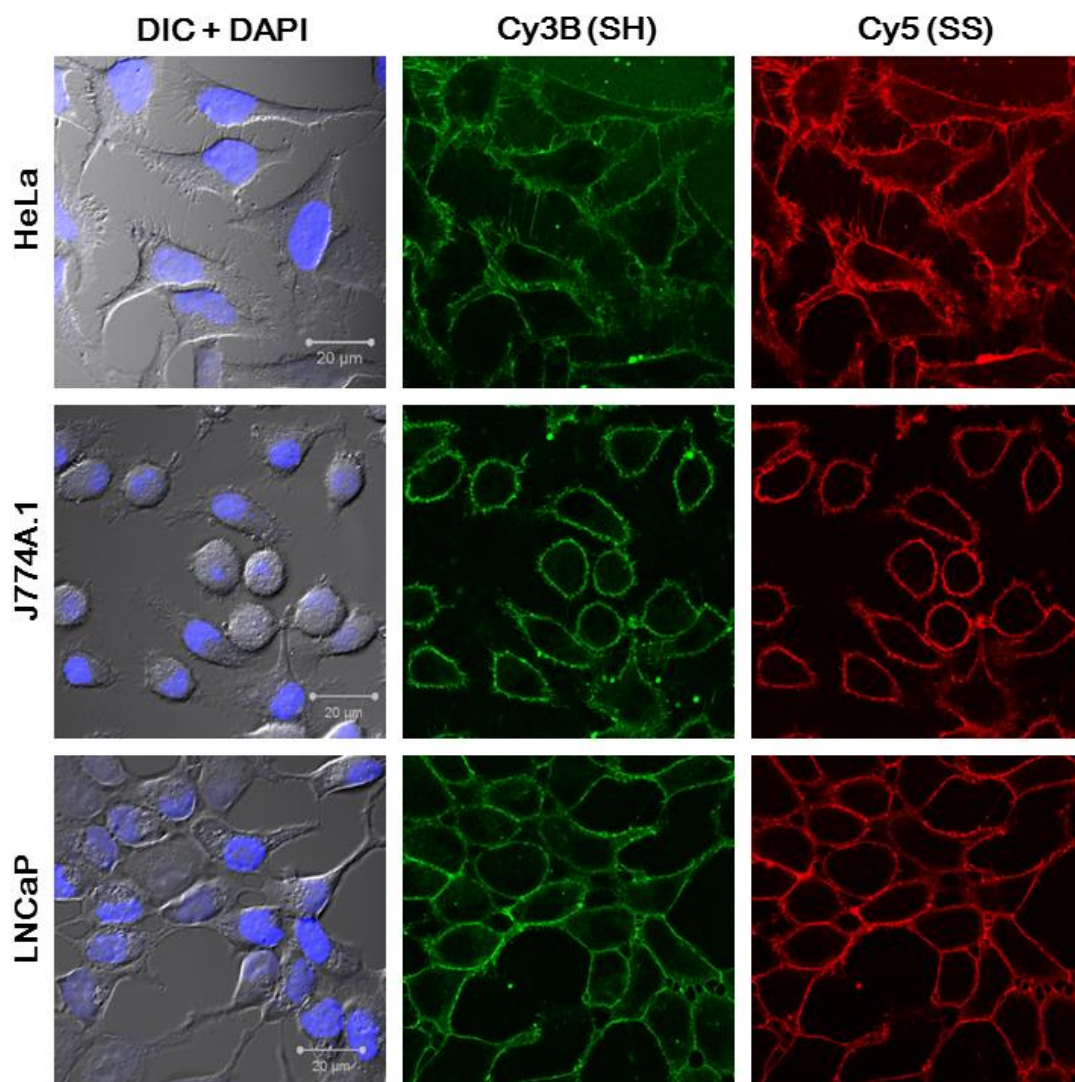


Figure 3.4 **SH/SS redox state of the cell surface of 3 cell lines.** The green channel indicates surface thiol staining and the red channel shows the surface disulfide staining. The nuclei are visualized with DAPI (blue). The differential interference contrast (DIC) channel shows the cell outlines at the left of the Figure. The intensities of green and red signals are adjusted here for ease of visualization.

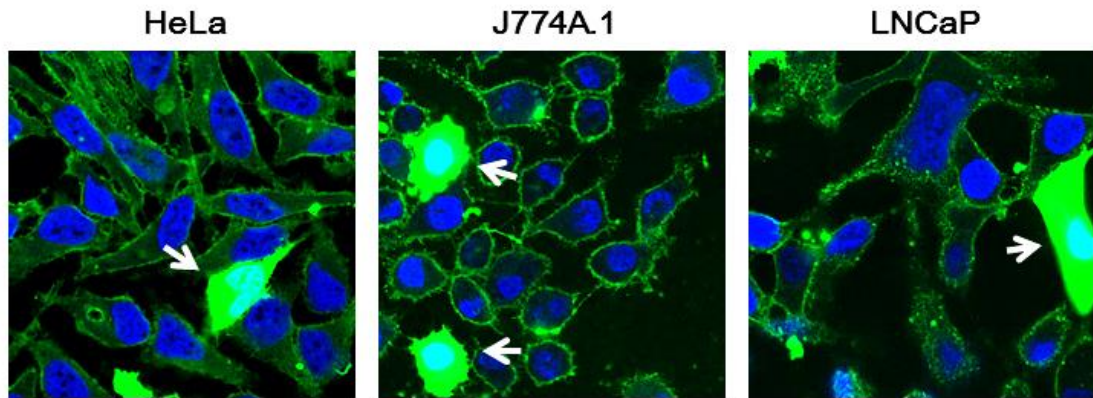


Figure 3.5 **Cells lacking a functional plasma membrane stain uniformly with sulfo-Cy3B-maleimide.** The white arrows show compromised cells that are permeant to fluorescent dyes. The nuclei are visualized with DAPI (blue).

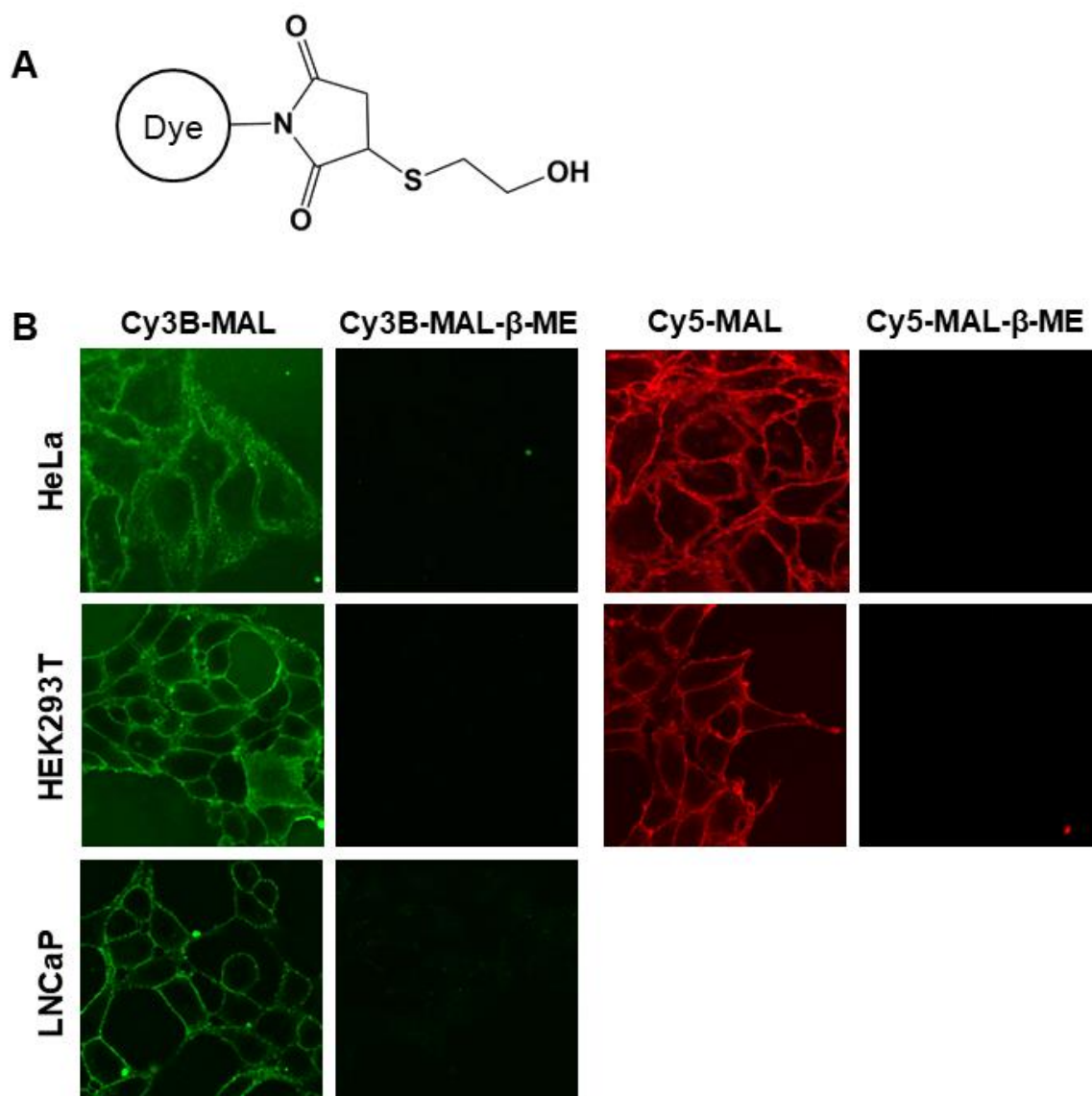


Figure 3.6 **Inactivated maleimide dyes cannot label cell surface thiols.** Panel A shows a schematic depiction of β -mercaptoethanol treated maleimide-dye conjugate. The maleimide dyes were pre-incubated with β -mercaptoethanol in a 1:1 molar ratio. Panel B shows the unmodified maleimide dye leads to clear cell surface staining while the β -mercaptoethanol-treated dyes cannot label the cells. Each laser intensity was maintained constant for comparison between non-treated and β -mercaptoethanol images. Signal intensities are increased uniformly for ease of visualization.

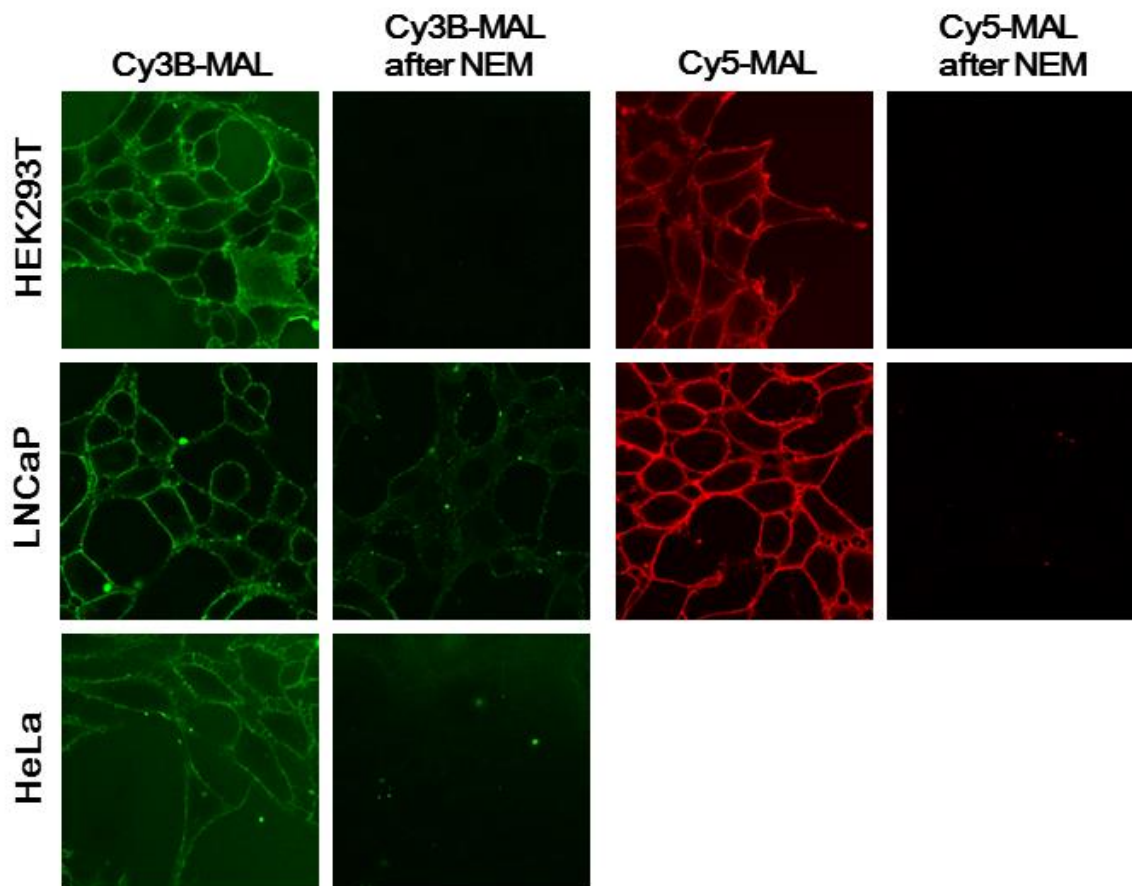


Figure 3.7 **Pretreatment with N-ethylmaleimide (NEM) prevents subsequent SH labeling on cell surfaces using either Cy3B or Cy5 maleimides.** NEM (1 mM) in DPBS was applied to the fixed cells for 10 min before the maleimide dyes were added. The NEM pretreatment significantly decrease the thiol labeling of the cell surface. Each laser intensity was maintained constant for comparison.

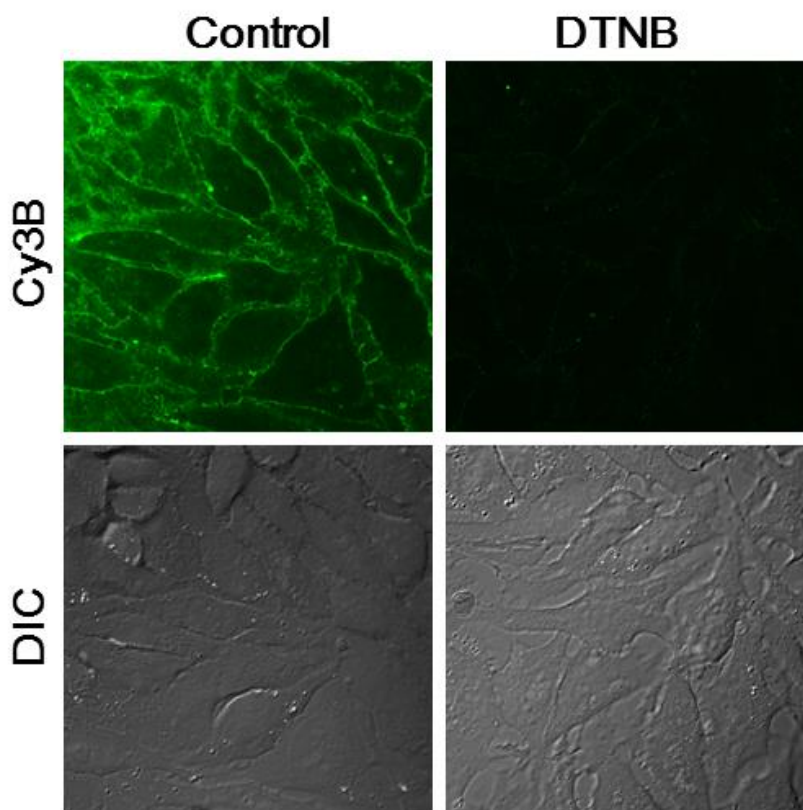


Figure 3.8 **DTNB pretreatment ablates cell surface thiol labeling.** HeLa cells were treated with DPBS only (control) or DPBS containing 1 mM DTNB for 10 min. Then the Cy3B-maleimide dye was applied to label the cell surface. The green channel shows the Cy3B fluorescence and the DIC channel shows the cell outlines. The laser intensity was maintained constant for comparison.

3.3.3 Quantitation Calibration Using Fluorescent Beads

Since fluorescent signals are all relative, the fluorescence in two channels cannot be compared without standards. We note that the much lower SH (green) signal necessitates the use of much higher laser power for effective visualization. For this reason, we have developed double labeled fluorescent beads as internal standards. Figure 3.9 shows a scheme of the bead preparation procedure. Beads loaded with different concentration of dyes will give proportional fluorescence signals (Figure 3.10 A, B). Because beads have a size distribution (~50 to ~150 μm), the loading and integrated fluorescence signals is not consistent between beads at each concentration, but the ratios shows linearity (see below). When beads were loaded with equal amount of two fluorophores, the integrated fluorescent intensity of each channel show linearity against the laser power, Figure 3.10 C shows the signal of one bead under different laser powers. In another batch, when beads were loaded with certain ratio of the two fluorophores, the fluorescence intensity is proportional to the ratio of dye. Figure 3.10 D shows the data of 4 beads at each concentration ratio. Although the beads examined have different sizes and thus carry different total amounts of dye, the green/red ratio of each bead is almost identical, as shown by the minimal error bars obscured by the symbols in Figure 3.10 D.

3.3.4 Quantitation of SH/SS Ratio for Mammalian Cell Surfaces

Several mammalian cell lines were investigated using the ratiometric two-color staining methods. The data for Figure 3.11 was collected staining all the cells on the same day using common reagents and conditions. Using the calibration procedure

outlined earlier, the ratio of cell surface SH/SS can be calculated. Notably the thiols released on treatment with 5 mM TCEP add to the pre-reduced surface SH by ~16 to 30-fold. The cell surface SH/SS ratio of these 4 cell lines show similarity.

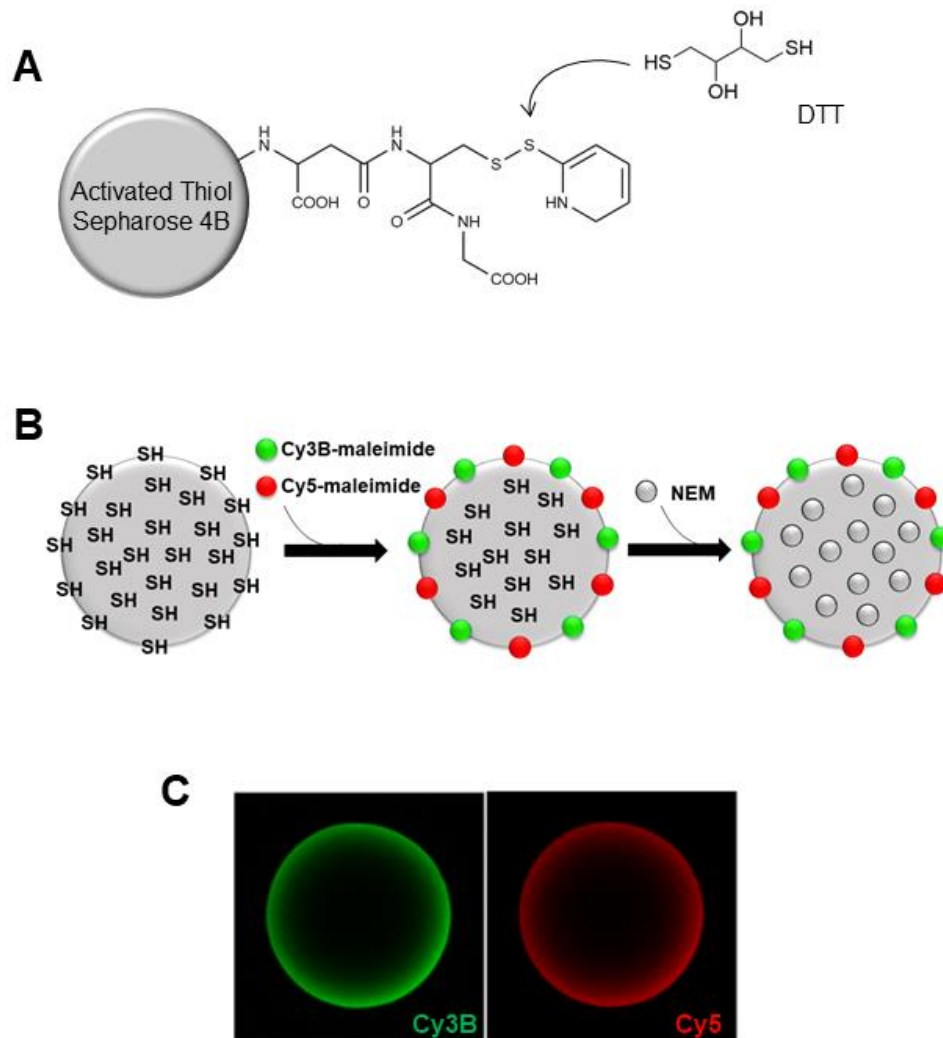


Figure 3.9 **Scheme for double labeling of thiopropyl bead with green and red fluorescent maleimides.** Activated thiol Sepharose 4B beads were treated with 10 mM DTT in PBS to expose free thiols (Panel A). The beads were incubated with limiting concentrations of mixture of Cy3B- and Cy5-maleimides (see Experimental procedures). Upon completion, the large excess of unreacted bead -SH groups were alkylated with 10 mM NEM (Panel B). Panel C shows two channels of one bead stained with two maleimides.

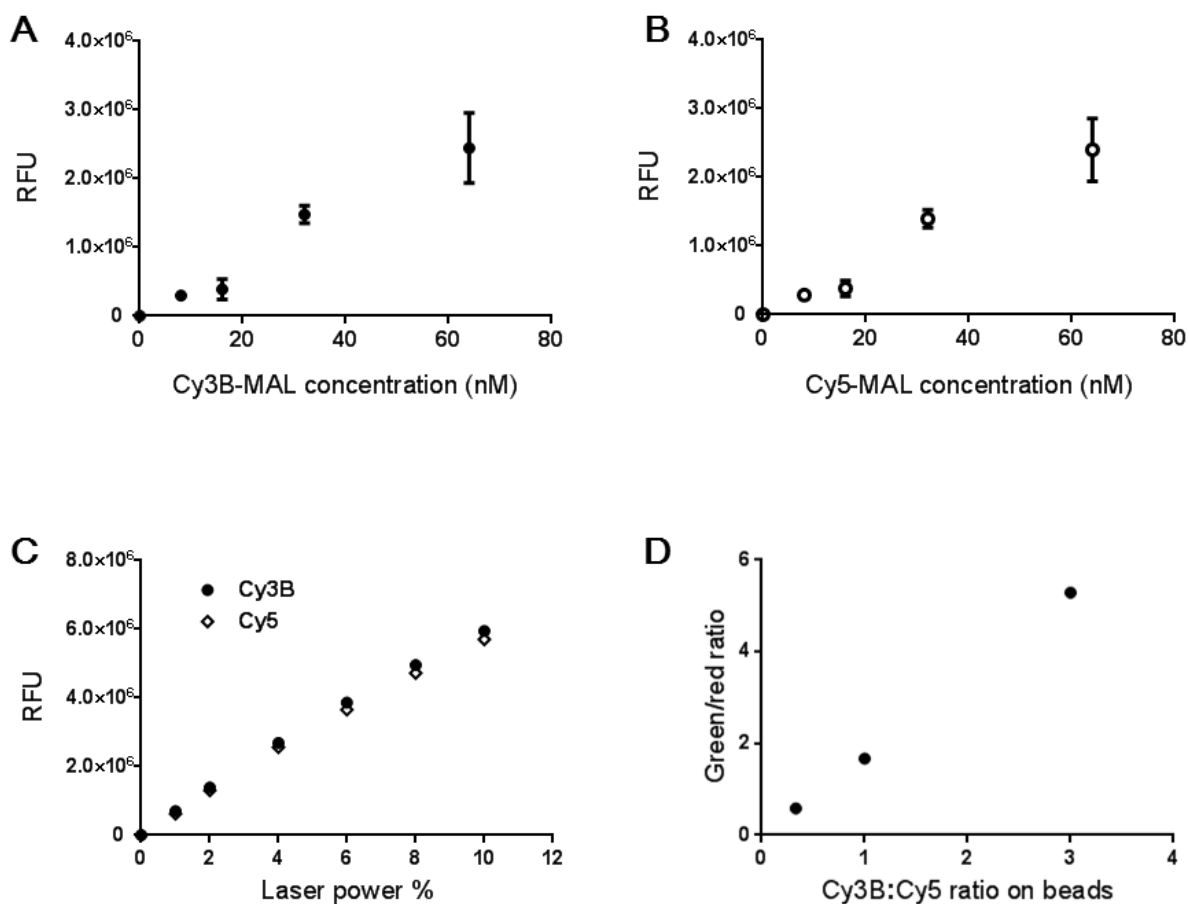


Figure 3.10 **Fluorescent beads can be used for ratiometric calculations.** Panel A, B show proportional fluorescence signals against increasing concentration of Cy3B and Cy5 loaded on the beads, respectively. The x-axis represents the dye concentration of the solution incubating the beads, the y-axis represents the integrated fluorescent signals of 1-3 beads at each concentration. Panel C shows the data of one bead loaded with equal amount of two fluorophores. The integrated fluorescent intensity of each channel is proportional with increasing laser power. Panel D shows the data of another batch of beads. Here beads were loaded with green and red maleimides at the three ratios shown. The fluorescence intensity is proportional to the ratio of dye ($n=4$ at each concentration ratio).

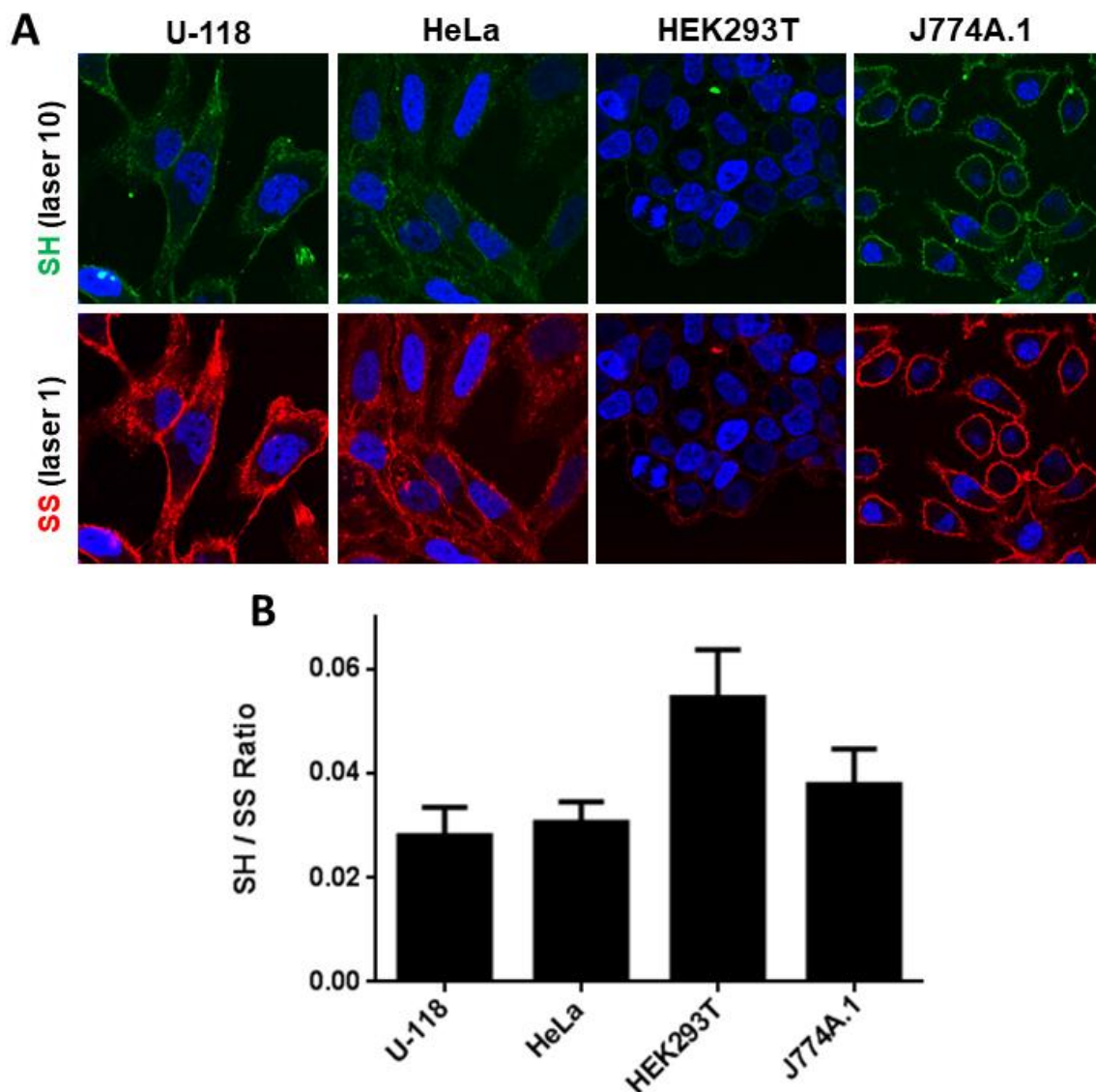


Figure 3.11 **Quantitation of SH/SS ratio for mammalian cell surfaces.** Panel A shows some representative cells under confocal microscopy. The green channel (with 10-fold higher laser power compared to the red channel) shows the free thiol staining while red channel shows the disulfide staining. Panel B shows the bar graph of SH/SS ratio of each cell lines calculated as before. Images were analyzed using ImageJ. Four representative images of each cell line were selected and 4-6 cell membrane areas of interest were picked in each image using ImageJ selection tools and calculated for fluorescence intensity (see Experimental procedures. U-118, n=20; HeLa, n=20; HEK293T, n=23; J774A.1, n=23).

3.3.5 SH/SS Ratio Depends on the Reductants

Considering Figure 3.3 A it would be expected that the ratio of SH/SS determined as above would depend on the stringency of the reducing protocol. The ratios presented in the Figure 3.11 may overestimate of the SH/SS ratio because it is unlikely that any reductant would capture SS in all exofacial proteins. Clearly the SS content will be the aggregate of redox active SS (as in regulatory SH/SS pairs) and more routine structural SS. Figure 3.12 shows the SS/SH ratio of HeLa cells using two different reducing agents: TCEP and glutathione (GSH). Because TCEP is a more potent reductant than GSH¹⁷, it results in significantly higher amount of SS reduced to free SH and labeled with red dye. Figure 3.12 A shows that the SS/SH ratio approaches an apparent limit above ~20. Figure 3.12 B shows that GSH at 10 mM is almost 25-fold less effective reductant of the aggregate SS bonds in exofacial proteins. Low concentrations of GSH are particularly ineffective at generating de novo SH groups. This may reflect the fraction of kinetically unreactive glutathionylated proteins as noted in Chapter 2 (see Figure 2.11).

3.3.6 Quantitation of SH/NH₂ Ratio for Mammalian Cell Surfaces

As a complementary method we have normalized the SH signal to protein using an NHS ester to label the lysine NH₂ groups that represent the total proteins on the cell surface (see Figure 3.3 B). One advantage of this method is that maleimide and NHS ester could be applied together. With the help of the standard beads, we could also calculate the normalized SH level on cell surface (see Figure 3.13).

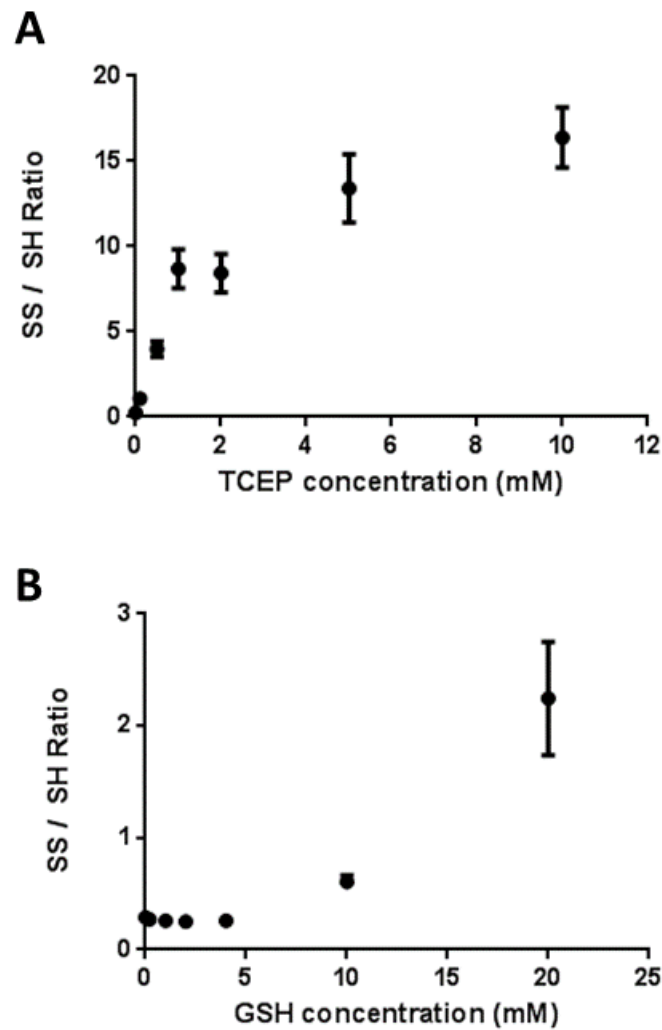


Figure 3.12 **SH/SS ratio depends on the reductants.** Panel A shows the HeLa cell surface SS/SH ratio with TCEP as the reductant. After labeling the free thiols with Cy3B-maleimide, a variety of concentrations of TCEP were applied to reduce the disulfide on the cell surface (at room temperature for 15 min) and then Cy5-maleimide was used for liberated SH labeling. Two representative images of each cell line were selected and 6 cell membrane areas of interest were picked in each image using ImageJ selection tools and calculated for fluorescence intensity (see Experimental procedures). For each concentration n=12. Panel B shows a comparable experiment using GSH as the reductant (here n=10).

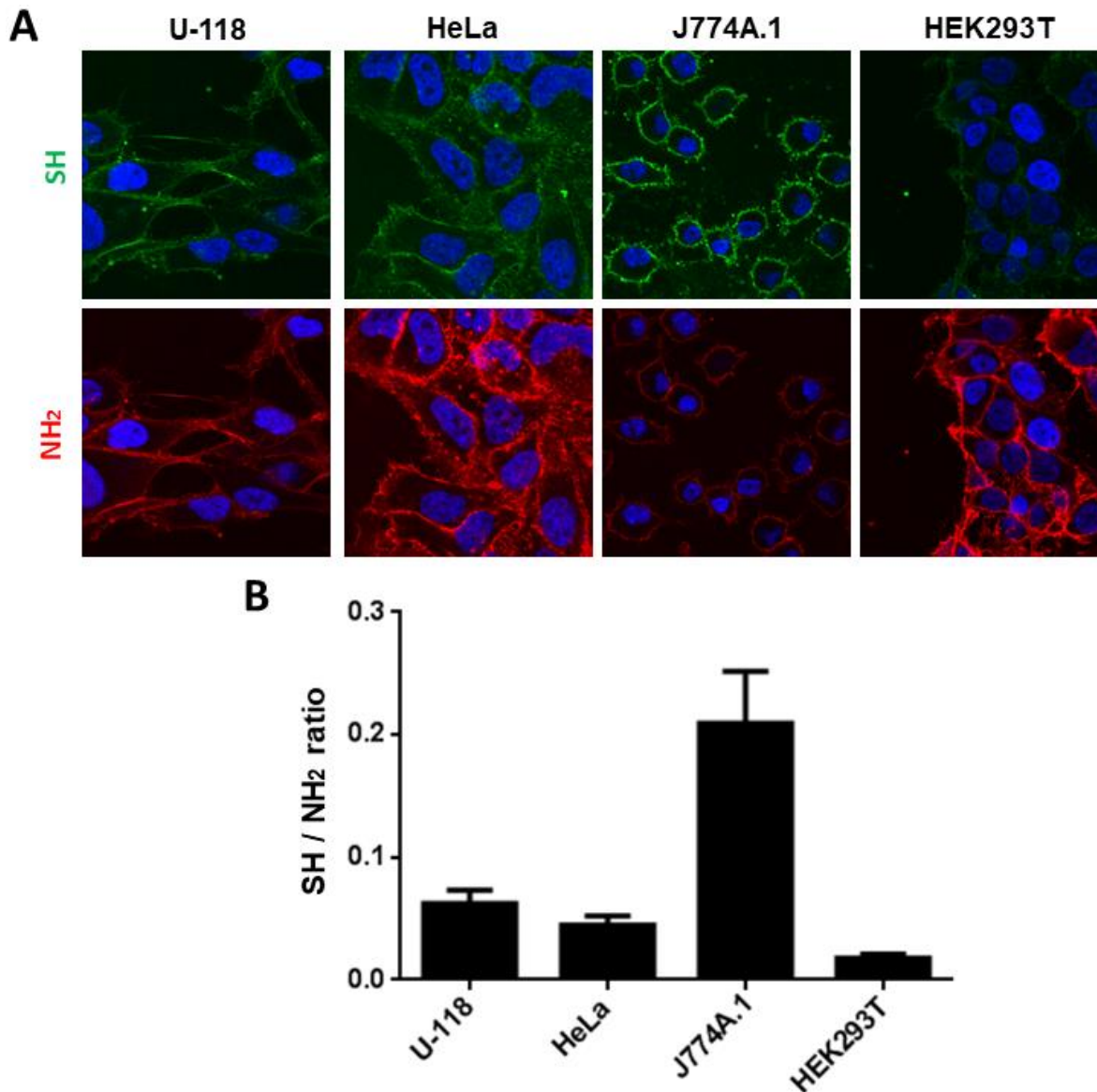


Figure 3.13 **Quantitation of SH/NH₂ ratio for mammalian cell surfaces.** Panel A shows some representative cells under confocal microscopy. The green channel shows the free thiol staining while the red channel shows the amino group staining. Panel B shows a bar graph of SH/ NH₂ ratio for each cell line. Images were analyzed using ImageJ. Three representative images of each cell line were selected and 5 cell membrane areas of interest were picked using ImageJ selection tools and calculated for fluorescence intensity (see Experimental procedures). The errors reflect the following measurements: U-118, n=15; HeLa, n=15; HEK293T, n=15; and J774A.1, n=15.

3.3.7 QSOX Activates on Cell Surface SH Oxidation

We have applied the SH/NH₂ labeling method on several researches, one is to visualize the QSOX activity on cell surface SH oxidation. Figure 3.14 shows the recombinant human QSOX1 works on GSH reduced surface of J774A.1. After GSH treatment the cell surface thiol level increased significantly, and QSOX1 reverse this effect. QSOX1 effect is also shown in HEK293T cells (data not shown).

3.3.8 Footprints of Cells on Cover Slides

In previous sections we have shown SH staining of cell surfaces. Additional cells may be secreting extracellular protein components carrying disulfides and some free SH groups¹³. Figure 3.15 A shows the strong staining of SH around the J774A.1 cells. Cells were incubated in DPBS containing 1 μ M Cy3B-MAL and 1 μ M Cy5-NHS ester for 30 min at 37 °C before fixation. The intensity of green staining may represent the higher local concentration of SH particularly around cells. The location underneath the cells is not stained with Cy3B. This lack of staining is not due to the steric exclusion of dye since these areas stain strongly for protein (Cy5), but not for Cy3B. Figure 3.15 B provides complementary information using a different cell type. HeLa cells are readily detached from glass coverslips using treatment with metal chelators (see Experimental procedures). Figure 3.15 B shows that after dislodging live HeLa cells the resulting footprint stain comparably to the surrounding surface protein. However, the area previously occluded by the HeLa cell stains weakly for protein thiols. These data then consolidate those found with mouse macrophage cells and show that in two cell types the SH signal is deepened immediately at the cell-glass contact site.

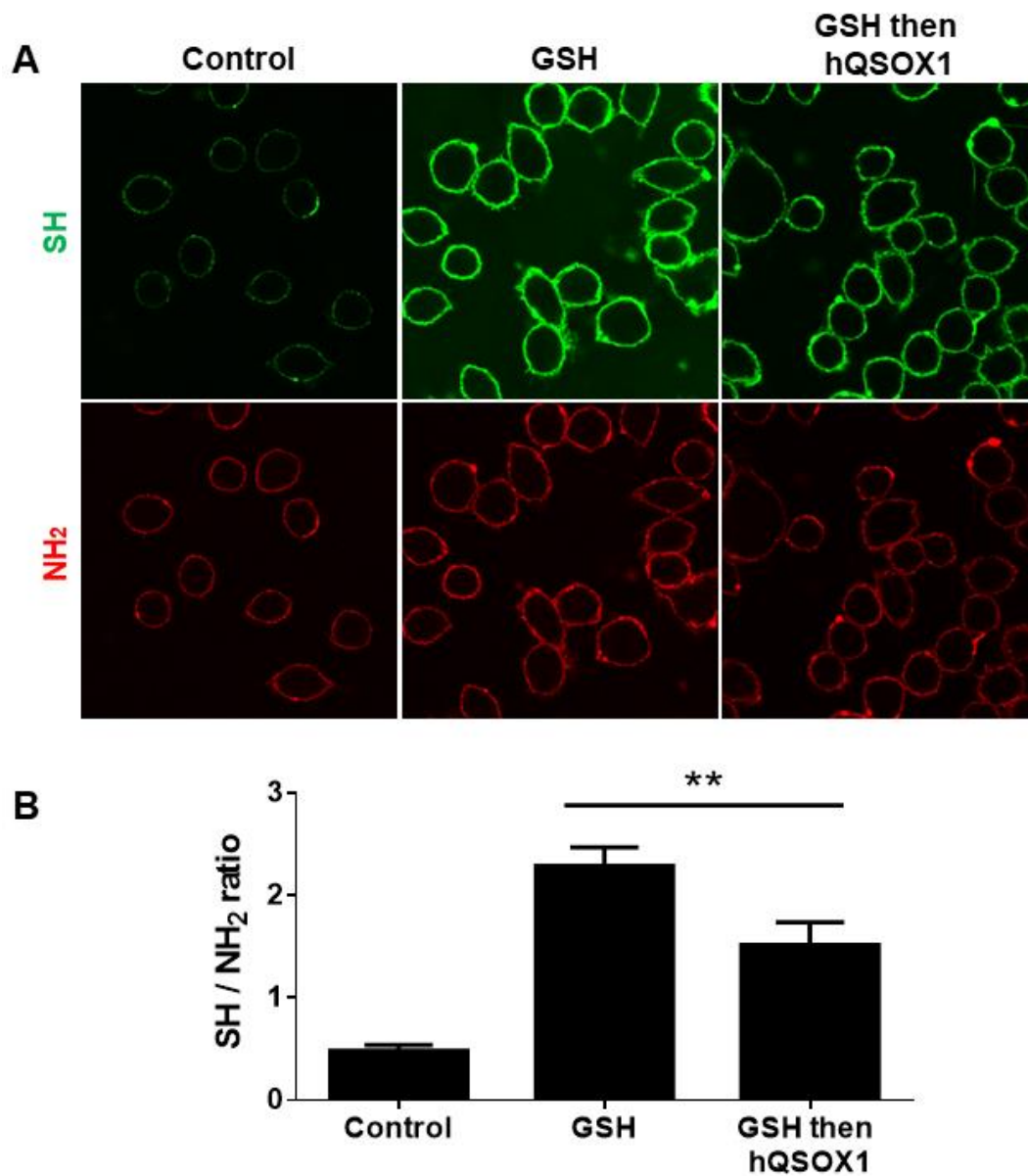


Figure 3.14 **QSOX catalyzes cell surface SH oxidation.** Panel A shows the staining of J774A.1 cells. Cells were incubated in media with or without 20 mM GSH at 37 °C for 20 min. Then 30 nM recombinant human QSOX1, or a DPBS control, was added and the cells were incubated for 40 min. Finally the cells were fixed using 2% PFA and stained with the regular SH/NH₂ procedure. Panel B shows the data, n=4. T-test ** P<0.01. The laser intensity was maintained constant within each cell type for comparison. Signal intensity was increased with the same level to show better view.

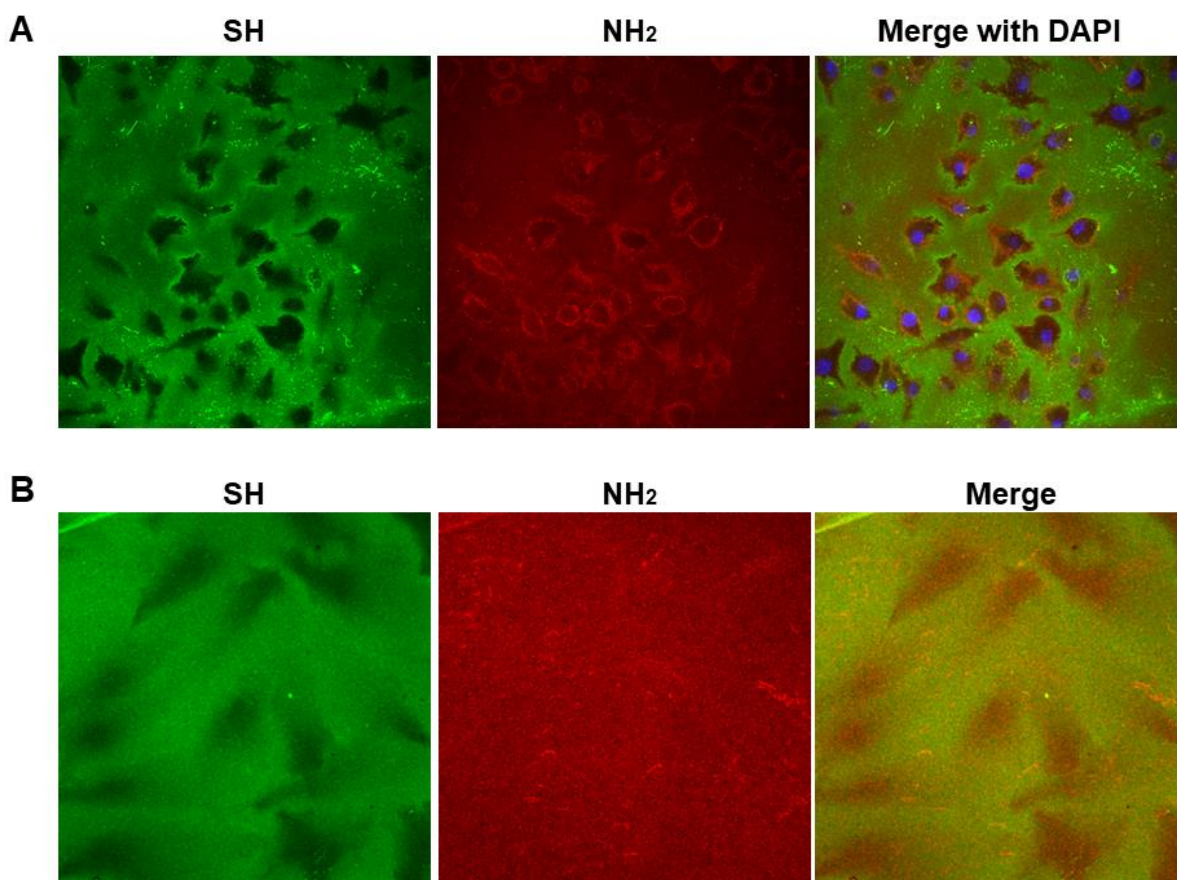


Figure 3.15 **Cells leave footprints on coverslips.** In these images green represents Cy3B-maleimide staining for thiols while red represents Cy5-NHS ester staining for protein as before. Nuclei are shown by DAPI (blue). Panel A shows the J774A.1 cells. The image focuses on the coverslip surface (coincident with the base of the macrophage cells). J774A.1 macrophage cells remain very tightly bound to the glass coverslip and it is clear that while the base of the cells and the substrate they occlude contain protein NH₂ group (staining red), thiol staining is notably absent within the margins of the cell. Thiol green staining covers the coverslip and is concentrated in the surrounding of certain cells. Panel B shows the stained coverslips that previously supported HeLa cells. Cells were dislodged by chelators before the regular SH/NH₂ staining procedure.

3.3.9 Macromolecular Crowding Agents Increase Cell Surface SH Levels

We were interested in evaluating the consequences of including agents to deepen the ECM. Macromolecular crowding agent have been used in bio-engineering research to deepen the deposition of the extracellular matrix¹⁸⁻²¹. Figure 3.16 shows the principle of crowding agents utilization. In standard 2-D cell cultures, cells anchored to the bottom of vessels bathe in a large volume of medium. This condition is hardly representative of the *in vivo* microenvironment that is highly crowded thus facilitating the interactions between of enzymes and their protein substrates^{22,23}. Figure 3.16 B shows chemical structures of several crowding agents. After 24 h growth in media supplemented with individual crowding agents, HeLa cells were washed and stained with the general thiol staining procedure. We found that polystyrene sulfonate (PSS) has a dramatic effect on cell surface SH staining (Figure 3.17). The PSS levels in this experiment is 50 µg/mL but this reagent is effective at much lower concentration (see later). The PSS effect observed here with HeLa cells is common to multiple cell types (Figure 3.18).

At first we thought that the PSS increases the expression and secretion of thiols on the cell surface. However, only 5 min incubation of PSS leads to significant effect on cell surface thiol labeling in all cell types examined (Figure 3.18). More surprisingly, experiments show that PSS treatment on cells pre-fixed with 2% paraformaldehyde also causes significant enhancement of surface labeling (Figure 3.18; right column). In this study, we have tried PSS with different average molecular weights (70 kD and 200 kD); both types have comparable effects on cell surface labeling (data not shown). In the studies presented here we used PSS 200 kD. We also surveyed the minimum concentration of PSS that promotes significant cell surface

labeling. Figure 3.19 shows that PSS down to 200 ng/mL also causes a significant increase in labeling. The corresponding SH/NH₂ ratio is shown in panel B.

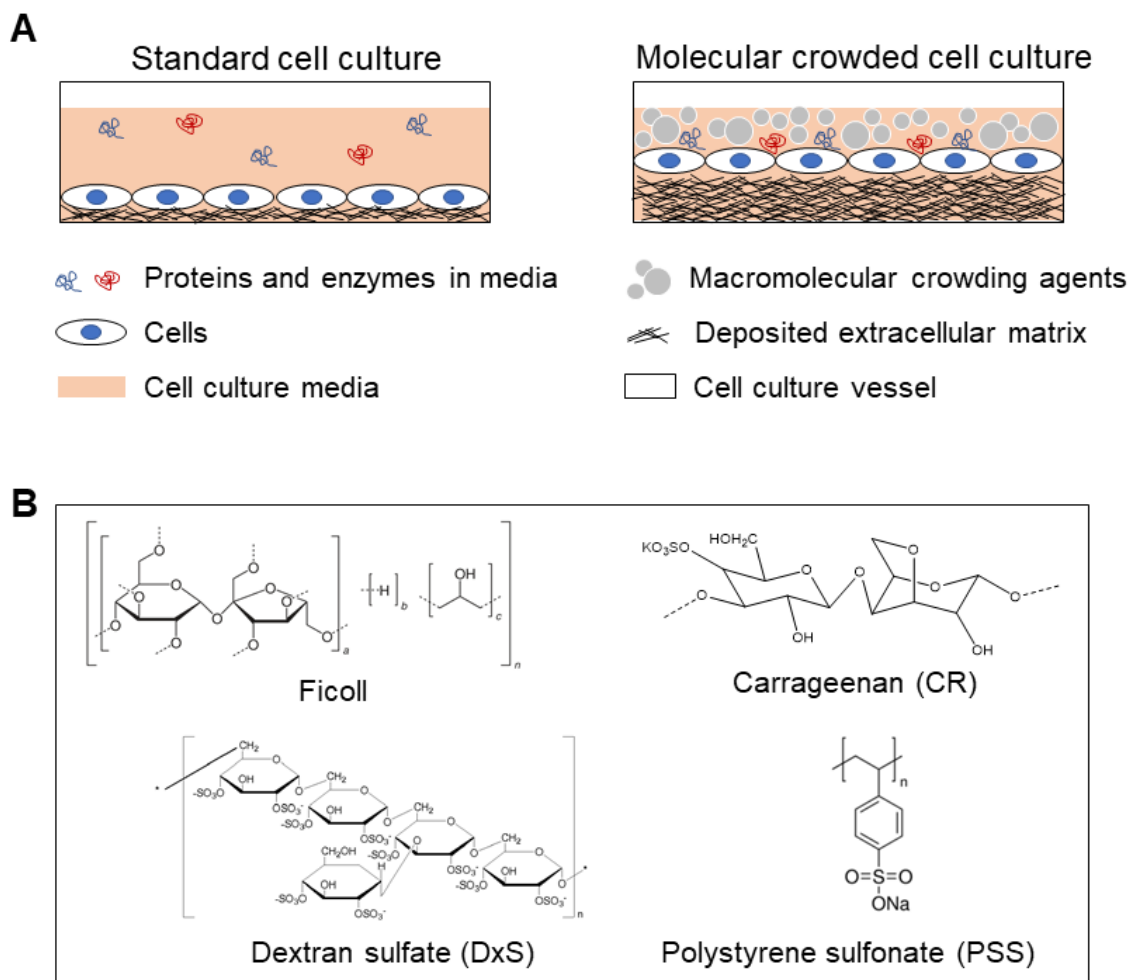


Figure 3.16 **Crowding agent utilization.** Under traditional 2-D cell culture conditions, the concentrations of extracellular matrix precursors and enzymes are low. The addition of polydispersed macromolecules (presented as spheres with different sizes) leads to a higher effective concentration of ECM precursors and enzymes that are involved in ECM generation, leading to increases in ECM deposition. Panel B shows several standard macromolecular crowding agents. Among these Ficoll is a neutral polysaccharide while CR, DxS and PSS are negatively charged sulfonated polymers.

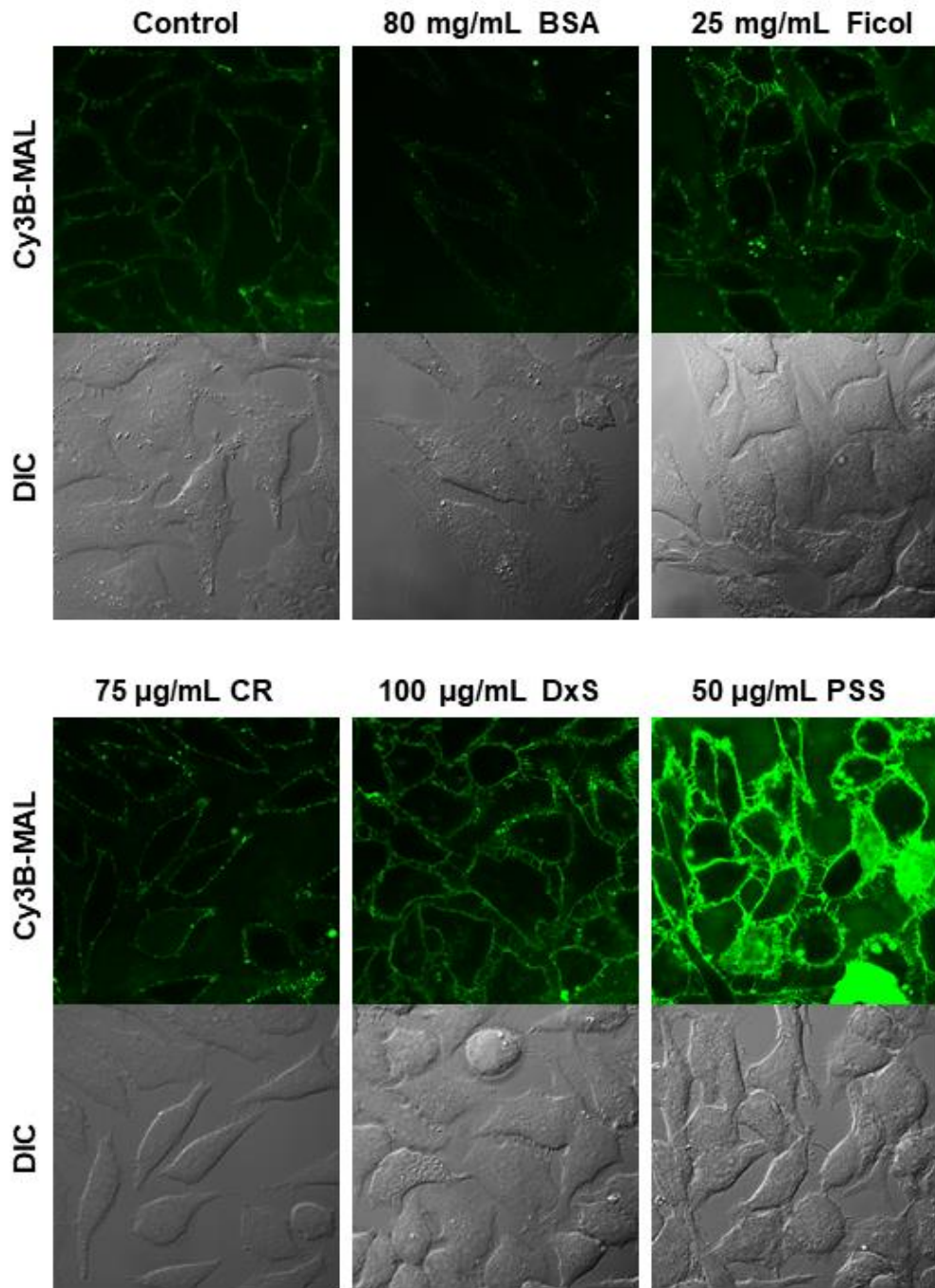


Figure 3.17 **PSS exerts a particular dramatic effect on HeLa cell surface SH staining.** The green channel shows the Cy3B-MAL labeled cell surface. The DIC channel shows the cell outlines. The laser intensity was maintained constant for comparison of SH staining.

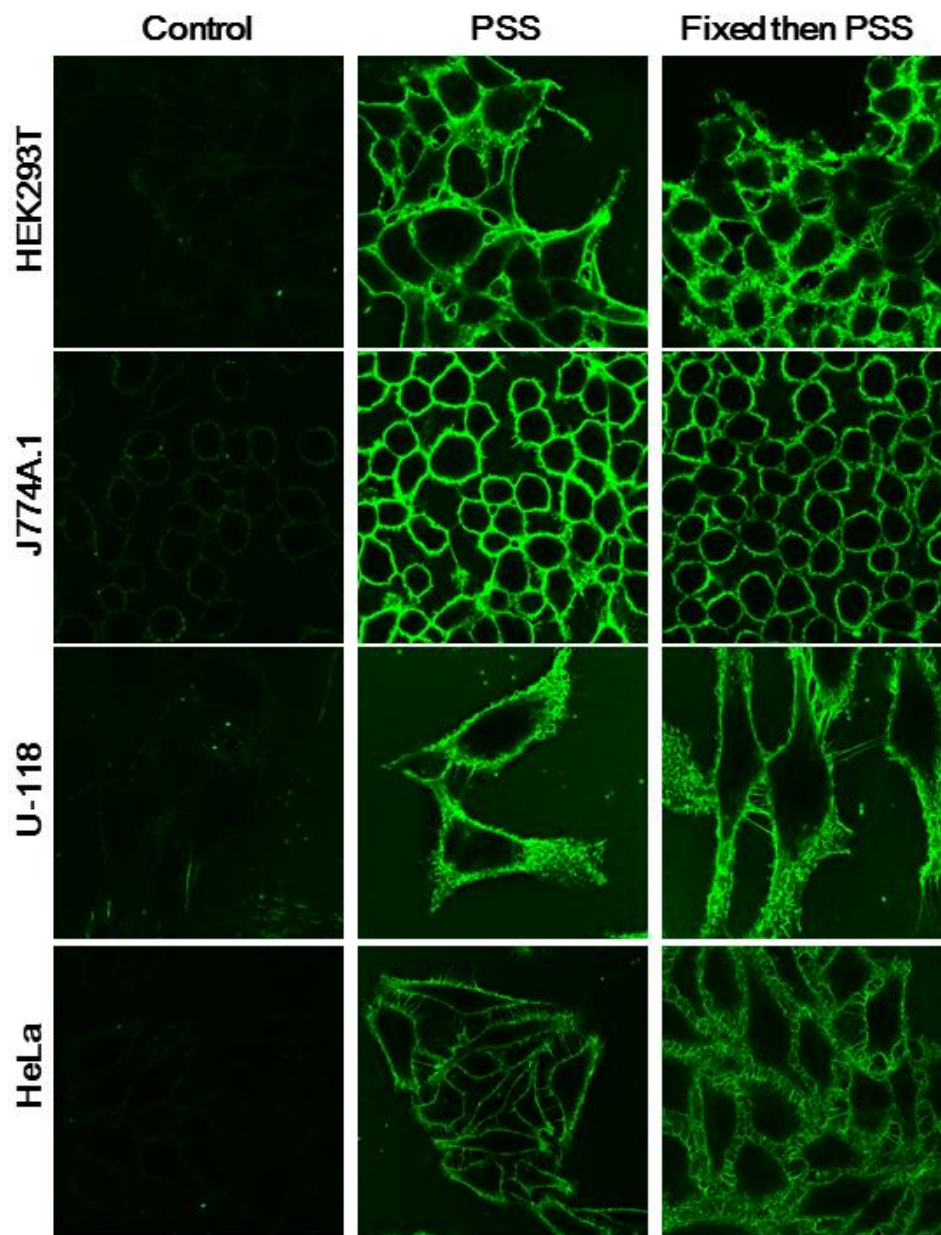


Figure 3.18 **PSS effect on cell surface thiol labeling is found in a range of cell lines.** Cells were washed and treated with DPBS (control) or DPBS containing 25 $\mu\text{g}/\text{mL}$ PSS (PSS) for 5 min at room temperature, in the control and PSS column, respectively. For the third column, cells were fixed with 2% PFA first and then treated with 25 $\mu\text{g}/\text{mL}$ of PSS. All the cells were labeled with 1 μM Cy3B-MAL for 10 min at room temperature. Laser power was maintained constant for each cell type. The 12 panels were then uniformly brightened for better visualization of the PSS effects.

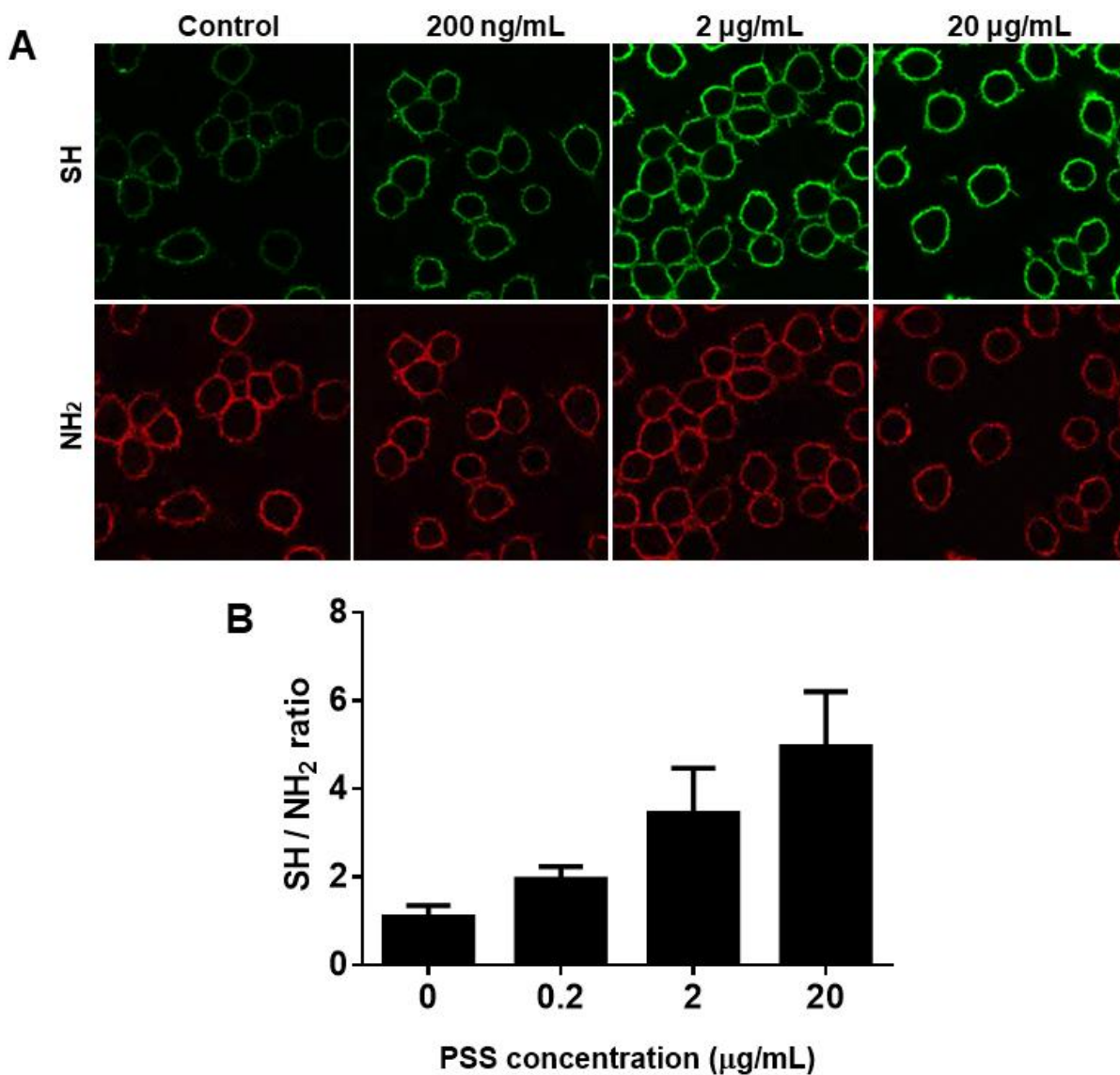


Figure 3.19 Low concentration of PSS increases cell surface thiol labeling.

J774A.1 cells were fixed first for 15 min with 2% PFA, and then incubated with DPBS containing different concentrations of PSS. After washing the standard SH/NH₂ staining procedure was applied. Panel A shows the images of cells. The green channel shows the thiol labeling by Cy3B-MAL while the red channel shows the NH₂ labeling by Cy5-NHS ester. The laser intensity was maintained constant for comparison. All images were brightened by the same factor for presentation purposes. Panel B shows the calculation of SH labeling normalized with NH₂ levels.

3.3.10 PSS Effect is SH Specific

To investigate the mechanism of the PSS effect we conducted several control experiments. Figure 3.20 shows that the maleimide treatment after PSS decreases the labeling. In addition the maleimide dye pre-inactivated by β -mercaptoethanol (see Experimental procedures) will also not label the cell surface thiols, shows that the PSS effect is not due to a non-specific absorption of the Cy3B dye. In addition we also tried other dyes (Cy5-MAL and Alexa568-MAL) for PSS effect investigation, and found that these dyes also show significant enhanced labeling after PSS treatment (Figure 3.21). Thus the PSS effect on surface fluorescent labeling is not dye specific.

Figure 3.22 shows that pre-treatment of cells with DTNB oxidize surface SH groups abolishes subsequent staining with the maleimide. Figure 3.23 show that the PSS effect on J774A.1 cells is also attenuated by QSOX1, which can oxidize extracellular matrix thiols (see Chapter 1)²⁴. QSOX1 was also found to reverse the PSS effect on other cell types, and control cells incubated with QSOX1 did not show significant change on cell surface thiol level (data not shown).

Finally we evaluated whether PSS itself could increase the intrinsic fluorescence of Cy3B, thus possibly contributing to the enhancement of fluorescence seen here. However PSS, at 23 $\mu\text{g/mL}$, has no significant effect on the Cy3B fluorescence (Figure 3.24)

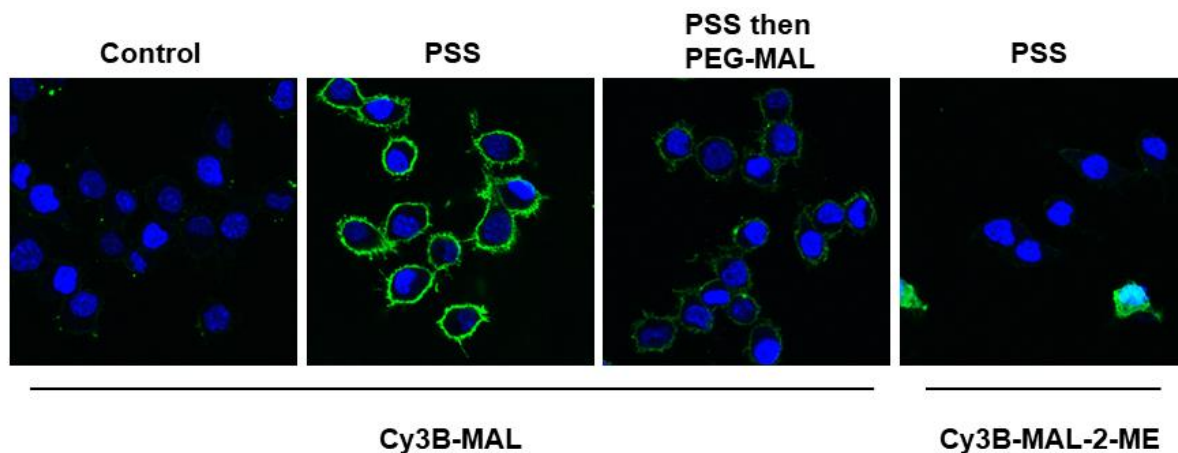


Figure 3.20 **PSS effect involves labeling of cell surface thiols by Cy3B-MAL.** J774A.1 cells were treated with or without 20 $\mu\text{g}/\text{mL}$ PSS for 10 min. The PSS treated cells were then incubated with or without 100 μM methyl-PEG₂₄-maleimide. The cells were labeled with the original maleimide dye or with β -mercaptoethanol inactivated dye (Cy3B-MAL-2-ME; see Experimental procedures). The green channel shows the SH labeling and the blue channel shows nuclei (DAPI).

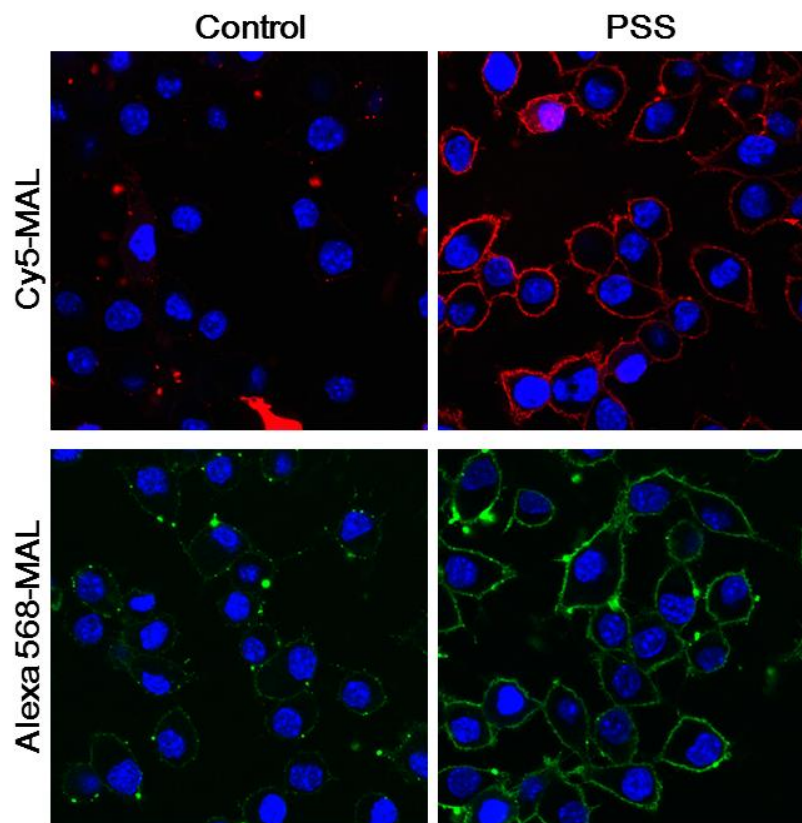


Figure 3.21 **PSS effect on cell surface thiol labeling is not a dye-specific effect.** J774A.1 cells were stained with 1 μ M Alexa 568-maleimide or 1 μ M Cy5-maleimide after treatment for 10 min with or without 25 μ g/mL PSS in DPBS at room temperature. The green channel shows the Alexa 568 fluorescence. The red channel shows the Cy5 fluorescence. In both cases nuclei are shown by DAPI. The laser intensity of each channel was maintained constant for comparison of the thiol levels for each dye set.

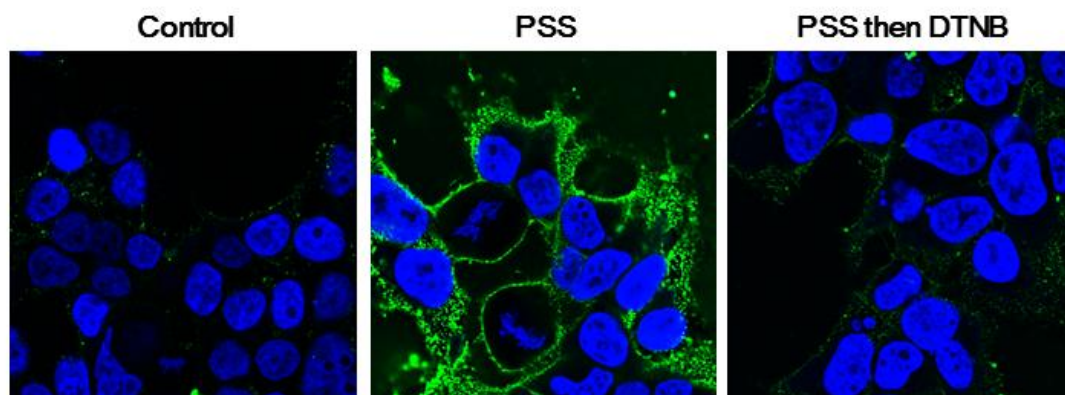


Figure 3.22 **PSS effect on cell surface thiol labeling is abolished by pretreatment with DTNB.** HEK293T cells were treated with DPBS (control) or DPBS containing 20 $\mu\text{g}/\text{mL}$ PSS for 10 min. The PSS treated cells were then incubated with or without 1 mM DTNB for 10 min. The green channel shows the SH labeling using Cy3B-MAL and the blue channel shows nuclei (Hoechst 33342).

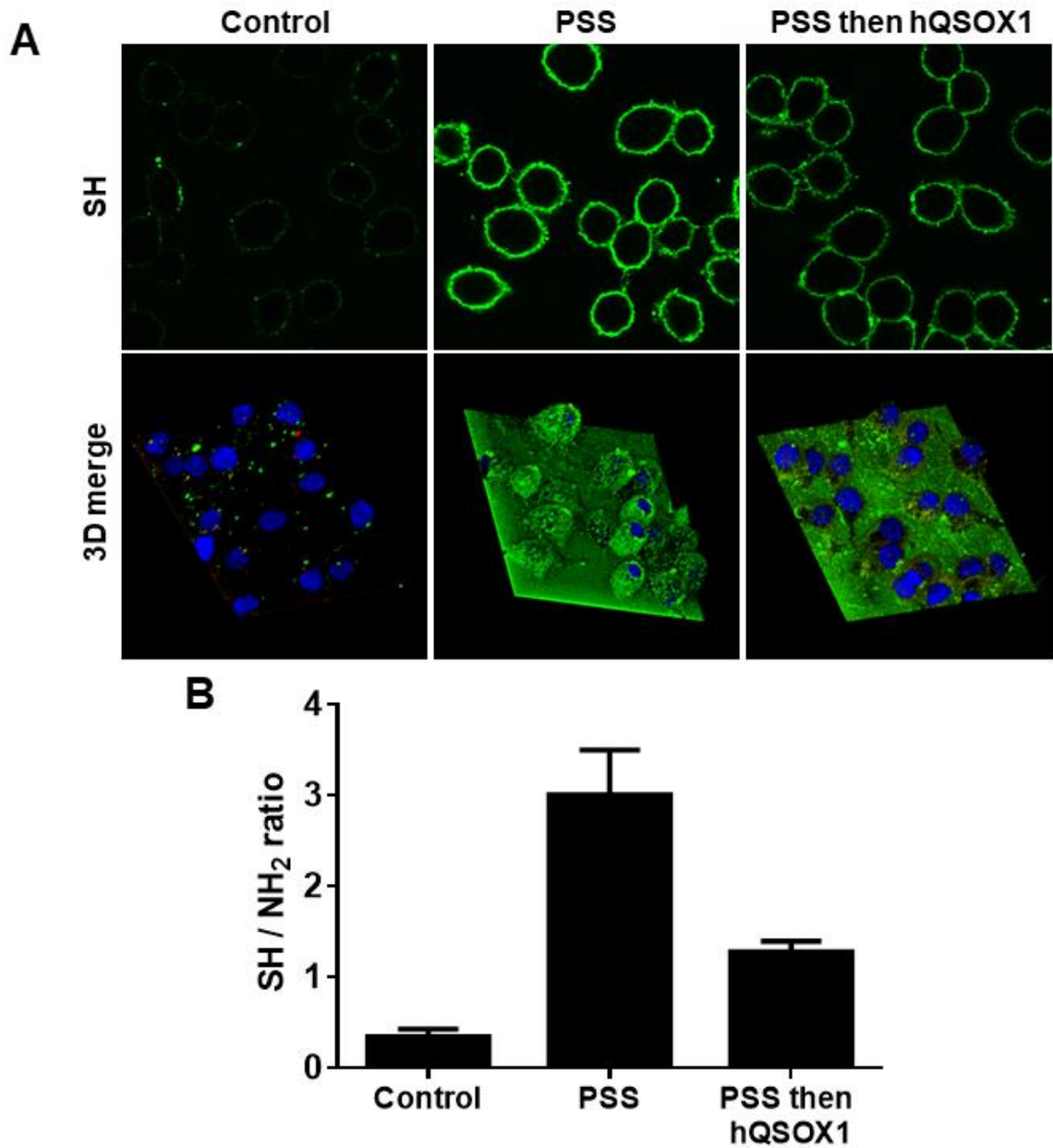


Figure 3.23 **PSS effect on cell surface thiol labeling can be reversed by recombinant human QSOX1.** J774A.1 cells were fixed with 2% PFA first and incubated with or without 20 $\mu\text{g}/\text{mL}$ PSS for 5 min. After washing with DPBS, the cells were treated for 15 min at 37 $^{\circ}\text{C}$ and then 10 min at room temperature with or without 50 nM recombinant human QSOX1. The green channel shows the SH staining with Cy3B-MAL. Nuclei are shown as blue (DAPI). The red channel (Cy5-NHS ester labeling NH₂) is not shown.

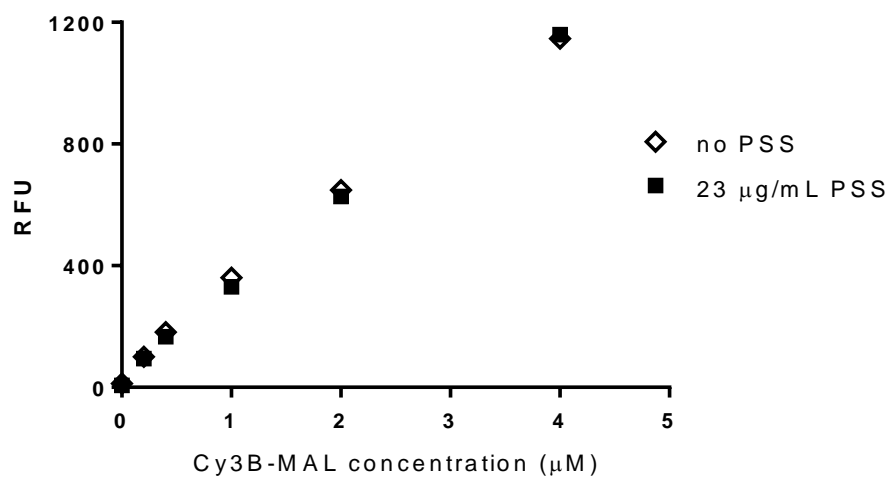


Figure 3.24 **PSS does not increase the fluorescence signal of Cy3B.** A variety of concentrations of Cy3B-MAL were added into a 96-well plate containing DPBS with (close squares) or without (open diamonds) 23 µg/mL PSS.

3.3.11 Further Experiments to Investigate the PSS Effect

The previous sections have shown definitively that PSS increases the exposure of surface -SH groups. We considered that the effect of PSS was related in some way to the polyanion recruiting the dye maleimide to the surface by some unknown mechanism. The enhanced dye concentration might then lead to PSS mediated staining of thiols. This section presents experiments to suggest that PSS exerts its effects by interacting directly or indirectly with proteins at the cell surface leading to increased exposure of surface thiols.

To investigate the possibility that PSS binds directly to sulfonated dyes in vitro, we performed the experiments described below. A PD-10 column (size exclusion) was used to analyze the interaction between Cy5-maleimide and PSS. DPBS (1 mL) containing 12 μ M Cy5-maleimide, 3.4 mg/mL PSS or the combination of both were loaded on three columns, respectively, and DPBS was used to elute. The elutions were analyzed by UV-vis to record the absorbance at 255 nm (PSS) and 645 nm (Cy5). Figure 3.25 shows the absorbance of each elution fraction. These data show that the Cy5-maleimide and PSS are eluting from column independently, indicating that the Cy5-maleimide dye is not binding the PSS in solution.

As mentioned before, both PSS molecular weight 70 kDa and 200 kDa increase the thiol labeling with maleimide dyes on cell surface. We then explored whether the monomeric unit can cause the same effect. J774A.1 cells were incubated in DPBS with either 25 μ g/mL sodium 4-vinylbenzenesulfonate (monomer) or 25 μ g/mL PSS (polymer) for 5 min, followed with the typical thiol labeling procedure with Cy3B-maleimide. Figure 3.26 shows the same concentration of monomer did not lead to increased thiol labeling on the cell surface. The PSS effect is thus not simply due to the monomeric unit.

During the investigation of macromolecular crowding agents (Figure 3.16) we found that the macromolecular crowders with negative charges (i.e. DxS, CR) show a mild effect on cell surface thiol labeling. We investigated one more synthetic anion polymer polyacrylic acid (PAA). Fixed HeLa cells were incubated in DPBS with 25 $\mu\text{g/mL}$ PAA and 25 $\mu\text{g/mL}$ PSS for 5 min, then underwent the typical thiol labeling with Cy3B-maleimide. Figure 3.27 shows that the PAA does not have comparable effect with PSS to increase the exofacial thiol labeling.

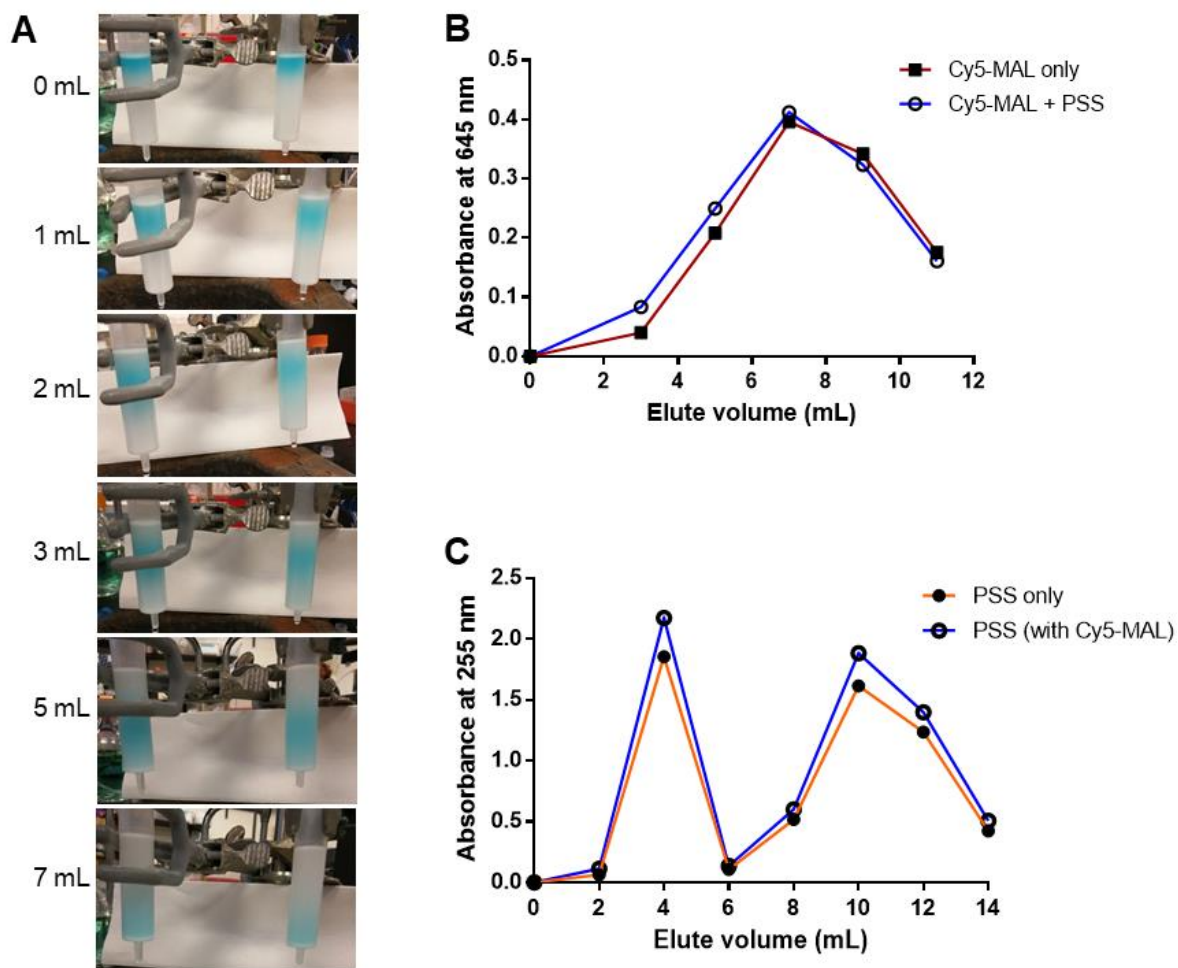


Figure 3.25 **PSS does not bind Cy5-maleimide dyes.** Panel A shows the two PD-10 columns with Cy5-MAL only (left column) and Cy5-MAL with PSS (right column). The numbers on the left hand presents the elution volume. Panel B shows the elution of Cy5-MAL (absorbance at 645 nm in UV-vis). Panel C shows the elution of PSS (absorbance at 255 nm in UV-vis).

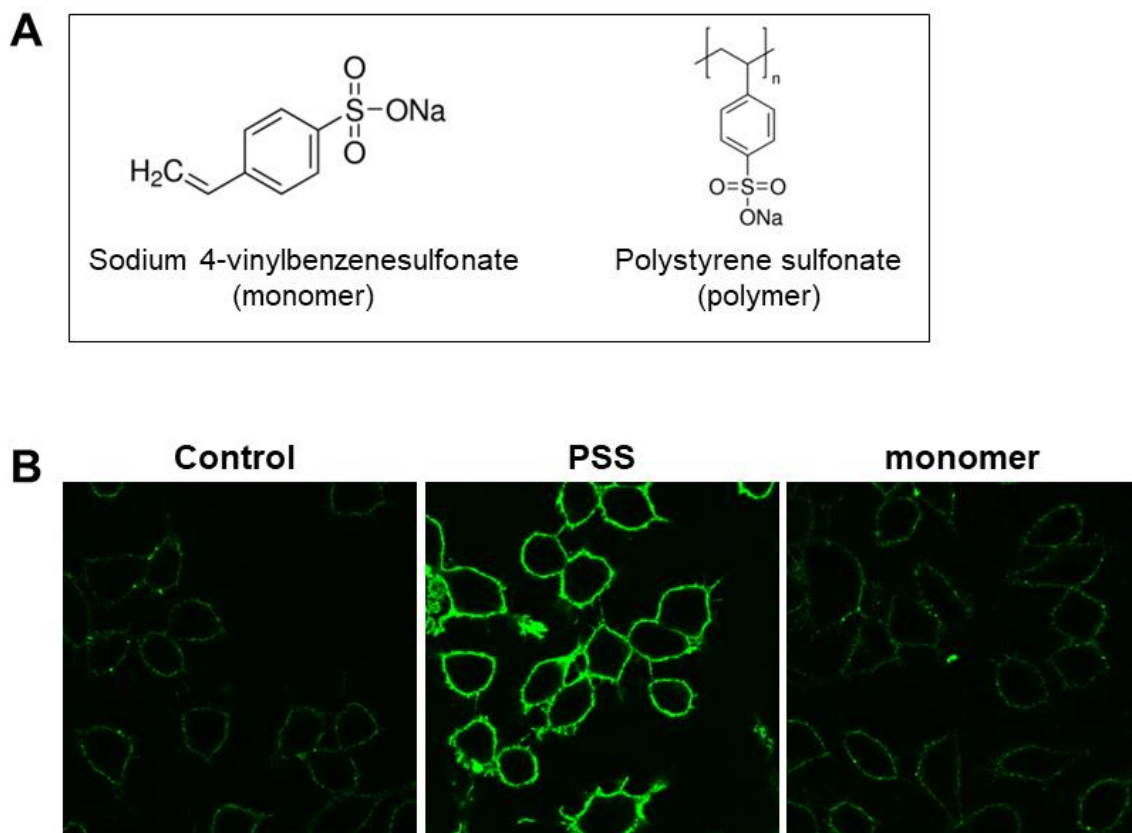
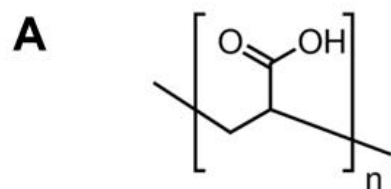


Figure 3.26 **The PSS monomeric unit, 4-vinylbenzenesulfonate, does not induce surface labeling.** Panel A illustrates the structure of the monomer of PSS. Panel B shows the effect of both compounds on surface thiols of J774A.1 cells. Cells were treated with DPBS containing 25 $\mu\text{g}/\text{mL}$ PSS or 25 $\mu\text{g}/\text{mL}$ monomer for 5 min, followed with the typical thiol staining procedure. The green channel shows the thiols labeled with Cy3B-MAL.



Poly Acrylic acid (PAA, pKa 4.2)

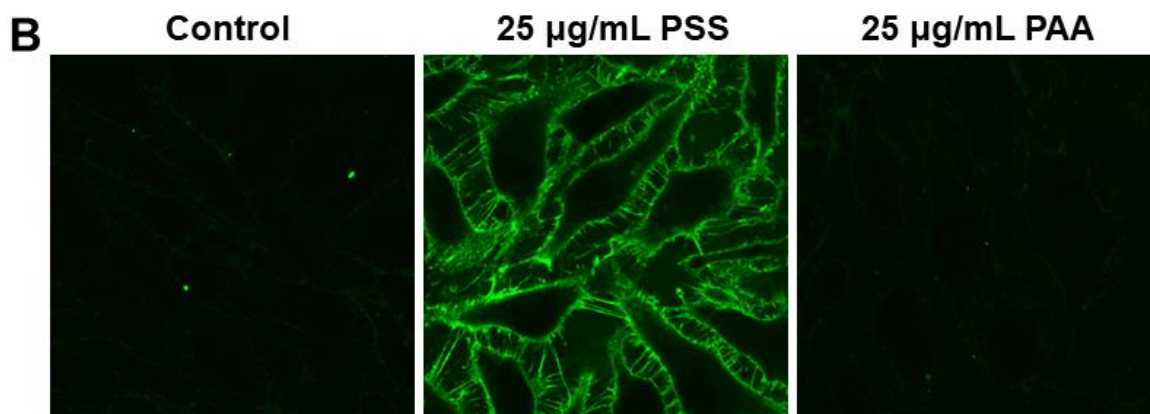


Figure 3.27 **Polyacrylic acid is unable to mimic the effects of polystyrene sulfonate.** Panel A shows the structure of PAA. Panel B shows the effect of PSS and PAA on HeLa surface thiols levels. The green channel shows the thiols labeled with Cy3B-MAL.

3.3.12 Surface Thiols Exposed with PSS Can be Internalized by Live Cells

During this project we have found that labeled thiols on cell surface can be internalized into cells, and the amount of internalized thiols is decreased with lowered temperature and shorter incubation times (data not shown). This phenomenon is consistent with thiols on the cell surface undergoing endocytic trafficking. Treatment with PSS significantly increases the cell surface labeling using maleimide dye, and almost all the surface Cy3B is internalized into mouse macrophages. However most of Cy5 (representing total proteins) still stays on the cell surface (Figure 3.28). Also we note the internalized proteins are increased in PSS group, possibly indicating an enhanced endocytic trafficking. This result indicates that cells are not killed by PSS treatment, but the dynamics of surface thiol transportation is changed.

We also tried to investigate the path of this internalization using LysoTracker to show the locations of lysosomes. Figure 3.29 shows that the internalized labeled thiols do not co-localize with lysosomes over 30 min of this experiments. Thus, the internalized thiols may not rapidly go to lysosomes for degradation.

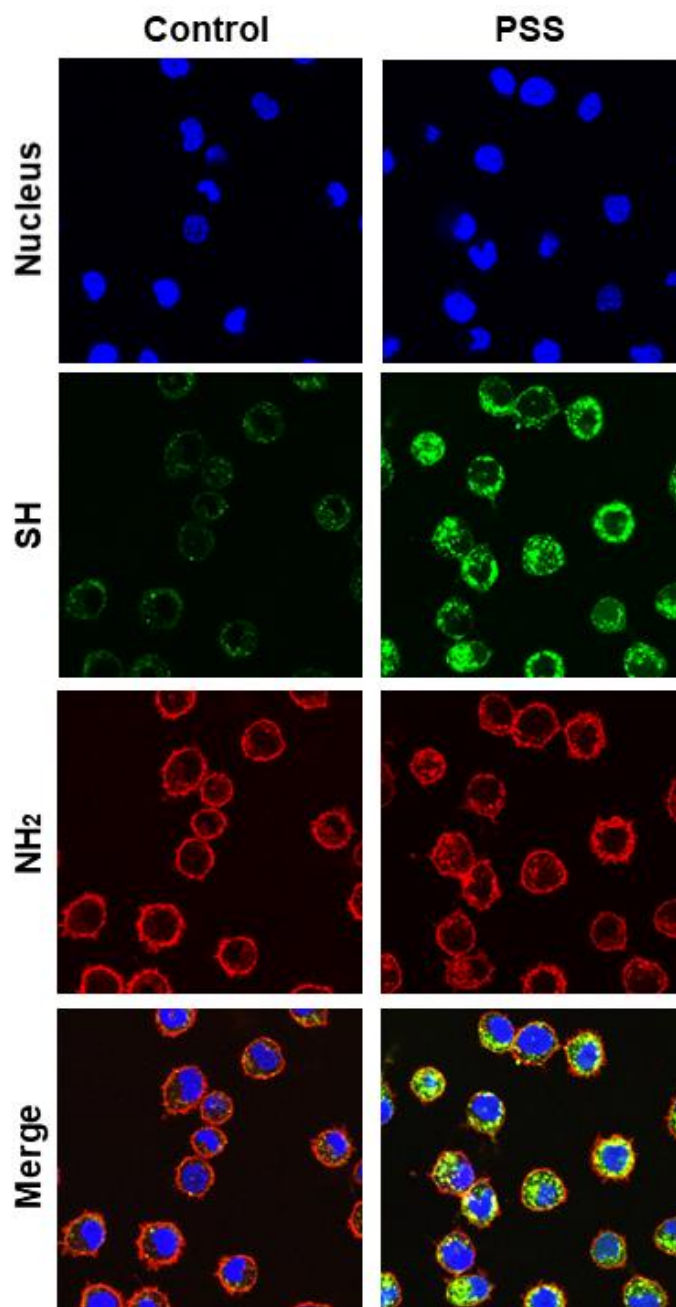


Figure 3.28 **PSS increased thiol labeling are internalized into cells.** J774A.1 cells were treated with DPBS or DPBS containing 20 $\mu\text{g}/\text{mL}$ PSS. Then cells were incubated with 1 μM Cy3B-MAL and 1 μM Cy5-NHS ester for 30 min at 37 $^{\circ}\text{C}$. The blue channel shows the nuclei, the green channel shows the Cy3B-MAL labeled thiols, the red channel shows the Cy5-NHS ester labeled proteins.

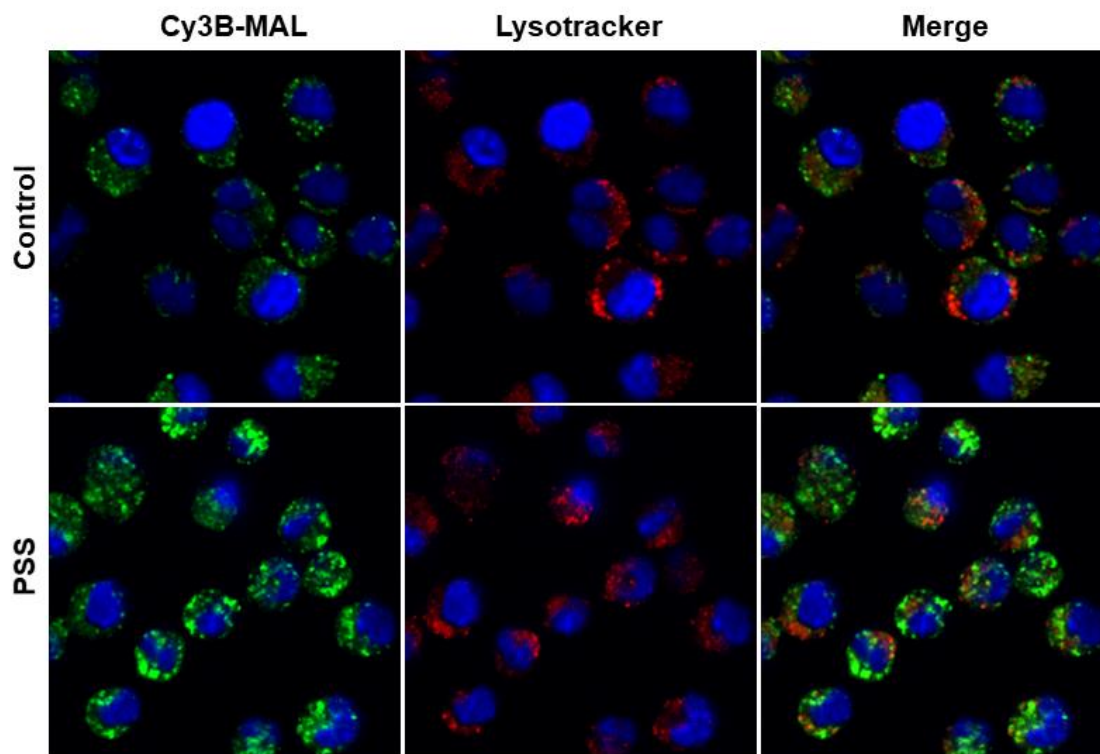


Figure 3.29 **Thiols internalized into cells do not co-localized with lysosomes.** J774A.1 cells were first incubated in complete DMEM media with 75 nM of Lysotracker Deep Red for 1 h at 37 °C. Then cells were washed and treated with or without 20 µg/mL PSS for 5 min, and then followed with 1 µM Cy3B-MAL and 1 µM Cy5-NHS ester incubation for 30 min at 37 °C. The green channel shows the thiols labeled with Cy3B-MAL, the red channel shows the lysosomes labeled by Lysotracker Deep Red.

3.3.13 Investigation of Protein Targets of PSS Effect

We would like to know what proteins are involved in the PSS effect on cell surface thiol levels. After PSS treatment, cell surface proteins were extracted and analyzed with SDS-PAGE (see Experimental procedures). Figure 3.28 shows this experiment. Panel A shows the flow of the experiment. Panel B shows the SDS-PAGE results of three cell types: HEK293T, U-118 and J774A.1. The left 2-3 lanes in the gel of each cell type shows the Cy5 fluorescent channel, and the right 2-3 lanes shows the Coomassie channel. The Cy5 channel and Coomassie channel are imaging the same gel. Note that in the Cy5 channel, PSS treated cells show significant higher level of labeling in several bands in gel than that in control cells. However, the same gel stained with Coomassie blue shows same intensity of bands in control lane and PSS lane, indicating comparable total protein levels in these two groups. This result is consistent with the confocal observations. Also, the harsh experimental procedure of SDS-PAGE preserves the fluorescent labelled proteins showing that the interaction is covalent.

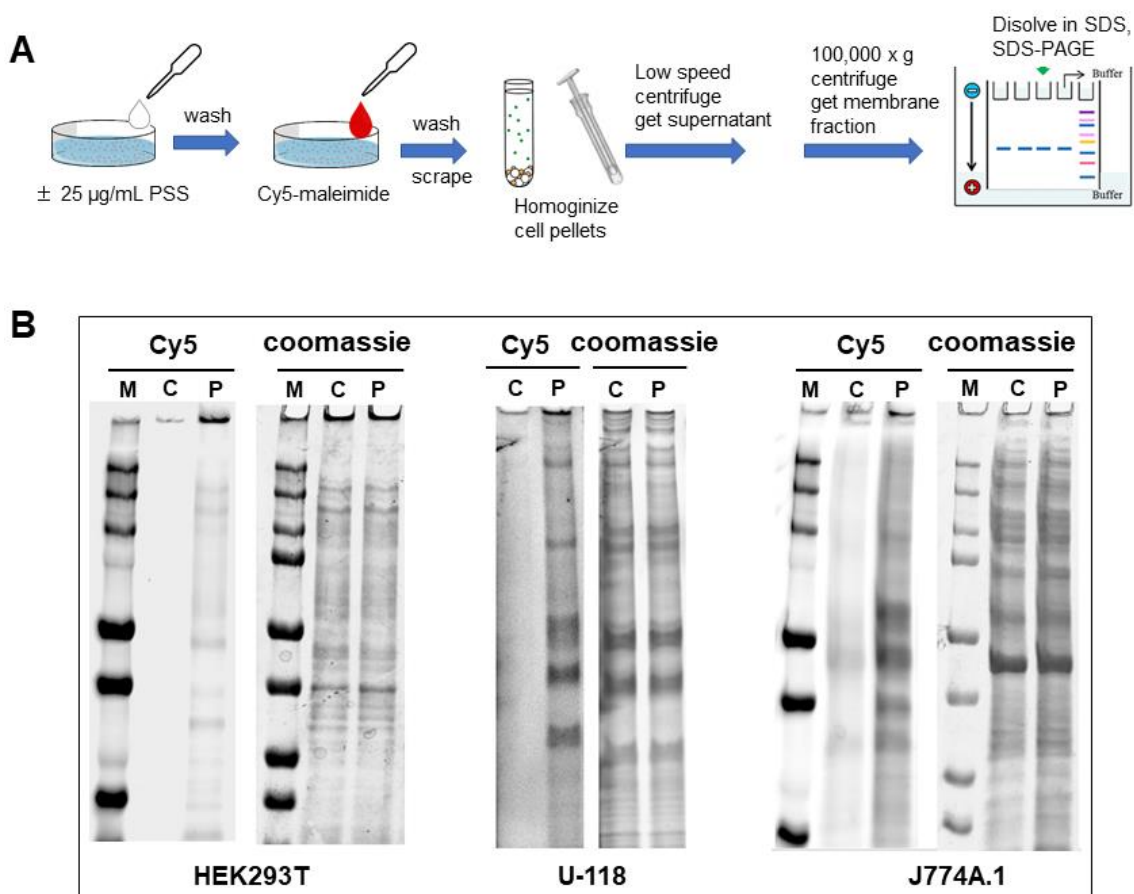


Figure 3.30 **SDS-PAGE shows higher thiol labeling on cell surface but same total protein levels after PSS treatment.** Panel A shows the flow of the experiment (see Experimental procedure). Panel B shows the SDS-PAGE results of three cell lines. The left 3 (HEK293T and J774A.1) or 2 (U-118) lanes show the Cy5 fluorescent channel, while the right lanes show the Coomassie channel. M, marker; C, control; P, PSS.

3.4 Conclusion and Discussion

The thiol/disulfide (SH/SS) redox state of the mammalian cell surface plays critical roles in modulation of different cell behaviors including cell adhesion¹, migration², proliferation³, metastasis^{4,5}, and viral fusion⁶⁻⁸. For example, the redox poise of thiols and disulfides located in exofacial protein domains on a range of blood cells are key modulator of biological functions²⁵⁻³⁴. In this chapter we describe confocal ratiometric fluorescence imaging methods specifically for cell surface thiols and disulfides and their applications to studying different cell types. These methods can be used not only on fixed cells but also on live cells for the analysis of endocytic trafficking. These procedures are also amenable for future super-resolution studies.

One interesting phenomenon was observed during this project. When cells were treated with crowding agents, especially the polystyrene sulfonate (PSS), the extracellular and cell surface thiol levels are significantly enhanced. PSS is in a class of medications called potassium-removing agents used to treat hyperkalemia (increased amounts of potassium in the body). There are several brand names on the market: Kalexate®, Kayexalate®, Kionex® and SPS®. As a cation-binding compound, PSS resin were also used to remove excessive K⁺ level in supernatants of stored red blood cells³⁵. PSS has also been investigated as a grafted coating for biomaterial science³⁶⁻³⁹. For example, Felgueiras et al.³⁹ showed that PSS grafted onto titanium alloy (Ti6Al4V) surfaces in the early stages of osteoblastic cultures increases cell viability, supports cell structure and morphology, and also facilitates adhesion strength of cells on biomaterial in serum-free conditions. PSS has also been demonstrated as an inhibitor of HIV-1 entry⁴⁰, although the inhibition effect decreases significantly in the presence of seminal plasma. Possibly, the positively charged

proteins in seminal plasma binds the negatively charged PSS in plasma, and limiting efficacy *in vivo*⁴¹. Voigt et al.⁴² discovered that nanoparticles modified with PSS exhibit specific affinity for caveolae of endothelial cells, and enhance particle uptake by cells.

The functional concentration of PSS as crowding agent is very low, much lower than the neutral crowder Ficoll. One explanation is that for negatively charged crowders the electrostatic forces amplifying steric exclusion effects are dependent on the charge distribution on the surface of the macromolecule²¹. Thus smaller concentrations of negatively charged crowders are needed to exert similar exclusion effects as their neutral counterparts. Several researches have demonstrated that PSS leads to denaturation of proteins. Saburova et al.⁴³ showed that low concentration of PSS disrupts the native structure of horse heart hemoglobin (Hb) and spermwhale muscle myoglobin (Mb). Kowalczyńska et al.⁴⁴ showed that the efficiency of bovine serum albumin (BSA) adsorption became markedly higher on polystyrene surfaces that had been sulfonated. Cells interacted differently with the polystyrene and sulfonated surfaces depending on the arrangement of adsorbed albumin. The same group also demonstrated that sulfonated polystyrene increases fibronectin adsorption, which involves conformational changes induced by the surface polarity⁴⁵. In an interesting report, Ahn et al.⁴⁶ demonstrated that PSS deposited on glass not only recruits but also stabilizes fibrillar ECM proteins, facilitating spontaneous and highly ordered large-scale ECM network formation. The hypothesized mechanism involves fibronectin unfolding due to a strong electrostatic interaction with the sulfonic groups exposed from the PSS.

In the present study, the PSS treatment significantly increases the cell surface thiol labeling, which might be due to conformational changes to exofacial proteins with enhanced exposure of thiols. Several experiments have shown that the PSS effect is thiol specific. Experiments with live cells show very substantial internalization of PSS-induced thiol labeling. In extensions of this work the targets of this labeling will be identified by traditional proteomics approaches.

REFERENCES

- 1 Eble, J. A. & de Rezende, F. F. Redox-Relevant Aspects of the Extracellular Matrix and Its Cellular Contacts *via* Integrins. *Antioxidants & Redox Signaling* **20**, 1977-1993, doi:10.1089/ars.2013.5294 (2014).
- 2 Hurd, T. R., DeGennaro, M. & Lehmann, R. Redox regulation of cell migration and adhesion. *Trends in Cell Biology* **22**, 107-115, doi:10.1016/j.tcb.2011.11.002 (2012).
- 3 Jonas, C. R., Ziegler, T. R., Gu, L. H. & Jones, D. P. Extracellular thiol/disulfide redox state affects proliferation rate in a human colon carcinoma (Caco2) cell line. *Free Radical Biology and Medicine* **33**, 1499-1506, doi:10.1016/S0891-5849(02)01081-X (2002).
- 4 Chaiswing, L., Zhong, W., Cullen, J. J., Oberley, L. W. & Oberley, T. D. Extracellular redox state regulates features associated with prostate cancer cell invasion. *Cancer research* **68**, 5820-5826, doi:10.1158/0008-5472.CAN-08-0162 (2008).
- 5 Katchman, B. a. *et al.* Quiescin sulfhydryl oxidase 1 promotes invasion of pancreatic tumor cells mediated by matrix metalloproteinases. *Molecular cancer research : MCR* **9**, 1621-1631, doi:10.1158/1541-7786.MCR-11-0018 (2011).
- 6 Barbouche, R., Miquelis, R., Jones, I. M. & Fenouillet, E. Protein-disulfide isomerase-mediated reduction of two disulfide bonds of HIV envelope glycoprotein 120 occurs post-CXCR4 binding and is required for fusion. *Journal of Biological Chemistry* **278**, 3131-3136, doi:10.1074/jbc.M205467200 (2003).
- 7 Cerutti, N., Killick, M., Jugnarain, V., Papathanasopoulos, M. & Capovilla, A. Disulfide reduction in CD4 domain 1 or 2 Is essential for interaction with HIV glycoprotein 120 (gp120), which impairs thioredoxin-driven CD4 dimerization. *Journal of Biological Chemistry* **289**, 10455-10465, doi:10.1074/jbc.M113.539353 (2014).
- 8 Wan, S.-W. *et al.* Endothelial cell surface expression of protein disulfide isomerase activates β 1 and β 3 integrins and facilitates dengue virus infection. *Journal of cellular biochemistry* **113**, 1681-1691, doi:10.1002/jcb.24037 (2012).
- 9 Laragione, T. *et al.* Regulation of redox-sensitive exofacial protein thiols in CHO cells. **387**, 1371-1376, doi:10.1515/BC.2006.172 (2006).
- 10 Jiang, X.-m. M., Fitzgerald, M., Grant, C. M. & Hogg, P. J. Redox Control of Exofacial Protein Thiols / Disulfides by Protein Disulfide Isomerase *. *The Journal of Biological Chemistry* **274**, 2416-2423 (1999).

- 11 Zai, A., Rudd, M. A., Scribner, A. W. & Loscalzo, J. Cell-surface protein disulfide isomerase catalyzes transnitrosation and regulates intracellular transfer of nitric oxide. **103**, 393-399 (1999).
- 12 Laragione, T. *et al.* Redox regulation of surface protein thiols: Identification of integrin $\alpha 4$ as a molecular target by using redox proteomics. *Proceedings of the National Academy of Sciences* **100**, 14737-14741, doi:10.1073/pnas.2434516100 (2003).
- 13 Angelini, G. *et al.* Antigen-presenting dendritic cells provide the reducing extracellular microenvironment required for T lymphocyte activation. **99**, 1491-1496 (2002).
- 14 Sahaf, B., Heydari, K., Herzenberg, L. a. & Herzenberg, L. a. Lymphocyte surface thiol levels. *Proceedings of the National Academy of Sciences of the United States of America* **100**, 4001-4005, doi:10.1073/pnas.2628032100 (2003).
- 15 Sahaf, B., Heydari, K., Herzenberg, L. A. & Herzenberg, L. A. The extracellular microenvironment plays a key role in regulating the redox status of cell surface proteins in HIV-infected subjects. **434**, 26-32, doi:10.1016/j.abb.2004.11.015 (2005).
- 16 Skalska, J. *et al.* Modulation of cell surface protein free thiols: A potential novel mechanism of action of the sesquiterpene lactone parthenolide. *PloS one* **4**, doi:10.1371/journal.pone.0008115 (2009).
- 17 Cline, D. J. *et al.* New water-soluble phosphines as reductants of peptide and protein disulfide bonds: reactivity and membrane permeability. *Biochemistry* **43**, 15195-15203, doi:10.1021/bi048329a (2004).
- 18 Kumar, P. *et al.* Macromolecularly crowded in vitro microenvironments accelerate the production of extracellular matrix-rich supramolecular assemblies. *Scientific Reports* **5**, 8729, doi:10.1038/srep08729 (2015).
- 19 Lareu, R. R. *et al.* Collagen matrix deposition is dramatically enhanced in vitro when crowded with charged macromolecules: The biological relevance of the excluded volume effect. *FEBS Letters* **581**, 2709-2714, doi:10.1016/j.febslet.2007.05.020 (2007).
- 20 Lareu, R. R., Arsianti, I., Subramhanya, H. K., Yanxian, P. & Raghunath, M. In vitro enhancement of collagen matrix formation and crosslinking for applications in tissue engineering: a preliminary study. *Tissue engineering* **13**, 385-391, doi:10.1089/ten.2007.13.ft-344 (2007).
- 21 Chen, C., Loe, F., Blocki, A., Peng, Y. & Raghunath, M. Applying macromolecular crowding to enhance extracellular matrix deposition and its remodeling in vitro for tissue engineering and cell-based therapies. *Advanced Drug Delivery Reviews* **63**, 277-290, doi:10.1016/j.addr.2011.03.003 (2011).
- 22 Jiang, M. & Guo, Z. Effects of macromolecular crowding on the intrinsic catalytic efficiency and structure of enterobactin-specific isochorismate synthase. *Journal of the American Chemical Society* **129**, 730-731, doi:10.1021/ja065064+ (2007).

- 23 Norris, M. G. & Malys, N. What is the true enzyme kinetics in the biological system? An investigation of macromolecular crowding effect upon enzyme kinetics of glucose-6-phosphate dehydrogenase. *Biochemical and biophysical research communications* **405**, 388-392, doi:10.1016/j.bbrc.2011.01.037 (2011).
- 24 Ilani, T. *et al.* A secreted disulfide catalyst controls extracellular matrix composition and function. *Science (New York, N.Y.)* **341**, 74-76, doi:10.1126/science.1238279 (2013).
- 25 Essex, D. W. Redox control of platelet function. *Antioxidants & redox signaling* **11**, 1191-1225, doi:10.1089/ARS.2008.2322 (2009).
- 26 Jordan, P. A. & Gibbins, J. M. Extracellular Disulfide Exchange and the Regulation of Cellular Function. *Antioxidants & Redox Signaling* **8**, 312-324, doi:10.1089/ars.2006.8.312 (2006).
- 27 Matthias, L. J. & Hogg, P. J. Redox Control on the Cell Surface: Implications for HIV-1 Entry. *Antioxidants & Redox Signaling* **5**, 133-138, doi:10.1089/152308603321223621 (2003).
- 28 Sahaf, B., Heydari, K., Herzenberg, L. A. & Herzenberg, L. A. Lymphocyte surface thiol levels. (2002).
- 29 Yan, Z., Garg, S. K., Kipnis, J. & Banerjee, R. Extracellular redox modulation by regulatory T cells. **5**, 721-723, doi:10.1038/nchembio.212 (2009).
- 30 Go, Y. M. & Jones, D. P. Cysteine/cystine redox signaling in cardiovascular disease. *Free Radical Biology and Medicine* **50**, 495-509, doi:10.1016/j.freeradbiomed.2010.11.029 (2011).
- 31 Acosta-Serrano, A. *et al.* The surface coat of procyclic Trypanosoma brucei: Programmed expression and proteolytic cleavage of procyclin in the tsetse fly. *Proceedings of the National Academy of Sciences* **98**, 1513-1518, doi:10.1073/pnas.98.4.1513 (2001).
- 32 Metcalfe, C., Cresswell, P., Ciaccia, L., Thomas, B. & Barclay, A. N. Labile disulfide bonds are common at the leucocyte cell surface. *Open Biology* **1**, 110010-110010, doi:10.1098/rsob.110010 (2011).
- 33 Stegmann, M., Metcalfe, C. & Barclay, A. N. Immunoregulation through membrane proteins modified by reducing conditions induced by immune reactions. *European Journal of Immunology* **43**, 15-21, doi:10.1002/eji.201242849 (2013).
- 34 Swiatkowska, M. *et al.* Ero1 α is expressed on blood platelets in association with protein-disulfide isomerase and contributes to redox-controlled remodeling of α IIb β 3. *Journal of Biological Chemistry* **285**, 29874-29883, doi:10.1074/jbc.M109.092486 (2010).
- 35 Miyata, Y., Maeda, T., Odate, T., Shimanaka, K. & Kusano, E. Characterization of the Cation-Binding Capacity of a Potassium-Adsorption Filter Used in Red Blood Cell Transfusion. *Therapeutic Apheresis and Dialysis* **19**, 288-295, doi:10.1111/1744-9987.12278 (2015).

- 36 Vaquette, C. *et al.* The effect of polystyrene sodium sulfonate grafting on polyethylene terephthalate artificial ligaments on invitro mineralisation and invivo bone tissue integration. *Biomaterials* **34**, 7048-7063, doi:10.1016/j.biomaterials.2013.05.058 (2013).
- 37 Collazos-Castro, J. E., Polo, J. L., Hernández-Labrado, G. R., Padial-Cañete, V. & García-Rama, C. Bioelectrochemical control of neural cell development on conducting polymers. *Biomaterials* **31**, 9244-9255, doi:10.1016/j.biomaterials.2010.08.057 (2010).
- 38 Oughlis, S. *et al.* The osteogenic differentiation improvement of human mesenchymal stem cells on titanium grafted with polyNaSS bioactive polymer. *Journal of Biomedical Materials Research - Part A* **101 A**, 582-589, doi:10.1002/jbm.a.34336 (2013).
- 39 Felgueiras, H. & Migonney, V. Sulfonate groups grafted on Ti6Al4V favor MC3T3-E1 cell performance in serum free medium conditions. *Materials Science and Engineering C* **39**, 196-202, doi:10.1016/j.msec.2014.03.013 (2014).
- 40 Clark, M. R. *et al.* Enzymatic triggered release of an HIV-1 entry inhibitor from prostate specific antigen degradable microparticles. *International Journal of Pharmaceutics* **413**, 10-18, doi:10.1016/j.ijpharm.2011.04.004 (2011).
- 41 Neurath, A. R., Strick, N. & Li, Y.-Y. Role of seminal plasma in the anti-HIV-1 activity of candidate microbicides. *BMC Infectious Diseases* **6**, 150, doi:10.1186/1471-2334-6-150 (2006).
- 42 Voigt, J., Christensen, J. & Shastri, V. P. Differential uptake of nanoparticles by endothelial cells through polyelectrolytes with affinity for caveolae. *Proceedings of the National Academy of Sciences of the United States of America* **111**, 2942-2947, doi:10.1073/pnas.1322356111 (2014).
- 43 Saburova, E. A., Basova, L. V., Dybovskaya, Y. N. & Sukhorukov, B. I. Destructive Effect of Polystyrene Sulfonate on the Structure of Hemoproteins. **80**, 1325-1335, doi:10.1134/S0036024406080280 (2006).
- 44 Kowalczyńska, H. M. *et al.* Albumin adsorption on unmodified and sulfonated polystyrene surfaces, in relation to cell-substratum adhesion. *Colloids and Surfaces B: Biointerfaces* **84**, 536-544, doi:10.1016/j.colsurfb.2011.02.013 (2011).
- 45 Kowalczyńska, H. M. *et al.* Atomic force microscopy evidence for conformational changes of fibronectin adsorbed on unmodified and sulfonated polystyrene surfaces. *Journal of Biomedical Materials Research - Part A* **91**, 1239-1251, doi:10.1002/jbm.a.32473 (2009).
- 46 Ahn, S. *et al.* Self-organizing large-scale extracellular-matrix protein networks. *Advanced Materials* **27**, 2838-2845, doi:10.1002/adma.201405556 (2015).

Chapter 4

THE APPLICATION OF THIOL/DISULFIDE AND THIOL/NH₂ IMAGING TO A MULTICELLULAR ORGANISM AND A DISULFIDE-RICH BIOMATERIAL

4.1 General Introduction

In Chapter 3 of this dissertation we applied ratiometric imaging to address the redox status of the outer surface of a range of cells. In this final chapter we illustrate the broad applicability of these general methods using two entirely different examples. In the first, we use redox imaging to examine the cuticle of the worm, *Caenorhabditis elegans*. In the second, we apply the methods developed in Chapter 3 to probe the disulfide-rich fibers that are found in avian eggshell membranes. In the first part of the following sections we introduce aspects of *C. elegans* that are most relevant to the redox imaging that follows later in the Chapter.

4.2 *C. elegans* – an Introduction to Relevant Aspects

4.2.1 General

C. elegans has been central to many aspects of biological and biomedical research¹. The nematode has about a thousand cells enclosed in a largely proteinaceous cuticle (Figure 4.1). *C. elegans* develops rapidly - from egg to adult in 3 days (Figure 4.2) and is exceptionally easy to cultivate and maintain. The worm is a filter feeder receiving a suspension of bacteria through its mouth parts driven by

opening of the lumen formed from the corpus and isthmus regions (Figure 4.1)¹. In a complex series of events, the bacteria collected adjacent to the grinder are fragmented and passed to the intestine while contraction of the lumen forces the spent liquid back through the mouthparts¹. Following disruption of the microbial cells, digestion proceeds via an array of glycosidases, lipases and proteases².

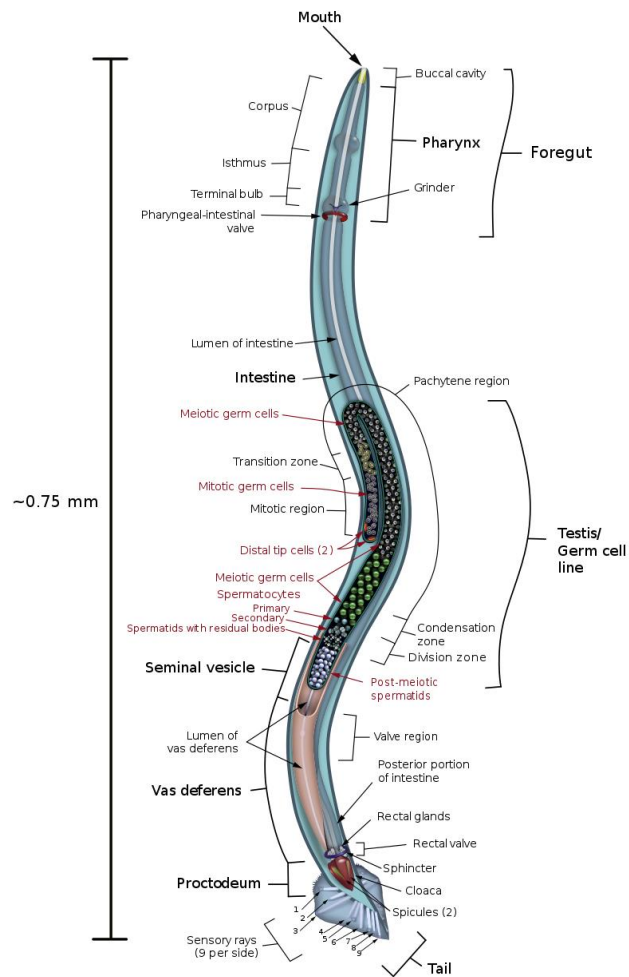


Figure 4.1 Schematic Depiction of a male *C. elegans* nematode. Figure is from Wikipedia.

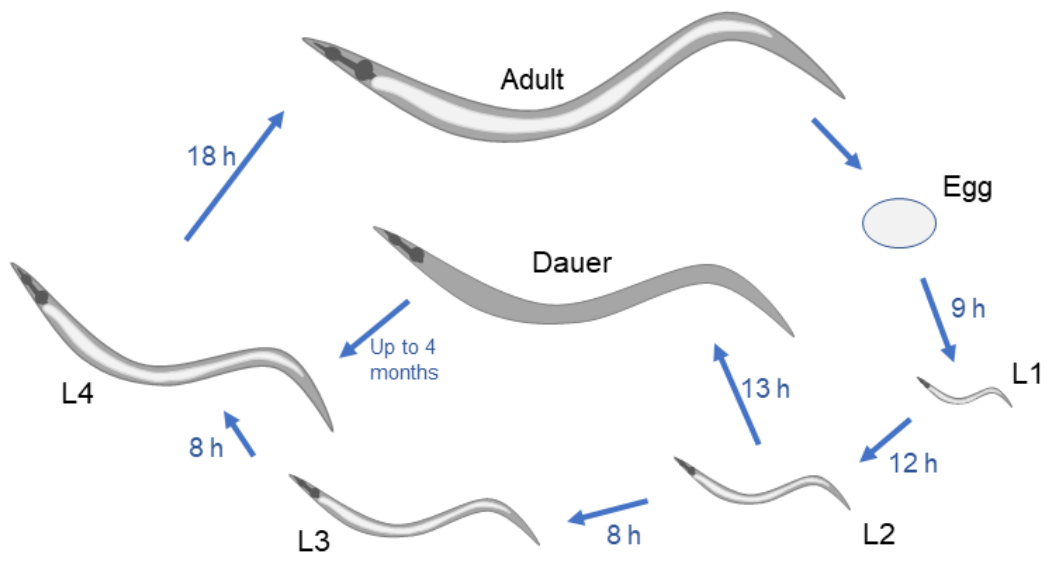


Figure 4.2 **Life cycle of *C. elegans***. Figure is adapted from Clark and Hodgkin³.

4.2.2 Cuticle Structure

The *C. elegans* cuticle is a flexible exoskeleton that serves to protect and insulate the worm from environmental stress. Starting with the embryonic cuticle, worms synthesize 5 iterations of this complex multilayered structure^{1,4,5}. Proceeding inwards, the cuticle has a negatively-charged glycoprotein surface coat, a lipid epicuticle, and then two mainly proteinaceous layers^{1,4,5} (see Figure 4.3 A). Collagens comprise about 80% of the total cuticular proteins, and are distinguished from their mammalian counterparts by being smaller and having several regions in which the canonical -GXY- repeat are replaced by non-triple-helical regions^{5,6}. Proteolytic processing of *C. elegans* collagens typically generates products which retain at least 2 disulfides⁶.

The second major protein component, the cuticulins, contain zona-pellucida domains that are widely distributed within structural proteins of the extracellular matrix⁷. These domains are of about 260 amino acids and contain 4 conserved disulfide bonds⁶. During the assembly of the cuticle, cuticulins are extensively crosslinked by peroxidase-mediated tyrosine coupling. This leads to critical stabilization of this outer protein layer^{1,5} (see Figure 4.3 A).

4.2.3 Moulting

Moulting in *C. elegans* begins with a period of relative physical inactivity (lethargus) during which a new cuticle is assembled under the old one^{1,4,5}. Immediately prior to lethargus, secretory cargo is accumulated in seam cells ready to be used in the layered assembly of the new cuticle. Lethargus begins with the breakage of the connections between the old cuticle and the underlying hypodermis

(apolysis)^{1,4,5} (see Figure 4.3 B). This critical event is initiated by reduction of cuticular disulfides using reduced thioredoxin and glutathione generated via the worm's selenoprotein thioredoxin reductase and glutathione reductase⁸. This key observation led us to test our redox imaging method with *C. elegans*. This work is not intended to be a comprehensive study of the details of nematode moulting. Instead, we just wish to showcase the quality of thiol/disulfide visualization that can be achieved in a multicellular organism.

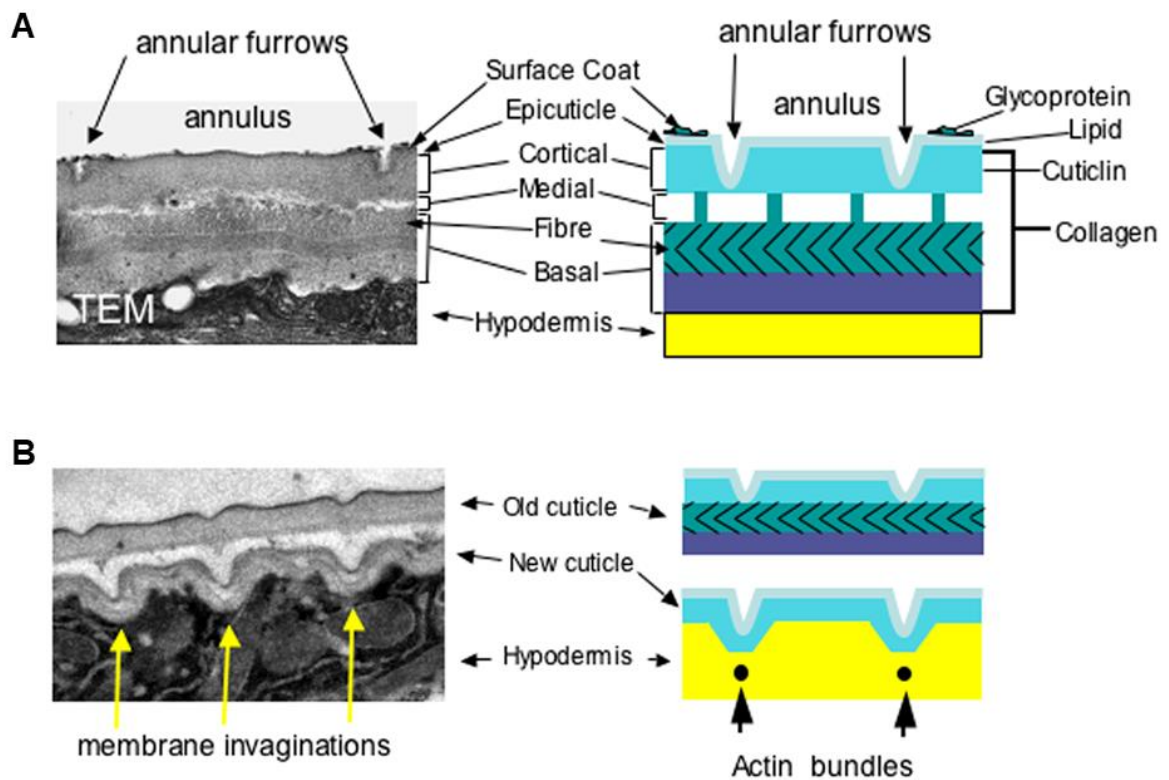


Figure 4.3 **The organization and structure of the *C. elegans* cuticle.** This figure is reprinted from Page & Johnstone⁶. Panel A is depicting a cross-section of the adult cuticle with distinct structural layers. Panel B depicts the synthesis of a new cuticle and the associated detachment of the old cuticle.

4.2.4 Experimental Procedures

4.2.4.1 Worm Preparation

The worms were prepared by Michael Clupper from Dr. Jessica Tanis' Lab in the Department of Biological Science. Briefly, *Caenorhabditis elegans* strains were maintained using standard conditions at 20°C on nematode growth medium (NGM) plates seeded with *Escherichia coli* OP50⁹. The wild-type N2 strain was used for all experiments.

The synchronization procedure is as follows. 3-4 plates of gravid adult hermaphrodites were washed off plates with M9 solution and pelleted at 350 x g for 1 minute. Pellets were resuspended in 10 mL of bleach solution (20% bleach, 5% 10 M NaOH in water) for 5 minutes with shaking, resulting in isolation of eggs. Eggs were rinsed 3 times by pelleting, discarding supernatant, and resuspending in 15 mL of M9 solution. Following a final rinse, the eggs were resuspended in 10 mL of M9 solution and allowed to incubate at 20°C on a rotary shaker overnight. This results in a synchronized population of larvae arrested at the L1 phase. Animals were then pelleted, and the supernatant was removed to allow approximately 1 mL of medium. Approximately 40-50 synchronized animals were plated onto a single OP50-seeded NGM plate.

4.2.4.2 Redox Staining of Worms

Worms were washed 3 times with Dulbecco's Phosphate-Buffered Salt Solution (DPBS, from Corning) and fixed with 4% methanol-free PFA at room temperature for 10 min. After 3 washes in DPBS, worms were incubated in the dark with 1 μM sulfo-Cy3B-maleimide and 10 μM methyl-PEG₂₄-maleimide in DPBS at

room temperature for 10 min. After 3 washes in DPBS, 5 mM tris (2-carboxyethyl) phosphine (TCEP) in DPBS was applied to cells at room temperature for 10 min, followed by 1 μ M sulfo-Cy5-maleimide and 10 μ M methyl-PEG₂₄-maleimide treatment again for 10 min at room temperature in the dark. Following 3 washes, worms were mounted with Fluoromount-G sealing the coverslip with clear nail polish.

During each staining or wash step, bench top centrifuges were applied to spin down the worms. In some later trials, a nylon mesh (Sefar) with 1 μ m holes immobilized between two pipet tips was used to filter the worms to avoid a large number of centrifugations. After the staining procedure, the mesh was recovered and worms were rinsed off and mounted.

4.2.4.3 Microscope Imaging and Image Analysis

Fluorescence images were acquired using a Zeiss LSM 780 upright confocal microscope in the Biological Department at the University of Delaware. The laser and filter sets were as follows: for Cy3B fluorophore, excitation at 561 nm, emission at 560-630 nm. For Cy5 fluorophore, excitation at 633 nm, emission at 637-758 nm. A 40x oil objective was used. Zeiss Zen software was used for image acquisition.

4.2.5 Results and Discussion

4.2.5.1 Redox Staining in Esophagus and Grinder

Figure 4.4 shows staining in esophagus and grinder of worms. Panel A and B show two representative adult worms, with the whole esophagus stained with green (representing SH) and the mouth part highly stained with red (representing SS). Panel

C shows a 3D reconstruction of the stained esophagus. The cross-like structure at the end of the esophagus is the grinder and it can be found strongly stained in almost all the worms (Figure 4.4, and later), no further area of the digestion track is stained. This SH staining might represent the high level of thiols of ground bacteria that are concentrated in the grinder. Note that the surface of adult worm is not stained. This might be due to the lipid layer on the cuticle (the epicuticle, Figure 4.3) that precludes staining.

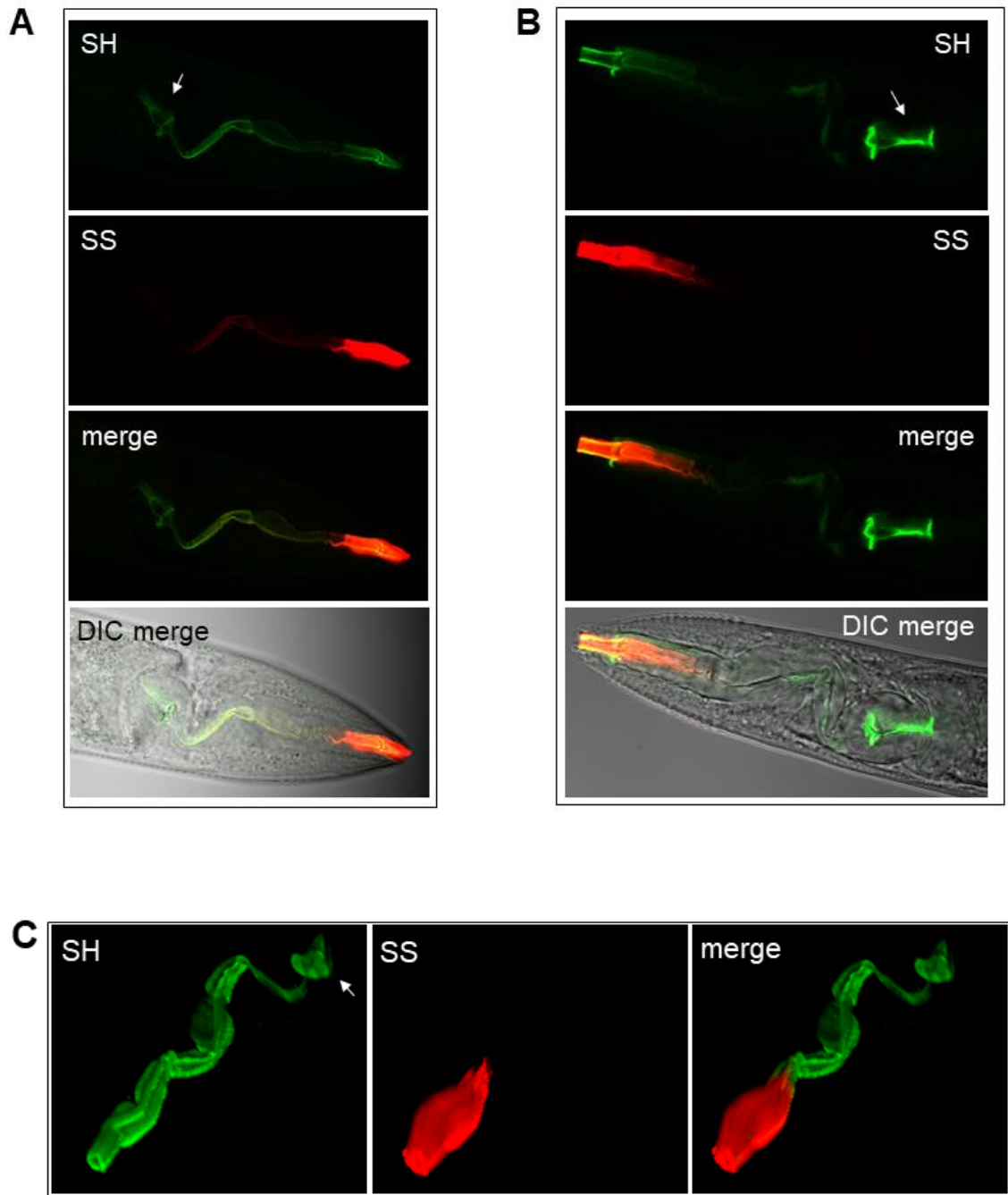


Figure 4.4 **Redox staining in esophagus and grinder of adult worms.** Panel A and B shows the two representative adult worms, the green channel shows SH staining and the red channel shows SS staining. Panel C shows a 3D reconstruction of a stained esophagus. The white arrows show the cross-like grinder structure at the end of the esophagus.

4.2.5.2 Level 1 Worms Show Strong Surface Staining

Unlike the adult worms, the young worms such as level 1 can be highly stained on the cuticle. Figure 4.5 shows images from two of the level 1 worms.

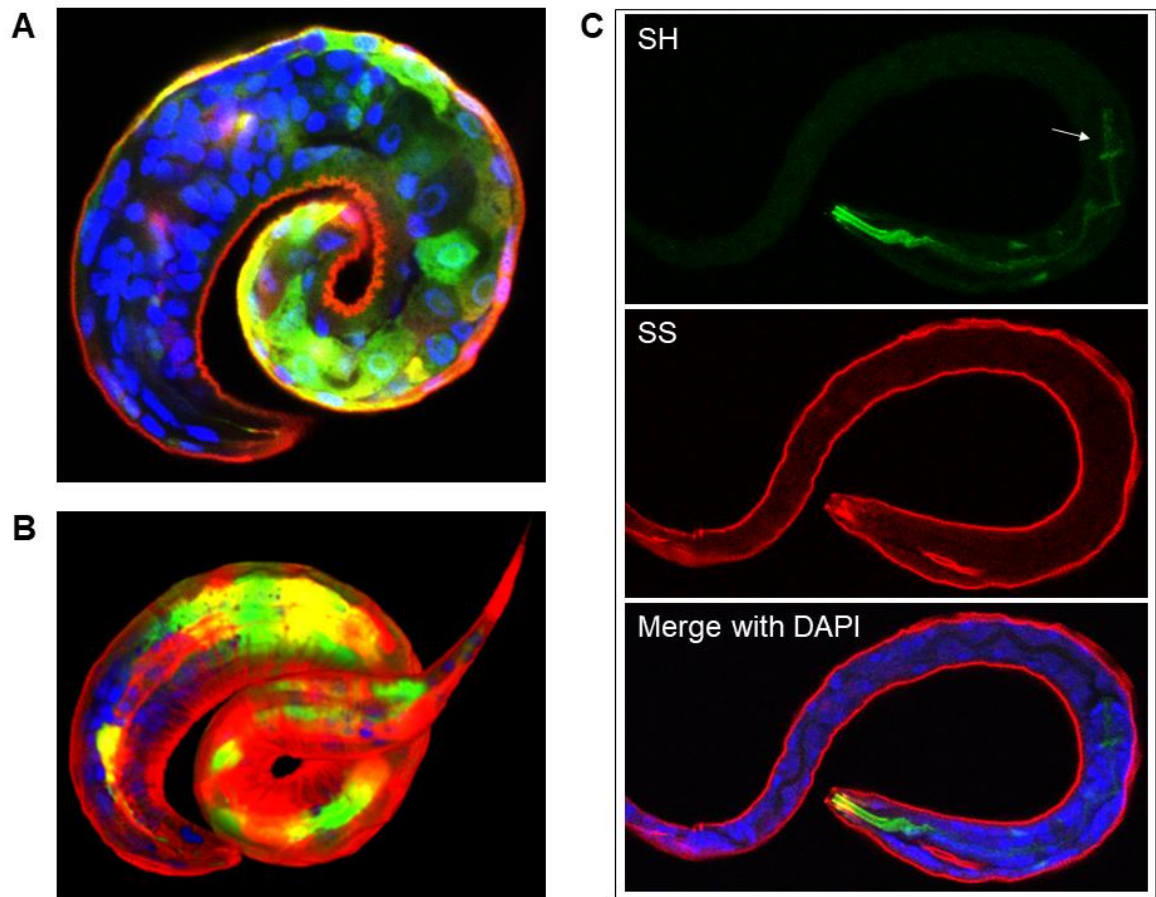


Figure 4.5 **Redox staining of two of the level 1 worms.** The green channel indicates the SH staining and the red channel shows the SS staining. Nuclei are shown in blue (DAPI). Panel A shows one section of a z-stack imaging of a level 1 worm. Panel B is the 3D reconstruction of the same worm. Panel C shows another worm with the esophagus and grinder (white arrow) stained as green.

4.2.5.3 Redox Staining on Molting Worms

Worms in lethargus were obtained and stained with the typical SH/SS staining procedure. Figure 4.6 shows one worm that is molting. The wrinkled surface indicates the formation of a new layer of cuticle. The red staining (representing SS) is all through the whole worm while the green staining (representing SH) is only from a certain point near the grinder to the tail. We can also find a shed old cuticle at the tail, indicating the half-way molting was captured in this image. As mentioned in the introduction, the breakage of the connections between the old cuticle and the new cuticle involves reduction of cuticular disulfides using reduced thioredoxin and glutathione. The green staining indicates the reduced environment between the old and new cuticles, while the red staining indicates the newly formed cuticle that contains high level of disulfides (the epicuticle lipid layer might have not yet formed so the cuticle can be stained).

Figure 4.7 shows another worm undergoing the molting process. Interestingly, this worm maintains a smooth outlook during molting. The outer (old) cuticle is stained as red, indicating disulfides on the surface. The esophagus and mouth are not stained at all, indicating a seeming protection of old cuticle to the worm inside.

4.2.5.4 Conclusion

With the SH/SS staining protocol we have visualized the redox state of specific stage of *C. elegans* worms for the first time. Although this work is not a comprehensive study of the details of nematode molting, it presents some information of redox state in certain structures of worms at different stages. Also, we have shown

the high quality of SH/SS visualization that can be achieved in a multicellular organism.

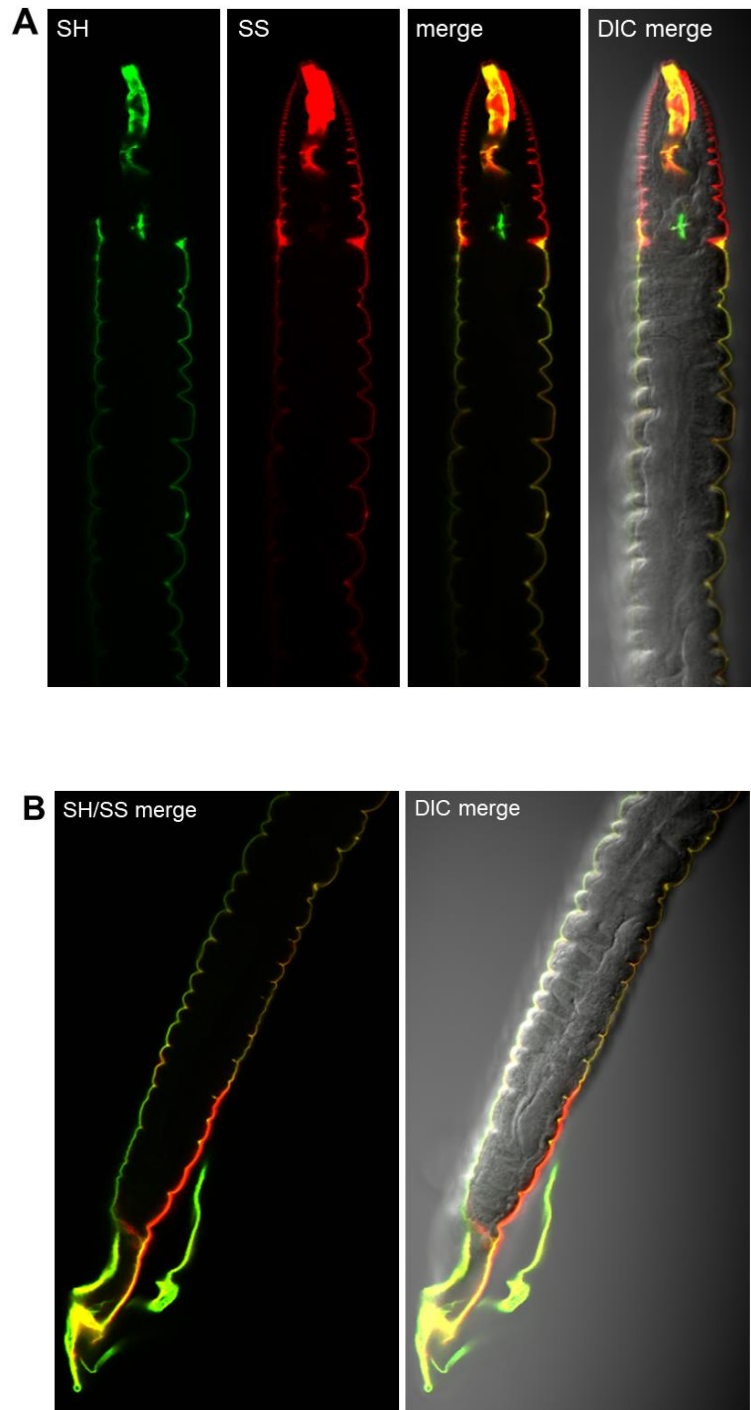


Figure 4.6 **Redox staining on a molting worm.** The green channel indicates the SH and the red channel shows the SS. Panel A shows the head part of the worm. Panel B shows the tail of the same worm.

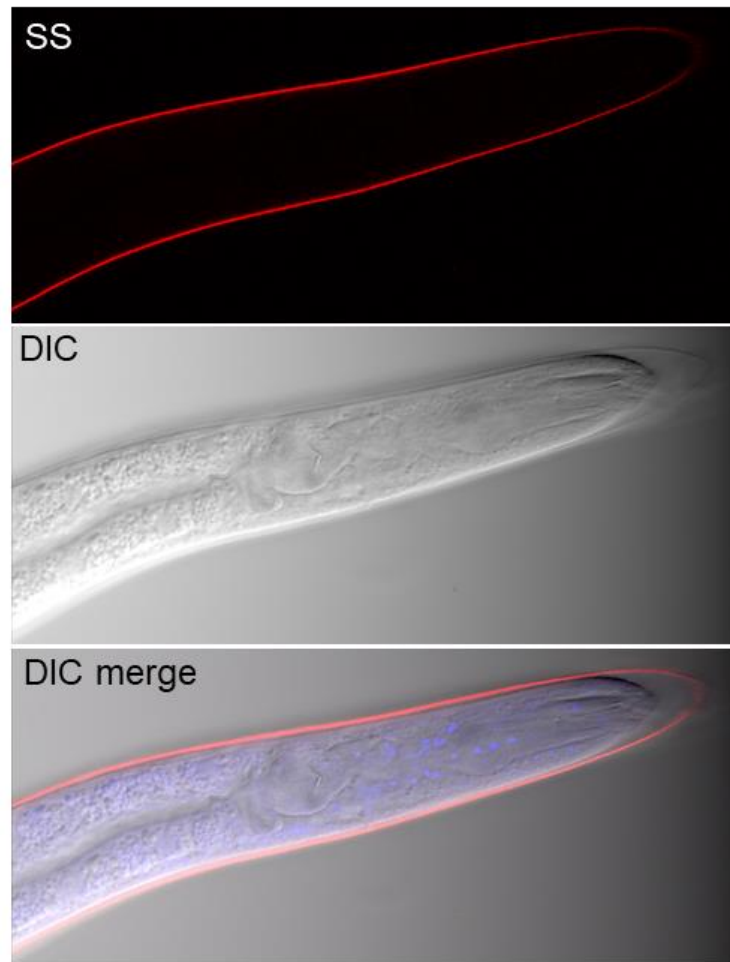


Figure 4.7 **Redox staining on a molting worm.** The red channel shows the SS, nuclei are stained with DAPI (blue). The green channel was not shown here because there is not signals.

4.3 Egg Shell Membrane

4.3.1 General Introduction

Bird eggs are formed in a series of discrete steps. The process is initiated by deposition of a yolk cell (the “yolk”) into the oviduct via a funnel-shaped structure called the infundibulum¹⁰. The massive secretion event that deposits the egg white around the yolk requires a 2-3 hour residence in the magnum region of the chicken oviduct. While egg white deposition has received a lot of attention¹⁰, the molecular details of the next three stages of egg construction remain cryptic. First, in the isthmus region of the oviduct, a thin membranous layer of uncertain composition (the “limiting membrane”), is deposited over the egg white¹⁰⁻¹⁴. Hincke and coworkers¹⁵ have found notable lysozyme immunoreactivity associated with this structure using immunogold staining. This limiting membrane (not shown in Figure 4.8) subsequently serves as a platform for the inner membrane. The inner membrane is an approximately 20 μm layer of adherent fibers (of typically less than 2 μm diameter). These fibers are extruded from tubular gland cells lining the isthmus¹⁶ and the layer deepens as the egg rotates within the oviduct. Further down the isthmus, a second ~ 60 μm deep layer of generally thicker fibers is deposited by a comparable mechanism¹⁰. Inner and outer layers remain in contact except in the area of the air sac (Figure 4.8). It has been suggested, on the basis of structural similarities¹², that inner and outer membranes share a common protein composition. Electron microscopy of stained and dehydrated cross sections of ESM fibers reveal an electron dense (medullary) core believed to be protein surrounded by a mantle (cortical) region of carbohydrate^{11,12,17,18}. Deposition of the calcium carbonate is the last major step in the synthesis of a bird's egg.

Calcification occurs within the shell gland of the oviduct and requires about 20 h for completion in the chicken¹⁰.

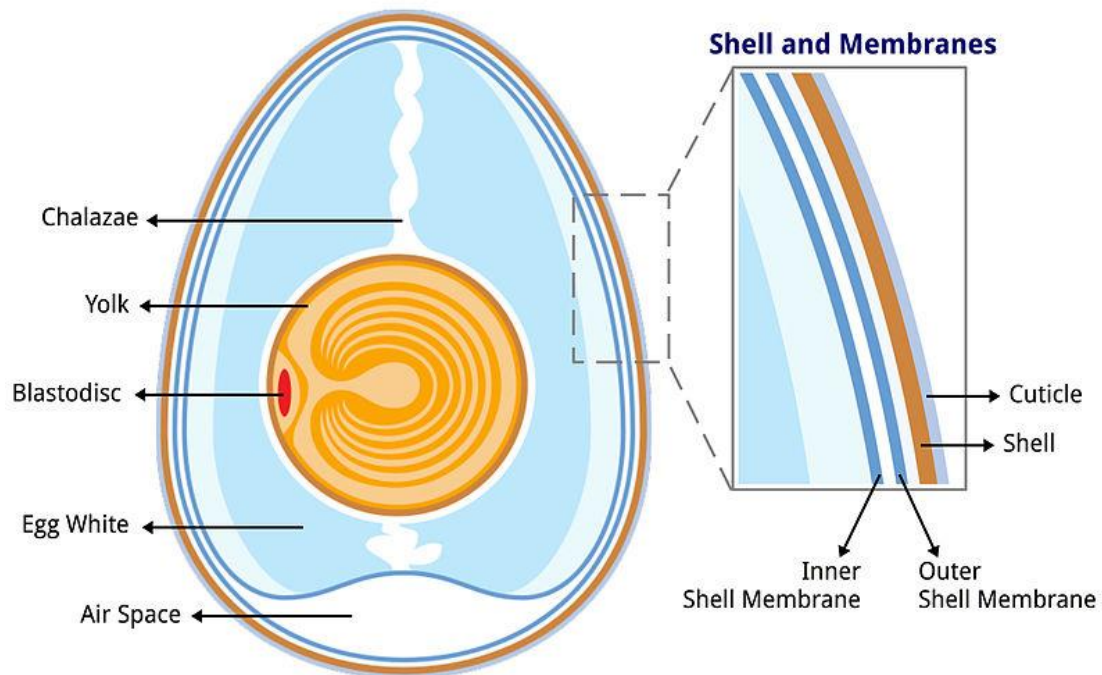


Figure 4.8 **Key components of a bird's egg.** The detail is not drawn to scale. The external cuticle layer is largely formed from protein, and may serve as a barrier to microbial attack and water loss. The calcified cell is a composite material consisting of calcium carbonate and small amounts of proteins that form a fibrous network. Outer and inner eggshell membranes are formed largely from protein fibers (see the Text). Not shown in this illustration is the limiting membrane. It lies between the egg white and the inner membrane. Illustration taken from: https://commons.wikimedia.org/wiki/File:Anatomy_of_an_egg_labeled.jpg

Eggshell membranes are largely proteinaceous. Both the inner and outer layers share similar amino composition, reinforcing the idea that they may be constructed from the same ratio of protein types^{10,19}. One persistent misconception is that the ESM fibers are largely made up of collagen. While collagens have been reported by immunochemical staining and by proteomic studies^{14,18,20-23}, our laboratory has shown that the presence of collagens as a major fraction of the total protein content of ESM is a mathematical impossibility¹⁹. Thus chicken collagens contain less than 1% cysteine, whereas amino acid analysis of total ESM show more than 10% cysteine¹⁹. In fact the composition of the fibrous layers coincides more closely to a novel disulfide-rich structural protein (CREMP) discovered by Kodali et al.¹⁹. CREMP proteins are composed of large numbers of very similar 2-disulfide containing modules arranged end to end to form structural proteins that are incorporated into the fibers.

Dissociation of intact ESM proteins from mature fibers proves impossible because the components are extensively and irreversibly crosslinked at lysine residues^{24,25}. This oxidative posttranslational modification is initiated by lysyl oxidase and leads to the coupling of 4 lysine residues to generate desmosine and isodesmosine derivatives¹⁰. The fibers are then resistant to dissolution with standard biochemical strategies including exposure to disulfide reductants such as dithiothreitol and TCEP^{19,24,25}.

Since the fibers are not destroyed by disulfide reductants, we attempted to visualize ESM fibers via selectively labeling of the reduced ESM with a fluorescent maleimide. However, in preparatory experiments for the paper by Kodali et al.¹⁹ these workers found that both fluorescein- and rhodamine-maleimides gave unacceptable background staining of the native oxidized ESM. Monobromobimane provided a

workable interim solution¹⁹ although the fluorescence was modest, and this dye is not optimal for modern confocal techniques. In the next section, we show that the bright sulfonated dyes we have used in Chapter 3 are well suited for fluorescence imaging of the disulfide rich ESM. Not only do these new findings lay the groundwork for future studies intended to use super-resolution confocal methods to probe fiber compositions, but these methods provide an additional way to visualize the limiting membrane without using electron microscopy.

4.3.2 Experimental Procedures

4.3.2.1 Preparation of ESM

Chicken eggs were purchased from a local grocery store. The eggs were cracked and the egg shell membrane was peeled away from the shell using gloved fingers. Care was taken to maintain the orientation of the membrane so that the side of the ESM facing the egg white was uppermost. Pieces were placed on thick plastic sheet in this orientation and then cut in rectangles of about 1.5 cm wide and 0.7 cm deep. A diagonal notch was cut in the top right of the pieces to allow for the orientation of the ESM pieces to be known following washing steps. Care was also taken to make sure that the pieces of ESM contained inner and outer layers of fibers by avoiding the area around the air sac (Figure 4.8). Membrane rectangles could be stored at 4 °C for several days. The pieces were then incubated in a range of conditions with or without denaturants and reductants (see later) with gentle rocking.

In some trials the ESM was first sectioned by Ms. Jean Ross at the Delaware Biotechnology Institute. Briefly, membranes were taken through a dehydration series

starting with 50% ethanol, then 75% and ending with 95%. Then samples were embedded in LR White resin and sectioned with a vibratome.

4.3.2.2 Redox Labeling of ESM

The membrane pieces in water were first washed with DPBS, and then treated with DPBS with or without 5 mM TCEP. Membranes were then washed and incubated in DPBS containing 0.5 μ M Cy5-maleimide dye diluted with 100 μ M NEM for 10 min. After washing in DPBS, the membranes were mounted on slides and imaged using confocal microscopy. In some trials Cy3B-maleimide was used instead of the Cy5 dye. It should be noted that ESM contains no free thiols¹⁹.

4.3.2.3 Microscope Imaging and Image Analysis

Fluorescence images were acquired using a Zeiss LSM 780 upright confocal microscope in the Biological Department at the University of Delaware. The laser and filter sets are as follows: for Cy3B fluorophore, excitation at 561 nm, emission at 560-630 nm. For Cy5 fluorophore, excitation at 633 nm, emission at 637-758 nm. A 40x oil objective was used. Zeiss Zen software was used for image acquisition.

4.3.3 Results and Discussion

4.3.3.1 Disulfide Staining on Both Sides of Membrane

ESM was treated with 5 mM TCEP in DPBS for 2 min at room temperature, and stained with 0.5 μ M Cy5-maleimide and 100 μ M NEM for 10 min. Figure 4.9

shows the staining of both sides of the membranes. Panel A shows the side facing the egg white (inner membrane). There is a layer of granule-like structures on this side with some fibers among them. Panel B shows the side facing the egg shell (outer membrane). The fibers are the main structures here, with some granules attaching on them.

According to preliminary experiments for the paper by Kodali et al.¹⁹, both fluorescein- and rhodamine-maleimides gave unacceptable background staining of the native oxidized ESM. However, the sulfo-Cy5-maleimide dye used in the current work does not show this problem. Figure 4.10 shows that the labeling is completely dependent on the reduction of disulfides using TCEP, thus the signals are not due to non-specific binding of dye but a selective labeling of liberated thiols from disulfides on the ESM. This is critical to future studies of the distribution of disulfide within the fiber cross sections using super-resolution studies.

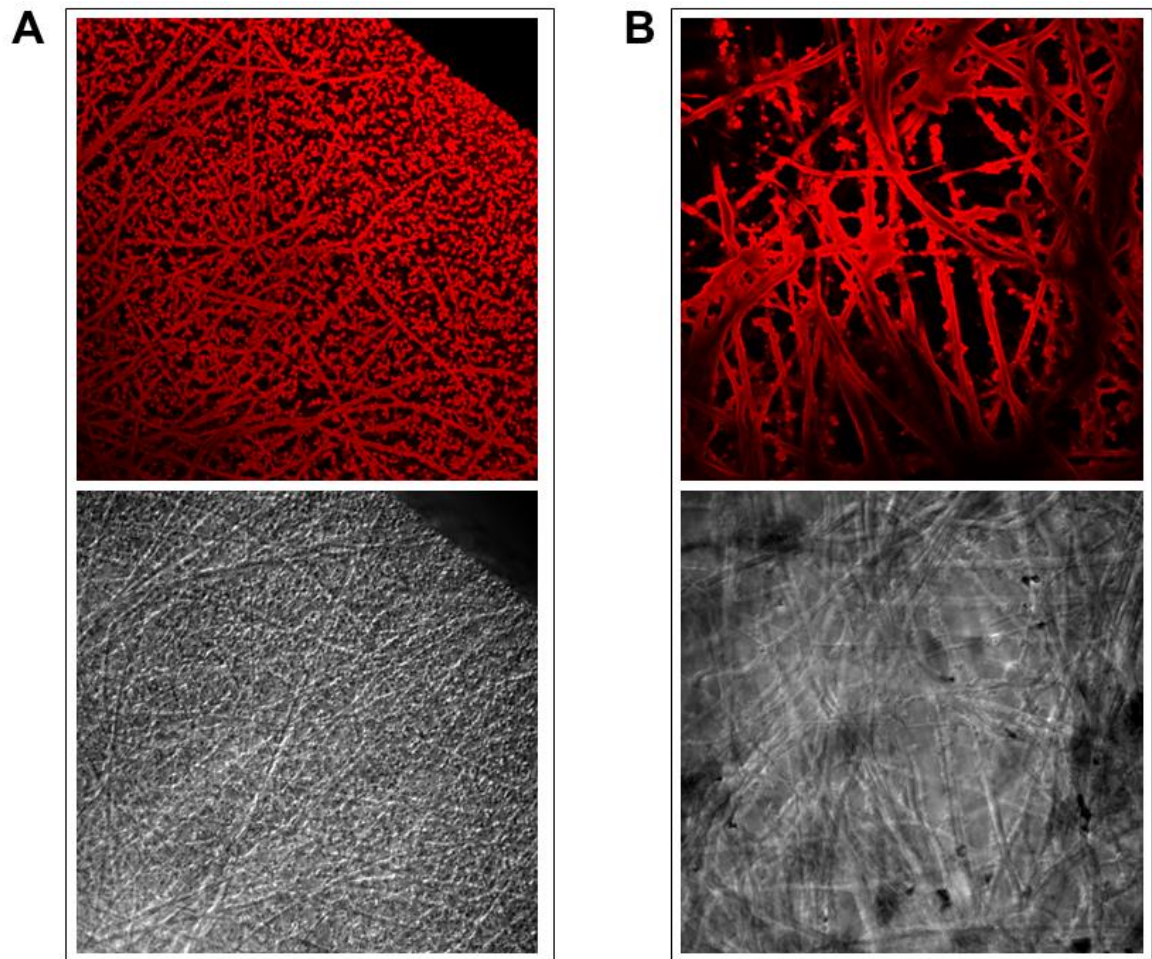


Figure 4.9 **Disulfide staining on both sides of egg shell membrane.** The red channel shows the Cy5-maleimide labeling disulfides, the grey channel is the DIC channel. Panel A shows the side facing the egg white. Panel B shows the side facing the egg shell. These two images are with the same magnification.

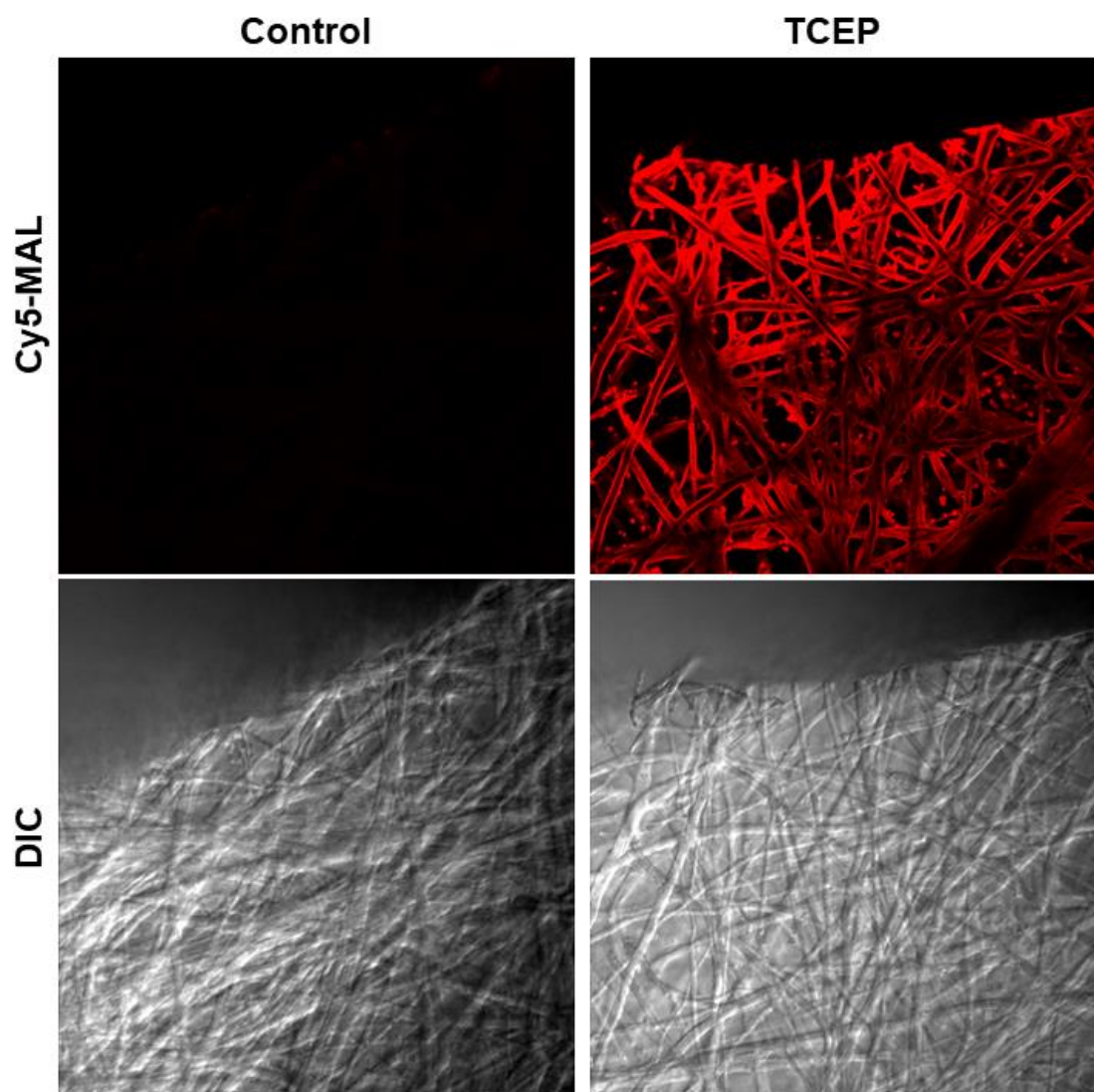


Figure 4.10 **The labeling of ESM by Cy5-maleimide is dependent on pre-reduction of protein disulfides.** The ESM was treated with or without 5 mM TCEP and stained with 1 μ M Cy5-maleimide diluted with 10 μ M PEG₂₄-maleimide.

4.3.3.2 GnCl and Reductants Disrupt the Thiol Distribution on the Membrane

Membranes were then treated with 4 M guanidine HCL (GnCl) with or without the disulfide reductant DTT to assess their effect on the structure of ESM. Membranes treated with or without protein denaturants and reductants overnight were subsequently treated with 5 mM TCEP followed with Cy5-maleimide labeling as before. Figure 4.11 shows that 4 M GnCl does not appear to change the structure of the inner membrane (the side facing the egg white), but GnCl together with 10 mM DTT leads to a major morphological change to the inner face of ESM. Here, there is an apparent loss of granules and the appearance of plate-like pieces. Figure 4.12 shows the results of another trial, in which sulfo-Cy3B-maleimide was used for SS staining, and Cy5-NHS ester was used to label the amino groups. The membrane treated with only DPBS shows granule structures in both channel (green for SS, red for NH₂), but on the membrane treated with GnCl and DTT, the red channel shows regular structure while the green channel shows an apparently degraded structure. Treatment with the combination of other denaturants (such as SDS) and other reductants (such as THP) show similar results (data not shown), indicating that the denaturants and reductants together impact the granular structures containing thiols.

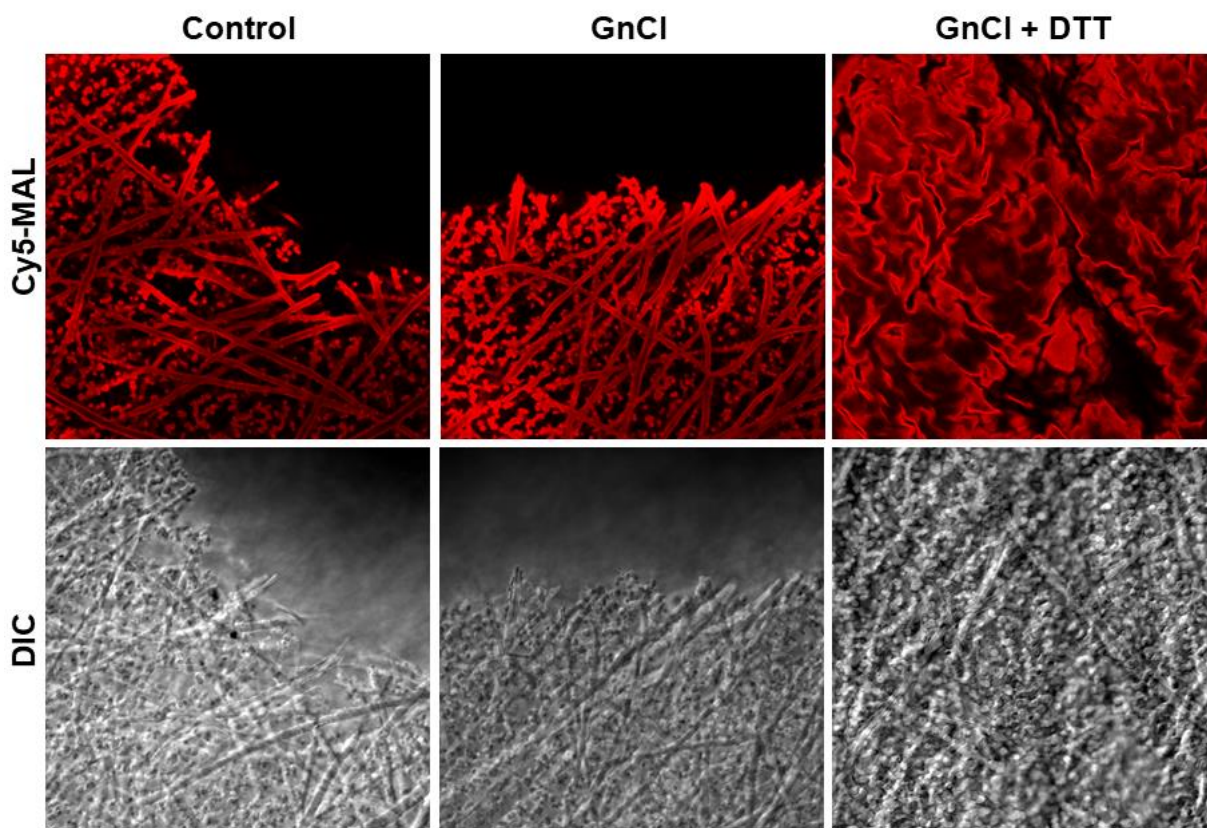


Figure 4.11 **GnCl and reductant disrupts the structure on ESM.** ESM pieces were treated with DPBS, 4 M GnCl, and 4 M GnCl with 10 mM DTT for 14 h with rocking. The treated membranes were reduced by TCEP and stained with Cy5-maleimide.

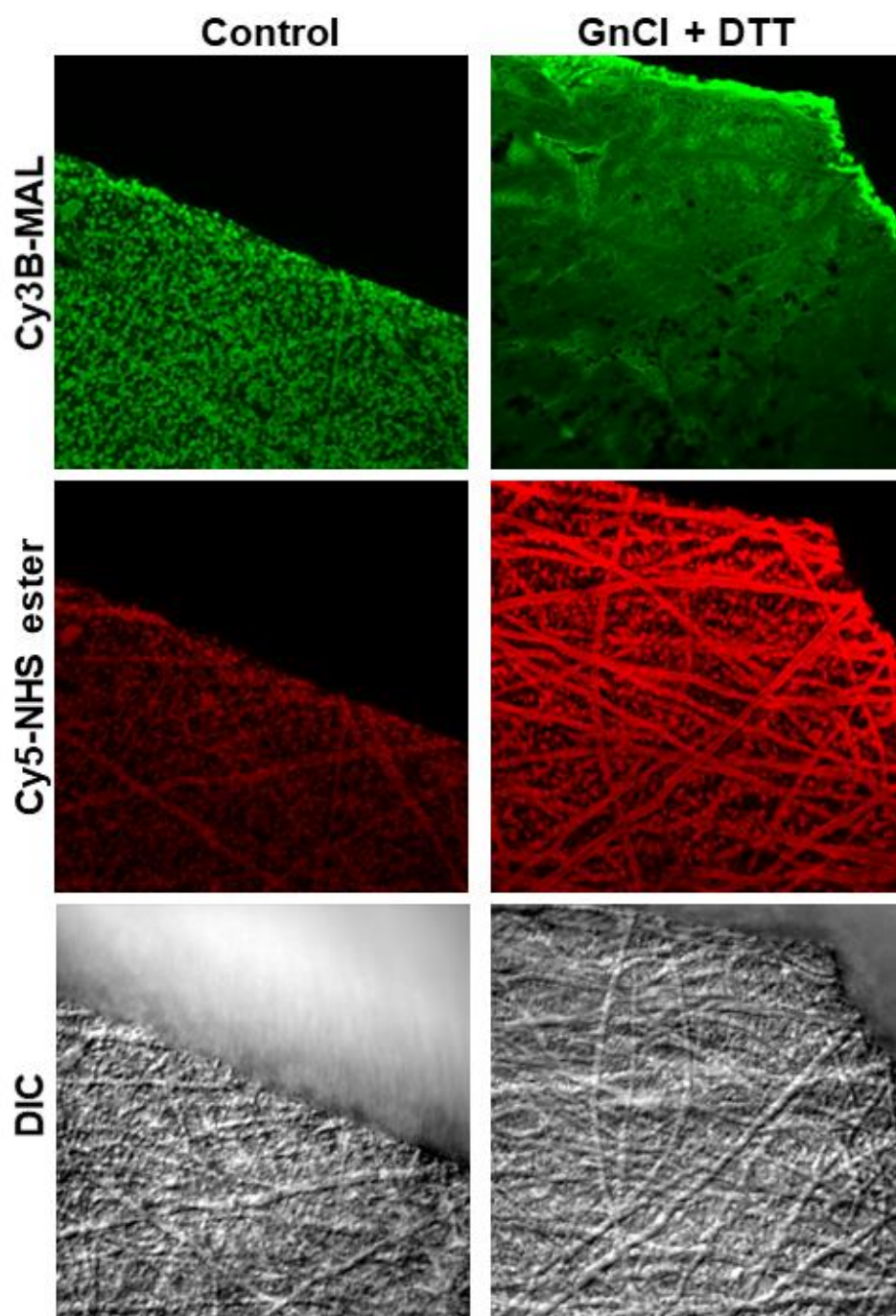
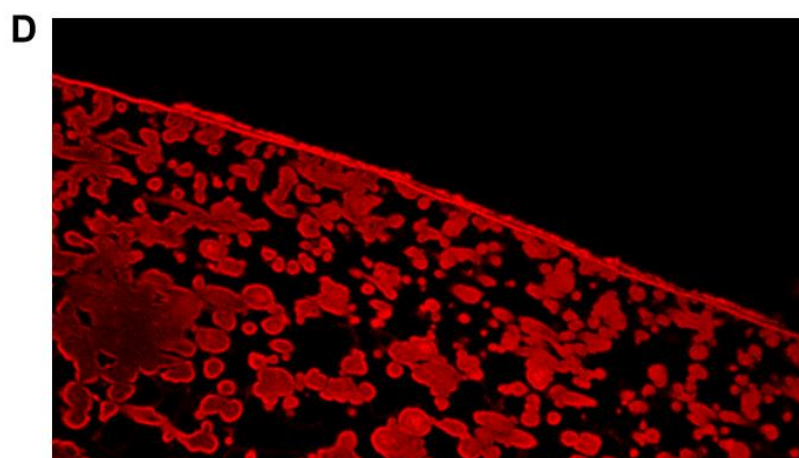
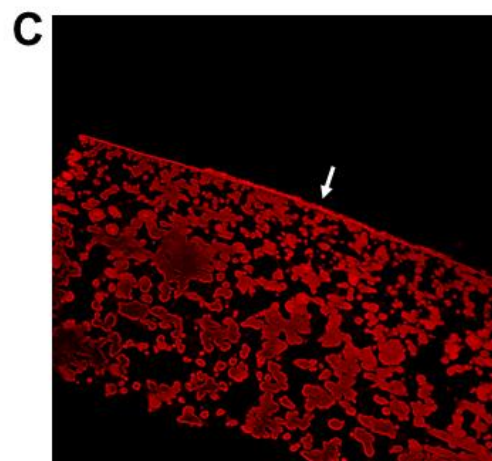
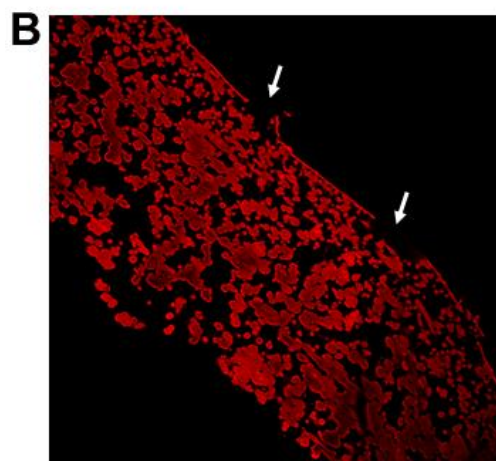
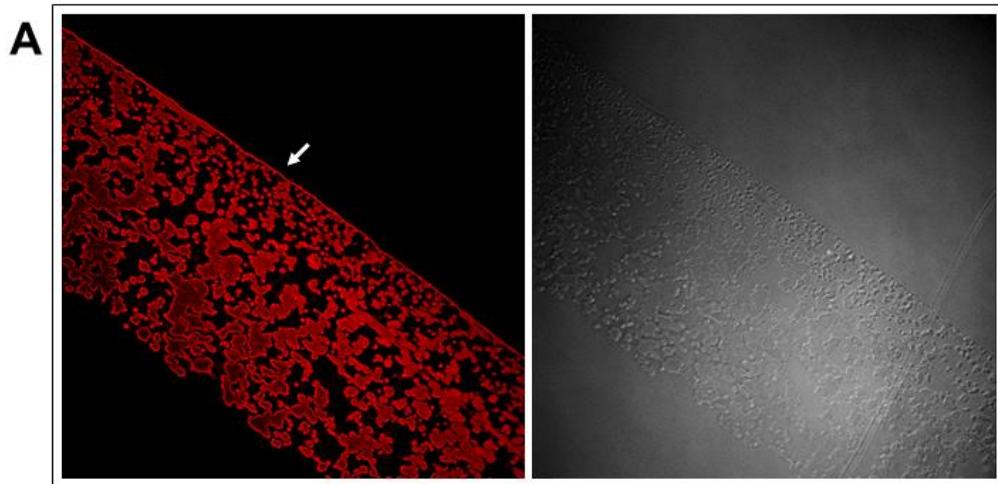


Figure 4.12 **GnCl and reductant disrupts the morphology of the inner layer of the ESM.** The green channel shows the SS labeling, the red channel shows the NH₂ labeling.

4.3.3.3 The Limiting Membrane is Disulfide Rich and Proteinaceous

The dehydrated ESM was embedded in LR White and cut using a vibratome to give 1 μM sections (see Experimental procedure). After mounting on glass slides, the fixed membranes were treated with or without 5 mM TCEP and stained with Cy5-maleimide. As before, the staining is selective to thiols since the control does not show fluorescence under the confocal microscope (data not shown). Figure 4.13 shows several sections of the ESM. Panel A shows a typical section, the white arrow shows the limiting membrane next to small granules that are observed previously. The organization of the cross section observed here is consistent with what we observed before, one side of the ESM contains a layer of small granules embedded in fibers while the other side contains thicker fibers with many fewer granules. Panel B presents a broken limiting membrane (the white arrows show the broken locations) and panel C shows a double layer of limiting membrane (white arrow). This surprising feature is shown in an enlargement in Panel D. Panel E shows several 3D reconstructions of the ESM sections. This experiment indicates that the limiting membrane is a disulfide rich structure next to inner membrane. While the dehydration step makes it difficult to know the natural structure of the limiting membrane, the staining gives some indication of the organization and features of this interesting structure.



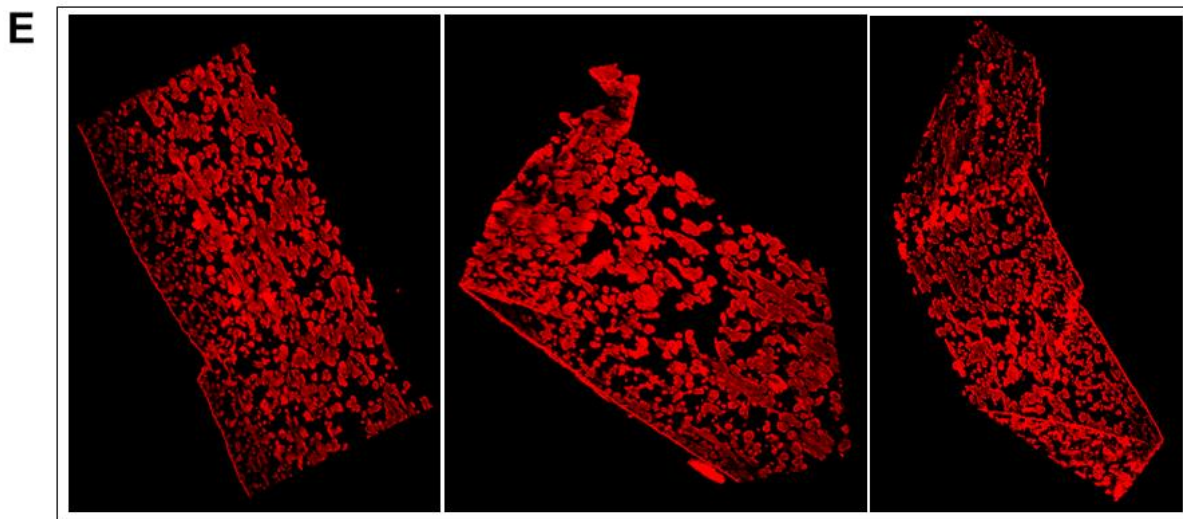


Figure 4.13 **The limiting membrane is a thiol rich structure.** The red channel shows the SS labeling of the cross sections of ESM. Panel A shows a typical cross section of ESM, the white arrow shows the limiting membrane. Panel B shows the limiting membrane that is broken (white arrows). Panel C shows a double layer of limiting membrane (white arrow). Panel D shows a magnification of the double layer area. Panel E shows three of the 3D reconstruction of z-stack ESM images.

4.3.4 Conclusion

We show that the bright sulfonated dyes conjugated with maleimide are well suited for fluorescence imaging of the disulfide rich ESM. This method can selectively label the thiols without the problem of non-specific binding that was encountered before and can be a potential way for future studies intended to use super-resolution methods to probe fiber compositions. We believe that our studies represent the first time that the limiting membrane has been visualized by traditional confocal microscopy instead of electron microscopy.

REFERENCES

- 1 Riddle, D. L. *C. elegans II*. (Cold Spring Harbor Laboratory Press, 1997).
- 2 McGhee, J. D. The Caenorhabditis elegans intestine. *Wiley interdisciplinary reviews. Developmental biology* **2** (2013).
- 3 Clark, L. & Hodgkin, J. *Caenorhabditis microbiota: Worm guts get populated*. Vol. 14 (2016).
- 4 Page, A. *The nematode cuticle: Synthesis, modification and mutants*. (2001).
- 5 Page, A. P., Stepek, G., Winter, A. D. & Pertab, D. Enzymology of the nematode cuticle: A potential drug target? *International journal for parasitology. Drugs and drug resistance* **4**, 133-141, doi:10.1016/j.ijpddr.2014.05.003 (2014).
- 6 Page, Antony P. & Johnstone, Iain L., The cuticle (March 19, 2007), WormBook, ed. The C. elegans Research Community, WormBook, doi/10.1895/wormbook.1.138.1, http://www.wormbook.org.
- 7 Jovine, L., Darie, C. C., Litscher, E. S. & Wassarman, P. M. Zona pellucida domain proteins. *Annual review of biochemistry* **74**, 83-114, doi:10.1146/annurev.biochem.74.082803.133039 (2005).
- 8 Stenvall, J. *et al.* Selenoprotein TRXR-1 and GSR-1 are essential for removal of old cuticle during molting in Caenorhabditis elegans. *Proceedings of the National Academy of Sciences of the United States of America* **108**, 1064-1069, doi:10.1073/pnas.1006328108 (2011).
- 9 Brenner, S. The genetics of Caenorhabditis elegans. *Genetics* **77**, 71-94 (1974).
- 10 Burley, R. W. & Vadehra, D. V. *The avian egg : chemistry and biology*. (Wiley, 1989).
- 11 Hoffer, A. P. The ultrastructure and cytochemistry of the shell membrane-secreting region of the Japanese quail oviduct. *The American journal of anatomy* **131**, 253-287, doi:10.1002/aja.1001310302 (1971).
- 12 Bellairs, R. & Boyde, A. Scanning electron microscopy of the shell membranes of the hen's egg. *Zeitschrift fur Zellforschung und mikroskopische Anatomie (Vienna, Austria : 1948)* **96**, 237-249 (1969).
- 13 Candlish, J. K. The outer membrane of the avian egg shell as a reticular structure. *British Poultry Science* **11**, 341-344, doi:10.1080/00071667008415824 (1970).
- 14 Hamilton, R. M. G. The Microstructure of the Hen's Egg Shell - A Short Review. *Food Structure* **5** (1986).
- 15 Hincke, M. T. *et al.* Identification and localization of lysozyme as a component of eggshell membranes and eggshell matrix. *Matrix biology : journal of the International Society for Matrix Biology* **19**, 443-453 (2000).
- 16 Draper, M. H., Davidson, M. F., Wyburn, G. M. & Johnston, H. S. The fine structure of the fibrous membrane forming region of the isthmus of the oviduct

- of *Gallus domesticus*. *Quarterly journal of experimental physiology and cognate medical sciences* **57**, 297-310 (1972).
- 17 A., T. M. & F., R. J. ULTRASTRUCTURE OF THE HEN'S EGG SHELL MEMBRANES BY ELECTRON MICROSCOPY. *Journal of Food Science* **37**, 277-281, doi:doi:10.1111/j.1365-2621.1972.tb05835.x (1972).
- 18 Wong, M., Hendrix, M. J., von der Mark, K., Little, C. & Stern, R. Collagen in the egg shell membranes of the hen. *Developmental biology* **104**, 28-36 (1984).
- 19 Kodali, V. K. *et al.* A novel disulfide-rich protein motif from avian eggshell membranes. *PloS one* **6**, e18187, doi:10.1371/journal.pone.0018187 (2011).
- 20 Arias, J. L., Fernandez, M. S., Dennis, J. E. & Caplan, A. I. Collagens of the chicken eggshell membranes. *Connective tissue research* **26**, 37-45 (1991).
- 21 Arias, J. L. *et al.* Role of type X collagen on experimental mineralization of eggshell membranes. *Connective tissue research* **36**, 21-33 (1997).
- 22 Torres, F. G., Troncoso, O. P., Piaggio, F. & Hajar, A. Structure-property relationships of a biopolymer network: the eggshell membrane. *Acta biomaterialia* **6**, 3687-3693, doi:10.1016/j.actbio.2010.03.014 (2010).
- 23 Du, J. *et al.* Identifying specific proteins involved in eggshell membrane formation using gene expression analysis and bioinformatics. *BMC genomics* **16**, 792, doi:10.1186/s12864-015-2013-3 (2015).
- 24 Leach, J. R. M. Biochemistry of the Organic Matrix of the Eggshell1. *Poultry Science* **61**, 2040-2047, doi:10.3382/ps.0612040 (1982).
- 25 Leach, R. M., Jr., Rucker, R. B. & Van Dyke, G. P. Egg shell membrane protein: a nonelastin desmosine/isodesmosine-containing protein. *Arch Biochem Biophys* **207**, 353-359 (1981).

Appendix A

COPYRIGHTS

Chapter 1

Figure 1.11 is reprinted from:

Thorpe, C. & Coppock, D. L. Generating disulfides in multicellular organisms: emerging roles for a new flavoprotein family. *J Biol Chem* 282, 13929-13933, doi:10.1074/jbc.R600037200 (2007).

Chapter 2

Figures and text are largely adapted from:

Israel BA, Jiang L, Gannon SA, & Thorpe C. Disulfide bond generation in mammalian blood serum: detection and purification of quiescin-sulfhydryl oxidase. *Free Radic Biol Med* 69: 129–135 (2014).

Chapter 4

Figure 4.2 is adapted from:

Clark, L. & Hodgkin, J. *Caenorhabditis* microbiota: Worm guts get populated. Vol. 14 (2016).

Figure 4.3 is reprinted from:

Page, Antony P. & Johnstone, Iain L., The cuticle (March 19, 2007), WormBook, ed.
The C. elegans Research Community, WormBook, doi/10.1895/wormbook.1.138.1,
<http://www.wormbook.org>.



RightsLink®

Home

Account
Info

Help



Title: Disulfide bond generation in mammalian blood serum: detection and purification of quiescin-sulfhydryl oxidase

Author: Benjamin A. Israel, Lingxi Jiang, Shawn A. Gannon, Colin Thorpe

Publication: Free Radical Biology and Medicine

Publisher: Elsevier

Date: April 2014

Logged in as:
Lingxi Jiang
Account #:
3001301365

LOGOUT

Copyright © 2014 Elsevier Inc. All rights reserved.

Please note that, as the author of this Elsevier article, you retain the right to include it in a thesis or dissertation, provided it is not published commercially. Permission is not required, but please ensure that you reference the journal as the original source. For more information on this and on your other retained rights, please visit: <https://www.elsevier.com/about/our-business/policies/copyright#Author-rights>

BACK

CLOSE WINDOW

Copyright © 2018 Copyright Clearance Center, Inc. All Rights Reserved. [Privacy statement](#). [Terms and Conditions](#).
Comments? We would like to hear from you. E-mail us at customercare@copyright.com